

**An Assessment of the Photostability of South African
Commercial Sunscreens**

by

Tavengwa Bunhu

Submitted in fulfillment of the academic
requirements for the degree of
Master of Science in the School of Chemistry,
University of KwaZulu-Natal,
Durban

ABSTRACT

The many deleterious effects of the sun's ultraviolet radiation (UVR) on the skin are well-documented. The increasing public awareness of the adverse effects of overexposure to solar UVR has led to a heightened use of sun protection products. Sunscreens have been developed to mitigate the acute and chronic skin damage caused by this radiation. The active ingredients incorporated into sunscreens are either chemical absorbers or physical blockers. However, the photostability of these sunscreens has been under much scrutiny as there is an alarming worldwide increase in skin cancer.

The photostability of commercial sunscreens available on the South African market has been investigated. A known amount of sunscreen was smeared onto quartz plates to achieve an application density of 1 mg cm^{-2} which is a more realistic estimate of what is typically used. Ultraviolet/visible transmission spectroscopy was employed for the photostability assessment of sunscreens. The transmission spectra of these samples were recorded before and after exposure to solar radiation in Durban, South Africa. The actinic flux incident on the samples was measured by means of chemical actinometry (valerophenone actinometer). Changes in the transmission profiles of the sunscreen products during the course of exposure were monitored at set time intervals.

It was shown that 35% of the sunscreen products tested are photounstable especially in the UVA region. Photostability assessment of sunscreen products by high performance liquid chromatography (HPLC) revealed that photoinstability was mainly a result of the photodegradation and/or photoisomerisation of the two chemical absorbers, octylmethoxycinnamate and avobenzone. The sunscreen products exhibited a high photostability in the UVB region. The sunscreen products were also analysed in solution to check if there was any correlation between solution analysis and the quartz plate results. The sunscreen products analysed displayed higher photostabilities in solution than on a quartz plate.

Since some sunscreen agents can cause photo-allergic reactions and photo-contact dermatitis, regulations limit the permissible amounts of these active ingredients in a formulation. Hence, quantification of the organic UV-filters was carried out by reversed-phase HPLC with a Phenomenex Synergi Max-RP-C₁₂ 80 Å column. Physical blockers are increasingly utilised in combination with organic UV-filters to boost the sun protection factor and to improve the

broad-spectrum protection of a sunscreen formulation. However, the most commonly used physical blocker, titanium dioxide (TiO₂), is known for its photocatalytic activity. Therefore, TiO₂ in the sun care products was determined by inductively coupled plasma - optical emission spectroscopy (ICP-OES).

The levels of sunscreen active ingredients were found to be within the European Cosmetics and Personal Care Association (COLIPA) approved limits.

The application of the *in vitro* critical wavelength method for the assessment of photostability and the broad-spectrum protection classification of commercial sunscreens was also explored. A strong correlation between the increase in photoinstability and the decrease in the calculated critical wavelength was observed. The broad-spectrum protection information on the labels also agreed very well with the calculated critical wavelength data.

PREFACE

This thesis presents work performed by the author in the School of Chemistry, University of KwaZulu-Natal, King George V Avenue, Durban, 4041, from August 2004 to February 2006 under the supervision of Prof. B. S. Martincigh.

This work is the original work of the author and has not been submitted in part, or in whole, to any other university. Where use has been made of the work of others, it has been duly acknowledged in the text.

TAYENGIWA BUNTHU  19/09/2006

ACKNOWLEDGEMENTS

I would like to thank my supervisor, Prof B. S. Martincigh for her invaluable guidance and support throughout my M.Sc. research. Many thanks go to Prof. A. Kindness for his much valued advice on the determination of titanium dioxide. I also want to thank Prof. I. L. MacDonald of the University of Cape Town for assistance with calculations.

I extend my gratitude to my colleagues: Janine Elizabeth Kasavel, Georges Jasper Mturi, Ali Mohammed Salim and Walyambillah Waudu, for their encouragement and support in the laboratory. The project would not have been successful if it was not for the technical assistance provided by Anita Naidoo and Bathabile Soko with the HPLC, ICP-OES and GC-FID operation.

I owe special thanks to Kishore Singh, Logan Murugus, Gregory Moodley, Thulani Sishi and Enoch Mkhize for their assistance.

I would like to thank my family for their encouragement and support, and I am especially grateful to my brother Mugove Essau Bhunu for financing my trip to South Africa.

Finally, I would like to thank the National Research Foundation (NRF), the Cancer Association of South Africa (CANSA) and the University of KwaZulu-Natal for financial support for the duration of this study.

TABLE OF CONTENTS

Chapter 1

INTRODUCTION	1
1.1 Solar ultraviolet radiation and its consequences	2
1.1.1 Ultraviolet C	2
1.1.2 Ultraviolet B	3
1.1.3 Ultraviolet A	3
1.1.4 Induction of skin cancer by ultraviolet radiation	4
1.2 The need for photoprotection	7
1.3 Sunscreen molecules and their photochemistry	9
1.3.1 Photochemistry of physical blockers	11
1.3.2 Photochemistry of chemical absorbers	15
1.3.2.1 Photochemistry of organic sunscreens	15
1.3.2.2 UVB absorbers	21
1.3.2.3 UVA absorbers	22
1.3.3 Chemical absorbers investigated in this study	24
1.4 Photostability of sunscreens	26
1.5 Aims and outline of this study	29

Chapter 2

EXPERIMENTAL	31
2.1 Materials	31
2.2 Equipment	31
2.3 Determination of UV filters by high performance liquid chromatography	33
2.3.1 Instrumentation	35
2.3.2 HPLC equipment and operation	36
2.3.3 Preparation of standard solutions	39
2.3.4 UV/VIS absorption spectra of sunscreen active ingredients	40
2.3.5 Determination of optimum separation conditions	42
2.3.6 Analysis of standard solutions	44
2.3.7 Preparation of sunscreen samples and analysis	45

2.3.8	Validation of the HPLC quantitation method	46
2.4	Determination of titanium dioxide by inductively coupled – optical emission spectroscopy	46
2.4.1	ICP-OES	47
2.4.2	Instrumentation	48
2.4.3	Preparation of standard solutions	48
2.4.4	Preparation of sunscreen samples and analysis	49
2.4.5	Validation of the ICP-OES quantitation method	49
2.5	Photostability analysis of sunscreens by UV/VIS transmission spectrophotometry	50
2.5.1	Instrumentation	51
2.5.2	Analysis of sunscreens on quartz plates	52
2.5.2.1	Evaluation of sunscreen application method	52
2.5.2.2	Assessment of the reproducibility of instrument readout	53
2.5.2.3	Analysis of sunscreen products on quartz plate by using the hand-smearing method	55
2.5.3	Analysis of sunscreens in solution	56
2.5.4	Data analysis	58
2.5.4.1	Calculation of photoinstability	58
2.5.4.2	Calculation of the critical wavelength	58
2.6	Photostability analysis of sunscreens by HPLC	60
2.7	Chemical actinometry measurements	61
2.7.1	Actinometry	62
2.7.2	Gas Chromatography	64
2.7.3	Instrumentation	64
2.7.4	Preparation of solutions for actinometry	66
2.7.5	GC-FID equipment and operation	67
2.7.6	GC-FID analysis of valerophenone solution	67
2.7.7	Data analysis	70

Chapter 3

RESULTS AND DISCUSSION	72
3.1 Determination of UV filters by high performance liquid chromatography	73
3.1.1 Variation of retention times	73

3.1.2	Linearity of calibration curves	74
3.1.3	Validation of the HPLC quantitation method	76
3.1.4	Levels of organic UV filters in commercial sunscreens	76
3.2	Determination of titanium dioxide by inductively coupled – optical emission spectroscopy	79
3.2.1	Linearity of calibration curves	79
3.2.2	Validation of the ICP-OES quantitation method	80
3.2.3	Levels of TiO ₂ in commercial sunscreens	81
3.3	Photostability assessment of sunscreens	82
3.3.1	Characterisation of sun care products	82
3.3.2	UV/VIS absorption spectra of sunscreen active ingredients	84
3.3.3	Assessment of sunscreen photostability by UV/VIS transmission spectrophotometry and HPLC	84
3.3.3.1	Sunscreens containing OMC	86
3.3.3.2	Sunscreens containing OMC and Bz-3	87
3.3.3.3	Sunscreens containing OMC and AVO	92
3.3.3.4	Sunscreens containing OMC, AVO and TiO ₂	96
3.3.3.5	Sunscreens containing OMC, AVO, MBC and TiO ₂	100
3.3.3.6	Sunscreens containing OMC, MBC, Bz-3 and OS	109
3.3.3.7	Sunscreens containing OMC, Bz-3, OS and TiO ₂	113
3.3.3.8	Sunscreens containing AVO, OT, DOBT and TiO ₂	115
3.3.3.9	Sunscreens containing OMC, OCR, BEMT and TiO ₂	116
3.3.3.10	Sunscreens containing OMC, MBC, MBBT and BEMT	117
3.3.3.11	Sunscreens containing OMC, MBC, MBBT, BEMT and TiO ₂	120
3.3.3.12	Sunscreens containing OMC, MBC, Bz-3, OS and TiO ₂	121
3.3.3.13	Sunscreens containing OMC, Bz-3, AVO, OS and TiO ₂	122
3.3.3.14	Sunscreens containing OMC, AVO, OT, BEMT, DOBT and TiO ₂	123
3.3.4	Discussion	127
3.4	Application of the <i>in vitro</i> critical wavelength method	131
3.4.1	Broad-spectrum classification of sunscreens	132
3.4.2	Photostability assessment of sunscreens using the critical wavelength method	134

Chapter 4

CONCLUSION 140

REFERENCES 145

APPENDICES

Appendix A	-	Materials	157
Appendix B	-	Equipment	159
Appendix C	-	Calibration and actinometry data	160
Appendix D	-	Calibration curves and residual plots	167
Appendix E	-	Straight-line calibration with intercept zero	177
Appendix F	-	Chromatograms for sun care products	182
Appendix G	-	Raw data for sun care products	198
Appendix H	-	Conference presentations	201

Chapter 1

INTRODUCTION

It is well appreciated that any form of life on earth would be virtually impossible without the sun. Plants directly use sunlight to convert carbon dioxide and water to carbohydrates through the process of photosynthesis. They then supply higher levels of the food chain in the ecosystem. In the human body, small amounts of ultraviolet radiation trigger the synthesis of vitamin D and help to boost the body's immune system.

However, overexposure to the sun also causes a number of adverse effects on the skin. Acute and chronic exposures are linked to the chronic development of various pathologies such as photoaging and skin cancers. Compelling evidence has demonstrated that the ultraviolet part of the solar spectrum is the aetiologic agent responsible for these effects.^{1, 2} Therefore, sun protection at any age is important to prevent short-term and long-term effects from the sun's ultraviolet radiation (UVR). Sunscreens were primarily designed for the prevention of sunburn but are now recognised to be an important strategy in the prevention of squamous cell carcinoma, photoaging and ultraviolet-induced immunosuppression.³⁻⁵ Sunscreen products work by scattering, reflecting and absorbing the harmful UVR that reaches the skin. These suncare products come in a variety of forms ranging from sprays, lotions, creams, lipsticks and powders. The sunscreen active ingredients are of two types: physical and chemical absorbers. The two are normally used in combination to boost the ultraviolet (UV) protective capacity of a formulation. However, the photostability of chemical absorbers has been under much scrutiny as there is an alarming worldwide increase in the incidence of skin cancer. This is despite a heavy campaign by medical groups and dermatologists for the use of sunscreen products. The purpose of this study was to assess the photostability of sunscreens commercially available in South Africa. The photostability analysis of sunscreens was carried out by use of ultraviolet/visible (UV/VIS) spectrophotometry and high performance liquid chromatography (HPLC).

Since some sunscreen active agents can cause photo-allergic reactions and photo-contact dermatitis, regulations limit the permissible amounts of these active ingredients in a formulation.⁶ Hence, quantification of organic UV-filters was carried out by reversed-phase HPLC. Inductively coupled plasma-optical emission spectroscopy (ICP-OES) was employed for the determination of titanium dioxide (physical blocker) in the commercial sunscreens.

1.1 Solar ultraviolet radiation and its consequences

Optical radiation within the electromagnetic spectrum includes UV, visible (VIS) and infrared radiation. In the electromagnetic spectrum, the UV region spans the wavelengths 100 - 400 nm, the VIS region covers the wavelengths 400 - 760 nm and infrared radiation, 760 - 10^6 nm. Visible light does not appear to be harmful to normal individuals.

Cell death, chromosome changes, mutation and morphological transformations are observed after UV exposure of procaryotic and eucaryotic cells.⁷ Many different genes and several viruses (including the human immunodeficiency syndrome - HIV) are activated by UV exposure.⁸ Studies of deoxyribonucleic acid (DNA) repair-defective disorders have clearly established a link between UV-induced DNA damage in skin and various types of skin cancer.

Besides causing skin cancer, solar UVR also increases the risk of developing cataracts and certain other eye problems and can cause impairment of the immune system. Impairment of the immune system as a result of exposure to suberythemal doses of UV has been shown to increase the risk of infections in rodents.⁹

We will focus on the UV region of the solar spectrum as it is the most potent and energetic radiation that falls on the earth's surface. UVR is further characterised according to its biological effects into ultraviolet C (100 - 280 nm), ultraviolet B (280 - 320 nm) and ultraviolet A (320 - 400 nm).⁹

1.1.1 Ultraviolet C

Radiation from the ultraviolet C (UVC) region is the most energetic and carcinogenic. UVC radiation is absorbed by DNA, thus causing damage in the form of pyrimidine dimers and 6-4 photoproducts.^{10, 11} Fortunately, all UVC is completely filtered out by nature's own sunscreen, the ozone layer as well as molecular oxygen and water vapour in the atmosphere, and does not reach the earth's surface in any measurable amounts.¹² Exposure to UVC is damaging to skin cells and is a hazard in occupations such as welding where exposure is common.

1.1.2 Ultraviolet B

Ultraviolet B (UVB) is radiation of wavelengths between 280 - 320 nm and makes up only 5% of the UV photons reaching the earth's surface.¹³ The shorter wavelength UVB radiation (280 - 290 nm) is absorbed by the ozone layer and the atmosphere such that solar UVR reaching the earth's surface is of wavelengths from 290 - 400 nm. The increasing depletion of the ozone layer worldwide is of major concern as that leads to shorter wavelengths (<290 nm) of biologically effective UVB radiation reaching the earth's surface. Low doses of UVB trigger the synthesis of vitamin D in the skin and support the immune system.¹⁴ It is the most important component of sunlight for human skin as it causes sunburn and skin cancer. UVB is considered the major action spectrum for both melanoma and non-melanoma skin cancer formation.^{15, 16} Although it does not penetrate as deeply as UVA,^{15, 17} and does not interact with the epidermis as vigorously as UVC, UVB combines depth of penetration and reactivity with macromolecules in such a way that it is the most biologically potent portion of the UV spectrum in terms of short- and long-term consequences.¹⁵ It inhibits DNA, ribonucleic acid (RNA) and protein synthesis and induces erythral responses.¹⁸ UVB causes direct DNA damage by inducing three major base modifications: cyclobutane-type pyrimidine dimers, (6-4) photoproducts and thymine glycols.^{19, 20} It is said that the majority of biological effects of UV radiation including cell killing, sister chromatid exchange, mutagenesis,²¹ and inhibition and recovery of DNA and RNA synthesis, appear to be due to the (6-4) photoproduct though it is produced in very low yields.^{22, 23}

1.1.3 Ultraviolet A

Radiation from this region is the most abundant of the solar UVR comprising about 95% of UV energy reaching the earth's surface at the equator and covers the wavelengths 320 - 400 nm.¹⁷ It is also the major radiation produced by tanning beds. UVA is poorly absorbed by DNA but can interact with cellular chromophores²⁴ (riboflavins, porphyrins, quinines and reduced nicotinamide cofactors).^{25, 26} These photosensitisers in turn can produce reactive oxygen species (ROS) which induce DNA strand-breaks, DNA-protein cross-links and many oxidized base derivatives such as 8-hydroxyquanosine.²⁵ The presence of ROS results in enhanced epidermal ferritin expression, lipid and protein oxidative damage, and reduced skin hydration and elasticity.²⁷ UVA penetrates much deeper into the skin than any of the other ultraviolet regions, and can enhance the carcinogenic effects of UVB.²⁸ Possibly because of its ability to penetrate

deeply into the skin, UVA contributes substantially to chronic sun damage and can cause photoimmunosuppression.²⁹ Premature aging of the skin has been shown to be a result of UVA with effects that include sagging, roughening, blotchiness and wrinkles. UVA also contributes to the development of skin cancer but it is only during the last decade that the damaging effects of UVA have been fully appreciated. Budai *et al.*³⁰ and other studies showed that UVA radiation induces collagenase and apoptosis in human fibroblasts *in vivo* and *in vitro*. The same was also shown to occur by Bernerd *et al.*³¹ and Soriani *et al.*²¹ Protection in this range of the UVR region is now recognized as important in the fight against skin cancer.

1.1.4 Induction of skin cancer by ultraviolet radiation

The importance of sun exposure in the development of skin cancers in humans was recognized as early as 1894.³² Animal models (using rodents) have shown that solar UVR causes predominantly non-melanoma skin cancers (NMSC): squamous cell carcinomas (SCC's) and basal cell carcinomas (BCC's). The action spectrum for the induction of SCC's and BCC's is considered to be in the UVB region.³³ UVA has been shown to produce the same, but only at much higher intensities. Studies have shown that the highest incidence rates of NMSC are on chronically exposed areas. It is generally accepted that chronic repeated exposures to solar UVR increase the risk of developing NMSC.^{33, 34} The two types of skin carcinomas are the most common but less fatal than malignant melanoma (MM).

Epidemiological studies have shown that the annual incidence and mortality rates of both melanoma and NMSC are rapidly rising.² The global mortality rate was shown to have increased five-fold with an annual increase of 11% in the incidence of skin cancer.³⁵ An epidemiological study of melanoma by Marks³⁶ showed that the global incidence rates have increased by 3-7% annually in recent decades. This increase is mainly attributed to the changing lifestyles of modern societies, with families participating more in outdoor leisure activities and outdoor occupations.

MM is the most serious of all skin cancers though it is less common than BCC's and SCC's. The risk of developing melanoma is high in people who are overexposed to the sun (especially the UVB region).^{37, 38} MM is thought to be caused by intermittent overexposure of untanned skin as well as excessive exposure during childhood.³⁹ UVB has been shown to transform

melanocytes from SV40 transgenic mice.^{16, 40} Setlow *et al.*⁴¹ working with *Xiphophorus* fish demonstrated that the action spectrum peak for melanoma lies in the UVB region.

The increase in the incidence of melanoma was observed despite the availability of sunscreens. Sunscreens were developed primarily to protect against sunburn (caused by UVB). However, it is now accepted that UVA plays a major role in the induction of skin cancer. Some researchers have come to suspect that it is the UVA, instead of the UVB region, responsible for causing melanoma.^{18, 27} A more recent study by Setlow *et al.*⁴² tends to support the suspicion that UVA may be responsible for melanoma. They found that UVA induced melanoma lesions in *Xiphophorus* fish (platyfish and swordtails).

It took several decades of research for scientists to unravel the mechanisms by which sunlight can transform normal cutaneous tissue into tumor tissue. Normally epidermis can absorb radiation in the UVB and UVC range, reflect 5% to 10% of the spectral range of 250 nm to 350 nm, and scatter most visible light.^{43, 44} The major cellular chromophores absorbing in the UVB are pyrimidine and purine bases in DNA, and proteins (especially tryptophan and tyrosine).⁴⁵ There is a general agreement that deoxyribonucleic acid (DNA) is the principal target of UV-induced skin damage. UVR damages DNA in the nucleus and transforms normal skin cells into malignant (cancerous) cells through a combination of complex cellular and molecular processes. Underlying these processes are the following two distinct but interacting pathways:

- a) direct alteration of DNA in the keratinocytes⁴⁶ within the skin by the UV energy itself (keratinocytes produce keratin, one of the structural proteins of the epidermis), and
- b) suppression of immune responses, which normally control the growth of abnormal cells.⁴⁷

The first mechanism causes the keratinocytes to grow abnormally, and this leads to formation of abnormal structures within the epidermal layer. Pyrimidine bases are more sensitive to UV damage than purines and undergo a number of photochemical modifications. Cyclobutane dimers formed from adjacent pyrimidines are a major form of direct UV-induced DNA damage.^{48, 49} The formation of these pyrimidine dimers is largely ascribed to UVB wavelengths. The presence of these dimers may result in mutations that can lead to skin cancers.

However, the body has mechanisms for repairing such abnormalities in the structure of DNA,⁵⁰ but if left un-repaired or mis-repaired may lead to mutations. In individuals with genetically

compromised DNA-repair capacity (*xeroderma pigmentosum* patients), lack of repair leads to several skin cancers early in life. Pyrimidine dimer formation and repair in human skin has been reported by Sutherland *et al.*⁵¹ and Sinha *et al.*⁴⁹

The second mechanism facilitates the growth of these emerging tumors by compromising the body's natural anti-tumor defenses.⁴⁷ The Langerhan's cells limit damage to the immune system by recognising and destroying malignant cells. Unfortunately the function of Langerhan's cells is impaired by UV radiation and their numbers are reduced.²⁷ The radiation that is the cause of carcinogenic change is also responsible for reducing the body's natural defence mechanisms.⁵²

Recent studies have also shown that alterations in a particular gene, the p53 tumor suppressor gene, play an important role in the development of skin carcinomas.⁵³⁻⁵⁵ This gene codes for a special protein (the p53 protein), that attaches itself to a specific place on the DNA and regulates gene transcription.²⁰ This in turn controls the cell cycle of growth and division. Normally, a very small amount of p53 protein is present in cells. However, upon exposure to UV radiation, this protein is produced in large quantities. This in turn inhibits cell division and enables the cell to repair its damaged DNA before undergoing cell division.⁵⁶

However, following repeated exposures to UV radiation, the p53 gene is also damaged resulting in keratinocytes carrying mutant p53 genes, which are resistant to cell death. In contrast, normal cells (with normal p53 protein) surrounding the cell that contains a p53 mutation commit massive suicide (apoptosis).⁵⁷ This programmed cell death is triggered by UV exposure. The result is the proliferation of mutant p53 carrying cells due to their lower sensitivity to UVR than the normal p53 cells. Both the UVA and UVB wavelengths have been found to be effective in the induction of cell damage and cell apoptosis in normal and mutant p53 melanoma cells and the damage elicited is dose dependent.⁵⁶

A few years ago, UV-specific p53 mutations were found in more than 90% of human SCC's and 50% of BCC's.⁵⁸ Cells containing p53 mutations have also been found from patients with *xeroderma pigmentosum*. The same have also been found in actinic keratoses, the most common pre-cancers.⁵⁹

Apart from the two mechanisms described above, there is also indirect damage to DNA. Indirect DNA damage is caused by free radicals and singlet oxygen that are generated by the action of UV radiation on the skin. The presence of free radicals and singlet oxygen may trigger a chain

of phototoxic reactions in the skin that may damage DNA, resulting in the development of cancerous cells. As described above, UVA is the most effective in photosensitizing the formation of singlet oxygen, thus creating conditions of oxidative stress.¹⁸

One of the clinically detectable effects of UV damage that deserves particular attention is erythema (sunburn), since this forms the basis of the current sunscreen efficacy measurement and has been correlated with melanoma risk. It is now appreciated that erythema *per se* is linked to the carcinogenic effect of sunlight, especially UVB radiation.⁶⁰ The wavelengths that are the most efficient at producing erythema are also the most efficient at producing pyrimidine dimers.⁴⁸ The fact that the action spectrum of erythema is similar to the absorption spectrum of DNA is consistent with this concept.⁶¹

It should be mentioned that repeated suberythema UV exposure can induce skin cancer since skin damage builds up with continued exposure to UV radiation, whether sunburn occurs or not. This is because the lower energy UVA radiation damages connective tissue at deeper levels, even if the skin surface feels cool.¹⁵

Preventive measures against the detailed deleterious effects of the sun are definitely required if the fight against skin cancer is to be successful. Section 1.2 describes the possible measures people can take in order to protect their skin from the harmful effects of solar radiation.

1.2 The need for photoprotection

In the light of the above-cited literature, prevention of skin cancer depends on preventing the genetic alterations that lead to tumor development by avoiding carcinogenic UV radiation. It is now accepted that incremental damage occurs with each exposure to UV radiation even with doses that do not produce erythema. This damage is cumulative and over the years the total time in the sun is reflected by wrinkles, blotchy pigmentation and with enough exposure, skin cancer. This damage could have been elicited in childhood. Therefore, sun protection is important at any age if the deleterious effects of excessive exposure to solar UVR are to be prevented.

The most effective way for people to reduce skin cancer risk is to protect their skin from burning in the sun. This can be achieved by staying out of the sun during the peak hours of the day, always being properly dressed including putting on broad-rimmed hats and sunglasses.

Although sun avoidance is more desirable, outdoor occupations and lifestyles make total avoidance impossible for many individuals. The regular use of sunscreens represents a practical compromise but more feasible way of sun protection in this regard.

The use of sunscreens as a protective measure against the deleterious effects of solar UVR is mired in a lot controversy. Some reports in the body of literature available have attributed the increase in the incidence of melanoma and non-melanoma skin cancers to the use of sunscreens.^{18, 62, 63} This hypothesis arises from epidemiologic studies which have demonstrated that there has been an increase in the incidence of skin cancer since the advent of commercial sunscreens.⁶⁴ Some researchers have even suggested that rigorous sun protection (wearing clothes and sunscreens) may result in an abnormally low level of vitamin D, thus compromising on the body's defense system, paradoxically leading to a high risk of skin cancer and other infections.⁶⁵ Nonetheless, there is overwhelming evidence supporting the potency of sunscreens in moderating the harmful effects of solar radiation.

Thompson *et al.*⁶⁶ reported that regular use of high potency (at least SPF 17) sunscreens reduces the risk of actinic keratoses. Sunscreens are especially effective against erythema. Diligent use of sunscreens has been shown to be effective in reducing the occurrence of SCC's and the induction of p53 gene expression.⁶⁷ An investigation by van der Molen *et al.*⁶⁸ has shown that broad-spectrum sunscreens offer protection against urocanic acid (an important mediator of UVR-induced immunosuppression) photoisomerisation.⁶⁸ A study by Seite *et al.*⁶⁹ demonstrated that sunscreens reduced the level of nuclear p53 expression after irradiation with UVA radiation. In a similar study, it was shown that the daily use of full-UV spectrum absorbing suncare creams protected against biological changes occurring in photoaging.⁷⁰ Fournier *et al.*⁷¹ found that sunscreens with increased UVA protection were effective in reducing solar-simulated radiation-induced immunosuppression. The body of literature on the potency of sunscreens against the harmful effects of excess exposure to the sun is inexhaustible.

The efficacy of these sunscreen products is dependent on the UV filters contained in their formulations. Section 1.3 presents the photochemistry of sunscreen molecules. This seeks to elucidate how sunscreens work and the possible photochemical changes that can take place upon their exposure to solar UVR.

1.3 Sunscreen molecules and their photochemistry

The susceptibility of human skin to acute burning, chronic photoaging, cancer and immunosuppression when exposed to solar UVR has been the impetus behind the continuing search by scientists for the ideal photoprotectant. Sunscreens have been proven able to provide substantial protection against the injurious responses to sunlight and there is experimental evidence to suggest that the chronic, repeated use of sunscreens does reduce the risk of photoaging and photocarcinogenesis. Sunscreens are selected and tested for their ability to prevent erythema. From the above-cited literature, the moderation of the harmful effects of solar UV irradiation by sunscreen use cannot be overstated.

Sunscreen products come in a variety of forms ranging from sprays, lotions, creams and powders. The first commercial sunscreen product is believed to have been launched in 1928 in the United States of America (USA) and it contained benzyl salicylate and benzyl cinnamate.⁵² Sunscreen development has evolved over the years and a lot of research is going on in the development of UVA-filters with new organic nanoparticles such as Tinosorb M and Tinosorb S having been approved for use in Europe recently.⁷²

Sunscreen active ingredients or UV absorbers are normally dispersed in a vehicle (emulsion) containing a number of other ingredients. The vehicle, to a greater extent, influences the absorption properties and the photostability behaviour of a sunscreen formulation. Producers decide on the type of formulation depending on cost, packaging and the protection desired. The cosmetic chemist is faced with the challenge of optimising his formula for efficacy, safety, stability, and last but not least, organoleptic considerations. There is a wide variety of sunscreen formulations available in the market place today. A compilation of the commonly used formulations can be found elsewhere.⁷³ A typical sunscreen formulation is shown in Table 1.1.

Sunscreens work by absorbing, scattering or reflecting the solar radiation, thus reducing the nature and amount of UV radiation reaching viable cells in the skin. Commercial sunscreens come in a variety of strengths called sun protection factor (SPF) values. The SPF is defined as the ratio of the minimal erythemal dose (MED) required to produce a minimal erythema (skin reddening or minimal sunburn) through the sunscreen compared to the MED required to produce the same reaction in the absence of the sunscreen. In mathematical terms,

$$SPF = \frac{MED \text{ with Sunscreen}}{MED \text{ without Sunscreen}}$$

To further elaborate on the above definition, an individual who burns after 30 minutes of sun exposure can extend the period of time until a burn begins to two hours with an SPF 4 sunscreen. The SPF value is essentially a measure of the UVB protective capacity of a sunscreen formulation since it has been shown that the action spectrum for erythema lies in the UVB region.^{48, 60} This value does not account for the UVA protective efficiency of a formulation. It should also be noted that though UVA is now understood to contribute significantly in the induction of both melanoma and non-melanoma skin cancer,^{18, 56} there is still no internationally accepted method to evaluate the UVA efficacy of a formulation.¹⁹

Table 1.1: Ingredients of a sunscreen formulation and the approximate concentrations of each.⁷³

Ingredient	Content/% m/m
Cetyl alcohol	2
Waxes	1 - 5
UV-absorbers	1 - 25
Stearic Acid	1-5
Glycerin	≤5
Stearyl dimethicone	10
Triethanolamine	≤1.5
Preservatives	≤1
Deionised water	55-80

Sunscreen active ingredients are of two types: physical blockers and chemical absorbers. Physical blockers include metal oxides such as *micronized* titanium dioxide (TiO₂), *ultrafine* zinc oxide (ZnO), and iron oxide (Fe₂O₃); with TiO₂ being the most commonly used. Chemical absorbers are typically aromatic compounds conjugated with carbonyl groups.

The continuing increase in the incidence of skin cancer since the advent of commercial sunscreens has now drawn the attention of scientists to the photostability of sunscreens. Though much has been said and a lot of literature is available on the photoprotective power of sunscreens against the harmful solar UVR, new evidence is emerging that these products may

not be as protective *per se*.⁷⁴ Sections 1.3.1 and 1.3.2 explain in more detail the photochemistry of the two types of sunscreen agents.

1.3.1 Photochemistry of physical blockers

Physical blockers are also referred to as inorganic oxides or microreflectors. They work by scattering and reflecting harmful solar UVR. As stated earlier, it is now well appreciated that UVA radiation plays an important part in the induction of skin cancer, chronic photoaging, photo-immunosuppression, and wrinkling of the skin. Therefore, modern sunscreens must offer broad-spectrum ultraviolet protection against both the UVB and UVA wavelengths. In order to achieve broad-spectrum protection and boost the SPF value of a formulation,⁷³ cosmetic manufacturers have turned to metal oxides such as *micronized* titanium dioxide (TiO₂), *ultra-fine* zinc oxide (ZnO) and iron oxide (Fe₂O₃). TiO₂ is the most commonly used of these physical blockers. This study will focus more on TiO₂ since it is the only physical blocker declared to be present in the commercial products analysed in this study.

If present in sufficient quantities, inorganic blockers will offer broad protection against both UVB and UVA wavelengths. Due to a limited number of suitable UVA absorbers, these micronized particles are used in conjunction with chemical absorbers in order to achieve high SPF values. Their inertness and broad-spectrum protective ability make them attractive alternatives to chemical absorbers.⁷³

Titanium dioxide is effective in blocking out both the UVA and UVB wavelengths and because of the micron size of TiO₂, it remains invisible on the skin.^{73, 75} Investigations have shown that for submicron TiO₂, UVB attenuation is predominantly due to its absorption while UVA attenuation is largely due to its scattering.⁷⁶ Rayleigh's principle best explains the optical behaviour of ultrafine TiO₂. It states that the intensity of light scattered is inversely proportional to the fourth power of the wavelength. Therefore, TiO₂ particles of size ranging 20 - 50 nm would effectively scatter and absorb UVR in the region, 200 - 400 nm, while wavelengths approaching the visible region are transmitted through the material, making it virtually transparent to the naked eye.⁷⁷ Also, the intensity of light scattered is proportional to the difference in the refractive indices of the pigment and its surrounding vehicle. Hence, ZnO with a refractive index of 1.99 is expected to be more transparent than TiO₂ with a refractive index of

about 2.60.⁷⁸ Figure 1.1 shows the effect of particle size on the UV/VIS absorption properties of TiO₂.

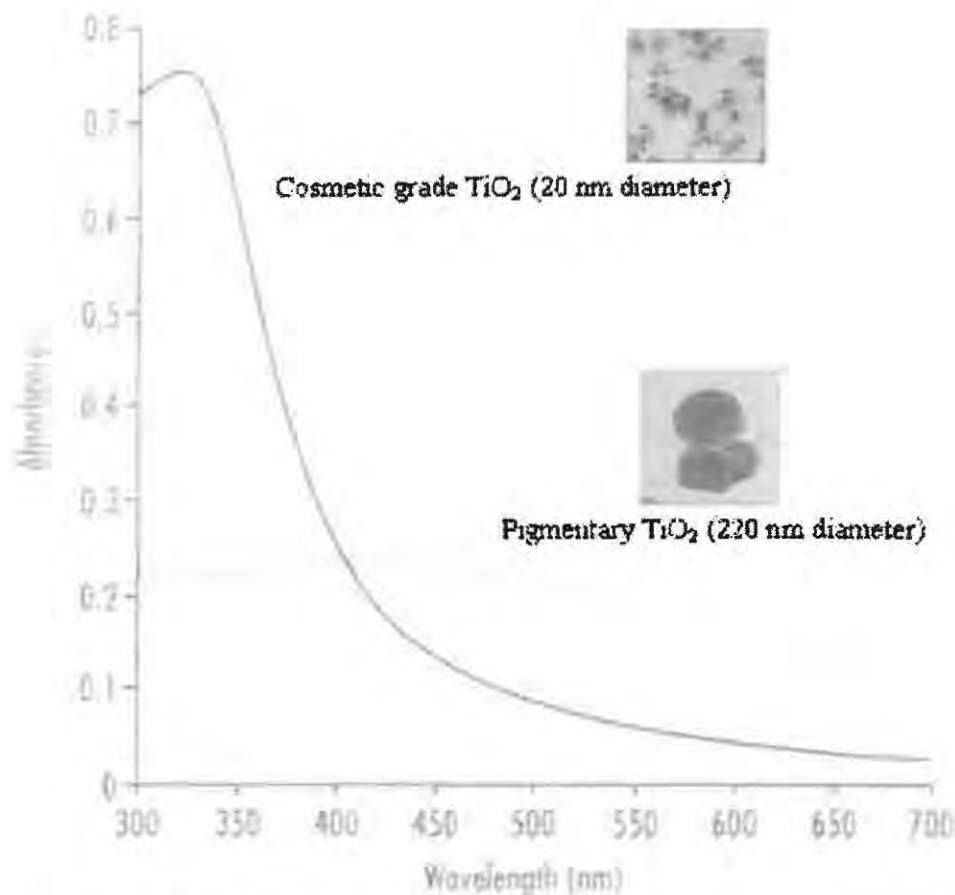
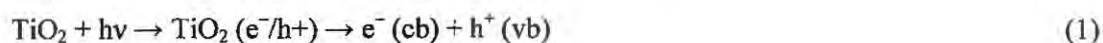
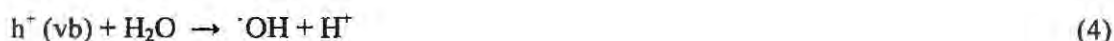


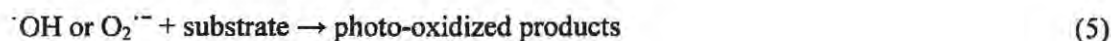
Figure 1.1: The effect of particle size on the UV/VIS absorption properties of TiO₂.⁷⁶

The most common crystalline forms of TiO₂, *anatase* and *rutile*, are both photocatalytic and semiconductors with band gap energies of about 3.23 eV and 3.06 eV respectively, corresponding to radiation of 385 and 400 nm. Radiation at or below these wavelengths can excite electrons from the valence band (vb) to the conduction band (cb) generating single electrons and positively charged spaces called holes (h⁺). After formation, electrons and holes either recombine or migrate rapidly to the particle surface, where they now react with adsorbed species. In an aqueous environment, electrons react with oxygen, and h⁺ with hydroxyl ions or water forming superoxide or hydroxyl radicals according to the reaction scheme shown below:





The superoxide and, in particular, the hydroxyl radicals formed are the active agents for the degradation of organic compounds:



Anatase is more photoactive than rutile.^{76, 79, 80} This has been ascribed to a lower rate of electron-hole recombination and a better efficiency to adsorb oxygen. Therefore rutile should be the preferred form for use in sunscreen products. However, over-the-counter sunscreens were found to contain either anatase or rutile or a mixture of the two,⁸¹ and Ricci *et al.*⁸² state that anatase is the form used in sunscreen and cosmetic products. Brezová *et al.*⁸³ found that nine commercial sunscreen preparations containing TiO₂ did indeed generate reactive radical species, such as superoxide anion radical and hydroxyl radical, when irradiated with wavelengths of light greater than 300 nm.

Since most sunscreen formulations employ a combination of physical and chemical (organic) UV-filters to provide broad-spectrum protection, the possibility exists that TiO₂ can photocatalyse the degradation of the organic filters. Indeed it has been shown that TiO₂ can cause a significant loss of the most commonly used absorbers, namely avobenzene,⁸⁴ octylmethoxycinnamate,⁸² benzophenone-3,^{74, 82} octocrylene,⁸² and octylsalicylate.⁸² Ricci *et al.*⁸² further found that the process occurs more rapidly in the presence of a surfactant which is often present in the formulation as an emulsifying agent. These interactions between the components of the formulation reduce the efficacy of the product and lead to loss of photoprotection.

The ability of photo-excited TiO₂ to generate free-radicals also accounts for its photocytotoxic effects,⁸⁵⁻⁸⁷ and its ability to degrade biomolecules such as amino acids,⁸⁷⁻⁸⁹ nucleic acids^{81, 90, 91} and their bases,⁹⁰ and proteins.⁹² Investigations by Dunford *et al.*⁸¹ have shown that TiO₂ particles isolated from commercial sunscreen products cause damage to DNA. Irradiation of the TiO₂ particles with simulated solar radiation caused single and double strand breaks in DNA plasmids and in human cells.⁸¹ Consequently, the presence of TiO₂ in sunscreen formulations can initiate or lead to photo-oxidative damage of the skin or as mentioned above even the

photodegradation of the organic chemical absorbers used in the formulation. The latter compromises the effectiveness of the preparation and hence, leads to more potential damage to the skin.

Moreover, the small size of these physical blockers makes it easy for them to penetrate the skin⁹³ via intercellular routes, or through hair follicles, pores or sweat glands. A number of studies have been reported on the percutaneous absorption of microfine titanium dioxide^{94, 95} and although they reach different conclusions because of the different protocols used, titanium dioxide has been detected no further than the *stratum granulosum*.⁹⁵ The fact that microfine TiO₂ does not appear to penetrate into viable skin tissue is fortunate since it has been found to be incorporated into cells^{85, 91} and once inside the cells, can trigger a chain of reactions (involving reactive oxygen species such as hydroxyl radical) that can lead to DNA mutations and cell death.⁹⁶ Kubota *et al.*⁸⁵ found TiO₂ particles in the cell membrane and in the cytoplasm, incorporated through the process of phagocytosis. van der Molen *et al.*⁷⁵ showed that some forms of TiO₂ changed the integrity of the intercellular spaces of the stratum corneum. Such a scenario is highly undesirable. It suffices to say that the higher the concentration of TiO₂ in the skin, the greater the amount of damage elicited.

In order to prevent the deleterious effects enumerated above, the surface of the TiO₂ must be deactivated. Consequently, coating of semiconductor TiO₂ is an area of active research.⁹⁵ The coating has the added advantage that it ensures a good dispersability of the very fine TiO₂ particles. However, it has been noted that surface treatment of TiO₂ particles may or may not prevent photo-oxidative reactions, and that some coatings work better than others.⁸² Aluminium hydroxide and stearic acid (ASHA) are the most popular for cosmetic-grade TiO₂. It is generally done in a wet process to give the smallest particle size. Many other organic materials are frequently used for surface treatment, and these include dimethicone, isopropyl titanium triisostearate (ITT), lecithin, etc.⁸⁴ Doping of the crystal lattice with transition metal ions can also alter the photoactivity of TiO₂. However, the choice of dopant is critical as it can either enhance or reduce the photoactivity. Wakefield *et al.*⁹⁷ have shown that doping micronised TiO₂ with 1% manganese has a number of beneficial effects including enhanced UVA absorption, less degradation of other organic constituents of the formulation and a reduction in free radical generation. Shen *et al.*¹³ have also shown that zeolite encapsulation of TiO₂ reduces the generation of reactive oxygen species in cultured human fibroblasts.

Since the coating or doping of TiO₂ nanoparticles cannot guarantee that they become photoinactive and hence ensure their safety, it is imperative that the levels of physical blockers incorporated in sunscreen formulations be closely monitored. In view of this, this study sought to quantify the levels of TiO₂ in commercial sunscreens available on the South African market. The quantitation of TiO₂ is reported in Section 2.4 and the results obtained are discussed in Section 3.2.

Section 1.3.2 details the photochemistry, as well as the different classes of chemical absorbers commonly used in commercial sunscreens.

1.3.2 Photochemistry of chemical absorbers

The majority of sunscreen absorbers are aromatic compounds conjugated with a carbonyl group with an electron-releasing amine or methoxy group substituted in the *ortho*- or *para*-position of the aromatic ring. Chemical absorbers are classified into either UVA or UVB filters depending upon the type of radiation they protect against. Organic sunscreen agents essentially work by absorbing UVR, which excites them to a higher energy state. The molecule may dissipate this energy as long wave (>380 nm) radiation and return to its original ground state or photoisomerisation can occur or the material may fragment into non-absorbing photoproducts. The excited molecule can also photo-react with neighbouring molecules.

Section 1.3.2.1 describes the possible photophysical and photochemical processes that take place upon exposure of chemical absorbers to UV radiation.

1.3.2.1 Photochemistry of organic sunscreens

In order to appreciate how sunscreens work, one must understand how organic molecules interact with light energy. Absorption of light by a molecule is associated with the part of its structure called a chromophore which may or may not encompass the whole molecule. Sunscreens, as typical conjugated aromatic compounds, contain delocalized π -electrons. Of interest to the sunscreen field are transitions involving the promotion of an electron from a non-bonding molecular orbital n to an anti-bonding π^* orbital ($n \rightarrow \pi^*$), and from a bonding π to an anti-bonding π^* orbital ($\pi \rightarrow \pi^*$). The spectral bands for such transitions fall within the 200 - 400 nm wavelength region.

Absorption of a photon of light by such a molecule sees an electron being excited from the highest occupied molecular orbital (HOMO) to a higher energy level (the lowest unoccupied molecular orbital, LUMO). The molecule is now in an excited state. The most common excited state for organic molecules is the first singlet excited state (S_1), in which the promoted electron is still spin-paired with the one left in the lower energy state (ground state).⁹⁸

Now, what happens to the excited molecule?

Since the lifetime of the excited state is short, the molecule must lose the excess energy and return to the ground state. Ideal sunscreen molecules quickly dissipate the excess energy as harmless long wave radiation (fluorescence) or as heat to the surrounding via vibrational relaxation, and return to the ground state. The molecule is now available to absorb more UVR in the next cycle, thus protecting the skin.

It must be realised that sunscreen molecules, being conjugated, are rather reactive: the π -electrons are very polarisable (being far from the carbon nuclei), and therefore readily engage in new chemical bonds. The situation is even worse when the molecule is excited, because then the electronic cloud has been given extra energy, which can be used to cross photochemical barriers, or gives access to more new states for the excited electron. The well-known Jablonski diagram (Figure 1.2) schematically shows the possible pathways accessible to an excited molecule.

As shown in Figure 1.2, there are several pathways available through which the excited molecule can lose the excess energy and return to the ground state. Important to note is that, the first step is radiationless transition (vibrational relaxation) from a higher excited state to the first singlet excited state, S_1 . The excited molecule is subjected to collisions with the surrounding molecules and as it gives up energy non-radiatively, it steps down the ladder of vibrational levels, S_1^v , to the lowest vibrational level of the electronically excited state.⁹⁹ The molecule quickly (within 10 picoseconds) loses heat energy to the surrounding medium and returns to ambient temperature.

From the first singlet excited state, S_1 , the molecule can proceed in one of many ways: it may undergo a chemical reaction, transfer charge, pass energy to other molecules through collisions, change spin multiplicity, or lose energy by emitting a photon.¹⁰⁰

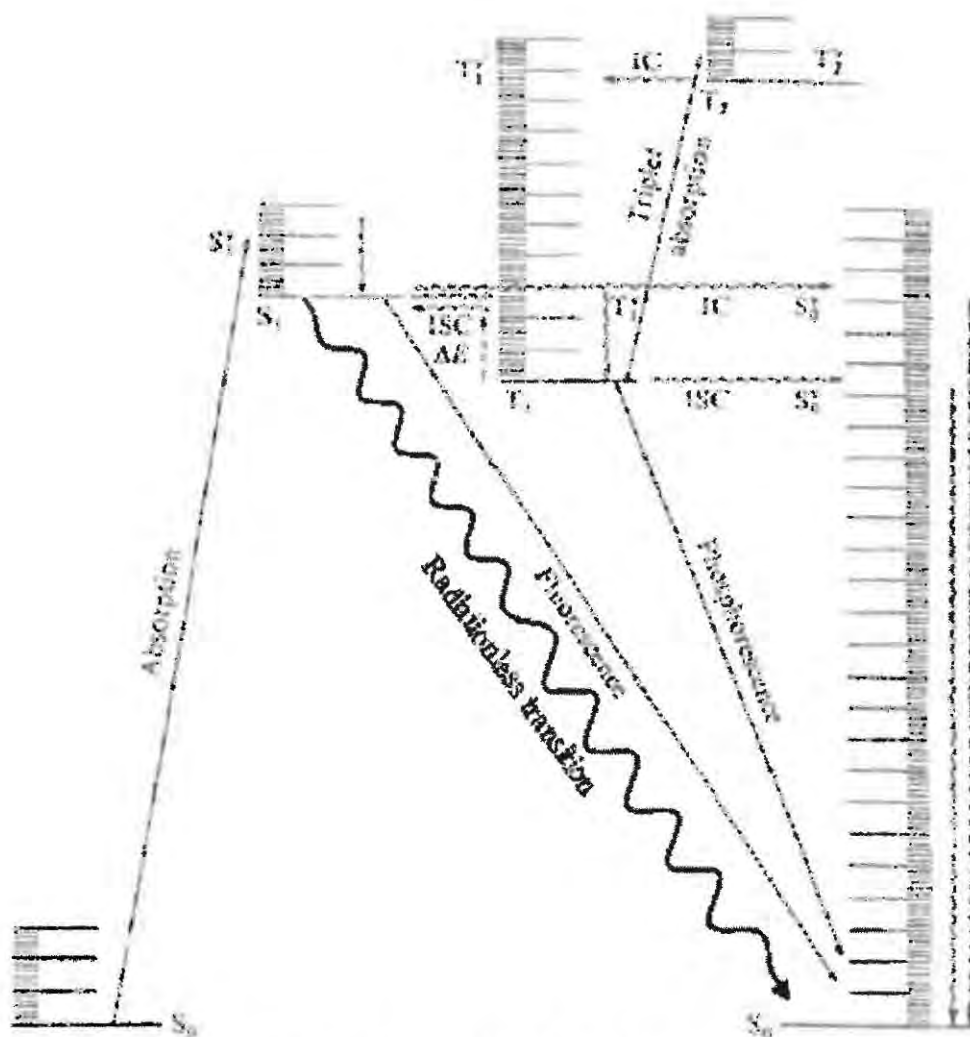


Figure 1.2: A Jablonski diagram showing the fate of an excited molecule.¹⁰¹

a) Radiationless transition to the ground state

This process is synonymous with vibrational relaxation from higher excited states to the first singlet excited state described above. The only difference is that the electron now moves from the lowest unoccupied molecular orbital (LUMO) of the first excited electronic state (S_1) to the ground state, S_0 . There are no photons emitted in this process and the excess energy is converted to heat, which is quickly released to the surrounding medium. The process occurs on a nanosecond timescale, substantially longer than radiationless transitions from higher excited states.

b) Fluorescence

After being subjected to collisions with the surrounding molecules and losing energy non-radiatively, the surrounding medium might now be unable to accept the large energy difference needed to lower the molecule to the ground electronic state. It might therefore survive long enough to undergo spontaneous emission. The molecule begins in a first excited state with no net spin (since all the electron spins cancel one another). Within nanoseconds, a photon is emitted and the molecule returns to the ground state; the net spin remains zero. The downward electronic transition is vertical (in accord with the Frank-Condon principle) and the fluorescence spectrum has a vibrational structure characteristic of the ground state.¹⁰²

c) Internal conversion (IC)

This is a radiationless decay process where the excited molecule moves to another state of the same multiplicity, e.g. the excited triplet states, T_2 to T_1 . The process occurs most readily at the point of intersection of the two molecular potential energy curves. This is because the nuclear geometries of the two states are the same at this point.

d) Intersystem crossing (ISC)

The transitions between singlet and triplet electronic states are called intersystem crossing, ISC. In ISC the molecule starts from an excited state with a net spin of 0 (S_1) and ends in a lower excited state with a net spin of 1 (T_1), or from the T_1 (spin 1) to S_0 (spin 0) state. Quantum mechanically, ISC is spin forbidden, and therefore is caused only by weak interactions such as spin orbit coupling. The triplet, T, and singlet states share a common geometry at the point where their potential energy curves intersect. Hence, if there is a way of unpairing the two spins, transition to the triplet state occurs. Triplets have long lifetimes, ranging from a fraction of a millisecond to several seconds. They last until the electrons encounter a strong electric field disturbance or another high spin molecule. For example, a triplet state organic molecule readily reacts with a triplet state oxygen molecule (normal state of molecular oxygen, 3O_2), deactivating both to the singlet state:



Singlet oxygen ($^1O_2^*$) is a very reactive free radical. In people suffering from porphyria, sunlight activates most of the metal-free haems near the surface of the skin to the triplet state. When they react with molecular oxygen, 3O_2 , in the skin, singlet oxygen is formed which reacts

to inflame nearby tissue. Patients often experience extreme photosensitivity and must avoid sunlight. A former sunscreen agent, *para*-aminobenzoic acid (PABA), is known to photosensitise the formation of singlet oxygen causing photoallergic reactions upon irradiation.¹⁰³⁻¹⁰⁷ Schimdt *et al.*⁶ have also shown that the current widely used sunscreen active agents like 3-(4-methylbenzylidene camphor) in combination with octylmethoxycinnamate cause photoallergic contact dermatitis.

e) Phosphorescence

The presence of a triplet-excited state plays a decisive role here. The process occurs from the triplet-excited state, T_1 , to return the molecule to its ground state, S_0 . This transition from the triplet state to the ground state violates spin angular momentum. In phosphorescence, quantum processes cause the excited state to become slightly "impure", entering a metastable triplet state.¹⁰² When this occurs, the molecule can then emit a photon and return to the ground state. Because triplet states are so long-lived, the process can last from seconds to minutes. The competing processes here are: vibrational relaxation to the ground state and charge transfer.

f) Excitation transfer (energy transfer)

Here, an excited molecule passes its energy to a nearby molecule in its ground state. No real photons are emitted or exchanged during this process; the electron movement from the excited molecule is sensed and its energy picked up by the ground state molecule. The extent and duration of this process is largely dependent on the distance between the two molecules. Such energy transfer processes can excite surrounding photosensitive molecules, making them photoactive, resulting in phototoxic reactions. If the energy transfer process occurs from a sunscreen molecule to a benign molecule or a less reactive molecule, it affords photoprotection. It has been shown that in addition to photosensitising the formation of singlet oxygen, PABA can penetrate the cell¹⁰⁸ and photosensitise the dimerisation of thymine bases (which are building blocks of DNA) via energy transfer.^{109, 110} Such structural changes in DNA are highly mutagenic and can result in the development of skin cancer.¹¹¹

g) Charge transfer

Instead of energy exchange between the excited molecule and ground state molecule, the excited electron is exchanged. In an aqueous environment, such transfer reactions lead to the formation of hydroxyl and superoxide radicals. The generation of superoxide and hydroxyl radicals will trigger a chain of reactions resulting in photoproducts which may be potentially

photocarcinogenic. Such photochemical reactions can occur from the singlet-excited state (S_1) but especially from the long-lived excited triplet state, T_1 .

h) Photofragmentation (Dissociation)

Another fate of an excited molecule is dissociation. When absorption occurs to unbound states of the upper electronic states, the molecule dissociates and the absorption is a continuum. The vibrational structure of a band terminates at a certain energy. Absorption occurs in a continuous band above this dissociation limit because the final state is an unquantised translational motion of the fragments. Below the dissociation limit, the electronic spectrum shows a normal vibrational structure. This is the phenomenon displayed in the chemical actinometer, valerophenone. The commonly used sunscreen agent, avobenzone, has been shown to photofragment upon exposure to UVR.^{112, 113}

i) Photochemical reactions

Besides the pathways discussed above, an excited molecule (in the S_1 or T_1 state) can also undergo rearrangement resulting in photoaddition, substitution and dimerisation. Photodimerisation has been reported in OMC through 4-6-cycloaddition and this results in loss of protective capacity in the photoadduct.^{114, 115} Some UV filters in a formulation can destabilize co-ingredients. This has been reported in the AVO/OMC combination, with avobenzone reportedly photosensitising the photolysis of OMC, thus destabilizing the cinnamate molecule.^{116, 117} The excited sunscreen molecule can also undergo photoisomerisation as reported with OMC and 3-(4-methylbenzylidene camphor).¹¹⁸ AVO is known to undergo keto-enol tautomerisation following exposure to UVR.¹¹³

A number of reports have appeared in literature citing photoallergic and photocontact dermatitis reactions that are induced by some sunscreen active ingredients. Octyldimethyl PABA (Padimate-O) has been shown to induce more single strand breaks in DNA when exposed to UVR than when compared to UV irradiation alone.¹¹⁹ The substance is also known to penetrate the skin.¹²⁰ A survey by Allen *et al.*¹⁰⁷ showed that the most important photosensitisers of singlet oxygen are PABA, padimate-O, OMC and octocrylene. Benzophenones are known to also cause photoallergic contact urticaria in addition to causing delayed contact and photocontact dermatitis.¹²¹ The negative reactions highlighted here are essentially a result of the photosensitising effects of the sunscreen molecules after formation of a stable triplet state. The triplet-excited state molecule is then able to transfer some of its energy to molecular oxygen to generate singlet oxygen as depicted in Equation 6 above. It is known that singlet oxygen is

highly reactive and quickly attacks macromolecules. If generated inside the cell, singlet oxygen can attack DNA causing single strand breaks.¹²²

As such, it is necessary to ensure that the concentration levels are within the internationally set permissible levels. In order to determine if levels of active ingredients in commercial sunscreen products available on the South African market are within the internationally stipulated levels, a high performance liquid chromatography (HPLC) method was employed.

Sections 1.3.2.2 and 1.3.2.3 give an overview of the different classes of chemical absorbers and their representative molecules. The weaknesses and strengths of each class in as far as UV absorption properties and photostability will be highlighted.

1.3.2.2 UVB absorbers

Para-aminobenzoic acid (PABA with a maximum absorption wavelength, λ_{\max} , of 283 nm) was one of the first widely available organic sunscreen agents. PABA is water soluble and is a very effective UVB filter.¹²³ It was discontinued due to its photosensitisation,^{108, 124} staining of clothes and photoallergic reactions,¹²⁵ apart from its poor photostability.¹²⁶ It was also found to be a potent carcinogen *in vitro*.^{124, 127} Shaw *et al.*¹²⁸ and Aliwell¹²⁹ have demonstrated *in vitro* that PABA can react with DNA bases like thymine to form pyrimidine dimers and non-dimer photoproducts of thymine such as 5,6-dihydrothymine and 5-hydroxymethyluracil.¹⁰⁹ As mentioned above, Sutherland *et al.*¹⁰⁸ have reported that PABA can sensitise pyrimidine dimer formation in the DNA of human fibroblasts. Derivatives of PABA were then developed in order to moderate such negative effects. The widely used PABA derivative today is Padimate-O (λ_{\max} = 311 nm), but it is less effective in photoprotection than PABA and has been found to be mutagenic.¹³⁰

Cinnamate derivatives largely absorb in the UVB region (290 - 320 nm). Octyl methoxycinnamate (OMC) is the most common UVB filter from this class and is usually used in combination with other UVB filters in order to achieve high SPF values in the final product. OMC has been reported to be photounstable, it photoisomerises¹³¹ to the *cis*-form which has a low molar absorptivity,^{115, 132} thus leading to decreased photoprotection.⁷⁴ It has also been reported to form photodimers through [2+2] cycloaddition reactions with itself.^{114, 115} Kowlaser¹¹⁵ reported that OMC can also form DNA photoadducts when irradiated with mixtures

of thymine-5'-monophosphate and 2'-deoxyguanosine-5'-monophosphate. Any such sunscreen-DNA photoadduct could be potentially mutagenic. Reports also exist in the literature that OMC has an estrogenic and antiosteoporotic effect.¹³³ There are many reports on attempts to photostabilise OMC.¹³⁴ Perugini *et al.*¹³⁵ investigated the photostabilisation of OMC by nanoparticle encapsulation in cyclodextrins.

Salicylate derivatives are weaker UVB absorbers so they must be used in relatively high concentrations. They are used to augment the efficacy of other UVB absorbers. Octylsalicylate and homomenthyl salicylate are commonly used to minimise the photodegradation of other sunscreen ingredients including 4-*t*-butyl-4'-methoxydibenzoyl methane (avobenzone).⁷³

Phenylbenzimidazole sulfonic acid (PBSA) is a water-soluble UVB filter. It is an aesthetically pleasing agent that is used to enhance the SPF of the final product in combination with other organic and inorganic UV absorbers. However, work by Sewlall¹²² showed that PBSA causes DNA cleavage, and studies by Bolton *et al.*¹³⁶ showed that PBSA photosensitises thymine dimer formation when irradiated with UV radiation at wavelengths greater than 300 nm.

Camphor derivatives (e.g. methylbenzylidene camphor) are moderately effective UVB filters. A notable exception is terephylidene dicamphor which is a broad UVA filter. This class of UV filters is approved for use in the European Union but not in the 1999 US FDA monograph.⁴⁵ Methylbenzylidene camphor is reported to have an estrogenic activity,¹³⁷ besides its photoinstability.¹¹⁸

1.3.2.3 UVA absorbers

Benzophenone derivatives are all UVA absorbers and the most commonly used is benzophenone-3. It absorbs most efficiently in the UVB region and the UVA2 (320 - 340 nm) range with two absorption peaks at 290 and 325 nm. It has for a long time been reported to be photostable. However, emerging evidence indicates that the sunscreen agent is easily photo-oxidized, leading to the inactivation of antioxidant systems.¹³⁸ Investigations by Sewlall¹²² showed that benzophenone-1 and benzophenone-9 cause DNA strand breaks. Bolton¹³⁹ showed that benzophenone-9 photosensitises thymine dimer formation. Other benzophenone derivatives commonly used in commercial sun care products include, benzophenone-4 and benzophenone-8.

Dibenzoyl methane derivatives are essentially all UVA absorbers. 4-*t*-butyl-4'-methoxydibenzoyl methane (avobenzone or Parsol 1789) is the most commonly used from this class, and has strong absorption in almost all the UVA region. Its wavelength of maximum absorption (λ_{max}) is 358 nm in methanol. Unfortunately, it has been shown that its photoprotective power decreases by more than 50% in 1 hour of exposure to solar radiation.^{113, 140, 141} The photostability of avobenzone is reported to be largely influenced by solvent effects, being more photostable in protic and less stable in aprotic organic solvents.^{112, 113} Roscher *et al.*¹⁴² showed that the irradiation of avobenzone in cyclohexane yielded *tert*-butylbenzene, *p*-*tert*-butylbenzoic acid and *p*-methoxybenzoic acid as the major photodegradation products. Moreover, investigations have implicated avobenzone in enhancing the photodegradation of OMC in a formulation where the two are in combination.^{116, 117, 143} The other derivative used in sunscreens, 4-isopropylidibenzoyl methane, has been reported to be photolabile again. Avobenzone is normally used in combination with octocrylene to improve its stability.¹⁴⁴

Anthranilate derivatives absorb in the UVA region and the most common are menthyl anthranilate and homomenthyl-*N*-acetyl anthranilate. Menthyl anthranilate has a weak molar absorptivity with a λ_{max} around 340 nm and has been shown to photosensitise the formation of singlet oxygen in a range of solvent systems.¹⁴⁵

Tinosorb S is an oil soluble UV filter recently developed in Europe (by Ciba Specialty Chemicals, Basel, Switzerland). The active ingredient offers broad-spectrum protection against both the UVA and UVB ranges. Apart from being photostable in the UVB and UVA regions, the active agent also can photostabilise both avobenzone and OMC.¹³⁴ Another agent, from Ciba Chemicals, is *Tinosorb M* which shares more or less the same attributes with *Tinosorb S*. *Tinosorb M* is dispersible in water and is insoluble in cosmetic oils. It has been reported that none of these *tinosorbs* possess intrinsic estrogenic/antiestrogenic or androgenic/antiandrogenic activity *in vitro*.⁷²

Section 1.3.3 details the structures of the different sunscreen active ingredients contained in the suncare products studied in this study.

1.3.3 Chemical absorbers investigated in this study

A total of nine different sunscreen agents were analysed in this study. All the active ingredients were declared on the bottles, which occurred in various combinations. The nine active agents have been classified according to the UV radiation they protect against, and the molecular structures are shown Figures 1.3 and 1.4. The chemical name, molecular formula and mass, and the wavelength of maximum absorption, λ_{\max} , of each ingredient are also given.

Figure 1.3 shows the chemical structures of the UVA absorbers investigated in this study.

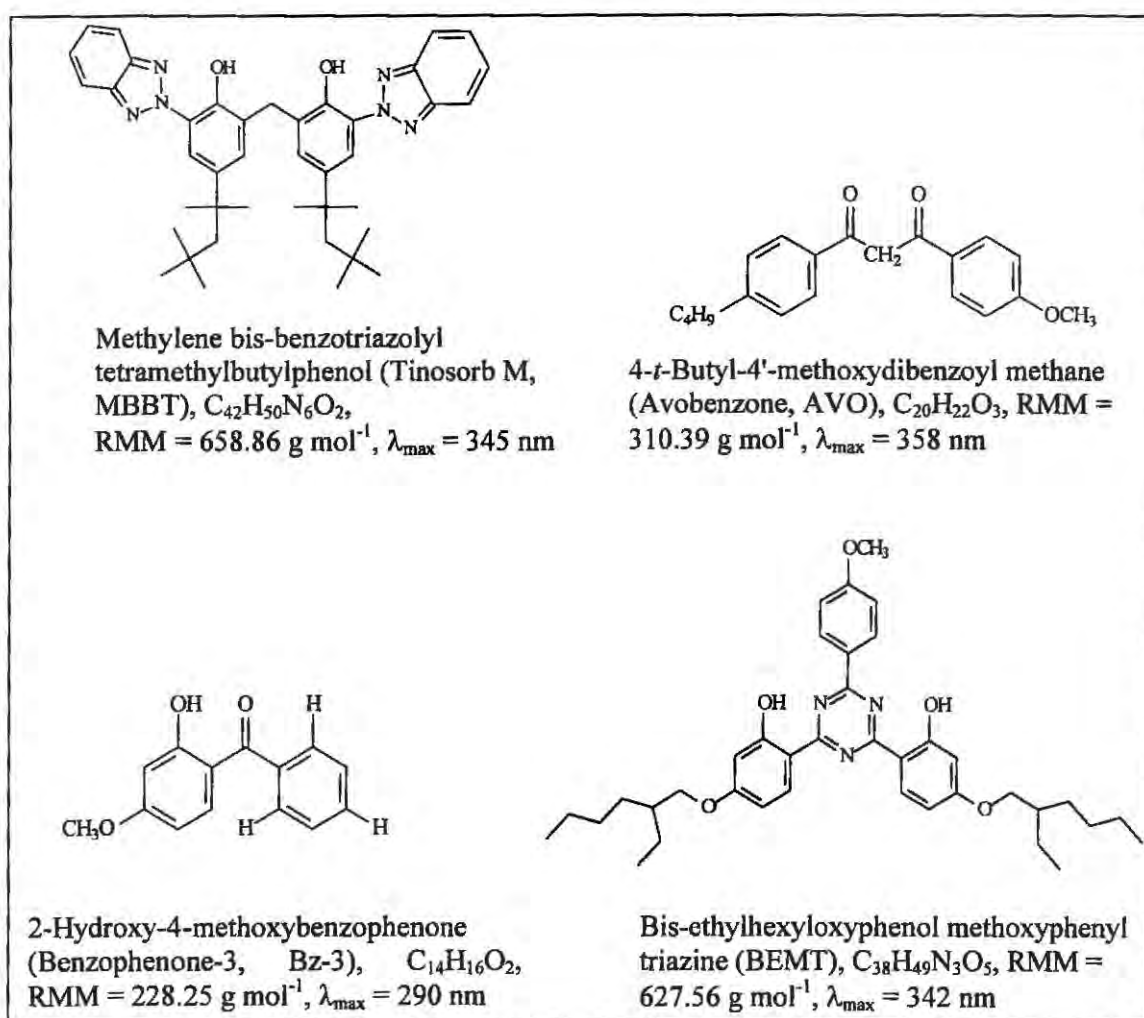


Figure 1.3: Structures of UVA absorbers investigated in this study.

Figure 1.4 presents the chemical structures of the UVB absorbers analysed in this study.

The high conjugation in chemical sunscreen molecules makes them particularly sensitive to photochemistry as explained in Section 1.3.2.1. Any photochemical change of a sunscreen molecule not only reduces the photoprotective capacity of a formulation, but the resulting photoproducts may be potentially photocarcinogenic. Ideal sunscreens would have the following attributes: well tolerated, cosmetically pleasant, non-toxic, water resistant, offer broad-spectrum ultraviolet protection and they should be photostable upon exposure to solar UVR.

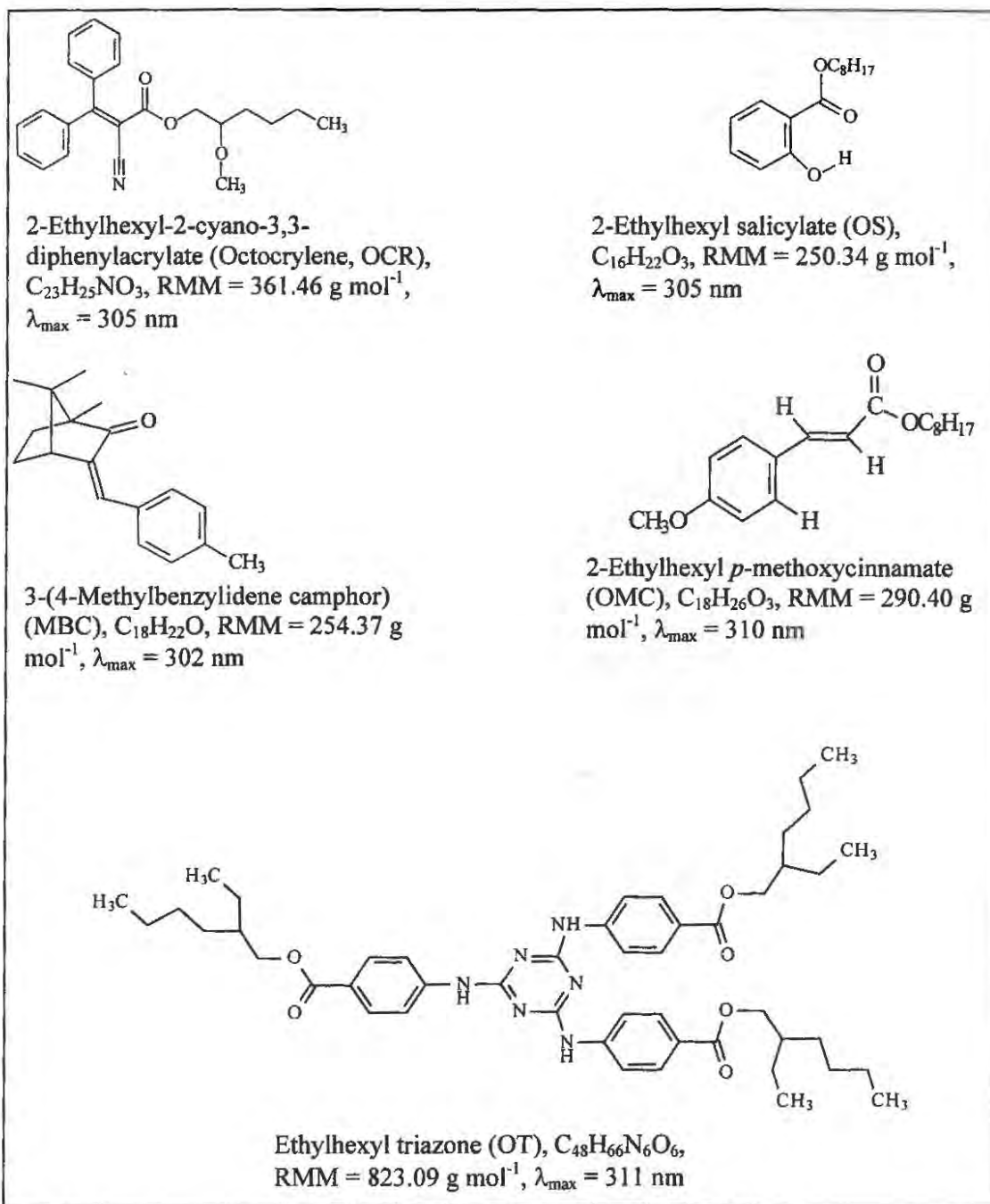


Figure 1.4: Structures of UVB absorbers investigated in this study.

The photostability of commercial sunscreen products has come under much scrutiny as there is an alarming worldwide increase in skin cancer. It should be noted that there is no legal requirement for cosmetic manufacturers to test the photostability of their products. As such, there is also no accepted protocol for the photostability assessment of sunscreen formulations.

Section 1.4 describes the different methods that have been previously employed in the assessment of the photostability behaviour of sunscreens.

1.4 Photostability of sunscreens

There are two main concerns responsible for limiting sunscreen chemicals for topical application: their potential for causing irritation and allergy, and the possibility of photochemical instability. Indeed, a number of investigations have shown that consumer sun care products lose their photoprotection upon exposure to solar UVR. Maier *et al.*¹⁴⁶ found that commercial sunscreens were photolabile following solar-simulated irradiation. An investigation by Sayre *et al.*¹¹⁶ showed that sun care products containing avobenzone lost their photoprotective capacity after exposure to solar-simulated radiation. Another study by Maier *et al.*¹⁴⁷ where the vehicle or emulsion effect was removed (since the products analysed were all photoprotective lipsticks in a waxy matrix) showed that commercial photoprotective lipsticks lost photoprotection especially in the UVA region, while the products displayed high photostability in the UVB region.

It is therefore, increasingly becoming necessary to routinely test the photostability behaviour of sunscreens before they are marketed in order to ensure that the public is fully protected from harmful solar UVR. This also keeps to a minimum, the potential risk of phototoxicity from photoproducts formed after degradation of photounstable sunscreen molecules.

Consequently, it is necessary to develop *in vitro* methods for the routine determination of the effectiveness of commercial sun care products.¹⁴⁸ The SPF value of a sunscreen formulation is determined *in vivo* on human subjects, using an erythema end-point.¹⁴⁹ However, the *in vivo* tests are costly and time-consuming, making them impractical for routine product evaluation. There are also still questions about the scientific accuracy and reproducibility of *in vivo* measurements, besides the potential hazards to subjects.¹⁵⁰ As such, *in vitro* methods are increasingly attracting the interest of scientists.

If *in vitro* methods are to be reliable in the prediction of *in vivo* results, especially in the determination of the SPF, broad-spectrum protection and photostability assessment, sample preparation is very crucial. There are two objectives in a sample preparation method. The first is to simulate the application conditions used for *in vivo* testing, both the applied quantity and substrate interaction. This would allow positive prediction of the result from a subsequent *in vivo* test. The second objective is for the method to be consistent enough to generate reproducible results, sample to sample for the same sunscreen formulation.

A number of methods have been proposed for the assessment of sunscreen photostability and photochemical behaviour. Rosenstein *et al.*¹⁵¹ in their study to determine theoretical sun protection factors, dissolved sunscreen products in a solvent mixture of 12.5:37.5:50% (v/v) dichloromethane-cyclohexane-isopropanol according to the protocol outlined in the Australian/New Zealand UV Transmittance Standard. The solutions were prepared in a way so as to mimic the recommended amount of 2 mg cm⁻² on the skin. The solutions were placed in a 1-cm pathlength quartz cell and then measurement (either transmission or absorption) was done in the UV region (290 - 400 nm), where the quartz cell is transparent.

Some have proposed using a thin film method.¹⁵² In this method, the authors applied sunscreen product onto a stratum corneum sheet, the sheet was sandwiched between two quartz plates and compressed into a thin capillary film. The sandwiched sample was irradiated with solar simulated radiation.

However, besides the inaccessibility of the stratum corneum, this method excludes oxygen from the system. It is a fact that sunscreens are used under aerobic conditions. Therefore, use of such films in photostability studies might give misleading results since it is well known that UVR photosensitises the formation of singlet oxygen^{45, 107, 122, 139, 153} which may attack co-ingredients in a formulation.

The use of synthetic skin to model the photophysical and photochemical processes occurring in sunscreens under application conditions has also been proposed.¹⁵⁰ It is recommended to use one of the three commercially available substrates of which several published studies are available: Transpore Tape[®],^{74, 154} Vitro Skin[™] or poly(vinyl chloride).¹⁵⁰ These synthetic substrates possess the porosity and texture close to that of human skin. Marginean *et al.*¹⁵⁵ measured the photoprotective efficacy of topical sunscreens smeared on human epidermis

supported on quartz plate by diffuse transmittance. It is needless to say that the human epidermis they proposed is not easily accessible. Springsteen *et al.*¹⁵⁰ have reviewed the different sample preparation methods for each of the synthetic skin substrates. Though ideal for mimicking human skin, most of the substrates are not readily available.

Maier *et al.*^{146, 147} assessed the photostability of sun protective lipsticks and sunscreens by smearing 1 mg cm⁻¹ of product directly onto quartz plates and then irradiated with increasing doses of solar-simulated radiation. Unlike Kammeyer *et al.*,¹⁵² they did not sandwich the sunscreen film. In their investigation to assess the photoisomerisation of benzylidene derivatives, Deflandre *et al.*¹⁴⁰ used roughened quartz plates to simulate the texture of human skin. They however, sandwiched the sunscreen film between two quartz plates, thus again excluding oxygen. The sandwiched samples were irradiated using solar simulated radiation. The authors ran an independent parallel high performance liquid chromatography method to confirm the validity of their method.

As noted above, since UVA radiation is known to play an important role in the induction of skin cancer,⁴² modern sunscreens are expected to offer broad-spectrum protection. However, there is no uniformly accepted standard method for the assessment of the protective capacity of a sunscreen formulation against UVA radiation. The commonly used *in vivo* methods are the immediate pigment darkening (IPD), persistent pigment darkening (PPD) and protection factor in UVA (PFA) with PPD being the most commonly used.⁴⁵ Diffey *et al.*¹⁵⁶ have proposed the *in vitro* critical wavelength method (which is evaluated by using ultraviolet/visible spectrophotometry) as a measure of the broad-spectrum UV protection of sunscreens. The *in vitro* critical wavelength method has been employed in this study in evaluating the broad-spectrum protection, and its applicability in assessing the photostability of commercial sunscreens.

Almost all the *in vitro* methods (quoted in the foregoing) used for the assessment of sunscreens require the use of an integrating sphere to allow for accurate capturing of light transmitted from a sunscreen, since the sunscreen film may scatter both the incident and transmitted radiation. The collected light is channeled to the detector. However, in this study no integrating sphere was available. Besides the use of an integrating sphere in most investigations reported, it should be noted that most investigations have used solar-simulated radiation instead of the terrestrial solar radiation to which people are exposed, and under which the sunscreen products are expected to perform. The dispersion of sunscreens in solution is the most widely used system in

the photostability assessment of UV filters.^{74, 107, 114, 157, 158} Although crucial for understanding the photochemical behaviour of UV filters, the methods are not relevant to practical conditions. Besides, the photochemistry of sunscreen absorbers is altered in different solvents.^{112, 113, 117}

A simple *in vitro* method for the assessment of the photostability of finished suncare products is proposed in this study. The beauty of the proposed method is that it provides a reliable, inexpensive way of measuring photostability and ultraviolet broad-spectrum protection of different sunscreen formulations. There is no need for an integrating sphere and expensive, sometimes inaccessible synthetic skin substrates. It eliminates the need of human subjects who are exposed to acute, high and non-terrestrial UVR, the human health risks which are still poorly understood.

1.5 Aims and outline of this study

In view of the potential photoinstability of topical sunscreens highlighted in Section 1.3, the main aim of this work was to assess the photostability behaviour of commercial sunscreens available on the South African market. It is important that in carrying out such photostability studies, they must be carried out under conditions that as close as possible mirror the application ones. In order to simulate application conditions, the sunscreen products were analysed as thin films smeared on quartz plates.¹⁴⁷ After a diligent search of literature, an appropriate application density was chosen based on what previous researchers^{146, 159, 160} determined as the amount normally applied by the public. A number of photostability^{142, 160, 161} and *in vitro* SPF determination¹⁵¹ studies have also been carried out in solution. This study also sought to compare the photostabilities of commercial sunscreens dispersed in solution and those smeared on quartz plates. The irradiation of the sunscreens was carried out in terrestrial solar radiation to which the public is exposed. The photostability analysis was carried out by UV/VIS transmission spectrophotometry and HPLC. It was desirable to quantify the actinic flux incident on the samples and to try and relate this to the photostability behaviour of sunscreens. Chemical actinometry was employed (with the valerophenone actinometer) for the quantitation of the amount of radiation received by the samples.

The need to produce high potency sunscreens (with high SPF) has seen manufacturers often using complex combinations of UV filters. One tempting option is to increase the concentration of the individual active agents in a formulation in order to achieve high potency suncare

products. Since it has been shown that some sunscreen active ingredients cause a number of negative effects after topical application, it is important to monitor the levels of these active ingredients in suncare products. Sunscreen active agents have been reported to cause irritation,^{103, 104} contact urticaria,¹²¹ photocontact dermatitis,^{6, 121} photosensitization reactions,¹³⁴ photocarcinogenesis induction,¹¹⁹ phototoxicity^{85, 86, 91} and estrogenic activity.^{133, 162} Therefore, the second aim was to determine the levels of active ingredients (both physical blockers and chemical absorbers) in commercial sunscreens. A high performance liquid chromatography method was developed for the quantitation of organic UV filters in commercial sunscreens. Titanium dioxide is the most employed physical blocker and the commercial sunscreens analysed in this study only contained titanium dioxide as the physical blocker. For the determination of titanium dioxide, inductively coupled plasma – optical emission spectroscopy was employed.

The details of all the experimental work performed in this study are reported in Chapter 2, and the results obtained from the different experiments are reported and discussed in Chapter 3.

Chapter 2

EXPERIMENTAL

This chapter details the experimental work carried out to investigate the photostability of commercially available sun care products, both on quartz plates and in solution. This required the use of chromatographic and spectroscopic techniques to quantify the active ingredients and assess the photostability of the commercial products. The valerophenone chemical actinometer was used to measure the photon flux incident on the sunscreen samples.

2.1 Materials

Commercial sun care products were purchased from retail outlets in Durban, South Africa in February 2005. Twenty-two (22) sun care products were purchased; the selection contained almost all brands that are available on the South African market. The samples were kept in the dark at room temperature and were taken out only on the day of analysis. Sun care products were labelled SA1-22. Table 2.1 lists the information regarding the brand name, the SPF, the declared active ingredients and the protection claimed on the label of each product.

The chemicals used in this study and their respective grades and suppliers are listed in Appendix A.

2.2 Equipment

The equipment used for ultraviolet/visible (UV/VIS) transmission spectrophotometry, actinometry and quantitative analysis is listed in Appendix B.

Table 2.1: Details of the commercial sunscreen products investigated in this study.

Sample Label	Brand Name	SPF No.	Active Ingredients	Antioxidants	Protection claim	
					UVA	UVB
SA1	EverySun Aquasport	5	OMC, Bz-3	-	✓	✓
SA2	EverySun Aquasport	10	OMC, Bz-3	-	✓	✓
SA3	EverySun Sensitive	30	OMC, Bz-3, OS, MBC	-	✓	✓
SA4	EverySun Aquasport	40	OMC, Bz-3, OS, TiO ₂	-	✓	✓
SA5	EverySun Kids	40	OMC, Bz-3, OS, TiO ₂ , AVO	-	✓	✓
SA6	Johnson's Suncare	8	OMC, MBC, AVO, TiO ₂	Vitamin E, ProVitB5	*** (3/4)	✓
SA7	Johnson's Suncare	15	OMC, MBC, AVO, TiO ₂	Vitamin E, ProVitB5	**** (4/4)	✓
SA8	Johnson's Suncare	30	OMC, MBC, AVO, TiO ₂	Vitamin E, ProVitB5	**** (4/4)	✓
SA9	Johnson's Suncare Baby	40	OMC, MBC, TiO ₂ , BEMT, MBBT	Vitamin E, ProVitB5	*** (3/4)	✓
SA10	Tropitone	15	OMC, Bz-3, TiO ₂ , OS	-	✓	✓
SA11	Tropitone	30	OMC, Bz-3, TiO ₂ , OS, MBC	-	✓	✓
SA12	Nivea Sun	5	OMC, AVO	Vitamin E	*** (3/4)	✓
SA13	Nivea Sun	15	OMC, TiO ₂ , OCR, BEMT	Vitamin E	*** (3/4)	✓
SA14	Nivea Sun	30	OMC, TiO ₂ , AVO, DOBT, OT, BEMT	Vitamin E	*** (3/4)	✓
SA15	Piz Buin	4	OMC, AVO, TiO ₂	Vitamin E	*** (3/4)	✓
SA16	Piz Buin	30	OMC, MBC, BEMT, MBBT	Vitamin E	*** (3/4)	✓
SA17	Labello	-	--	Vitamin A, B, E & B5	-	-
SA18	Labello MED	6	OMC	-	-	-
SA19	Labello Sun	25	AVO, TiO ₂ , OT, DOBT	Vitamin E	✓	-
SA20	Lip Balm	30	OMC, AVO	-	-	-
SA21	Lip-Ice Sunblock	40+	OMC, MBC, AVO, TiO ₂	Vitamin E	-	-
SA22	Aloe ferox	36	TiO ₂ , Parsol family	Vitamin E	-	-

Key to abbreviations: MBBT -- methylene bis-benzotriazolyl tetramethyl butylphenol, BEMT -- bis-ethylhexyloxyphenol methoxyphenyl triazine, OT -- octyl triazone, DOBT -- dioctyl butamido triazone, OS -- octyl salicylate, AVO -- avobenzone, MBC -- 3-(4-methylbenzylidene camphor), OMC -- octylmethoxycinnamate, Bz-3 -- benzophenone-3, TiO₂ -- titanium dioxide

* - UVA protection rating

2.3 Determination of UV filters by high performance liquid chromatography

It was desirable to first quantify the active ingredients in the sun care products and to qualitatively determine whether the active ingredient information supplied by the manufacturers agreed with experimental findings.

Rapid and reliable methods for the determination of UV-filters in commercial sun care products are required to check whether products conform to the existing legislation, and also for quality control purposes. A number of techniques have been reported including UV/VIS spectrophotometry, gas chromatography (GC) and high performance liquid chromatography (HPLC). Chisvert *et al.*¹⁶³ successfully determined the amount of Bz-3 in the presence of OMC by flow injection-isodifferential derivative UV/VIS spectroscopy. Azevedo *et al.*¹⁶⁴ also quantified a mixture of 2-hydroxy-4-methoxybenzophenone-5-sulfonic acid and 2-phenylbenzimidazole-5-sulfonic acid by second derivative UV/VIS spectrophotometry. Felix *et al.*¹⁶⁵ determined Bz-3 and its metabolites in water and human urine samples by solid-phase microextraction and quadrupole ion-trap gas chromatography with mass spectrometry.

In UV/VIS derivative spectroscopy, second derivative spectra are predominantly used for quantitative analysis. This is mainly because of the enhanced resolution of overlapping peaks especially for the separation of superimposed spectra in multicomponent analysis. However, the resolution becomes poor with an increase in the number of analytes in a mixture due to a strong overlap of peaks. In the sunscreen field, the technique has been successfully applied to mixtures of up to two active ingredients which was reported by Azevedo *et al.*¹⁶⁴

An attempt was made to apply the second derivative UV/VIS spectroscopy method in the quantitative analysis of some sun care products prior to the analysis of the commercial sunscreens reported in this study. The method was successfully applied for the quantitative analysis of two component mixtures such as OMC and AVO or OMC and Bz-3 (results not reported). However, it was difficult to resolve the second derivative spectra of a simple three-component mixture of Bz-3, MBC and OMC because of too much overlap between the derivative spectra. As a result, the quantitation work with the second derivative UV/VIS spectrophotometry method was dropped. In view of the complex combinations of sunscreen active ingredients in the products listed in Table 2.1, this method becomes virtually inapplicable.

Salvador *et al.*¹⁶⁶ published a comprehensive review on the different analytical methods used in the determination of UV-filters in cosmetic products and other samples for the period 1976-2004. Chromatographic techniques have been the most commonly employed methods for both qualitative and quantitative analysis of sunscreen active agents.

Chromatography is the physico-chemical process by which the components of a mixture are separated. The principle is based on the concentration equilibrium of the components in a mixture between two phases; one of which is called stationary because it is immobilized in a column, the other is called mobile because it is the transport mechanism through the system. The differential migration of compounds through the column leads to their separation.

Because of its versatility, HPLC has been the method of choice for the simultaneous determination of several UV filters in suncare products. This analytical technique evolved from preparative chromatography and its performance (resolution and efficiency) has been greatly enhanced by the use of elaborate stationary phases composed of spherical particles with diameters of between 2 and 5 μm . However, because the particles are small, the head pressure needed to force the mobile phase through the column packing must be greatly increased compared to that used in preparative chromatography. The high pressures needed are achieved by use of pumps which can be alternating or single pumps.¹⁶⁷

Several reports have been published on the determination of multi-component mixtures of sunscreens by HPLC. However, the resolution of a mixture containing a combination of OS, OMC and AVO usually presents difficulties for proper quantitation. Most studies have been carried out exclusively on C_8 or C_{18} reversed¹⁶⁸⁻¹⁷¹ or normal stationary phases. Sarveiya *et al.*¹⁷² developed a reversed phase HPLC method (with a C_{18} column) for the determination of common sunscreens in a number of biological matrices including bovine serum albumin, human urine, plasma and human epidermis where they showed that Bz-3 is systematically absorbed by the body. Salvador *et al.*¹⁷³ attempted to develop a HPLC method for the determination of eighteen sunscreens active agents in both model formulations and commercial sunscreens. Though it is desirable, especially in an industrial set-up, to develop a HPLC method for the quantitative determination of many active ingredients in one step, the widely different solubilities of sunscreen agents in a given solvent makes it difficult to develop such an all encompassing method. Simeoni *et al.*¹⁷⁴ used normal phase HPLC (with a cyanopropyl-bonded silica column) for the simultaneous determination of eight sunscreen active ingredients in

suncare products. Smyrniotakis *et al.*¹⁷⁵ simultaneously quantified MBBT along with OCR, OMC and OS in suncare products by reversed phase HPLC (C₁₈ column) using a non-aqueous mobile phase. Chisvert *et al.*¹⁷⁶ used a reversed phase HPLC (C₁₈ column) method with an isocratic mobile phase system modified with cyclodextrins to separate seven UV filters in commercial sunscreens. Cyclodextrins were employed to increase the aqueous solubility of some of the active ingredients.

The field of application of HPLC overlaps that of gas chromatography (see Section 2.7.2) to a great extent. In addition, HPLC allows the analysis of analytes that are thermolabile, very polar or of high molecular mass. One important attribute of HPLC is that resolution can be increased simply by modifying the composition of the mobile phase. It is thus possible to modify interactions that occur between analyte and mobile phase, analyte and stationary phase, and mobile phase and stationary phase.

Single pumps are sufficient if the mobile phase composition is expected to remain constant (isocratic elution). The other type of elution in HPLC systems is called gradient elution where the composition of the mobile phase is preprogrammed so that it changes as the separation continues. Gradient elution is employed when trying to resolve components which do not separate and elute under isocratic conditions. This mode of elution is synonymous with temperature programming in gas chromatography. Section 2.3.1 describes the major components of a HPLC system and the principle of separation in more detail.

2.3.1 Instrumentation

A schematic diagram showing the major components of a HPLC system is shown in Figure 2.1.

The mixture of interest is injected into the system through the injector (with an injection syringe) as shown in Figure 2.1. The sample mixture is carried by the mobile phase to the column where separation takes place through the differential partitioning of the components between the mobile and stationary phases. From the column, the mixture is fed to the detector which is connected to a microprocessor or computer for identification. A more comprehensive description of this technique can be found elsewhere.^{177, 178}

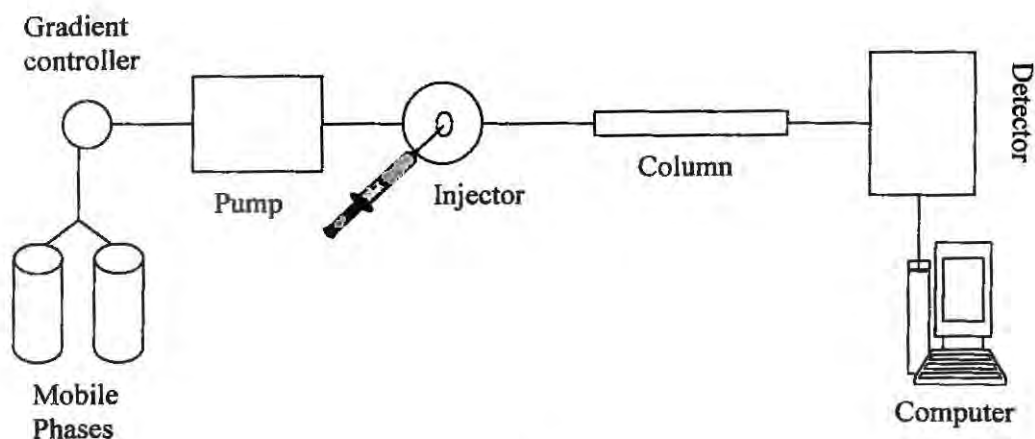


Figure 2.1: Schematic representation of a HPLC system.

A number of detectors are available for use in HPLC systems. The detector, irrespective of its nature, is required to have a number of fundamental properties. It should give a response that is proportional to the instantaneous mass flow, be sensitive, have a small inertia, be stable with time and yield very low background noise. Common detectors for HPLC are based on the optical properties of the analytes: absorption, fluorescence and refractive index. A detailed description of the different detectors is given elsewhere.¹⁶⁷

The HPLC system used in this study has photodiode array detection (PDA) which is based on the absorption properties of the analytes. PDA detectors are robust and can be used over a wide dynamic range. They are especially useful for recording the full UV/VIS absorption spectrum of each component as it rapidly passes through the sample flow cell. The following sections give a description of the procedures followed in the quantitative analysis of the active ingredients contained in the commercial sunscreens investigated in this study.

2.3.2 HPLC equipment and operation

For the separation and quantitative analysis of sunscreens and potential photoproducts, a Waters 600 HPLC multisolvent delivery system with 225 μL pumpheads and a Waters 996 photodiode array (PDA) detector was used. The PDA detector allows for variable wavelength scanning. Sample injection was achieved by using a Perkin Elmer Series 200 autosampler. Data acquisition and processing was accomplished by using a De'Mark Pentium II computer with Waters Millennium³² software.

The Waters 600 HPLC multisolvent delivery system has programmable features to facilitate the use of gradient and isocratic elution modes. Each day of use, the autosampler was first flushed with 100% methanol (MeOH) to remove any dirt that may have accumulated overnight. If the autosampler was not used for 24 hours, the autosampler was first flushed with isopropanol to kill all microbes that may have grown in the injection needle as well as the flush syringe. This was then followed by a double flushing with MeOH. The detector was only used after a warm-up period of 1 hour to allow the PDA lamp to stabilize. The flow rate of the system was increased in steps of 0.2 mL min^{-1} in order to protect the pump-heads and prolong the duration of the pumps, which easily wear away as a result of drastic changes in flow rates.

Initially, a Nucleosil 100 C_{18} column was tried for the quantitation of sunscreen active ingredients in the different suncare products. However, a number of problems were encountered with this column. A good resolution of peaks could not be achieved despite several modifications of the mobile phase composition, flow rate, as well as the injection volume. The peaks of some of the active ingredients appeared split at the apex. Some of the active ingredients like MBBT, OT, AVO and BEMT failed to elute completely.

After failing to get good separation with the Nucleosil 100 C_{18} column, a Phenomenex Ultracarb 5 ODS 20 semi-preparative column was tried. Again the resolution of active ingredients (Bz-3, OS, MBC, AVO and OMC) was poor yet these were the most common combinations in the suncare products analysed. MBBT and BEMT would not elute if any water was present in the mobile phase. All work with the two columns was then abandoned. Optimum separation was eventually achieved on a Phenomenex Synergi Max-RP- C_{12} 80 Å column.

Separation of the active ingredients was achieved on a reversed phase Phenomenex Synergi Max-RP- C_{12} 80 Å column with $4 \mu\text{m}$ particles, a length of 150 mm and an internal diameter of 4.6 mm. The separation and quantitation of the active ingredients was carried out under isocratic elution. Since the column had not been used for a long time, it was first conditioned by making use of the solvents listed in Table 2.2 and the respective volumes at a flow rate of 1 mL min^{-1} . Gradient elution was employed here to pass the different solvents through the column. The conditioning solvents were passed through the column in the order given in Table 2.2 as per the instructions detailed in the manufacturer's manual.¹⁷⁹

Table 2.2: Solvents and their respective volumes used for conditioning the Phenomenex Synergi Max-RP-C₁₂ 80 Å column.

Solvent	Volume used/mL
Millipore Water (55°C)	50 (with 4 x 100 µL injections of DMSO)
MeOH	50
Chloroform	50
MeOH	50
84:16% (v/v) MeOH-H ₂ O (mobile phase)	50

After the conditioning process, the column was allowed to equilibrate by allowing five column volumes of the mobile phase to pass through the column. Once the column had equilibrated, priming of the pump was carried out in order to remove any air bubbles from the system. The analysis of the standard solutions was then carried out. All the sunscreen standard solutions were passed through a syringe filter before injection.

The mobile phase (84:16% (v/v) MeOH-H₂O) was prepared by using ultra-pure water from a Millipore Milli-Q⁵⁰ water-purifying unit. The preparation of the solvent was carried out by separately measuring the MeOH and purified water in a measuring cylinder prior to mixing. This was done to avoid inconsistencies in mobile phase compositions that result from the contraction of solvents (MeOH-H₂O). The mobile phase was filtered through a Millipore 0.45-µm filter and allowed to stand for two minutes before being fed into the mobile phase reservoir.

The mobile phase was sparged with ultra-pure helium gas at a rate of 100 mL min⁻¹ at the beginning, which was then reduced to 30 mL min⁻¹ after 10 minutes. The flow rate of the mobile phase was 1 mL min⁻¹. An injection volume of 20 µL was used for all injections. Quantitative analysis was carried out under ambient temperature. The total elution time for both standards and samples was not more than 17 minutes.

2.3.3 Preparation of standard solutions

All the standard solutions of each sunscreen active ingredient were prepared in HPLC-grade MeOH. Standard stock solutions were prepared as detailed in Table 2.3. Table 2.3 gives details of the masses used to prepare a particular concentration of each active ingredient and the resulting concentrations of the solution.

One active ingredient, dioctyl butamido triazone (DOBT), could not be quantified because of the lack of a pure sample. An authentic sample could not be purchased commercially and all attempts to obtain it from the manufacturer failed. This substance was present in two sunscreen products (SA14 and SA19) as shown in Table 2.1.

MBBT (Tinosorb M) and BEMT (Tinosorb S) were especially difficult to dissolve in MeOH. Different solvent mixtures were initially tried but all failed to dissolve these two active ingredients. These include: 80:20% (v/v) tetrahydrofuran-acetonitrile,¹⁷⁵ ethanol and isopropanol. Subsequently, the two active agents were first dissolved in 25 mL of dimethylformamide (DMF) and then diluted with MeOH to achieve the final concentration as shown in Table 2.3.

Table 2.3: Details of the preparation of the standard stock solutions of sunscreen active agents dissolved in MeOH and diluted to 100 mL.

Sunscreen ingredient	Mass weighed/g	Concentration/M
Bz-3	0.0228	1.00×10^{-3}
OMC	0.0290	1.00×10^{-3}
OS	0.0234	1.00×10^{-3}
MBC	0.0254	1.00×10^{-3}
AVO	0.0310	1.00×10^{-3}
MBBT*	0.0324	2.46×10^{-4}
BEMT*	0.0053	8.44×10^{-5}
OT	0.0411	5.00×10^{-4}
OCR	0.0362	1.00×10^{-3}

* The active ingredients with an asterisk were first dissolved in DMF.

2.3.4 UV/VIS absorption spectra of sunscreen active ingredients

The UV/VIS absorption spectra of the pure sunscreen active ingredients were recorded on a Perkin Elmer Lambda 35 UV/VIS spectrophotometer. The spectra were used for qualitative analysis of the peaks from HPLC analysis. The associated UV/VIS absorption spectra in the HPLC chromatograms were compared to those in Figures 2.2a-c, thus positively identifying the peaks of the active ingredients. The absorption spectra of the active ingredients were also used to discuss the transmission spectra of the different sunscreen products analysed and presented in Section 3.3.2.

The sunscreen standard solutions were diluted in MeOH and the absorption spectrum of each active ingredient was recorded. The absorption spectra were recorded in a 1-cm pathlength quartz cuvette with MeOH in the reference beam. The spectra are shown in Figures 2.2a-c with the respective concentrations of each active ingredient used.

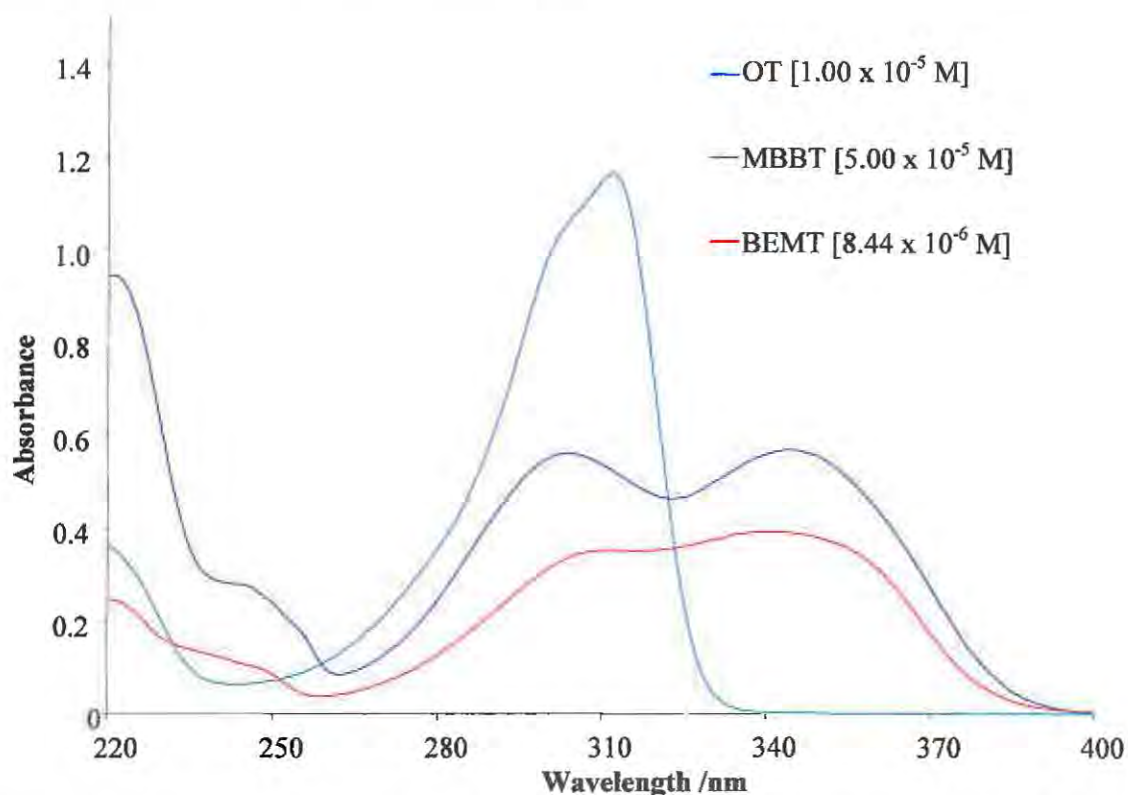


Figure 2.2a: Absorption spectra of the pure sunscreen active ingredients (dissolved in MeOH) contained in the sunscreen products investigated in this study. Absorption spectra were recorded in a 1-cm pathlength quartz cuvette against MeOH in the reference beam.

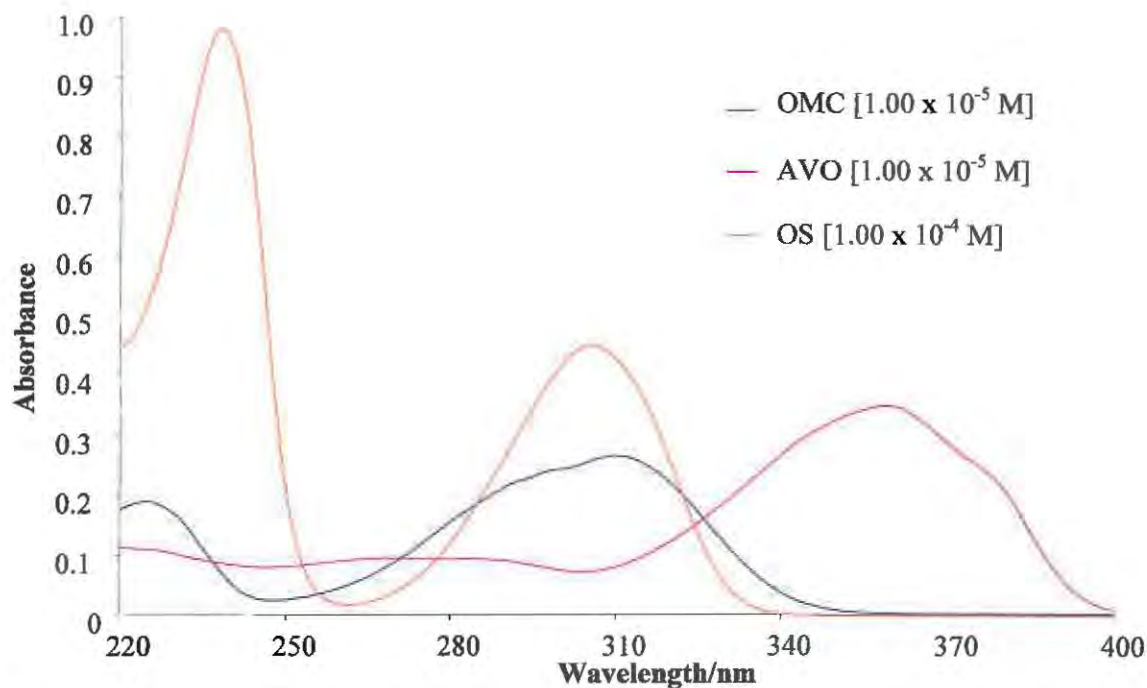


Figure 2.2b: Absorption spectra of the pure sunscreen active ingredients (dissolved in MeOH) contained in the suncare products investigated in this study. Absorption spectra were recorded in a 1-cm pathlength quartz cuvette against MeOH in the reference beam.

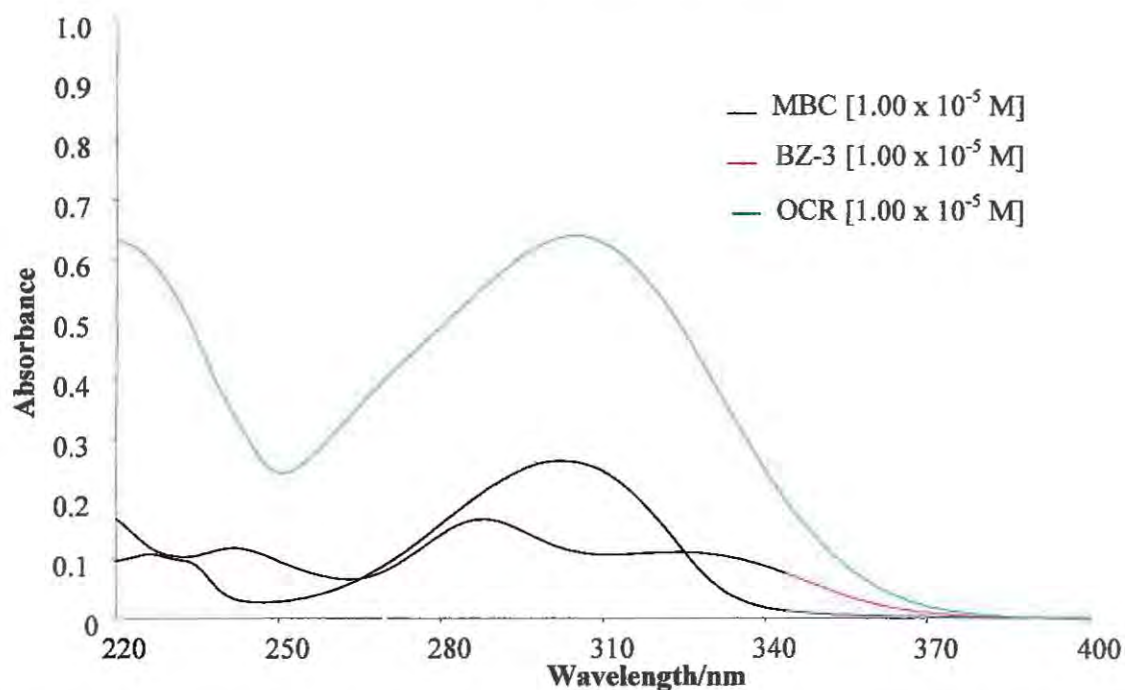


Figure 2.2c: Absorption spectra of the pure sunscreen active ingredients (dissolved in MeOH) contained in the suncare products investigated in this study. Absorption spectra were recorded in a 1-cm pathlength quartz cuvette against MeOH in the reference beam.

2.3.5 Determination of optimum separation conditions

The commercial sunscreen products were divided into two groups. The first one comprised those products without *tinosorbs* in their formulations. The second group constituted all the products with *tinosorbs* (BMMT, BEMT) and OT. Different solvent mixtures were tried in order to determine the optimum conditions for the separation of the active ingredients in the different commercial sunscreens. Mixtures of standard solutions of the active ingredients were used in the determination of the optimum separation conditions. For the non-*tinosorb* set, a mobile phase composition of 90:10% (v/v) MeOH-H₂O was tried at first. Poor separation of OCR, AVO, OMC and OS was observed and therefore, the solvent mixture was modified by increasing the polarity. This was achieved by increasing the content of water and reducing the amount of MeOH. Optimum separation was finally achieved at a mobile phase composition of 84:16% (v/v) MeOH-H₂O. Figure 2.3 shows a typical chromatogram and the optimum chromatographic conditions used for the separation of Bz-3, MBC, OCR, AVO, OMC and OS.

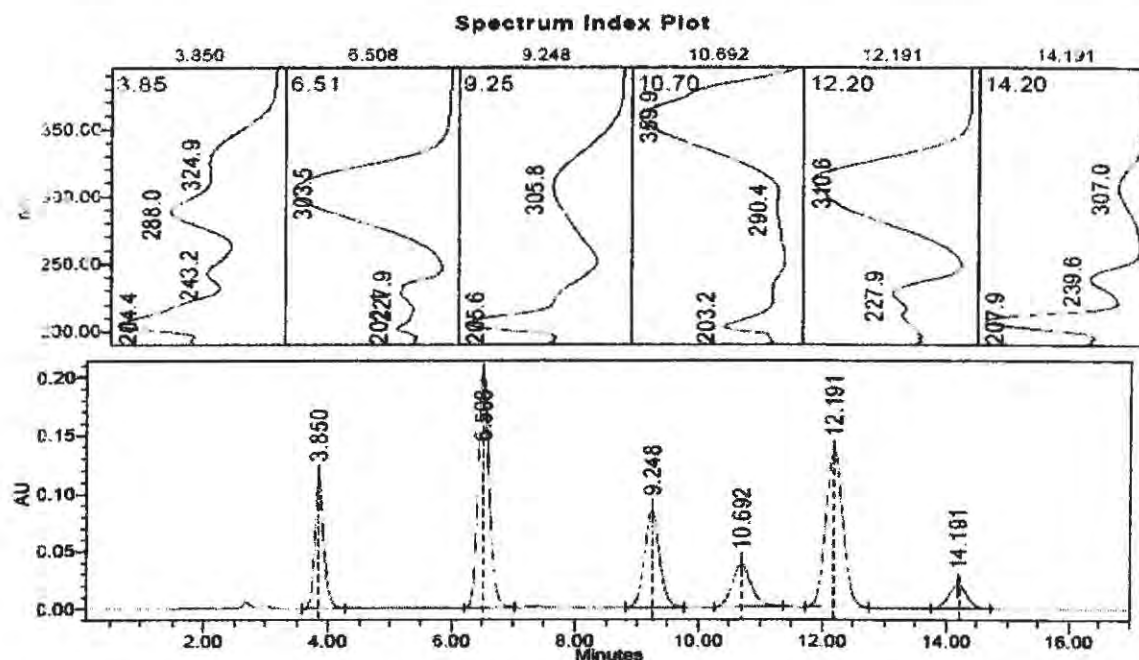


Figure 2.3: Typical chromatogram of a standard mixture of sunscreen agents for the non-*tinosorb* set. The chromatographic conditions used were: Phenomenex Synergi Max-RP-C₁₂ 80Å column, mobile phase MeOH-H₂O 84:16% (v/v), injection volume – 20 µL, flow rate - 1 mL min⁻¹, and detection wavelength – 310 nm. The order of elution is **Bz3**, **MBC**, **OCR**, **AVO**, **OMC** and **OS**.

As observed by Smyrniotakis *et al.*,¹⁷⁵ MBBT, and BEMT fail to elute when water is present in the mobile phase. A different mobile phase composition was therefore developed. A good resolution of the OT, MBBT and BEMT peaks was achieved by using 90:10% (v/v) MeOH-acetonitrile (ACN) as used by Smyrniotakis *et al.*,¹⁷⁵ and a typical chromatogram is shown in Figure 2.4.

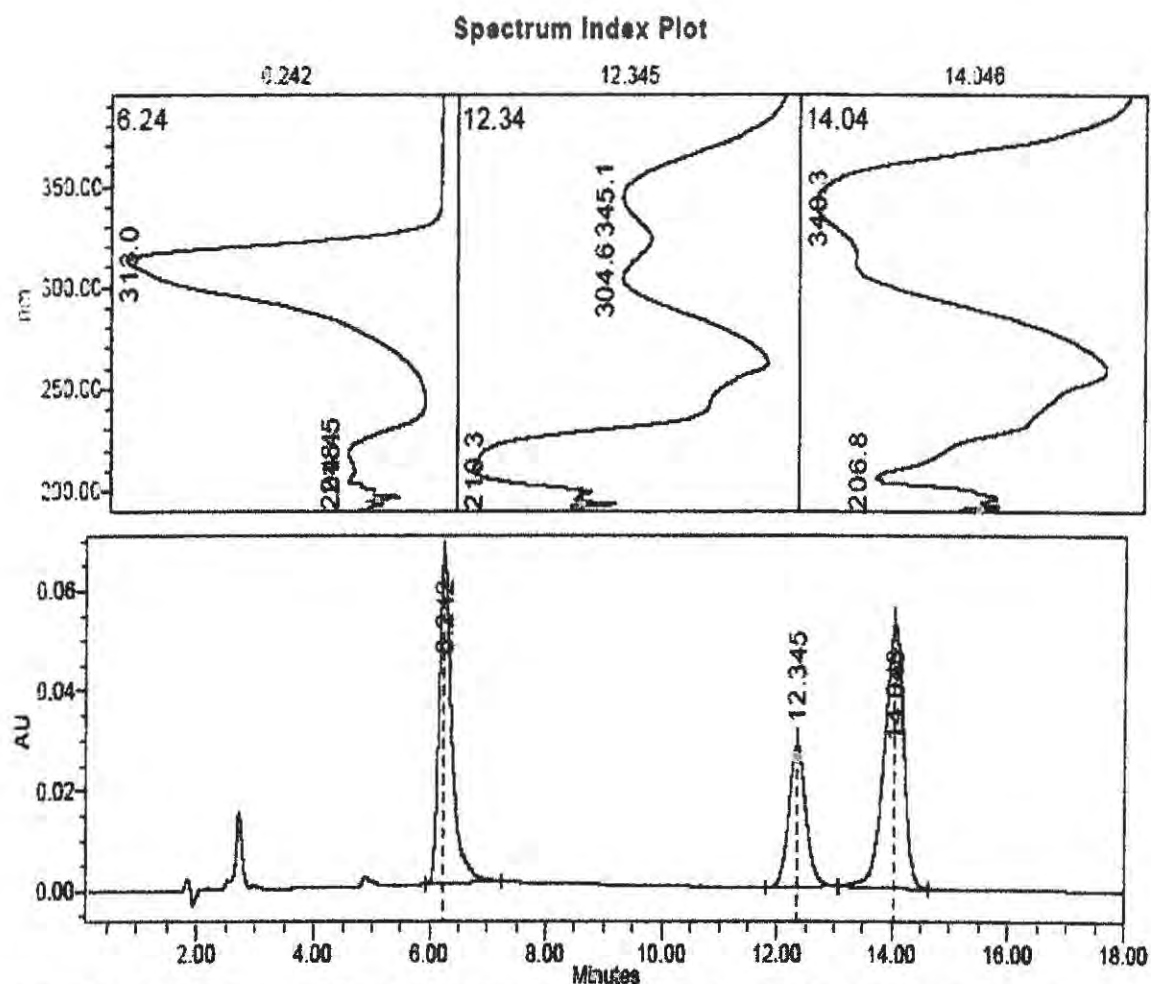


Figure 2.4: Chromatogram for a standard mixture of sunscreen active ingredients in the *tinisorb* set. The chromatographic conditions used were: Phenomenex Synergi Max-RP-C₁₂ 80 Å column, mobile phase MeOH-ACN 90:10% (v/v), injection volume – 20 µL, flow rate - 1 mL min⁻¹, and detection wavelength - 311 nm. The order of elution is OT, MBBT and BEMT.

It was difficult to separate MBC and OMC in the presence of MBBT and BEMT. Several parameters were changed including modifying the mobile phase composition, reducing the injection volume, reducing the flow rate as well as applying gradient elution. All these were explored in an effort to achieve good resolution but to no avail. Consequently, the analysis of the four products with the *tinisorbs* in combination with OMC and/or MBC was carried out

under two sets of chromatographic conditions. Quantitation of OT, MBBT and BEMT in sunscreen samples was carried out under the same chromatographic conditions as given in Figure 2.4, with the two active ingredients, OMC and MBC eluting early in the chromatogram as shown in Figures F13a and F17a of Appendix F. The determination of OMC and MBC was carried out as in Figure 2.3, and the column was flushed between injections with MeOH in order to elute OT, MBBT and BEMT.

2.3.6 Analysis of standard solutions

Once the optimum conditions for the separation of the active ingredients had been determined, a multi-component working standard stock solution was prepared for the two sets of active agents. From the working standard stock solution, auto-serial dilution was carried out with the aid of an autosampler in order to generate calibration curves. A total of seven standard solutions (with different concentrations) were made and these were subjected to HPLC analysis. The calibration ranges were: $1.0 \times 10^{-5} - 7.0 \times 10^{-5}$ M for Bz-3, MBC, AVO, OCR, OMC, MBBT and OS, $1.0 \times 10^{-6} - 7.0 \times 10^{-6}$ M for OT, and $4.0 \times 10^{-6} - 2.8 \times 10^{-5}$ M for BEMT.

The autosampler was programmed so as to perform five injections per sample, and solution injections were interspaced by blank injections to clear the column of any carry-over from previous injections. The detector was programmed to monitor the sunscreen ingredients at four wavelengths (290, 305, 310 and 358 nm) for the first set: Bz-3, MBC, OCR, AVO, OMC and OS. During the analysis of OT, MBBT and BEMT, the detector was programmed to monitor the separation of the sunscreen active agents at two wavelengths (311 and 342 nm). Nevertheless, the processing of the data used for calibration curves was carried out at the wavelength of maximum absorption of the particular UV filter as indicated in the captions of the calibration curves (Figures D1 to D18 of Appendix D).

The calibration curves given in Figures D1 to D18 were used for the quantitation of active agents in suncare products. The chromatographic conditions used for the separation of active agents are indicated in the individual calibration curves. The data used to construct these calibration curves are given in Tables C1 to C9 of Appendix C.

2.3.7 Preparation of sunscreen samples and analysis

There are several aspects to sample preparation. The most important one is to adapt the state of the sample to that accepted by the applied analytical technique. It is necessary to match the standard solution matrix to that of the sample as close as possible if the results are to be useful.

For HPLC analysis of sunscreens, the active ingredients are usually extracted into a suitable organic solvent prior to analysis. The commonly used solvents are ethanol and MeOH. Chisvert *et al.*¹⁶⁹ dissolved the commercial sunscreens in ethanol by ultrasonication. They eluted the sunscreens using a mobile phase of water-acetic acid-ethanol 29.5:0.5:70% (v/v). All their standard solutions were prepared in ethanol. Simeoni *et al.*¹⁷⁴ dispersed the sun-care products in MeOH, or 20% (v/v) acetonitrile in tetrahydrofuran for products containing MBBT, by ultrasonication. The samples were then filtered through 0.45- μm syringe filters and subjected to HPLC analysis. Dutra *et al.*¹⁶⁸ dissolved the sunscreen products in MeOH by ultrasonication for 5 minutes followed by filtration through Millipore 0.45- μm syringe filters. Elution was achieved using MeOH-H₂O 85:15% (v/v) as the mobile phase. A similar sample preparation method as described by Dutra *et al.*¹⁶⁸ was employed in this study.

For the samples not containing *tinosorbs* or OT, a mass of 0.150 g of the sunscreen product was accurately weighed into a 25 mL volumetric flask. The product was dissolved in 15 mL of MeOH under ultrasonication for one hour. The samples were then diluted to the mark with MeOH. However, those sunscreen products containing *tinosorbs* (SA9, 13, 14 and 16) were first dissolved in 10 mL of DMF by ultrasonication for 1 hour and then diluted to 25 mL with MeOH according to the method described by Smyriotakis *et al.*¹⁷⁵ All the sunscreen solutions were filtered through a Millipore 0.45- μm syringe filter to remove all particulate matter that would clog or block the column. Further dilution of the samples was carried out by using the autosampler so that the final concentration of product was 0.10 mg mL⁻¹, and this final solution was subjected to HPLC analysis. Three replicate samples of each product were prepared and the autosampler was programmed so that it performed three injections per sample. On each day of analysis of samples, standard solutions were also run in between sample injections to check if there was a shift in the calibration curve. Sample injections were interspaced with blank injections as was done for the injections of standard solutions.

The results of the quantitation analysis of the twenty-two commercial sunscreen samples are presented in Section 3.1.

2.3.8 Validation of the HPLC quantitation method

There is no requirement in South Africa for sunscreen manufacturers to declare the amounts of the sunscreen active ingredients used in their formulations. Therefore, to check the validity of the HPLC method employed in the quantitation of sunscreen active ingredients in the different suncare products analysed, a recovery analysis was carried out.

A known amount of the pure active ingredient was spiked into one of the commercial sunscreen products (SA2). The spiked samples were prepared in replicates of three. One set of samples was spiked with Bz-3, MBC, OCR, AVO, OMC and OS, and the second set with OT, MBBT and BEMT. The samples were mixed manually using a glass rod. A sample mass of 0.150 g of the mixture was weighed into a 25-mL volumetric flask and dissolved in MeOH (under ultrasonication for 1 hour) for the non-*tinorsorb* set. For the *tinorsorb* set, the samples were first dissolved in 10 mL DMF by ultrasonication and diluted to the mark with MeOH. The solutions were filtered through a Millipore 0.45- μm syringe filter. Further dilution was carried out by using the autosampler to give a final solution of 0.10 mg mL⁻¹. The HPLC analysis of these solutions was carried out under the chromatographic conditions given in Section 2.3.6 for the respective sample sets. The results from this section are presented in Section 3.1.3.

2.4 Determination of titanium dioxide by inductively coupled plasma – optical emission spectroscopy

The large variety and complexity of vehicles used in cosmetic formulations, and the high inertness of TiO₂ towards a number of chemicals, make the choice of analytical methodology for its determination in the sample of interest a challenge. At the industrial level, where quality control has to keep pace with the rate of production, one needs to develop a robust, quick and reliable method for its determination. Not only is it important to check the amount of TiO₂ in the final product, but it is also crucial that the purity of the incoming raw TiO₂ be accurately determined.

Only a few papers have reported on the determination of TiO₂ in sunscreen products. Gottbrath *et al.*¹⁸⁰ determined TiO₂ particles removed with an adhesive tape from the skin after topical application of a suncare product. They employed atomic absorption spectrometry. Mason *et*

*al.*¹⁸¹ also employed atomic absorption spectroscopy to determine titanium in a commercial sunscreen formulation. Another study was by Salvador *et al.*¹⁸² who determined the levels of metal oxides in sun protection products. The determination was basically a microwave-assisted wet digestion of the oily, organic matrix with a mixture of acids (HCl and HNO₃), followed by fusion with a suitable flux over a Bunsen burner. Detection was done by inductively coupled plasma – atomic emission spectrometry (ICP-AES). The following sections describe the use of the inductively coupled plasma – optical emission spectroscopy (ICP-OES) for the determination of TiO₂ in commercial sunscreens analysed in this study. The sample preparation procedure used here is a modification of that reported by Salvador *et al.*¹⁸²

2.4.1 ICP-OES

Inductively coupled plasma – optical emission spectroscopy (ICP-OES) is an attractive technique for the determination of the concentration of heavy metals in both the pharmaceutical industry and in environmental analysis of solid and liquid samples. ICP-OES uses the optical emission principles of excited atoms to determine the elemental concentration. Thus, it provides element-specific quantitative results. A detailed description of the operational principles of ICP-OES is given below.

The ICP-OES instrument uses argon gas flowing through a torch consisting of three concentric quartz tubes. A copper coil circumscribing to the top of the torch is connected to a radio frequency generator. When the radio frequency power is applied on the copper coil, it sets up an alternating current within the coil. The oscillation of an alternating current causes electric and magnetic fields at the end of the torch. A spark applied to the argon gas causes ionization of some of the argon atoms. Being confined within the magnetic field, these electrons collide with other argon atoms, producing a chain reaction which ionizes argon within the field creating the plasma. The liquid samples are nebulized into an aerosol and introduced into the center of the plasma; the plasma excites the sample atoms which subsequently relax to a lower energy state by emitting light at elementally characteristic wavelengths. The intensities of these characteristic wavelengths are detected, measured and compared to the intensities for known standards to provide quantitative results.

2.4.2 Instrumentation

Figure 2.5 shows a schematic of the plasma and torch. A Jobin Yvon JY24 inductively coupled plasma-optical emission spectrophotometer equipped with a cross-flow nebuliser was used. The experimental conditions were: wavelength, 337.280 nm; generator power, 1000 W; plasma gas flow rate, 12 L min⁻¹; auxiliary gas flow rate, 0.00 L min⁻¹; sheath gas flow rate, 0.2 L min⁻¹; nebuliser pressure, 3 bars; sample flow rate, 1 mL min⁻¹. The data was analysed by using JYESS software.

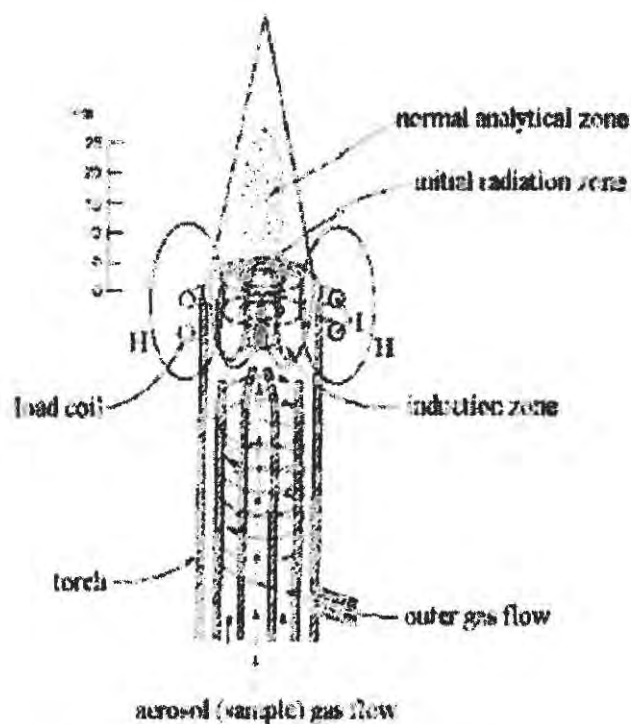


Figure 2.5: Schematic of the plasma and torch in ICP-OES instruments.¹⁸³

2.4.3 Preparation of standard solutions

A 300 mg L⁻¹ stock solution of Ti⁴⁺ was prepared by dissolving 0.050 g of pure TiO₂ in 100 mL of hot, concentrated sulfuric acid. An intermediate standard solution of 9.51 mg L⁻¹ was prepared by diluting the 300 mg L⁻¹ solution with deionised water. Working standard solutions were then prepared by serial dilution from the 9.51 mg L⁻¹ solution. Six standard solutions were prepared and subjected to ICP-OES analysis. Each solution was allowed to aspirate for at least a minute before sampling by the instrument. The instrument was programmed so that it sampled

each standard solution five times and four times for the samples. A typical calibration curve obtained from the analysis of a series of titanium dioxide standard solutions is shown in Figure D19 of Appendix D.

Standard solutions were run every day of sample analysis to check the constancy of the calibration curve. The calibration data for the calibration curve shown in Figure D19 can be found in Table C10 of Appendix C.

2.4.4 Preparation of sunscreen samples and analysis

A sample mass of 0.150 g of the commercial sunscreen product was weighed into a fused silica crucible. The sample was placed into an electrical furnace (with the temperature set at 600 °C). The sample was left in the furnace for 3 hours to give a carbon-free ash. After 3 hours, the sample was allowed to cool before being taken for fusion in which a mass of 0.50 g of potassium hydrogen sulfate (KHSO_4) was added into the crucible. The crucible was heated over a Bunsen flame for a few minutes to fuse the mixture. The molten product was then dissolved in hot, concentrated sulfuric acid and the solution transferred to a beaker. Further heating of the solution was done to ensure complete solubilization of the TiO_2 . The sample solution was diluted with deionised water to 50 mL. Further dilution was carried out to 10% (v/v) and the solution was subjected to ICP-OES analysis. This procedure was repeated for each sunscreen product that contained TiO_2 . The results from this section are presented in Section 3.2.3.

2.4.5 Validation of the ICP-OES quantitation method

In order to validate the method used for the quantification of titanium dioxide, a known amount of TiO_2 was spiked into a TiO_2 -free commercial product (SA16). The sample was mixed manually using a glass rod. After mixing, a sample mass of 0.150 g was then accurately weighed into a fused silica crucible. The crucible was placed in an electrical furnace at 600 °C for 3 hours. After 3 hours, the crucible was left to cool to room temperature. A mass of 0.50 g of KHSO_4 was added to the carbon-less ash product for fusion over a Bunsen burner. The sample was heated slowly and then left on the burner for a few minutes. The molten product was dissolved in hot, concentrated sulfuric acid and then diluted as required with deionised water. The diluted sample was subjected to ICP-OES analysis. The commercial sunscreen product

chosen for the recovery analyses was initially analysed to confirm the absence of TiO₂ in the same way as described above. Three replicate samples were prepared and analysed in the same way. The results from this analysis are given in Section 3.2.2.

2.5 Photostability analysis of sunscreens by UV/VIS transmission spectrophotometry

In this study, UV/VIS transmission spectrophotometry was applied to measure the transmitted radiation when a beam of light passes through a thin film of sunscreen on a quartz plate and in solution, and also in following the change in transmitted radiation upon irradiation of the sunscreen film in the sun. This section describes in detail the equipment and procedures used in the photostability analysis of the topical suncare products assessed in this study. The following paragraphs give brief background information on UV/VIS spectrophotometry.

Molecular absorption spectroscopy in the ultraviolet (UV) and visible (VIS) region is concerned with the measured absorption of radiation in its passage through a gas, liquid or solid. Molecules which absorb photons of energy corresponding to wavelengths in the range 190 nm to about 700 nm exhibit UV/VIS absorption spectra. Sunscreen agents, which are typically aromatic compounds conjugated with carbonyl groups, display absorption spectra in this region. That makes it possible to carry out qualitative analysis on finished suncare products by UV/VIS transmission spectrophotometry.

The technique is commonly used in many clinical and chemical laboratories today to give both quantitative as well as qualitative information. This is made possible by the fact that many organic and inorganic complexes exhibit absorption in this spectral region. However, the method becomes weak when it comes to quantitative analysis of complex mixtures. Since in this study, the products have complex UV-filter combinations with up to five active ingredients in a given formulation, the technique becomes effectively inapplicable due to a strong overlap of spectra (poor resolution of peaks) as explained in Section 2.3.

2.5.1 Instrumentation

A UV/VIS spectrophotometer consists of three components: the source, the dispersive system (combined in a monochromator) and a detector. These components are typically integrated into the same instrument to make spectrophotometers for chemical analysis. The sample can be placed in the optical path before or after the dispersive system and recorded spectra can be treated by using a number of different computer algorithms. Figure 2.6 shows a schematic representation of a double-beam spectrophotometer.

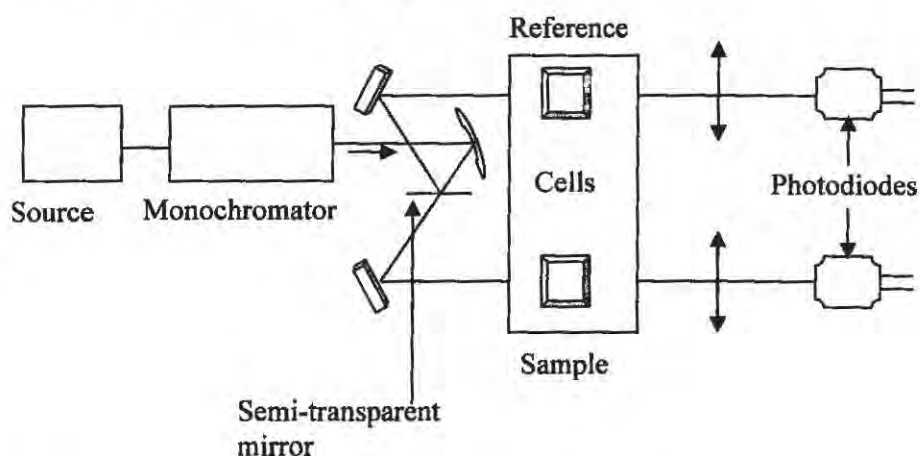


Figure 2.6: The optics of a double-beam UV/VIS spectrophotometer.

The light sources commonly used in this spectral domain are of two types. An incandescent lamp made from a tungsten filament housed in a glass envelope is used for the visible portion of the spectrum, for wavelengths longer than 350 nm. For the UV portion (wavelengths shorter than 350 nm), a medium pressure deuterium arc lamp is used. Detectors are again of two types: photomultiplier tubes and semiconductors (e.g. silicone photodiodes and charge transfer devices). More information on the components of a UV/VIS spectrophotometer can be found elsewhere.¹⁷⁸

Double-beam spectrophotometers allow differential measurements to be made between the sample and the analytical blank. A double-beam Perkin Elmer Lambda 35 UV-VIS spectrophotometer was used for UV/VIS transmission measurements in this work.

2.5.2 Analysis of sunscreens on quartz plates

In assessing the photostability of thin films of sunscreens on quartz plates, there is need to ensure that a uniform sunscreen film has been smeared. For that, it was necessary to carefully choose the right method of application of sunscreen on the quartz plate. It was also important to check for the reproducibility of the readout from the UV/VIS spectrophotometer to avoid inconsistencies in the results. Sections 2.5.2.1 and 2.5.2.2 describe how these two important parameters were evaluated.

2.5.2.1 Evaluation of sunscreen application method

Initially, attempts were made to achieve uniform distribution of sunscreen on quartz plates by dispersing the product in organic solvents according to the COLIPA protocol for the determination of photostability.¹⁸⁴ For this, two solvents were assessed. Firstly, the sunscreen product (an Australian purchased '*auScreen Ultrablock Lotion SPF15*') was dissolved in 80:20% (v/v) MeOH-H₂O to give a product load of about 11 mg mL⁻¹. A volume of 1 mL of the solution was delivered onto the quartz plate (surface area – 11 cm²) by carefully spotting the solution using a micropipette. Secondly, the sunscreen product was dissolved in dichloromethane and again dispensed onto the quartz plate by using a micropipette. The sunscreen product was also smeared onto the quartz plate with a gloved finger to give an application density of 1 mg cm⁻² (by mass) as with the solutions. The samples were left to dry for 30 minutes in the dark. However, since the solution samples took a long time to dry, they were placed in an oven set at 30 °C to speed up the drying process. The dry sunscreen films were taken for measurement. The reproducibility of the transmission spectra from the solution system and those from hand smearing were compared. Figure 2.7 shows the transmission spectra obtained with these two application methods.

It was found that the hand-smearing method gave more reproducible results than the solution system. Although the solvent system gave fair results, it was difficult to vaporise all the solvent so as to give a uniform, dry film. This required use of an oven set at a temperature of 30 °C or higher. That made the handling of the quartz plates covered with solution quite difficult due to spillages and the lack of a level surface. Dichloromethane gave very poor results (not shown), probably because of its high surface tension on quartz as compared to that of 80% MeOH-H₂O.

Consequently, the hand-smearing method was chosen for the photostability assessment of sunscreens.

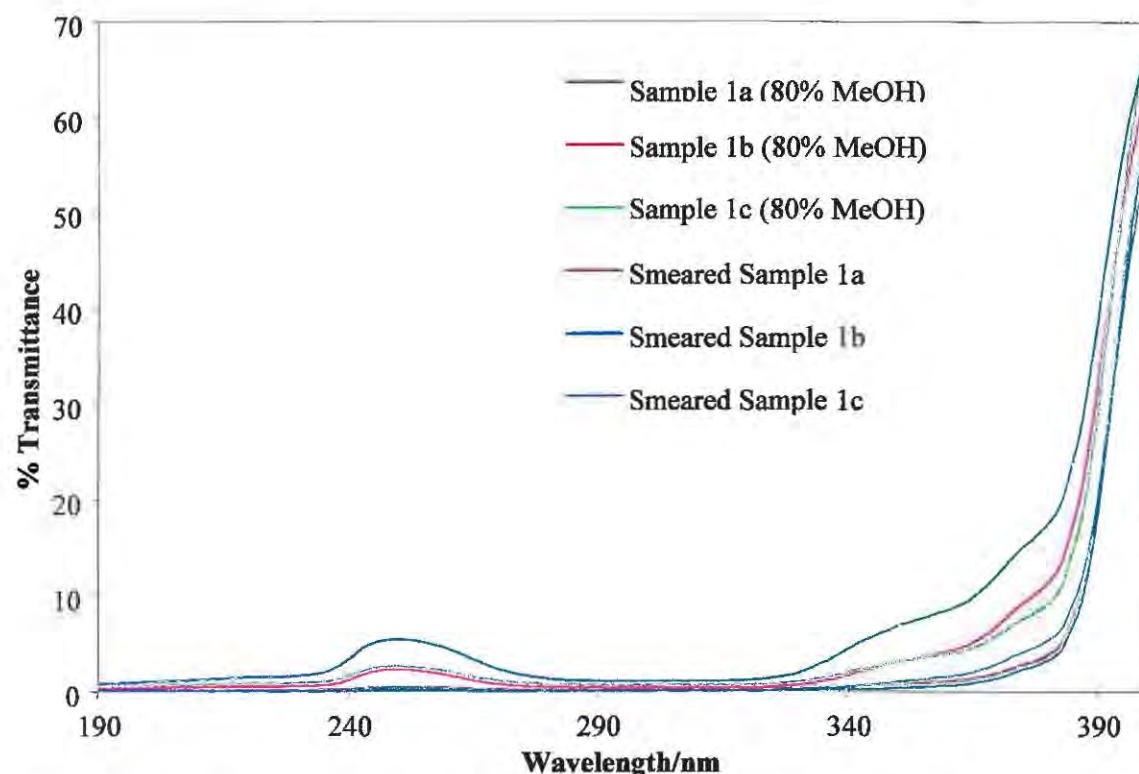


Figure 2.7: Comparison of the reproducibility of the transmission spectra of a sunscreen film (*auScreen Ultrablock Lotion SPF15*) prepared by hand-smearing and by dissolution in 80% (v/v) MeOH-H₂O.

2.5.2.2 Assessment of the reproducibility of instrument readout

Having determined that hand-smearing was the best application method, it was desirable to check the reproducibility of the readout from the instrument. A number of published reports to assess the photostability and the broad-spectrum protective capacity of sunscreens (as thin films on a substrate) have used an integrating sphere.^{146, 147, 185} This is used to capture all the light transmitted from a sunscreen film since the film may scatter both the incident and transmitted radiation, thus giving inconsistent readings.¹⁵⁰ The light collected by the sphere is then channeled to the detector.

The experimental work described here was designed to assess whether the integrating sphere offered superior results to those from measurements without an integrating sphere. Using an

application density of 1 mg cm^{-2} , the sunscreen sample (*auScreen Ultrablock Lotion SPF15*) was applied onto a quartz plate and the transmission spectrum of the film was recorded with a Perkin Elmer Lambda 35 UV/VIS spectrophotometer without an integrating sphere. The transmission spectrum of the same product recorded on a UV/VIS spectrophotometer (Varian Cary 3E, Varian Australia Pty Ltd, Mulgrave, Australia) connected to an integrating sphere (Labsphere DRA-CA-30, Labsphere, North Sutton, NH, USA) was made available by our collaborators (Konrad Brunnhofer of the Austrian Consumers' Association) in Vienna, Austria. The transmission spectra from the two instruments were compared and are shown in Figure 2.8.

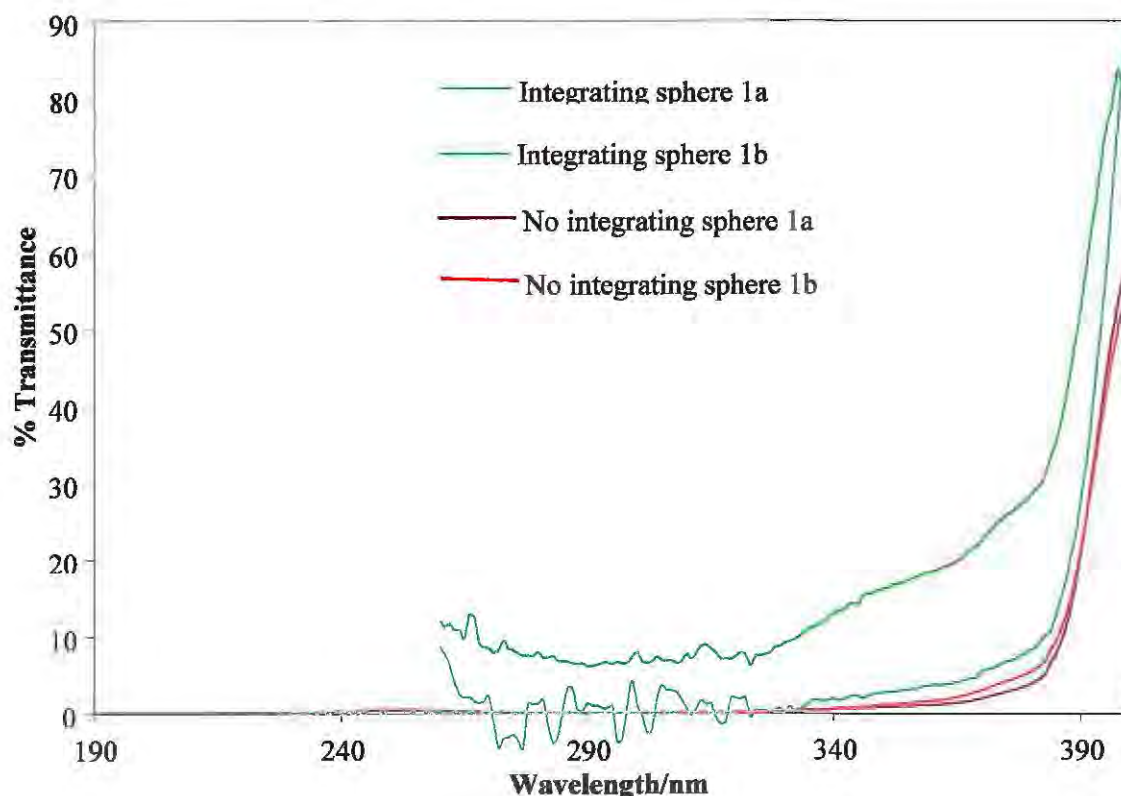


Figure 2.8: Comparison of the transmission spectra of 'auScreen Ultrablock Lotion SPF15' from a UV/VIS spectrophotometer with and without an integrating sphere.

As can be seen in Figure 2.8, the transmission spectra obtained without an integrating sphere show better reproducibility. These investigations demonstrate that UV/VIS transmission spectrophotometry with a quartz plate as substrate, and without an integrating sphere, can be successfully used to compare the photostability behaviour of sunscreen products.

2.5.2.3 Analysis of sunscreen products on quartz plates by using the hand-smearing method

Sunscreen products were smeared onto quartz plates with an average surface area of 11 cm². The quartz plates were weighed before application of sunscreen product. Using a gloved finger saturated with sunscreen product, the sunscreen was applied onto the quartz plate by circular motions of the finger according to the method described by previous investigators.^{146, 156, 185} The quartz plate was re-weighed to check the exact amount of sunscreen product applied. It is important to note that the efficacy of a sunscreen is highly dependent upon its correct application. A mass of 0.011 ± 0.001 g of each product was applied to give an application density of 1.00 ± 0.10 mg cm⁻². This is a more realistic amount since it has been demonstrated^{159, 160} that in actual use, people apply between 0.50 and 1.00 mg cm⁻². This amount is significantly lower than the COLIPA and FDA¹⁴⁶ recommended application density of 2 mg cm⁻² at which the SPF of sunscreens is measured.^{186, 187}

After application of sunscreen, the quartz plates were left in the dark for 30 minutes to allow for equilibration. The samples were then taken for transmission measurements. The transmission spectra of the smeared quartz plates were recorded with a double-beam Perkin Elmer Lambda 35 UV/VIS spectrophotometer. The measurement of transmission spectra was performed twice on the same side of the quartz plate (with the quartz plate turned upside down for the second measurement) to ensure that a uniform amount was applied onto the plate. The measurement of the transmission spectra was carried out against air in the reference beam. If the transmission spectra of the two measurements differed by more than 1% transmittance (across the whole spectrum), the quartz plate was washed clean and the product was re-applied. The ± 1% difference makes allowance for the unevenness of the skin surface and variation in amount of sunscreen applied *in vivo*, which are realities. After measurement of the transmission spectra, the smeared quartz plates were placed in a specially prepared sample holder for exposure to the sun.

The sample holder was designed in such a way as to have eight shallow rectangular troughs, which were cut out in a polystyrene block. The troughs measured about 12 cm² in area with a depth of about 2 mm to allow full exposure of the quartz plates to sunlight, and at the same time protecting them from windy weather. Provision was also made to accommodate a quartz cuvette containing the valerophenone chemical actinometer solution (see Section 2.7.6). The polystyrene block was mounted onto a heavy metal plate.

Exposure of the samples to sunlight was carried out on top of the Chemistry Building of the University of KwaZulu-Natal, from the 30th of May to the 30th of August, 2005. Transmission spectra were measured after every 1 hour of irradiation in the sun for a total period of 7 hours for each sample. The results from the photostability analysis of suncare products are reported in Section 3.3.

Because a number of photostability studies have been carried out in solution, selected sunscreen products were also assessed for their photostability in solution. Serpone *et al.*⁷⁴ reported on the photostability assessment of sunscreen agents in solvents of varying polarity. Shaath *et al.*¹⁶¹ also investigated the photostability behaviour of pure actives dispersed in solvents of different polarities, i.e. ethanol/water, isopropylmyristate and mineral oil. However, most of these studies are suspected not to be representative of the photophysical and photochemical processes occurring in thin, dry films of sunscreen on the skin. This analysis was carried out to compare the behaviour of sunscreens in solution and on quartz plates and to determine if there is any correlation. Section 2.5.3 describes in detail the experimental work carried out to determine the photostability behaviour of sunscreens in solution.

2.5.3 Analysis of sunscreens in solution

The selection of product was based on the photostability behaviour observed by UV/VIS transmission spectrophotometry studies carried out in Section 2.5.2.3. Moreover, for sunscreen products sharing a common UV filtering system, only one was assessed. This was based on the assumption that products with the same UV filtering system would produce the same photoproducts. The products analysed in solution include: SA1, SA2, SA3, SA6, SA15, SA20 and SA21.

The sunscreen product was dissolved in a solvent mixture of 12.5:37.5:50% (v/v) dichloromethane-cyclohexane-isopropanol as used by Rosenstein *et al.*¹⁵¹ according to the protocol outlined in the Australian/New Zealand UV Transmittance Standard. A mass of 0.010 ± 0.001 g of the sunscreen product was weighed into a 10 cm³ volumetric flask and the flask was placed in an ultrasonic bath for thirty minutes to dissolve the sunscreen product. The sunscreen solution was diluted to the mark with the solvent mixture.

The UV/VIS absorption spectrum of the solvent mixture was measured first before any transmission measurement commenced. The absorption spectrum is shown in Figure. 2.9. Clearly, this solvent mixture absorbs light starting from about 320 nm to shorter wavelengths.

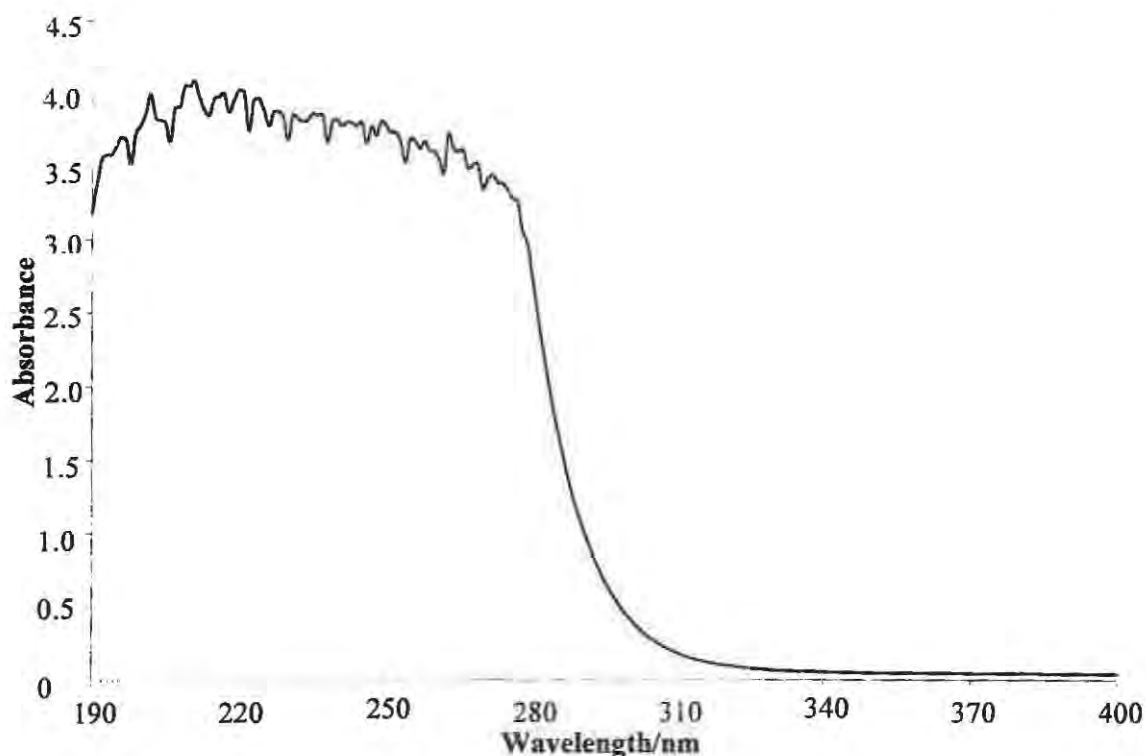


Figure 2.9: UV/VIS absorption spectrum of the solvent mixture: 50:37.5:12.5% (v/v) isopropanol-cyclohexane-dichloromethane, measured in a 1-cm pathlength quartz cuvette against air.

Nevertheless, the sunscreen sample was dissolved in the solvent mixture to give a solution load of 1 mg mL^{-1} . The solution was then pipetted into a 1-cm pathlength quartz cuvette for transmission measurement before irradiation. Another quartz cuvette with the solvent mixture was placed in the reference beam. In each case, a total sunscreen solution volume of 3 mL was used. Alongside the sunscreen solution cuvette, a quartz cuvette containing the valerophenone chemical actinometer was prepared for irradiation. Irradiation was carried out by putting the two quartz cuvettes in the sun at an angle depending on the direction of sunlight. The transmission spectra of the solution were recorded after every 1 hour of irradiation in the sun for a total of 7 hours in the same way as described in Section 2.5.2.3.

2.5.4 Data analysis

The transmission data obtained from the UV/VIS transmission spectrophotometry studies of commercial sunscreens were processed mathematically as detailed in Sections 2.5.4.1 and 2.5.4.2.

2.5.4.1 Calculation of photoinstability

The data obtained from Sections 2.5.2.3 and 2.5.3 were treated in the same fashion as reported by Maier *et al.*¹⁴⁷ The change in the spectral transmittance after a defined exposure period (UV dose), D , at a given wavelength, λ , $\Delta T_{\lambda, D}$, was calculated from the difference between the spectral transmittance before UV exposure, $T_{\lambda, 0}$, and the spectral transmittance, $T_{\lambda, D}$, for a defined UV dose, D at that wavelength. The value is termed spectral photoinstability, $\Delta T_{\lambda, D}$.

$$\Delta T_{\lambda, D} = T_{\lambda, 0} - T_{\lambda, D} \quad (2.1)$$

The arithmetic mean of the $\Delta T_{\lambda, D}$ values for both the UVA (320 - 385 nm), and the UVB (290 - 320 nm) range for exposure periods of 1 to 7 hours were calculated. A threshold photoinstability of 5% was set to assign products as photostable ($\Delta T_{\lambda, D} < 5\%$) and photounstable ($\Delta T_{\lambda, D} \geq 5\%$) after an exposure period of 2 hours in the UVB or UVA region. A period of 2 hours is reasonable since Guy *et al.*¹⁸⁸ showed that the average time school children in Durban spend outdoors was 2.3 hours which is close to 2.2 hours found by Gies *et al.*¹⁸⁹ for Australian children. The same period spent in the sun by children can be extrapolated to all people in general. The results of this analysis are discussed in Section 3.3.3.

2.5.4.2 Calculation of the critical wavelength

The UV/VIS transmission spectrophotometry data were also analysed by use of the critical wavelength, λ_c (CW) method. The CW method was used in the broad-spectrum classification of sunscreens as well as in assessing its suitability in the photostability analysis of sunscreens. The analysis of photostability data by the CW method was prompted by the claim made by Diffey *et al.*¹⁵⁶ that the method can be used to account for photoinstability in sunscreen products.

The CW *in vitro* method is based on the absorption spectrum of a sunscreen product which is obtained by means of UV/VIS spectrophotometry. In this study, the transmission spectra of product films were measured. Therefore, the transmission data were mathematically processed to yield absorption spectra for each product. The following equation was used for the conversion of transmittance data to absorbance:

$$A = 2 - \log(\%T) \quad (2.2)$$

where A is the absorbance and T is the transmittance. Once the absorbance values had been found, these were then used to calculate the CW. The critical wavelength was calculated with the following equation:

$$\int_{290}^{\lambda_c} A(\lambda)d\lambda = 0.9 \int_{290}^{400} A(\lambda)d\lambda \quad (2.3)$$

where λ_c is critical wavelength, A is absorbance and λ is wavelength. For each absorption spectrum, the integral, which represents the area-under-the-product absorbance curve, was estimated by using trapezoidal integration. For each product film, the CW was the average of four replicates for the broad-spectrum protection classification part.

The broad-spectrum protection claims made on the labels of sunscreen products were compared with the calculated critical wavelengths for each suncare product. It was assumed that the broad-spectrum classification method used by manufacturers (according to the information labelled on their products) was the same as that detailed by Diffey.¹⁹⁰ Table 2.4 gives the different CW ranges and the broad-spectrum protection rating or the number of stars for the respective wavelength ranges according to Diffey.¹⁹⁰

Table 2.4: The CW ranges and broad-spectrum rating (number of stars) according to Diffey.¹⁹⁰

Broad-spectrum classification of sunscreens	
Critical wavelength (λ_c)/nm	Broad-spectrum rating /no. of stars
$\lambda_c < 325$	0
$325 \leq \lambda_c < 335$	1
$335 \leq \lambda_c < 350$	2
$350 \leq \lambda_c < 370$	3
$370 \leq \lambda_c$	4

In the photostability assessment part, the change in the CW value of a product with irradiation time was used to assess the photostability of commercial sunscreens. For this part (photostability assessment), the CW value was estimated from one determination only. The data obtained were compared with the findings from Section 2.5.4.1. The results from this section are discussed in Section 3.5.

2.6 Photostability analysis of sunscreens by HPLC

Only a few selected sunscreen products were analysed by HPLC for their photostability behaviour. The products selected were SA1, 3, 15, 16, 20, and 21. The selection was based on the photoinstability observed from the photostability studies carried out by UV transmission spectrophotometry as described in Section 2.5.2.3. For products containing the same UV filter system, only one product was selected for analysis. It was assumed that those products with the same UV filter combination would likely produce the same photoproducts though the vehicle also influences the photostability and photochemical behaviour of the sunscreen active ingredients. The selection was a representative sample of both photounstable and photostable products. The interest was more on the possible photoproducts that could have formed during irradiation of the photounstable products (SA1, 3, 15, 20 and 21).

A mass of 0.245 ± 0.005 g of each selected product was accurately smeared onto glass petri-dishes with an average surface area of about 245 cm^2 . The exact mass weighed was checked by reweighing the petri-dishes. All the petri-dishes (smeared with sunscreen) were put in the sun for a total period of 6 hours except for SA3. The irradiation of sunscreen products was done for six hours to allow for the generation of enough photoproducts for HPLC analysis. For SA3, two petri-dishes were prepared; one was exposed for three hours and the other one for 6 hours. This particular product was treated differently because of its unique photostability behaviour as observed in the UV/VIS transmission studies (Section 2.5.2.3). Except for SA16, the rest of the dry sunscreen samples were dissolved in HPLC-grade MeOH by ultrasonication for one hour. SA16 was first dissolved in 10 mL of DMF by ultrasonication. The solutions were each diluted to 25 mL with MeOH. The sunscreen solutions were filtered through a $0.45\text{-}\mu\text{m}$ syringe filter. Further dilution was carried out by taking 10 μL and diluting to 500 μL . The diluted samples were then subjected to HPLC analysis. Analysis of the solutions was carried out in the same

manner as described in Section 2.3.6. The results from this analysis can be found in Section 3.3.3.

2.7 Chemical actinometry measurements

The solar UVR irradiance reaching ground level is influenced by two main factors: the solar zenith angle, θ_z (the angle between the local vertical direction and the direction of the centre of the solar disc) and the column of the total ozone. Besides these two factors, clouds and aerosol content of the atmosphere have an effect on the relative spectral distribution. As the photostability and photochemical behaviour of sunscreens depends on the hour-to-hour, and day-to-day intensity of the solar radiation incident on the samples, actinometric measurements were carried out to determine the irradiance received by the samples. Since irradiation was done by using terrestrial solar energy, the study also afforded a chance to quantify, within experimental error, the exact amount of light normally received by a sun bather on a clear and sunny day. The irradiation of sunscreens was carried out on clear days only.

Chemical actinometry has been employed since the 1920s in photochemistry as a relatively simple and accurate method for the measurement of the intensity of radiation. The recent progress in the development of radiation detectors, semiconductors and electronic equipment has also seen the development of physical devices for easy, fast and precise measurement of radiation. Photochemists often prefer these physical devices to chemical actinometers because of their simple irradiation geometries and easy handling. Physical devices are employed in many areas,^{191, 192} including environmental monitoring for the measurement of changes in erythemogenic UV irradiance reaching the earth's surface and measurement of the thickness of the ozone column.¹⁹³

However, these outstanding properties of physical devices are inherent in only a small number of electrically calibrated radiometers (ECRs) available in few highly equipped laboratories. ECRs are special thermopiles or piezoelectric radiometers, which can be calibrated in an absolute manner by electrical substitution without the need of any standard. The majority of physical detectors, like usual thermopiles, piezoelectric joulemeters, or photodiodes are only secondary standards, the response of which is subject to changes.¹⁹⁴

In contrast to the physical detectors, chemical actinometers lead to accurate absolute radiation measurements, provided that they are used according to the recommended procedures. As opposed to physical devices, chemical actinometers do not require any calibration. Instead, they can be used to calibrate joulemeters at low laser power in order to control the accuracy of the power meter.

2.7.1 Actinometry

A general definition of an actinometer is given as a chemical system or a physical device by which the number of photons in a beam absorbed into the defined space of a chemical reactor can be determined integrally or per time.¹⁹⁴ Furthermore, a chemical actinometer or dosimeter is a chemical system (fluid, gas, solid or in a micro-heterogeneous environment) that undergoes a light-induced reaction (at a certain wavelength, λ) for which the quantum yield, $\Phi(\lambda)$ is accurately known.¹⁹⁴ Measuring the rate of reaction allows the calculation of the absorbed photon flux. The rate of the light-induced reaction is related to the photon flux by the following equation:

$$-\frac{d[\textit{Actinometer}]}{dt} = I_0 \Phi f \quad (2.4)$$

where the left term is the change in concentration of the actinometer with time, I_0 is the incident photon flux, Φ is the quantum yield and f is the fraction of photons absorbed.

The determination of the rate of change of reactants, or the rate of formation of products, affords the total number of photons absorbed by the liquid or gas volume or solid surface, which may have any form or geometry. The quantum yield of a photochemical reaction is defined as $\Phi(\lambda)$ = the number of events, e.g., molecules changed, formed, or destroyed, divided by the number of absorbed photons at that particular wavelength in the same period of time. Expressed in mathematical terms, the quantum yield is:

$$\Phi(\lambda) = \frac{d[\textit{Actinometer}]}{ndt} \quad (2.5)$$

where n is the number of photons absorbed in the time period dt .

For accurate and reliable measurements of radiation by a chemical actinometer, the photochemical system should be simple and well-studied. The photoreaction must be reproducible under well-defined and easily controllable experimental conditions. Quantum yields should be accurately known for a wide range of wavelengths and the quantum yields should be independent of wavelength. The chemical components should be thermally stable to exclude complications due to dark reactions, and they should be detectable by simple analytical methods. It is desirable that the system displays large sensitivity. The handling of the photochemical system and the evaluation of the number of photons absorbed should be simple and straightforward. Lastly, the chemical actinometer should be commercially available and disposal of waste should be simple.

A number of chemical actinometers have been studied and their photochemistry is well established. Kuhn *et al.*¹⁹⁴ have published a comprehensive review of the different types of both chemical actinometers and physical devices that have been applied in different areas where quantification of radiation might be of interest.

1-Phenyl-1-pentanone (valerophenone) is an intensively studied photochemical system and has been used in the measurement of radiation in many light-induced reactions.¹⁹² Allen *et al.*¹⁵⁸ have used valerophenone to study the photolysis of the cosmetic fragrance, 6-methylcoumarin. Klán *et al.*¹⁹⁵ have studied the photochemistry of valerophenone in frozen solid solutions that comprised both non-polar organic solvents and water. It is documented that valerophenone undergoes the Norrish Type II photoreaction with quantum yields close to unity being realized. However, the alkyl phenyl photoreaction kinetics and product distribution is influenced by several factors that relate to the triplet and biradical nature and interactions with solvent (Zepp *et al.*¹⁹⁶). The major products of valerophenone photodegradation are acetophenone, propene and the phenylcyclobutanols, which are formed as a result of cleavage and cyclization. The quantum yield in aqueous solution was determined to be, $\Phi(290 - 330 \text{ nm}) = 0.98 \pm 0.04$.¹⁹⁶ All the calculations of the actinic flux incident on the sunscreen samples reported herein, were performed by employing a quantum yield of 0.98.

The study of the erythral influence of UVR has been largely based on the minimum dose of UV erythral radiation that will produce a noticeable reddening of the skin that has not been previously exposed to solar radiation. This dose is known internationally as the minimal erythral dose (MED – 200 J m^{-2}) and is always related to a specific skin type (phototype). However, the Commission Internationale de l'Eclairage (CIE) recently defined the standard

erythemal dose (SED), which corresponds to 100 J m^{-2} weighted at 297 nm. The SED does not depend on the skin type and must be used instead of the MED.¹⁹⁷ Hence, the UV doses received by the sunscreen samples analysed in the foregoing are reported in SEDs.

A number of analytical techniques can be used to follow the decrease in concentration of valerophenone with exposure to sunlight. These include high performance liquid chromatography (HPLC), gas chromatography with mass spectrometry (GC-MS), etc. In this study, the change in the concentration of valerophenone with irradiation time was monitored by gas chromatography with flame ionization detection (GC-FID) as detailed in the following sections.

2.7.2 Gas Chromatography

Gas chromatography is an analytical technique for separating compounds based primarily on their volatilities. The principle of separation in GC and HPLC is the same. The most distinctive feature between gas and liquid chromatography is that liquid chromatography employs a liquid as mobile phase. In GC, the samples to be analysed are vaporized and eluted with the aid of an inert carrier gas as a mobile phase through the column. The compounds partition between the stationary phase, which can either be solid or liquid, and a gas mobile phase. The predominant separation principle behind this technique is the differential partitioning of substances into the stationary phase which allows the compounds to be separated in time and space.

2.7.3 Instrumentation

The different components of a gas chromatograph are shown in Figure 2.10. Commonly used carrier gases include nitrogen, helium, argon and carbon dioxide. The choice of carrier gas is often dependent on the type of detector which is used.

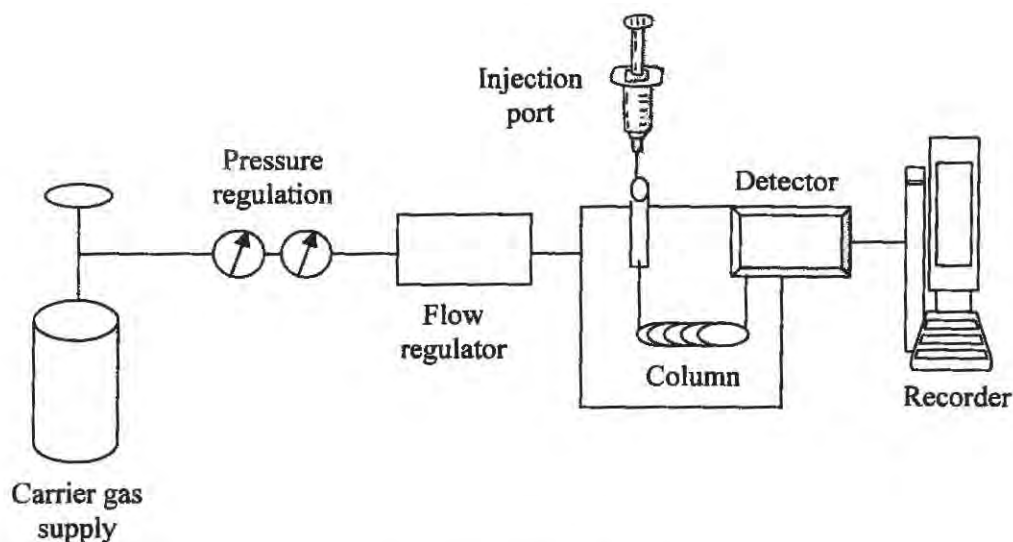


Figure 2.10: Schematic of a gas chromatographic system.

For optimum column efficiency, the sample should not be too large, and should be introduced into the column as a “plug” of vapour.¹⁹⁸ Normally, 1 μL of sample is injected into the GC system for analysis. Injection is usually achieved by means of a micro-syringe inserted through a self-sealing septum. Injection of sample should be done quickly to avoid band broadening and loss of resolution. Large sample volumes cause column overload. However, this can be solved by use of a stream splitter.

On injection, the sample is vaporized and mixed with a carrier gas. A fraction of this can be delivered to the column and the rest vented into the atmosphere. In this investigation, the GC was operated in the split-less mode. The temperature of the sample port is usually 50 $^{\circ}\text{C}$ higher than the boiling point of the least volatile component of the sample.

The separation of the components in a sample occurs in the column which is housed in an oven. Columns are generally of two types: packed and capillary (open tubular). In packed columns the stationary phase is set on a solid support material (commonly based on diatomaceous earth). The problem with packed GC columns was their high flow impedance which was solved by the development of the capillary column. Capillary columns contain no carrier material; the liquid stationary phase is discharged on the wall of the capillary.¹⁹⁹ The most recent capillary columns are the fused silica columns which are very strong and very inert (in contrast with glass columns) and can be used over a wide range of temperatures. A non-polar DB-5 column (fused silica) was used for the determination of the valerophenone concentration remaining following

irradiation in the sun. From the column, the eluate is channeled to the detector where a signal is generated and is captured by the data recorder or computer.

There are many detectors which can be used in GC. Different detectors will give different types of selectivity. A non-selective (universal) detector responds to all compounds except the carrier gas whereas a selective detector responds to a certain class of compounds. Detectors can also be grouped into concentration dependent detectors (sample integrity normally preserved) and mass flow dependent detectors (usually destroy the sample). The signal from a mass flow detector is related to the rate at which solute molecules enter the detector and the response is unaffected by make-up gas, in contrast with the former. A flame ionization detector (mass flow detector) was used in this work to quantify valerophenone. The flame ionization detector (FID) has high sensitivity, a large linear response and low noise. It is also robust and easy to use, but unfortunately, it destroys the sample. Figure 2.11 shows a schematic representation of a FID.

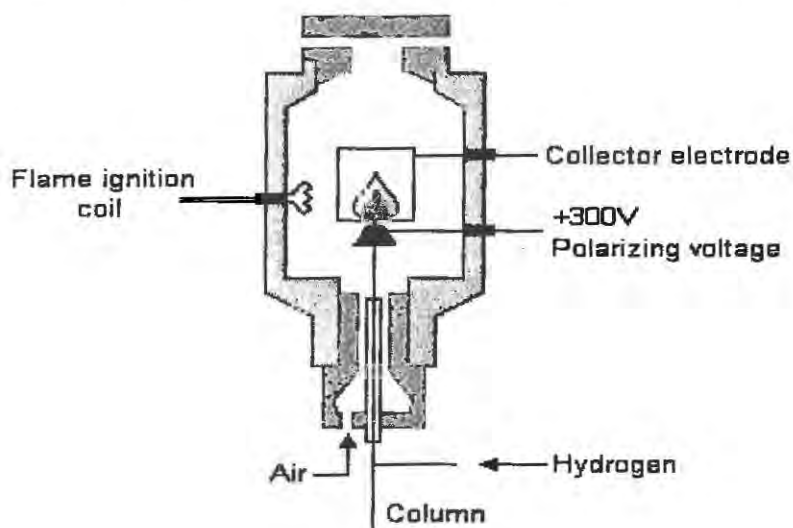


Figure 2.11: The Flame Ionisation Detector.²⁰⁰

2.7.4 Preparation of solutions for actinometry

The valerophenone actinometer was used to follow the dose of UV radiation falling on the sunscreen samples. Because of the inherently low precision in GC quantitative analysis, it was necessary to use an internal standard. Dodecane was used as the internal standard in this work to improve both precision and accuracy of actinometry data. Masses of 0.0435 g of valerophenone and 0.0459 g dodecane were dissolved in a 100 mL volumetric flask and made up to the mark with acetone to give a concentration of 1.1×10^{-3} M for both. The concentration of

valerophenone was made sufficiently high in order to make the kinetics of the reaction approximately zero order. In this way, the rate of reaction does not depend on the concentration of the reactant as it would if one assumed first-order kinetics. Zepp *et al.*¹⁹⁶ used lower concentrations of valerophenone (in the order of 10^{-5} M) than those used in this study. The UV absorption spectrum of a 1.1×10^{-5} M valerophenone solution was recorded with a Perkin Elmer Lambda 35 UV/VIS spectrophotometer and is shown in Figure 2.12.

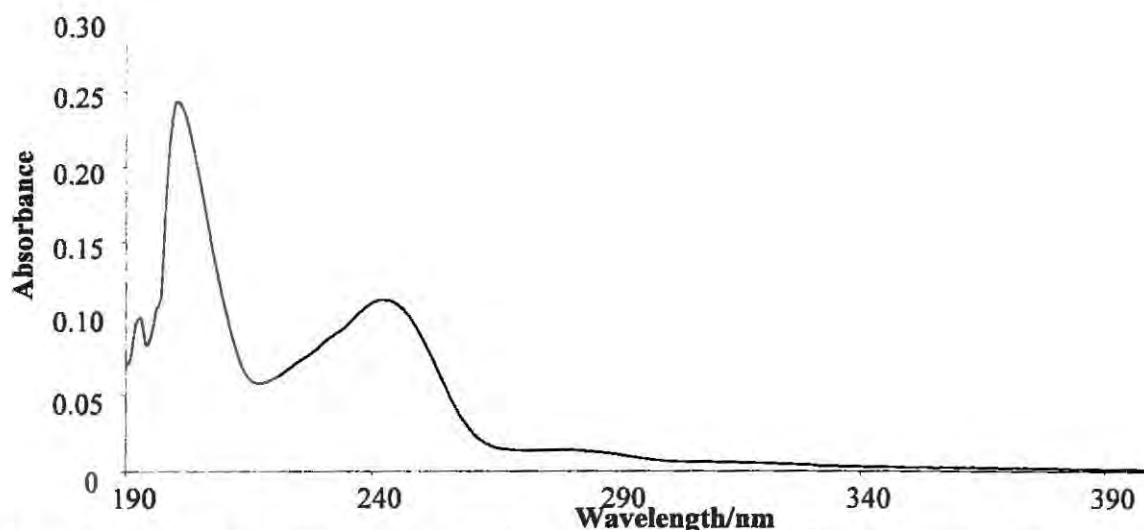


Figure 2.12: UV absorption spectrum of valerophenone (1.1×10^{-5} M) in acetone. Absorption spectrum was recorded in a 1-cm pathlength quartz cuvette with acetone in the reference beam.

2.7.5 GC-FID equipment and operation

A Perkin Elmer Autosystem XL gas chromatograph with flame ionization detection was used in this work. The column used was a DB-5 fused silica capillary column with the following dimensions: length – 50 m, diameter – 320 μm and a film thickness of 1 μm . Nitrogen was used as the carrier gas and was set at a flow rate of 2 mL min^{-1} . The FID used an air/hydrogen flame with flow rates of approximately 450 mL min^{-1} and 45 mL min^{-1} , respectively. The injector was used in a split-less mode.

2.7.6 GC-FID analysis of valerophenone solution

In order to quantify valerophenone, the optimum conditions for the determination of valerophenone had to be determined first. This was achieved by injecting the solvent (acetone)

alone. Once the retention time for the acetone peak was determined, the valerophenone actinometer solution dissolved in acetone was injected. The solution containing both valerophenone and dodecane (in acetone) was then injected to determine the retention time for dodecane. Having determined the retention times of the two analytes (valerophenone and dodecane), the actual analysis of samples that had been irradiated in the sun was then carried out.

A volume of 3 mL of the 1.1×10^{-3} M valerophenone solution was accurately pipetted into a 1-cm pathlength quartz cuvette. The quartz cuvette was placed in a specially cut out trough (at the centre of the eight quartz plate troughs) alongside the quartz plates smeared with the sunscreen products. The valerophenone solutions and sunscreen samples were exposed to sunlight. After irradiation for 1 hour, the valerophenone solution was injected into the GC by means of a 1 μ L microsyringe to determine the remaining amount of valerophenone. Figure 2.13 displays a typical gas chromatogram obtained in the determination of the optimum conditions for valerophenone analysis. Because of the high boiling temperature of valerophenone, it was necessary to have a high detector temperature.

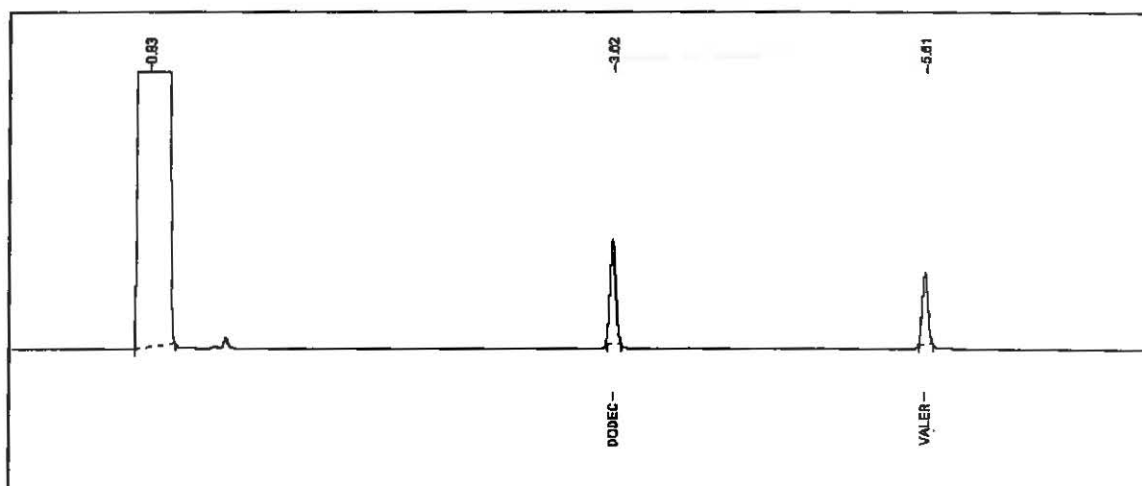


Figure 2.13: Typical gas chromatogram obtained in the determination of optimum conditions for the valerophenone actinometer analysis before irradiation. The chromatographic conditions were: DB-5 column with dimensions: length – 50 m, diameter – 320 μ m and a film thickness of 1 μ m, nitrogen gas flow rate – 2 mL min^{-1} detector temperature – 260 $^{\circ}\text{C}$, temperature programme – 120 $^{\circ}\text{C}$ held for 1 minute, then increased to 230 $^{\circ}\text{C}$ at a rate of 10 $^{\circ}\text{C} \text{ min}^{-1}$ and held at 230 $^{\circ}\text{C}$ for 2 minutes. The order of elution is acetone (solvent), dodecane (1.1×10^{-3} M) and valerophenone (1.1×10^{-3} M). Injection volume was 1 μ L.

A fresh solution of the actinometer was used for every hour of irradiation of the sunscreen samples. Initially, the loss in valerophenone concentration with irradiation time was measured after every 15 minutes but it was later realised that the slopes of the concentration versus time graphs for the 1-hour irradiation period and the 15-minute irradiation intervals were comparable.

Since the response and sensitivity of the detector could not be assumed to be constant in the day-to-day measurements of valerophenone, a relative response factor (RRF) was calculated as follows on a daily basis.

$$RRF = \frac{M_{Dodec}}{M_{Valer}} \times \frac{S_{Valer}}{S_{Dodec}} \quad (2.6)$$

where $M_{Valer:Dodec}$ is the mass of valerophenone or mass of dodecane, and $S_{Valer:Dodec}$ is the signal of valerophenone or dodecane, respectively. Before each irradiation, a GC chromatogram of the valerophenone solution was run in order to determine the RRF, which was then used in the determination of the remaining amount of valerophenone for each irradiation. Rearrangement of Equation 2.6 yields,

$$M_{Valer} = \frac{M_{Dodec}}{RRF} \times \frac{S_{Valer}}{S_{Dodec}} \quad (2.7)$$

From equation 2.7, calculation of the remaining concentration of valerophenone (M_{Valer}) can be done and a plot of concentration against time yields a linear curve as shown in Figure 2.14. The R^2 values obtained were all greater than 0.95 for the 15-minute irradiations. The data used to plot the curve shown in Figure 2.14 can be found in Table C11 of Appendix C.

The slopes of the hourly plots were used to determine the irradiance incident on the samples in any given hour. Moreover, the sum total of irradiance (in 7 hours) received by the sunscreen samples could be obtained.

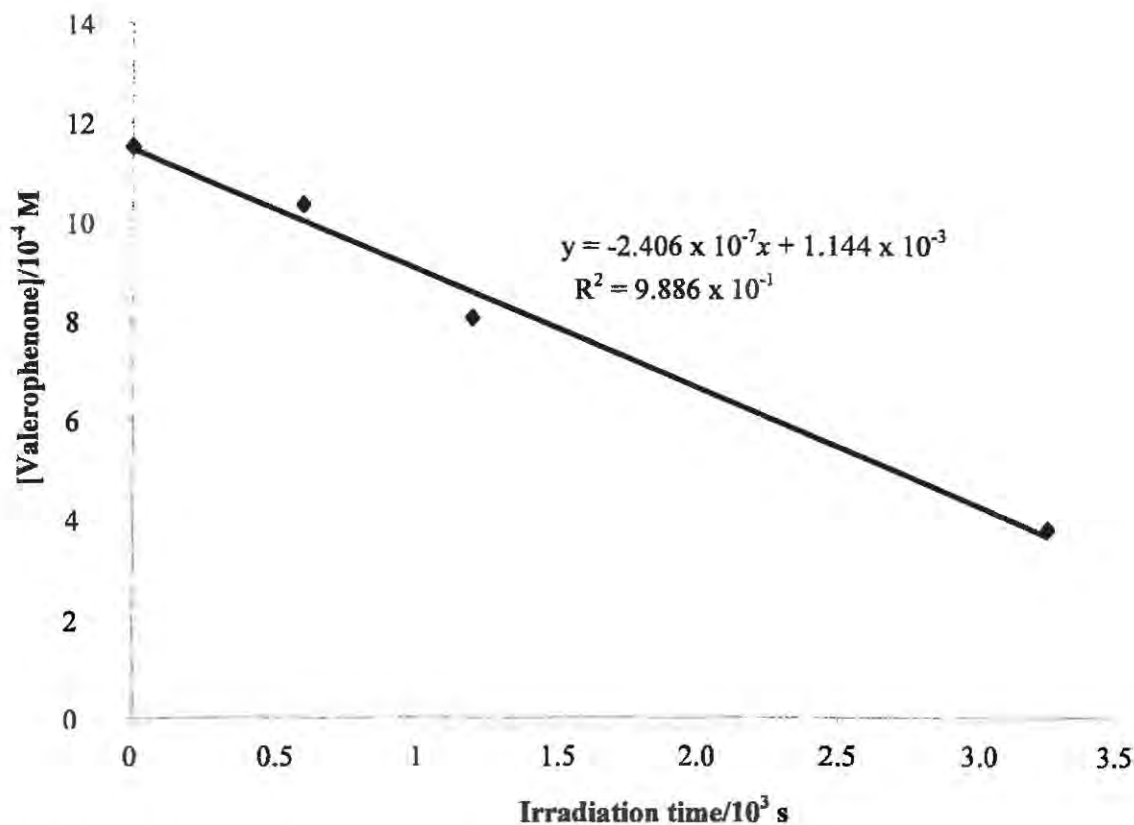


Figure 2.14: Change in valerophenone concentration with irradiation time.

2.7.7 Data analysis

The incident light intensity, I_0 , was calculated from the slope, k_0 , of the valerophenone concentration versus time curve and the quantum yield, Φ , for the photolysis of valerophenone as follows:

$$I_0 = \frac{k_0}{\Phi} \quad (2.8)$$

The units of k_0 are in $\text{mol L}^{-1} \text{s}^{-1}$, and those of I_0 are $\text{einstein L}^{-1} \text{s}^{-1}$ (i.e. the rate at which the photon concentration is delivered to the solution).

The goal was to measure the intensity of sunlight falling on the samples. This quantity is called the photon flux, F_0 , and is in units of Watts per square meter (W m^{-2}). A detailed explanation and derivation of Equation 2.9 for F_0 is reported elsewhere:²⁰¹

$$F_0 = \frac{I_0 V N_A E_\lambda}{A} \quad (2.9)$$

where F_0 is the photon flux, V is the volume (in litres) and A is the area (in m^2) of the exposed actinometric solution, N_A is Avogadro's number and E_λ is the energy of a photon of wavelength λ (in J photon^{-1}). Note that the product of I_0 and V is the flow of photons to the actinometric solution (in einstein s^{-1}) and that the ratio of V to A is the pathlength of the solution.

The energy of a photon is calculated from Planck's law:

$$E_\lambda = h\nu = \frac{hc}{\lambda} \quad (2.10)$$

where h is Planck's constant, c is the speed of light, and λ is the average wavelength over which the actinometer is used, 290 - 330 nm in this case. Values for the constants used in the equations above can be found in Table C12 of Appendix C.

Once the photon flux per given hour has been found, the standard erythemal dose, SED, (for that hour) can now be calculated by finding the product of irradiation time in seconds, T , and the photon flux, F_0 , in W m^{-2} divided by 100, as shown in Equation 2.11.

$$SED = \frac{F_0}{100} \times T \quad (2.11)$$

The units of standard erythemal dose (SED) are J m^{-2} . The cumulative SEDs for each hour of the 7 hours of irradiation are displayed in the individual photostability plots reported in Section 3.3.3.

Chapter 3

RESULTS AND DISCUSSION

The increasing awareness of the harmful effects of overexposure to sunlight has led to a heightened use of sunscreens in many cosmetic products. However, it is reported that there is an alarming global increase in the incidence of skin cancer. The incidence of skin cancer in South Africa is reported to be among the highest in the world with about ten thousand cases being diagnosed annually.²⁰² This is despite a heavy campaign by medical groups and dermatologists for people to use sunscreens. One would ask if we are losing the fight, when the necessary weapons (sunscreens) are at our disposal. Sunscreens should not only protect against UVR, but should maintain that protection throughout the period of exposure to sunlight. It has been observed that sunscreen combinations are often chosen based on their solubility compatibility rather than their inherent UVR absorption properties. As a result, that compromises their photostability and their photoprotective efficiency. Moreover, some cosmetic manufacturers claim broad-spectrum protection simply by virtue of having incorporated a UVA absorber, and not on the spectral coverage of a formulation. Investigations have shown that sunscreen products lose their photoprotective capacity upon exposure to sunlight. It is also documented that some sunscreen ingredients exhibit skin photoallergic sensitisation, contact dermatitis and estrogenic activity. It is necessary therefore, to monitor the levels of sunscreen ingredients in sun care products and assess the photostability of commercial sunscreens.

As detailed in Chapter 2, a number of experiments were carried out to assess the photostability behaviour of South African commercial sunscreen products. In addition, the levels of the different sunscreen active agents in the products were determined. This was achieved by use of chromatographic and spectroscopic techniques. This study is the first to assess the photostability, as well as to quantify the active ingredients, of a representative sample of commercially available sun care products (lipsticks, creams and lotions) on the South African market. The following sections present the results obtained from the different analyses carried out.

3.1 Determination of UV filters by high performance liquid chromatography

This section presents the results obtained from the quantitation of organic UV filters in commercial sunscreen products by HPLC. A total of 21 commercial products were analysed by HPLC. Seventeen of the 21 sun care products were analysed under the same chromatographic conditions. As has been reported in Section 2.3.5, it was difficult to separate MBC and OMC in the presence of MBBT and BEMT. This UV filter combination occurred in four products. Subsequently, the determination was carried out by separately resolving the MBBT and BEMT peaks under the different chromatographic conditions as shown in Figure 2.4. Quantitation of MBC and OMC was carried out under the chromatographic conditions shown in Figure 2.3. This essentially means that a product containing any of the *tinosorbs* in combination with OMC and/or MBC was analysed under two sets of chromatographic conditions.

3.1.1 Variation of retention times

Table 3.1 shows the details of the retention times and detection wavelengths of the different UV filters when separated by HPLC. As can be seen from the relative standard deviation (RSD) values, there is negligible variation in the retention times. This shows that parameters such as column equilibration, flow rate, and mobile phase composition were well controlled.

Table 3.1: Retention times of the different organic UV filters when separated by HPLC.

Active ingredient	Detection wavelength /nm	Retention times/minutes					
		1	2	3	Mean	Std Dev	RSD/%
OMC*	310	12.19	12.34	12.22	12.25	0.08	0.66
MBC*	302	6.56	6.57	6.51	6.54	0.03	0.49
Bz-3*	290	3.85	3.86	3.93	3.88	0.04	1.14
OCR*	305	9.26	9.25	9.25	9.25	0.01	0.06
AVO*	358	10.69	10.81	10.88	10.80	0.10	0.89
OS*	242	14.38	14.21	14.19	14.26	0.11	0.74
MBBT [#]	342	12.11	12.27	12.35	12.24	0.12	0.97
BEMT [#]	342	13.90	13.90	13.67	13.82	0.13	0.94
OT [#]	311	6.16	6.24	6.21	6.21	0.04	0.63

* Chromatographic conditions: Phenomenex Synergi Max-RP-C₁₂ 80 Å column, mobile phase -- MeOH-H₂O 84:16% (v/v), flow rate – 1 ml min⁻¹.

[#] Chromatographic conditions: Phenomenex Synergi Max-RP-C₁₂ 80 Å column, mobile phase – MeOH-ACN 90:10% (v/v), flow rate – 1 ml min⁻¹.

3.1.2 Linearity of calibration curves

Calibration curves were obtained using the external standard calibration method. For each curve, three repeat determinations (prepared and measured in the same way) were performed. These determinations were performed on different days. For each concentration, five repeat injections were performed. Hence fifteen data points were obtained for each concentration. The calibration data used to construct the calibration curves (shown in Figures D1 to D18 of Appendix D) are listed in Tables C1 to C9 of Appendix C. The calibration curves were constructed by plotting the peak areas against the concentration in mol dm⁻³. Linear regression analysis (at 95% confidence level) of the calibration data for each active ingredient was performed by using the Microsoft Excel add-in package called Analysis ToolPak and the data is listed in Table 3.2. Also shown along with the calibration curve of each active ingredient is the plot of the unweighted residuals against concentration. The residual plots did not show any characteristic pattern indicating a good fit of the experimental data to the linear model.^{203, 204}

The slope and standard error of the calibration lines (for each sunscreen agent) listed in Table 3.2 were used to calculate the limit of detection (LOD) and the limit of quantitation (LOQ) according to the method used by Chisvert *et al.*^{168, 169, 175} The LOD was calculated as $3S_{y/x}b^{-1}$ ($S_{y/x}$ is the standard deviation of the slope, and b is the mean slope) and LOQ was calculated as $3.33 \times \text{LOD}$, and the values are also shown in Table 3.2.

The LOD values for Bz-3, MBC, OCR, AVO, OMC, OS, OT, MBBT and BEMT were 0.015, 0.008, 0.009, 0.011, 0.015, 0.010, 0.014, 0.006 and 0.010 μM , respectively. Smyrniotakis *et al.*¹⁷⁵ found LOD values of 0.036, 0.170 and 0.044 μM for OCR, OS and MBBT, respectively. Chisvert *et al.*²⁰⁵ found LOD values of 1.380, 3.600 and 2.630 μM for OMC, OS and Bz-3, respectively. Dutra *et al.*¹⁶⁸ also found LOD values of 0.394, 0.276 and 0.760 μM for Bz-3, OMC and OS, respectively. The LOD values found in this study are comparable and lower than those from other investigations.

The precision test was carried out by assessing the intra-day and inter-day variability where authentic standard solutions were prepared and subjected to HPLC analysis. The quantity of each analyte was obtained from the corresponding calibration curve. Table 3.3 shows the precision data.

Table 3.2: Results of linear regression of calibration data for sunscreen active ingredients analysed by HPLC.

Parameters	OMC	Bz-3	AVO	MBC	OCR	OS	OT	BEMT	MBBT
Calibration range/ 10^{-5} M	1.0-7.0	1.0-7.0	1.0-7.0	1.0-7.0	1.0-7.0	1.0-7.0	0.1-0.7	0.4-2.8	1.0-7.0
Slope (b) / 10^{10} M ⁻¹	2.919	1.835	3.641	2.896	1.523	1.010	14.38	4.919	0.864
Standard error of slope/ 10^8	1.459	0.900	1.289	0.815	0.454	0.331	0.672	1.612	0.171
R ² / 10^{-1}	9.987	9.987	9.994	9.996	9.995	9.994	9.989	9.994	9.998
LOD/ 10^{-2} μM	1.499	1.472	1.062	0.844	0.894	0.983	1.402	0.983	0.592
LOQ/ 10^{-2} μM	4.993	4.901	3.537	2.809	2.978	3.273	4.668	3.273	1.971

- LOD calculated as $3S_{y/x}b^{-1}$ ($S_{y/x}$ is the standard error of the slope and b is the slope of the calibration line.)

- LOQ calculated as $3.33 \times$ LOD.

75

Table 3.3: Analytical results of intra-day and inter-day variability.

Active ingredient	Concentration/μM	Intra-day (n = 5)			Inter-day (n = 9)		
		Found	RSD/%	Accuracy/%	Found	RSD/%	Accuracy/%
OMC	40.00	40.67 ± 0.21	0.52	101.68	39.70 ± 1.27	3.20	99.25
MBC	50.00	51.12 ± 0.17	0.34	102.25	50.45 ± 0.58	1.14	100.90
Bz-3	30.00	31.00 ± 0.21	0.67	103.34	30.08 ± 0.99	3.30	100.26
OCR	70.00	68.97 ± 0.16	0.24	98.53	69.77 ± 1.18	1.69	99.68
AVO	20.00	19.89 ± 0.12	0.58	99.46	19.91 ± 0.08	0.40	99.50
OS	40.00	40.63 ± 0.25	0.61	101.58	40.58 ± 0.27	0.66	101.44
MBBT	30.00	29.56 ± 0.14	0.49	98.55	30.14 ± 0.11	0.38	100.47
BEMT	28.00	27.76 ± 0.12	0.42	99.16	28.06 ± 0.37	1.33	100.23
OT	6.00	6.11 ± 0.05	0.09	101.91	6.03 ± 0.01	0.22	100.42

Accuracy (%) = (mean of found concentration/theoretical amount) x 100%.

RSD (%) = (SD/mean concentration) x 100%.

The RSD was taken as a measure of precision. The intra-day variability was examined within one day by five replicate injections. The RSD values for intra-day variability were below 1% (see Table 3.3). The inter-day precision was calculated from nine determinations over three days for each active ingredient and the RSD values ranged from 0.22 to 3.30% (see Table 3.3).

3.1.3 Validation of the HPLC quantitation method

Validation of the HPLC quantification method was achieved by spiking sunscreen samples with known amounts of the pure active ingredients as described in Section 2.3.8. Table 3.4 displays results of the recovery analysis. As can be seen in Table 3.4, the mean percentage recoveries achieved ranged from 96.88 to 104% for the different UV-filters analysed. The recoveries were relatively high, though recoveries between 98-102% would be ideal. The RSD values obtained for the recoveries ranged from 0.36 to 3.86% for the sunscreen active agents. Other workers¹⁷¹ achieved recoveries of 94.4, 98.6, 93.0, 85.9 and 97.7% for MBC, OT, OCR, AVO and Bz-3, respectively. These recoveries were from an oil/water emulsion commonly used in cosmetics. Hence the recoveries obtained in this study are comparable to those from other studies.

Table 3.4: Recovery analysis data for each active ingredient analysed by HPLC.

Active ingredient	Retention time/min†	Spiked concentration /% m/m	Recovery/%†	Standard deviation	RSD/%
AVO	12.25	5.17	96.88	0.35	0.36
OMC	3.88	15.94	97.63	0.38	0.39
Bz3	10.80	10.81	98.25	0.97	0.98
MBC	6.54	8.62	103.37	2.24	2.16
OS	9.25	5.73	100.95	3.75	3.71
OT	14.26	7.14	102.33	1.72	1.68
OCR	6.21	10.15	99.20	3.83	3.86
MBBT	13.82	2.85	97.53	3.07	3.15
BEMT	12.24	1.86	101.55	3.92	3.86

† Each value is the mean of three determinations.

3.1.4 Levels of organic UV filters in commercial sunscreens

Quantification of active ingredients in suncare products was carried out by the use of external standard calibration curves as described in Section 3.1.2 and 3.1.3. Table 3.5 presents results of the mean percentage concentrations (% m/m) of the different active ingredients in the suncare

Table 3.5: Mean % m/m levels and 95% confidence interval of the various active ingredients in the different products analysed by HPLC.

Product	Concentration/% m/m†								
	OMC	Bz-3	AVO	MBC	OCR	OS	OT	BEMT	MBBT
SA1	1.63 ± 0.50	0.88 ± 0.04	-	-	-	-	-	-	-
SA2	2.84 ± 0.06	1.43 ± 0.06	-	-	-	-	-	-	-
SA3	7.70 ± 0.18	4.83 ± 0.14	-	1.17 ± 0.09	-	2.14 ± 0.10	-	-	-
SA4	9.99 ± 0.55	3.82 ± 0.42	-	-	-	6.37 ± 0.31	-	-	-
SA5	7.51 ± 0.12	6.28 ± 0.10	0.72 ± 0.09	-	-	3.69 ± 0.07	-	-	-
SA6	2.25 ± 0.04	-	1.83 ± 0.03	2.28 ± 0.02	-	-	-	-	-
SA7	5.12 ± 0.08	-	2.15 ± 0.06	3.87 ± 0.04	-	-	-	-	-
SA8	6.84 ± 0.09	-	1.69 ± 0.06	3.99 ± 0.04	-	-	-	-	-
SA9	7.03 ± 0.07	-	-	4.27 ± 0.03	-	-	-	1.90 ± 0.06	3.39 ± 0.09
SA10	4.49 ± 0.12	3.45 ± 0.10	-	-	-	1.61 ± 0.07	-	-	-
SA11	8.82 ± 0.35	5.34 ± 0.27	-	1.18 ± 0.17	-	3.28 ± 0.20	-	-	-
SA12	7.78 ± 0.15	-	2.41 ± 0.11	-	-	-	-	-	-
SA13	4.03 ± 0.06	-	-	-	3.89 ± 0.04	-	-	1.63 ± 0.03	-
SA14	5.23 ± 0.06	-	2.83 ± 0.04	-	-	-	1.20 ± 0.02	1.81 ± 0.05	-
SA15	4.06 ± 0.13	-	1.12 ± 0.09	-	-	-	-	-	-
SA16	6.31 ± 0.06	-	-	3.88 ± 0.03	-	-	-	2.59 ± 0.04	3.84 ± 0.07
SA17	-	-	-	-	-	-	-	-	-
SA18	4.78 ± 0.08	-	-	-	-	-	-	-	-
SA19	-	-	1.12 ± 0.07	-	-	-	3.43 ± 0.02	-	-
SA20	9.45 ± 0.12	-	0.53 ± 0.05	-	-	-	-	-	-
SA21	7.58 ± 0.23	-	1.49 ± 0.17	4.69 ± 0.11	-	-	-	-	-
SA22	6.31 ± 0.27	-	2.44 ± 0.20	2.18 ± 0.13	-	-	-	-	-
COLIPA	10	10	5	4	10	5	5	10	10

† Each value is the mean ± 95% confidence interval of nine determinations. The confidence interval was calculated according to the method detailed in Appendix E. The raw data can be found in Appendix G.

products, the 95% confidence interval (calculated as detailed in Appendix E) and the COLIPA maximum permissible levels for each active agent investigated in this study. Three determinations were performed for each product and for each determination three injections were performed.

The levels of active agents in the diverse products analysed were within the European Cosmetics and Personal Care Association (COLIPA)¹⁶⁶ stipulated levels. This was with the exception of OS in SA4 and MBC in SA9 and SA21 which were slightly higher than the stipulated levels. The amount of OS in SA4 was 6.37%. The concentrations of MBC were found to be 4.27 and 4.69% in SA9 and SA21, respectively. The allowed maximum levels are 4.00 and 5.00% for MBC and OS, respectively. Otherwise the amounts of active agents in all commercial suncare products analysed conformed to the internationally maximum allowable levels in a formulation. There is no legislation in South Africa requiring that manufacturers declare the amounts of active ingredients in suncare products. There was no correlation observed between the amounts of the individual active ingredients and the labelled SPF value.

A consolidated table of the concentrations of both the physical blockers and chemical absorbers, including the COLIPA limits can be found in Table C13 of Appendix C. Representative chromatograms for each product can be found in Figures F3 to F28 of Appendix F.

The HPLC method used in this work for the determination of sunscreen active ingredients in commercial suncare products afforded multicomponent analysis of up to six organic UV filters simultaneously. As can be seen in Figure 2.3, the resolution of Bz-3, MBC, OCR, AVO, OMC and OS achieved was very good, making it easy for quantitative analysis of the six active ingredients simultaneously without interference. The determination of the *tinisorbs* was carried out under the chromatographic conditions detailed in Section 2.3.5. Although it was difficult to resolve OMC and MBC in the presence of MBBT and BEMT, the method employed affords the quantitative analysis of the four active ingredients in the same product with good accuracy.

Commercial sunscreens are often formulated with physical blockers to boost the UV filtering capacity of a formulation. The suncare products investigated in this study contained TiO₂ as the only physical blocker. Products were also analysed for their TiO₂ content by ICP-OES as described in Section 2.4. The following section presents results from the determination of TiO₂ in the suncare products.

3.2 Determination of titanium dioxide by inductively coupled plasma – optical emission spectroscopy

The determination of titanium dioxide in sunscreen samples presented a number of challenges especially in the sample pretreatment stage. The sample was first dry-ashed to give a carbon-free ash product. The solubilisation of the titanium dioxide in the samples required use of hot, concentrated sulfuric acid. It was important to minimise the number of transfers so as to achieve maximum recovery and a high precision in the quantitative results. A detailed description of the sample preparation procedure is given in Section 2.4.4.

For accurate determination of titanium dioxide, it was necessary to choose an emission line with high intensity, low or without spectral interference, and with minimal background noise signal in the presence of the matrix. The emission wavelength chosen for the detection of titanium was 337.280 nm. The only interference expected at this emission line was from nickel. Consequently, all the equipment used for the determination of TiO₂ did not contain nickel. Moreover, there were no any other metal oxides in the samples that would interfere with the determination of titanium dioxide.

Sections 3.2.1, 3.2.2 and 3.2.3 present the data from calibration curves, detection limits and the quantitative results from the analysis of TiO₂ in the commercial sunscreen products.

3.2.1 Linearity of calibration curves

Standard solutions from 0.475 to 9.512 µg mL⁻¹ were used for the calibration. The external standard calibration method was used to generate calibration curves used for the quantitation of TiO₂ in suncare products. The calibration data can be found in Table C10 of Appendix C. Linear regression analysis of the calibration data from the three determinations was performed by using the Microsoft Excel add-in package called Analysis ToolPak. Figure D19 (Appendix D) displays a typical calibration curve for the determination of TiO₂. For each concentration, three determinations were performed on different days to give three data points for each concentration. The RSD values of the emission signals from the three determinations ranged from 1.40 to 4.84%. Table 3.6 displays the linear regression analysis results.

The correlation coefficients for all the calibration curves used in the quantitation of TiO₂ were greater than 0.995 ($R^2 > 0.995$). The standard error of the calibration line was found to be 10.11. The sensitivity of the instrument (estimated as the mean of the slopes of calibration curves) was in the order of $10^{-3} \mu\text{g mL}^{-1}$. The LOD was calculated to be $0.030 \mu\text{g mL}^{-1}$, determined from $3S_{y/x}b^{-1}$ ($S_{y/x}$ is the standard error of the slopes of calibration curves, and b is the mean slope). The LOQ was calculated as $3.33 \times \text{LOD}$,²⁰⁶ which was approximately $0.098 \mu\text{g mL}^{-1}$.

Table 3.6: Results of linear regression analysis of TiO₂ calibration data.

Parameters	Value
Calibration range/ $\mu\text{g mL}^{-1}$	0.475-9.512
Slope (b)/ 10^3 †	1.026
Standard error of slope ($S_{y/x}$)	10.110
Correlation coefficient	0.999
LOD/ $\mu\text{g mL}^{-1}$	0.030
LOQ/ $\mu\text{g mL}^{-1}$	0.098

- LOD calculated as $3S_{y/x}b^{-1}$ ($S_{y/x}$ is the standard error of the slope and b is the slope of the calibration line.)

- LOQ calculated as $3.33 \times \text{LOD}$.

3.2.2 Validation of the ICP-OES quantitation method

In order to validate the method used for the quantitation of TiO₂ in sunscreen samples, a recovery analysis was carried out. This was carried out by spiking a sunscreen sample with known amounts of TiO₂. The spiked samples were dry-ashed and subjected to ICP-OES analysis as described in Section 2.4.5. Table 3.7 shows the results from the recovery analysis. The recoveries of TiO₂ achieved were quite high. The mean recovery (of three replicate samples) for TiO₂ was $102.32 \pm 2.87\%$ with a RSD of 2.81%.

Table 3.7: Recovery analysis results for TiO₂.

Sample	Spiked concentration /% m/m	Found/% m/m	Recovery/%
1	1.03	1.07	104.51
2	1.26	1.31	103.38
3	1.01	1.00	99.06
Mean recovery			102.32
Standard deviation			2.87
RSD/%			2.81

The electrical furnace dry-ashing method reduces the number of steps and transfers during sample treatment, and hence leads to very good recoveries. The many chemical treatment steps involved in the classical, acid-assisted digestion methods are reduced to only the fusion of the dry-ashed product and finally the dissolution of the molten product. The method used by Salvador *et al.*¹⁸² is quite fast but has more transfer procedures that might result in sample loss besides the high risk of explosions associated with wet, microwave-assisted digestion methods. Moreover, the kind of equipment used here is less sophisticated and is accessible in almost every laboratory.

3.2.3 Levels of TiO₂ in commercial sunscreens

Table 3.8 shows the % m/m levels of TiO₂ determined in the commercial sunscreen products analysed in this study. The percentage levels of TiO₂ presented in Table 3.8 are the mean values of three replicate samples treated in the same way as described in Section 2.4.4.

Table 3.8: Mean % m/m concentrations of TiO₂ measured in 14 suncare products.

Product	SPF No.	% TiO ₂ †	Confidence interval (95%)	% RSD
SA4	40	3.21	0.06	0.79
SA5	40	1.41	0.12	3.39
SA6	8	0.33	0.05	5.78
SA7	15	1.14	0.12	4.12
SA8	30	1.58	0.08	2.03
SA9	40	1.09	0.14	5.07
SA10	15	1.42	0.10	2.95
SA11	30	1.28	0.15	4.65
SA13	15	1.61	0.17	4.25
SA14	30	1.79	0.13	2.82
SA15	4	0.05	0.00	1.23
SA19	25	1.26	0.26	8.20
SA21	40	1.03	0.11	5.78
SA22	30	0.82	0.06	3.12

† Each value is the mean of three replicates.

Fourteen (14) of the twenty-two suncare products purchased contained TiO₂. The levels of TiO₂ in all the samples analysed were less than 5%, with a minimum of 0.05% and a maximum of 3.21%. The RSD values for the TiO₂ percentage concentrations ranged from 0.70 to 8.20%. The

relatively low RSD values and the percent recoveries achieved are a good indication of the robustness of the proposed method. The concentration of TiO₂ in the suncare products was far below the COLIPA limits of 25%.

After quantitation of the active ingredients in the commercial suncare products, it was sought to assess the photostability and photochemical behaviour of the different products upon irradiation in the sun. I also sought to see, among other factors, how the presence of titanium dioxide at such low concentrations as shown in Table 3.8, or its absence would affect the photostability and photochemical behaviour of the different suncare products. These results are presented in Section 3.3.

3.3 Photostability assessment of sunscreens

This section describes the results obtained from the photostability assessment of sunscreens by both UV/VIS transmission spectrophotometry and HPLC techniques. Section 3.3.1 details the information that was labelled on the sunscreen bottles including the UV-filter combinations occurring in the different suncare products.

3.3.1 Characterisation of suncare products

The information on the labelled SPF, protection claimed, sunscreen agents included and antioxidant additives in each of the 22 suncare products is listed in Table 2.1. All the products in the table, except SA12 and SA17 were assessed for their photostabilities. SA12 was a sprayable oil which failed to give a dry film even after exposure to sunlight. Due to the fact that the samples were irradiated at an angle, this product flowed over the sides of the quartz plate making it difficult to handle and analyse its photostability. It was therefore difficult to achieve a uniform product film on the quartz plate. As a result, the photostability assessment of this product was abandoned. SA17 contained no any UV-filters in its formulation, therefore the product was not analysed.

All but five products declared broad-spectrum ultraviolet protection. Nine products used the star rating system to indicate protection in the UVA region, while the rest displayed 'UVA/UVB block' on the bottles. The five products with no claim of broad-spectrum ultraviolet protection were all lipsticks except SA22 which was a cream. The information on the active ingredients in

the formulation and the respective SPF value was given in 21 suncare products. In addition to the active ingredients, 13 products declared that they contained antioxidants especially vitamin E (see Table 2.1).

Table 3.9 displays the different UV-filter combinations contained in the suncare products. The UV-filter combinations are presented in order of increasing complexity and the photostability results are discussed in the order shown in Table 3.9. Only one product contained a single UV-filter (OMC) and that was SA18. The products, SA1, SA2, SA12 and SA20 contained two UV-filters. Only SA15 contained three UV-filters. Most products contained a total of 4 active agents in their UV filtering system and these include: SA3, SA4, SA6-8, SA10, SA13, SA16, SA19 and SA21. Five products (SA5, SA9, SA11 and SA22) contained five UV-filters and one product (SA14) contained 6 active ingredients.

Table 3.9: Characterisation of suncare products.

Suncare Product	Active agents					
SA18	OMC					
SA1, SA2	OMC	Bz-3				
SA12, SA20	OMC	AVO				
SA15	OMC	AVO	TiO ₂			
SA6, SA7, SA8, SA21, SA22	OMC	AVO	TiO ₂	MBC		
SA3	OMC	Bz-3	MBC	OS		
SA4, SA10	OMC	Bz-3	OS	TiO ₂		
SA19	OT	AVO	DOBT	TiO ₂		
SA13	OMC	OCR	BEMT	TiO ₂		
SA16	OMC	MBC	MBBT	BEMT		
SA9	OMC	MBC	MBBT	BEMT	TiO ₂	
SA5	OMC	Bz-3	AVO	OS	TiO ₂	
SA11	OMC	Bz-3	MBC	OS	TiO ₂	
SA14	OMC	OT	AVO	BEMT	DOBT	TiO ₂

OMC was the most common active ingredient, appearing in all but two products, SA17 and SA19. OMC was followed by TiO₂ which occurred in fourteen products. AVO and MBC occurred in about 50% of the suncare products analysed. Bz-3 occurred in seven sunscreens, and OS appeared in five products. The new broad-spectrum UV-filters, MBBT and BEMT, occurred in 4 and 2 products, respectively. Only one product contained OCR, and OT appeared in two products. Section 3.3.2 presents the UV/VIS absorption spectra of the active ingredients contained in the different suncare products analysed in this study.

3.3.2. UV/VIS absorption spectra of sunscreen active ingredients

The absorption spectra of the sunscreen active agents were recorded as described in Section 2.3.4. The UV/VIS absorption spectra of the active ingredients contained in the sun care products investigated in this study have been presented in Figures 2.2a-c.

UV-filters are usually formulated in combination to boost the SPF value of a formulation. This is because the high overlap (see Figures 2.2a-c) of the absorption spectra has an additive effect, resulting in an increase in the amplitude of the resultant absorption spectrum of the combined active ingredients. Thus, the protective capacity of a sunscreen formulation is enhanced. The combination of a UVB filter (OMC) and a UVA filter (AVO) also would result in a wider spectral coverage than would be achieved by the individual active agents.

The active ingredients, Bz-3, MBC, OMC, OCR, OT and OS all absorb maximally in the UVB region. Bz-3 is normally regarded as a UVA filter but it only covers the shorter UVA2 wavelengths (320 – 340 nm) with a maximum absorption around 290 nm in MeOH. There are only three UVA chemical absorbers which offer protection in the longer UVA1 wavelength (340 – 400 nm) range, and these are AVO, BEMT and MBBT. The absorption spectra of the recently approved broad-spectrum absorbers, MBBT and BEMT, span the whole spectral region from 290 nm to about 380 nm (see Figure 2.2a). Thus, they offer broad-spectrum ultraviolet protection. However, these two broad-spectrum UV absorbers are not readily available yet. The commonly used UVA-filter, AVO, shows absorption from about 320 nm to 400 nm and offers better protection in the 380 – 400 nm region than MBBT and BEMT. AVO is normally formulated in combination with UVB filters, thus affording a high SPF value and broad-spectrum protection for a formulation.

Sections 3.3.3 and 3.3.4 give the results obtained from the different experiments carried out to assess the photostability of commercial sunscreens.

3.3.3. Assessment of sunscreen photostability by UV/VIS transmission spectrophotometry and HPLC

This section presents the results from the experimental work (Sections 2.5.2.3, 2.5.3 and 2.6) carried out to assess the photostability behaviour of commercial sunscreen products both on

quartz plate and in solution. The details of the analyses carried out to assess the photostability of each sunscreen product are given in Table 3.10.

Table 3.10: Details of the photostability analyses performed on each sunscreen product.

Sunscreen Product	SPF No.	Type of Analysis		
		Quartz plate	Solution	HPLC
SA1	5	✓	✓	✓
SA2	10	✓	✓	✓
SA3	30	✓	✓	✓
SA4	40	✓	-	-
SA5	40	✓	-	-
SA6	8	✓	✓	-
SA7	15	✓	-	-
SA8	30	✓	-	-
SA9	40	✓	-	-
SA10	15	✓	-	-
SA11	30	✓	-	-
SA12	5	-	-	-
SA13	15	✓	-	-
SA14	30	✓	-	-
SA15	4	✓	✓	✓
SA16	30	✓	-	✓
SA17	-	-	-	-
SA18	6	✓	-	-
SA19	25	✓	-	-
SA20	30	✓	✓	✓
SA21	40+	✓	✓	✓
SA22	36	✓	-	-

For ease of comparison, the plots of the changes in the spectral transmittance of products dispersed in solution have been included after the quartz plate plot for each of the products analysed on quartz plate and in solution. For all the quartz plates, the application density was 1 mg cm^{-2} and for those in solution, the loading was 1 mg cm^{-3} . The method detailed in Section 2.5.4.1 was used to distinguish between photostable and photounstable products. In addition, the chromatograms of the sunscreen samples analysed for their photostability by HPLC after irradiation for 6 hours on petri-dishes are presented along with the spectral transmission plots. The application density for all the petri-dishes was 1 mg cm^{-2} as with the quartz plates.

3.3.3.1 Sunscreens containing OMC

Figure 3.1 displays the spectral transmission change of SA18 on quartz plate with irradiation time. As shown in Table 3.7, SA18 contained only OMC (see Figure 2.2b for absorption spectrum) in its UV filtering system. Therefore, SA18 would not be expected to offer any UVA protection. No claim of UVA protection was made on the label.

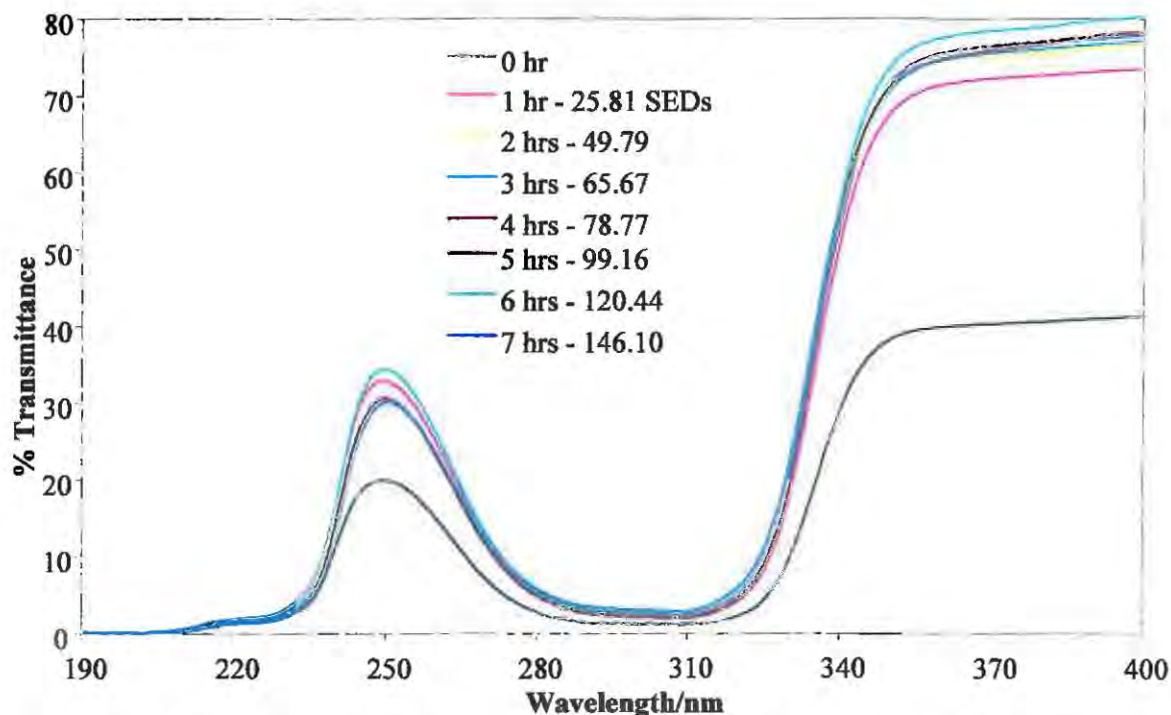


Figure 3.1: Changes in the spectral transmission of SA18 on a quartz plate (1 mg cm^{-2}) with increasing solar irradiation.

The large increase in transmitted radiation in the UVA region in the first hour shows that the vehicle or emulsion is affected by solar UVR, making it more transparent. This is because the bottom-most (0 hr) spectrum is reproducible for up to three hours without exposure to sunlight. Hence this increase in transmittance does not reflect any losses in drying of the sunscreen film. As shown in Figure 3.2 above, the product showed a good photostability in the UVB region. The slight change in photoprotection in the UVB region, though insignificant, can be speculated to be a result of the photoisomerisation of OMC to the *cis*-isomer, since OMC is known to photoisomerise to the *cis*-isomer upon exposure to solar radiation.¹³¹ The shape of the transmission spectra remained essentially the same throughout the irradiation period. Overall, the product lost 1.11 and 26.58 % of photoprotection in the UVB and UVA regions,

respectively. Although the product is not UVA protective, it was classified as photounstable in the UVA region based on the spectral transmission change observed after irradiation in the sun.

3.3.3.2 Sunscreens containing OMC and Bz-3

Figure 3.2 shows the change in the spectral transmission of SA1 on quartz plate with irradiation time. The product's UV filtering system consisted of Bz-3 (UVB and short UVA), and OMC (UVB). There is a slight improvement in the UVA filtering capacity of the product by the addition of Bz-3. Bz-3, however, only covers the shorter wavelength UVA (320 - 340 nm) region and is transparent in the longer wavelength UVA region (340 – 400 nm). The absorption spectrum of Bz-3 can be found in Figure 2.2c.

The product displayed a photoinstability of 31.13 and 3.14% in the UVA and UVB regions, respectively, after 2 hours of irradiation. The photoinstability in the UVB region (3.14%), though below the 5% threshold, is significantly higher than that observed for SA18 containing OMC alone. Bz-3 is generally considered a safe and photostable UV-filter. Sewlall¹²² found that Bz-3 did not cause single strand breaks in DNA as observed with benzophenone-1 and benzophenone-9. However, Serpone *et al.*⁷⁴ reported that OMC degraded faster when in combination with Bz-3. The increase in the photoinstability observed in SA1 in the UVB region can be surmised to be a result of the photoisomerisation of OMC caused by the photosensitising effect of Bz-3.²⁰⁷ SA1 was classified photounstable in the UVA region.

Figure 3.3 shows the change in the spectral transmission of SA1 dissolved in a solvent mixture of isopropanol-dichloromethane-cyclohexane (spectrum shown in Figure 2.18). The poor protection in the UVA region is quite clear, with radiation of wavelengths greater than 330 nm being transmitted. The product displayed very high photostability in solution throughout the irradiation period. This can be explained by the fact that, the solvent absorbs some of the UVR, thus stabilizing the UV filtering system.

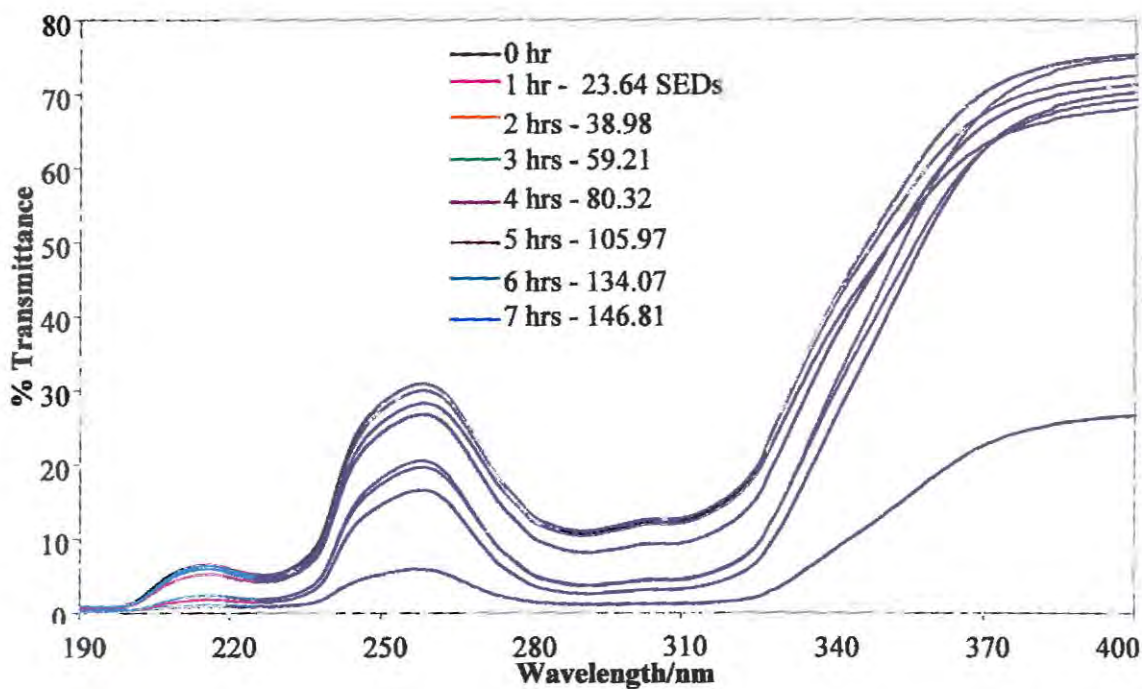


Figure 3.2: Changes in the spectral transmission of SA1 on a quartz plate (1 mg cm^{-2}) with increasing solar irradiation.

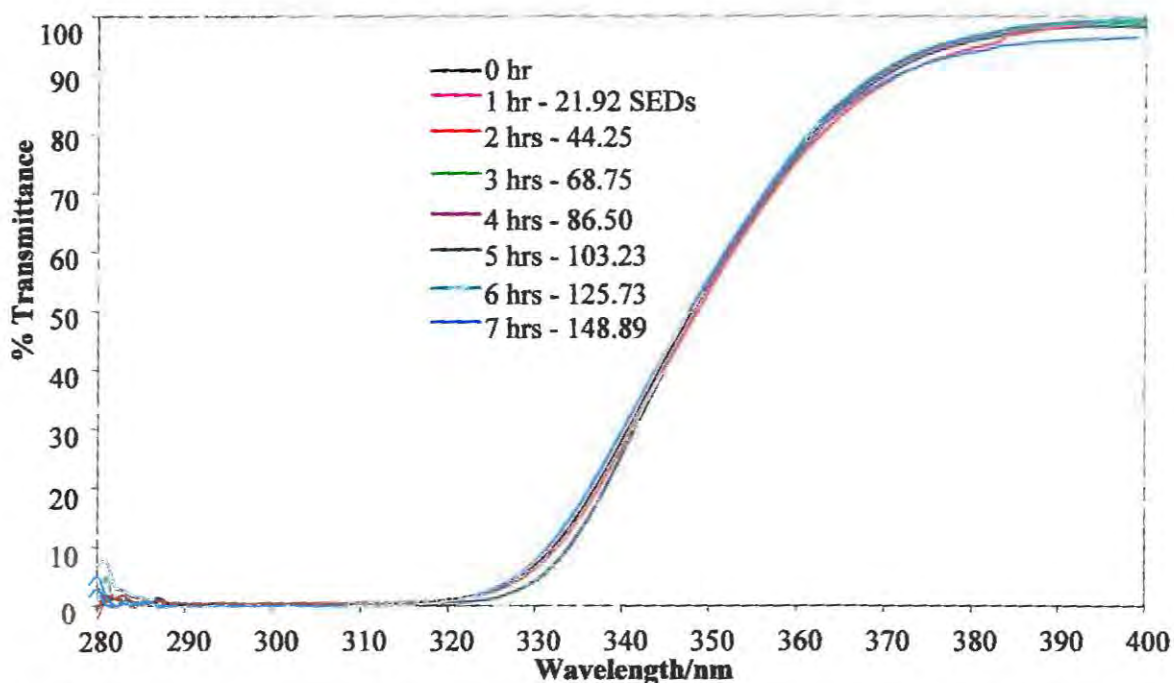


Figure 3.3: Changes in the spectral transmission of SA1 in solution (1 mg cm^{-3}) with increasing solar irradiation. Transmission spectra were recorded in a 1-cm pathlength quartz cuvette with the solvent (isopropanol-cyclohexane-dichloromethane 50:37.5:12.5% (v/v)) in the reference beam.

SA1 was also analysed for its photostability by HPLC. The chromatograms of both the un-irradiated samples and the irradiated samples are presented in Figures 3.4 and 3.5, respectively. As displayed in Table 3.9, SA1 only contained two active ingredients in its UV filtering system. This was confirmed by HPLC as shown in Figure 3.5. Bz-3 eluted at 3.858 minutes and OMC at 12.344 minutes. The chromatographic conditions used are as shown in the chromatograms.

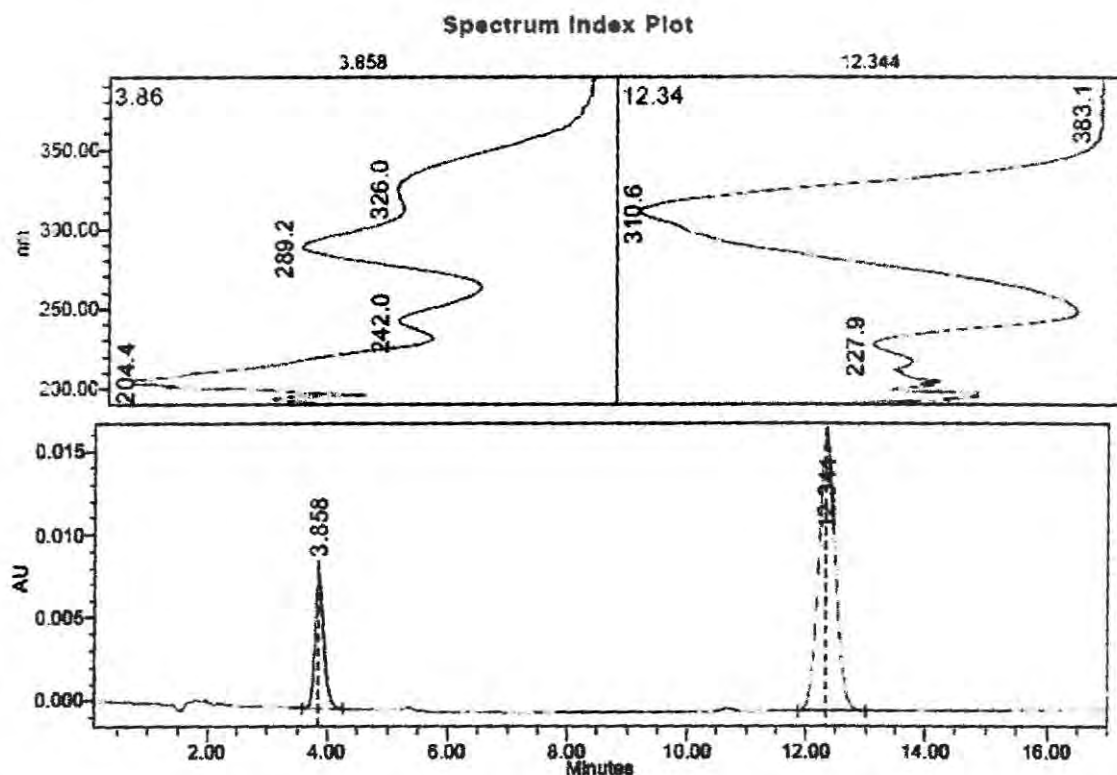


Figure 3.4: Chromatogram of an unirradiated sample of SA1. The chromatographic conditions used were: Phenomenex RP-C₁₂ 80 Å column, mobile phase - MeOH-H₂O 84:16% (v/v), injection volume - 20 µL, flow rate - 1 mL min⁻¹, and detection wavelength - 310 nm. The order of elution is Bz-3 and OMC.

Figure 3.5 shows the chromatogram of an irradiated sample of SA1. An additional peak can be seen at 11.158 minutes and this can be ascribed to the *cis*-form of OMC. It is well documented that upon exposure of OMC to UVR, it rapidly photoisomerizes to the *cis*-form until a photostationary equilibrium is established in both polar and non-polar solvents.^{117, 140} Kowlaser *et al.*¹³² showed that *cis*-OMC has a lower molar absorptivity ($1.84 \times 10^4 \text{ dm}^3 \text{ mol}^{-1} \text{ cm}^{-1}$) than the common *trans*-OMC ($2.45 \times 10^4 \text{ dm}^3 \text{ mol}^{-1} \text{ cm}^{-1}$). Again, *cis*-OMC absorbs maximally at a shorter wavelength of 305 nm than *trans*-OMC (310 nm) in MeOH. A comparison of the UV

absorption spectrum of this photoproduct with those from literature shows a good agreement.^{114,}
¹¹⁷ Therefore, the photoinstability observed in the UVB region for SA18 and SA1 can be ascribed to the photoisomerisation of OMC. The peak of the photoproduct was well resolved from the other two peaks. HPLC quantitation studies after exposure of the product to sunlight for 6 hours resulted in a percentage loss of 19.33% for OMC and a slight gain for Bz-3 of - 5.56%.

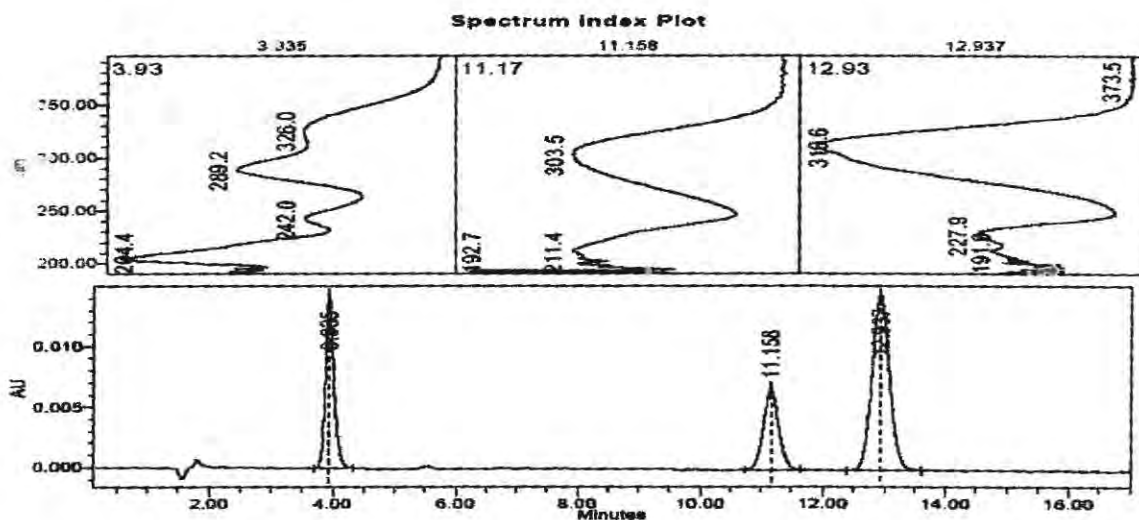


Figure 3.5: Chromatogram of an irradiated sample of SA1. The chromatographic conditions used were: Phenomenex RP-C₁₂ 80 Å column, mobile phase - MeOH-H₂O 84:16% (v/v), injection volume - 20 µL, flow rate - 1 mL min⁻¹, and detection wavelength - 310 nm. The order of elution is Bz-3, *cis*-OMC and *trans*-OMC.

Figure 3.6 displays the changes in the spectral transmission of SA2 on a quartz plate. This product contained the same UV filtering system as SA1. Hence, their transmission spectra are expected to be similar (see Figure 3.2). There is again poor UVA (320 – 400 nm) filtering capacity in this product as observed with SA1. However, there was not as large a change in transmittance in both the UVB (0.28%) and UVA (23.77%) regions as observed for SA1. This is perhaps because of a higher concentration of the individual actives in SA2 than SA1 (see Table 3.5).

Figure 3.7 shows the changes in the spectral transmission of SA2 in solution with irradiation time. The product exhibited a high photostability in both the UVB and UVA regions as observed for SA1 (see Figure 3.3). The spectral transmission curves of the two products appear similar.

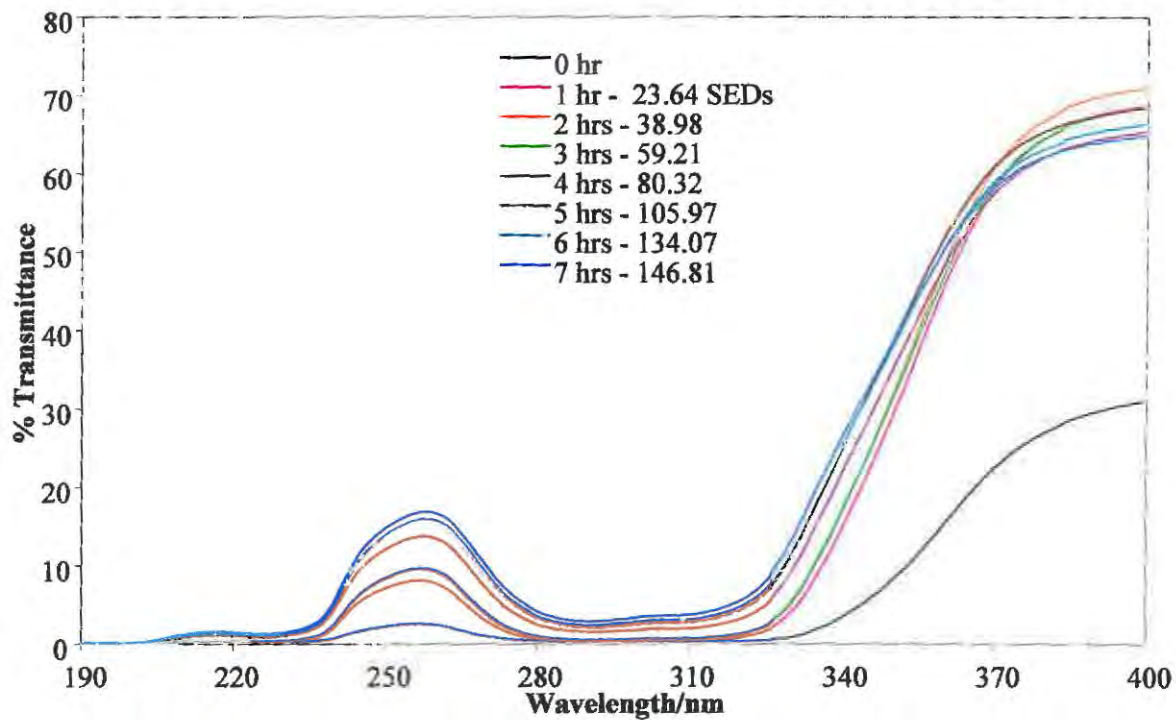


Figure 3.6: Changes in the spectral transmission of SA2 on a quartz plate (1 mg cm^{-2}) with increasing solar irradiation.

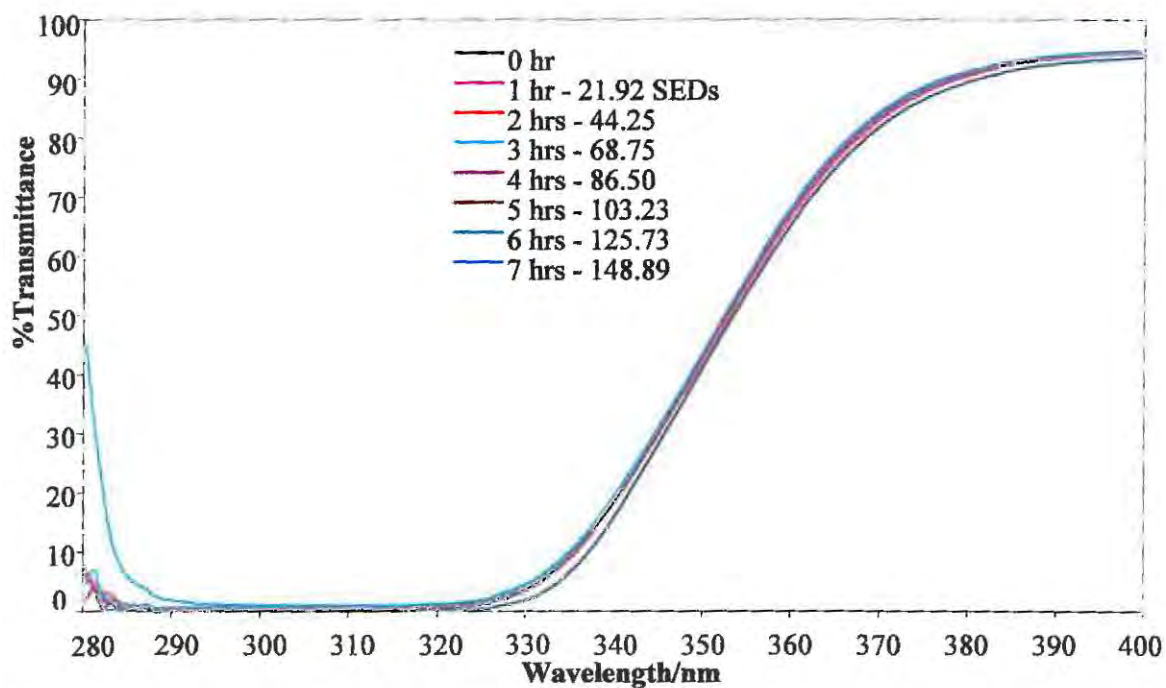


Figure 3.7: Changes in the spectral transmission of SA2 in solution (1 mg cm^{-3}) with increasing solar irradiation. Transmission spectra were recorded in a 1-cm path-length quartz cuvette with the solvent (isopropanol-cyclohexane-dichloromethane 50:37.5:12.5% (v/v)) in the reference beam.

3.3.3.3 Sunscreens containing OMC and AVO

Figure 3.8 presents the spectral transmission change of SA20 on a quartz plate with irradiation time. The product can be said to offer poor broad-spectrum protection. No claim of broad-spectrum protection was made on the label. The UV filtering system consisted of OMC and AVO. AVO is the most commonly used UVA filter. The UV/VIS absorption spectrum of AVO can be found in Figure 2.2b. The poor protection in the UVA region is probably due to the low concentration of AVO (0.53%) in the formulation (see Table 3.5).

Exposure of SA20 to sunlight resulted in a large loss in the photoprotective capacity of the product in the UVA range, whereas there was a high photostability in the UVB region. The product lost nearly 20% of its photoprotective power in the UVA range upon exposure to solar radiation for 2 hours. The product was classified as photounstable in the UVA region. As in other products containing AVO, the loss of photoprotection in the UVA region can be said to be due to the photoloss of AVO. Several studies on AVO have shown that the sunscreen agent photodegrades upon irradiation with UVR.^{113, 140, 143} AVO is reported to photodegrade in non-polar organic solvents like cyclohexane, and is more photostable in polar protic organic solvents such as MeOH.^{112, 113} Studies have shown that AVO photoisomerises upon irradiation to its keto form which absorbs in the UVC region.^{112, 113} AVO is also reported to photosensitise the photoloss of OMC when the two are formulated in combination.^{116, 117, 143} Nevertheless, the photosensitising effect of AVO on OMC was not evident at this point since there was no change in photostability of the product in the UVB region.

Overall, the product displayed an increase in transmittance of 0.07 and 35.88% in the UVB and UVA regions, respectively. The photoinstability increased with irradiation time. SA20 was also analysed for its photostability behaviour in solution.

Figure 3.9 displays the spectral transmission change of SA20 dispersed in solution with irradiation time. The initial transmission profiles (before irradiation) of SA20 in solution were very similar to those from the quartz plate.

Whereas the product (SA20) displayed a high photoinstability on quartz plate, there was a slight loss in photostability when the product was dispersed in solution. There was a small loss in photoprotection in the UVA region in solution (5.05%) as opposed to 19.18% for the quartz plate (Figure 3.8) after 2 hours of irradiation. Again, there was no change in transmission in the

UVB region. The product was photounstable both on quartz plate and in solution in the UVA region.

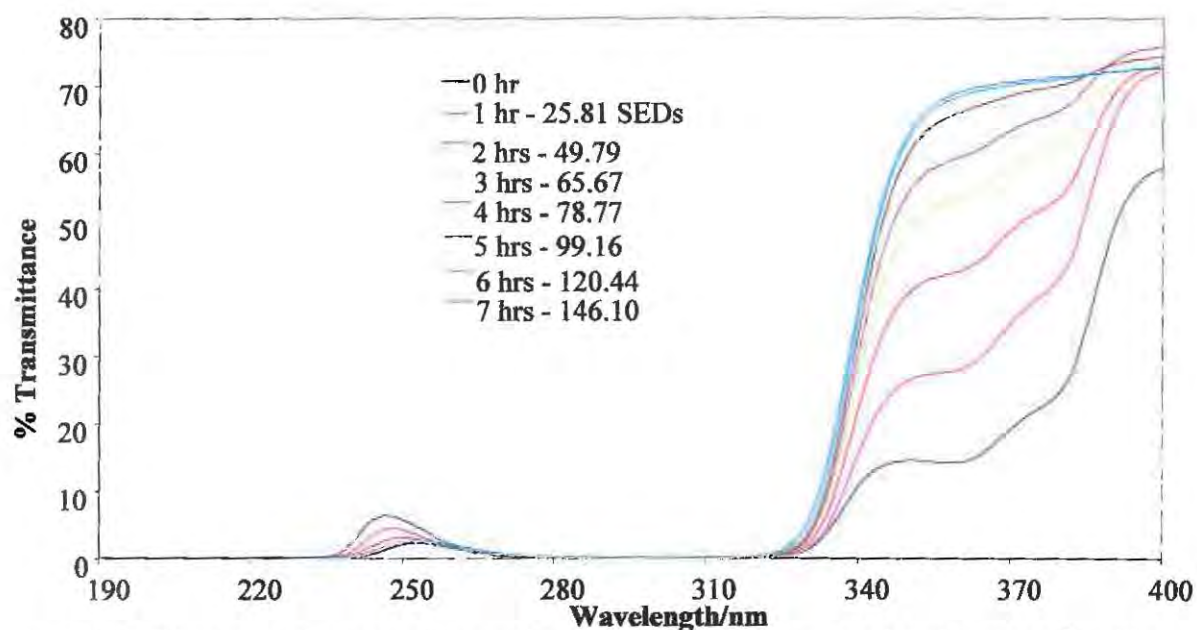


Figure 3.8: Changes in the spectral transmission of SA20 on a quartz plate (1 mg cm^{-2}) with increasing solar irradiation.

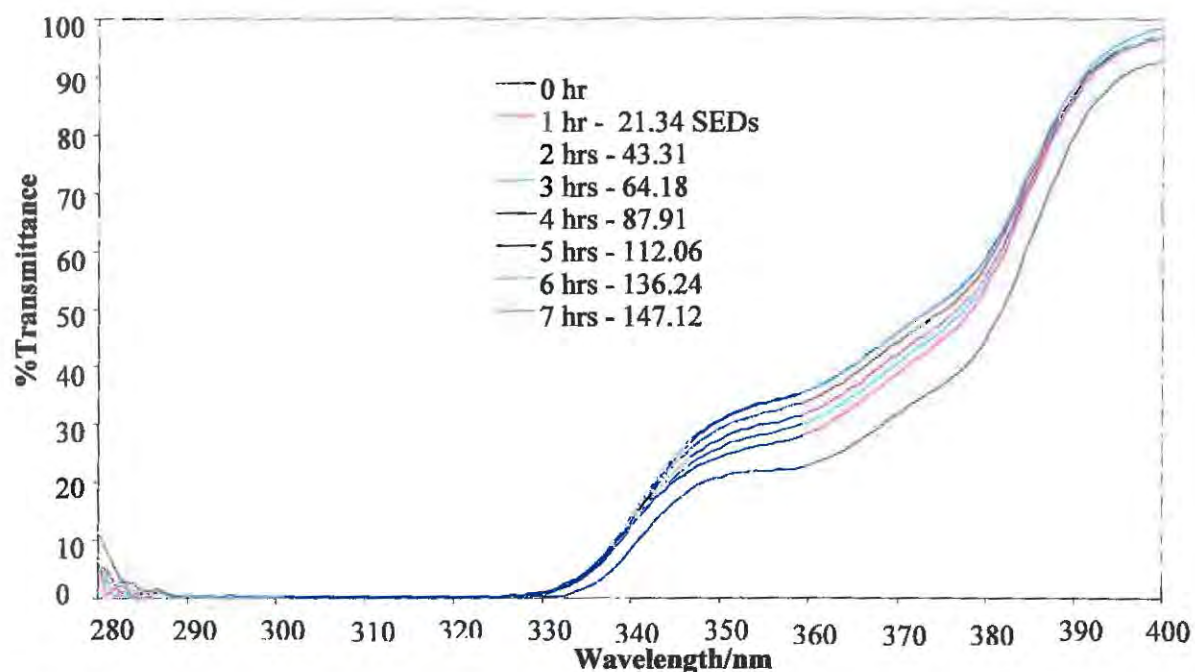


Figure 3.9: Changes in the spectral transmission of SA20 in solution (1 mg cm^{-3}) with increasing solar irradiation. Transmission spectra were recorded in a 1-cm quartz cuvette with the solvent (isopropanol-cyclohexane-dichloromethane 50:37.5:12.5% (v/v)) in the reference beam.

SA20 was analysed for its photostability behaviour by HPLC. Figure 3.10 displays the chromatogram of an unirradiated sample of SA20. The product contained two active ingredients as the UV filtering system. The chromatogram confirmed the presence of AVO and OMC as seen by the two peaks in the chromatogram and their associated UV absorption spectra. However, the level of AVO in the product was very low (Table 3.5). The low concentration of AVO in the formulation also explains the poor protection in the UVA region observed in Figure 3.9.

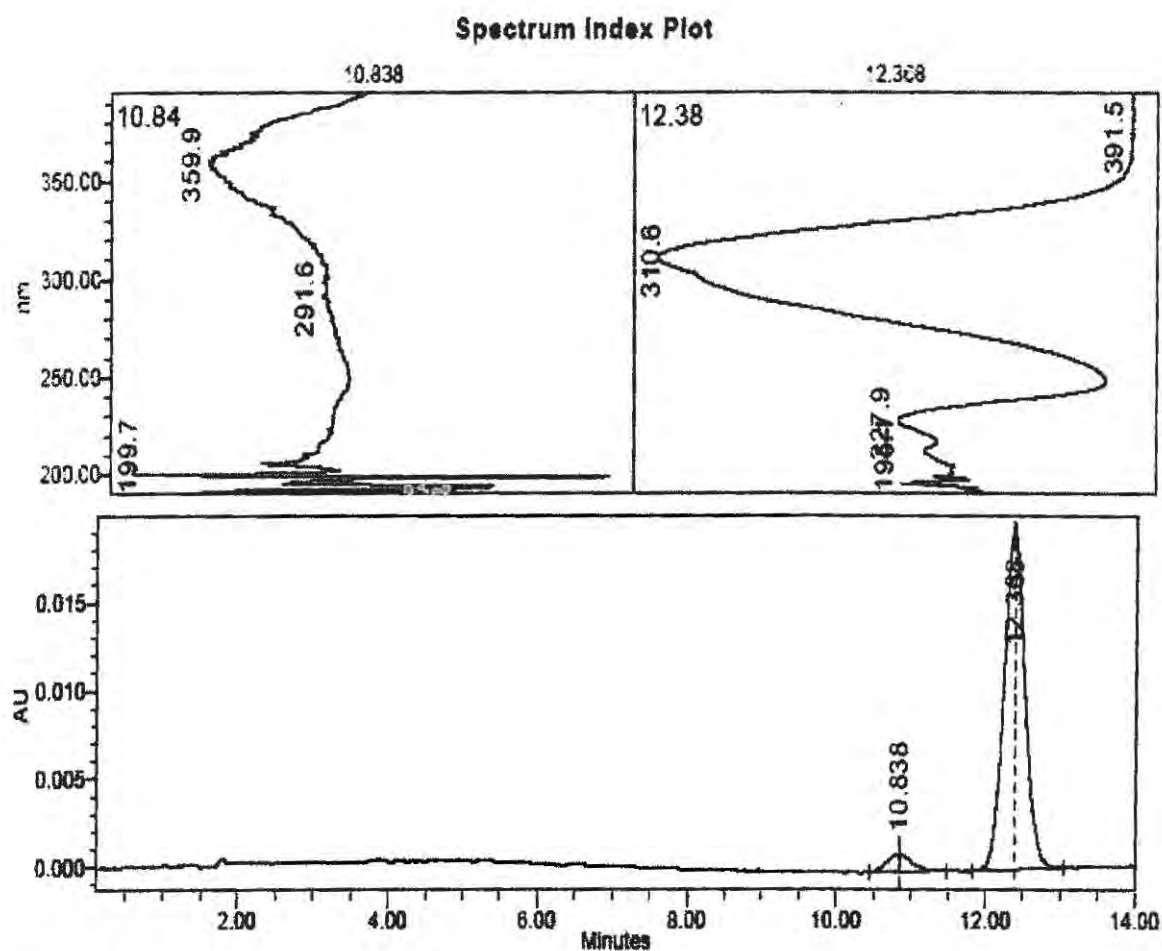


Figure 3.10: Chromatogram of an unirradiated sample of SA20. The chromatographic conditions used were: Phenomenex RP-C₁₂ 80 Å column, mobile phase - MeOH-H₂O 84:16% (v/v), injection volume - 20 µL, flow rate - 1 mL min⁻¹, and detection wavelength - 330 nm. The order of elution is AVO and OMC.

Analysis of the irradiated sample of SA20 by HPLC yielded the chromatogram shown in Figure 3.11. AVO was no longer detectable in the irradiated sample, and only one extra peak was observed eluting at 11.097 minutes (assigned as *cis*-OMC). The UV absorption spectrum of the

photoproduct looks similar to the one observed in Figure 3.5, for SA1. AVO was not detectable probably because its concentration was now below the detection limit of 2.32 μM (see Table 3.2) or it completely photodegraded to unknown photoproducts which do not absorb in the 250 to 400 nm wavelength window. Deflandre *et al.*¹⁴⁰ reported that AVO lost about 50% of its photoprotective power when exposed to solar UVR for just 1 hour. As mentioned above, AVO is more photostable in protic organic solvents (MeOH)¹¹³ and less stable in aprotic organic solvents (cyclohexane).¹¹²

HPLC quantitation of the irradiated product showed a loss of 35.35% for OMC. A significantly high amount of OMC was lost in this product as compared with SA1 discussed above. This result perhaps supports the previous findings that AVO photosensitises the photoloss of OMC as explained above.

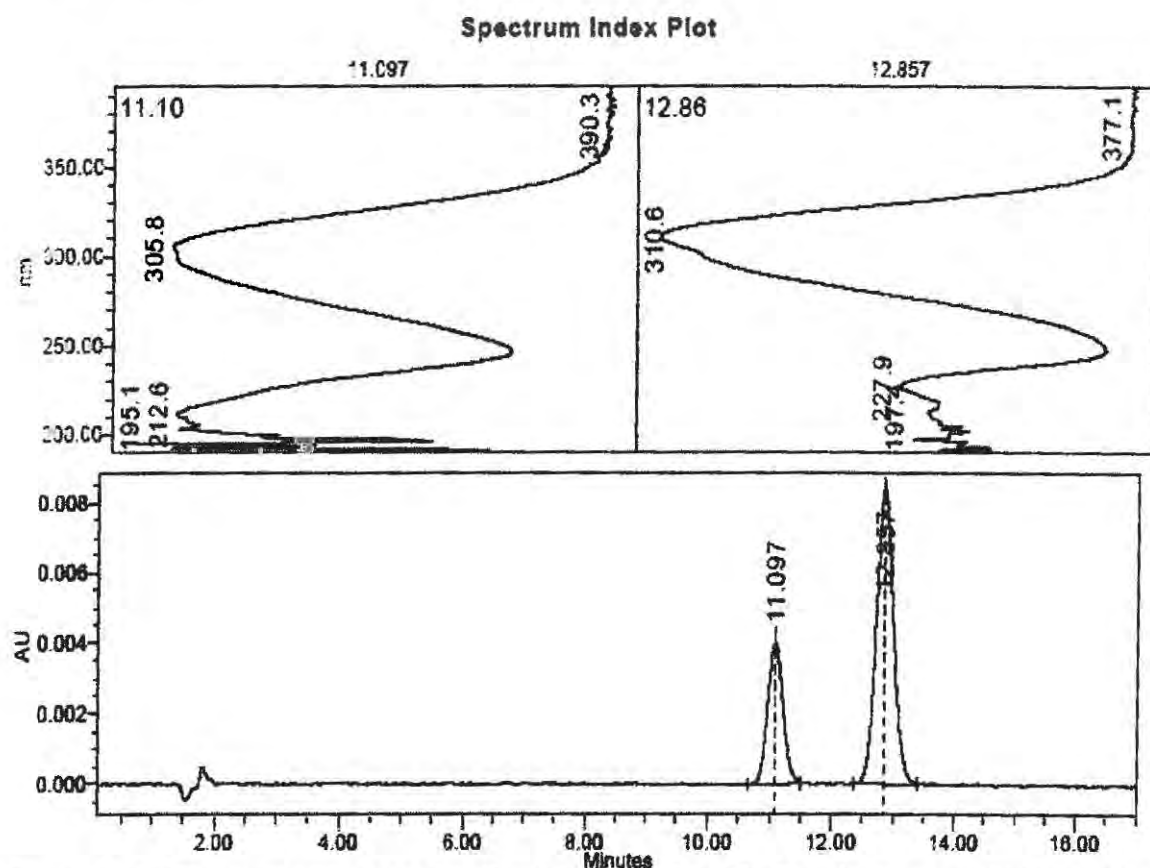


Figure 3.11: Chromatogram of an irradiated sample of SA20. The chromatographic conditions used were: Phenomenex RP-C₁₂ 80 Å column, mobile phase - MeOH-H₂O 84:16% (v/v), injection volume - 20 μL , flow rate - 1 mL min⁻¹, and detection wavelength - 330 nm. The order of elution is *cis*-OMC and *trans*-OMC.

3.3.3.4 Sunscreen containing OMC, AVO and TiO₂

Figure 3.12 displays the change in the spectral transmission of SA15 on a quartz plate with irradiation time. The product consisted of AVO, OMC and TiO₂ as the active ingredients. The UV filtering system of SA15 is close to that of SA20 except that SA15 contains TiO₂ (see Table 3.9). Evident from the 0 SED spectrum (dark blue line) is the good broad-spectral coverage which was in agreement with the claim of broad-spectrum protection on the label. SA15 displayed a broader spectral coverage than observed for SA20. This is probably because of a significantly higher concentration of AVO (1.12%) in SA15 than that found for SA20 (0.53%), as displayed in Table 3.5. The good broad spectral coverage of SA15 can also be attributed to the presence of TiO₂. TiO₂ is normally employed to boost the SPF value and improve the broad-spectrum protection of a formulation. The absorption spectrum of the cosmetic grade TiO₂ can be found in Figure 1.1.

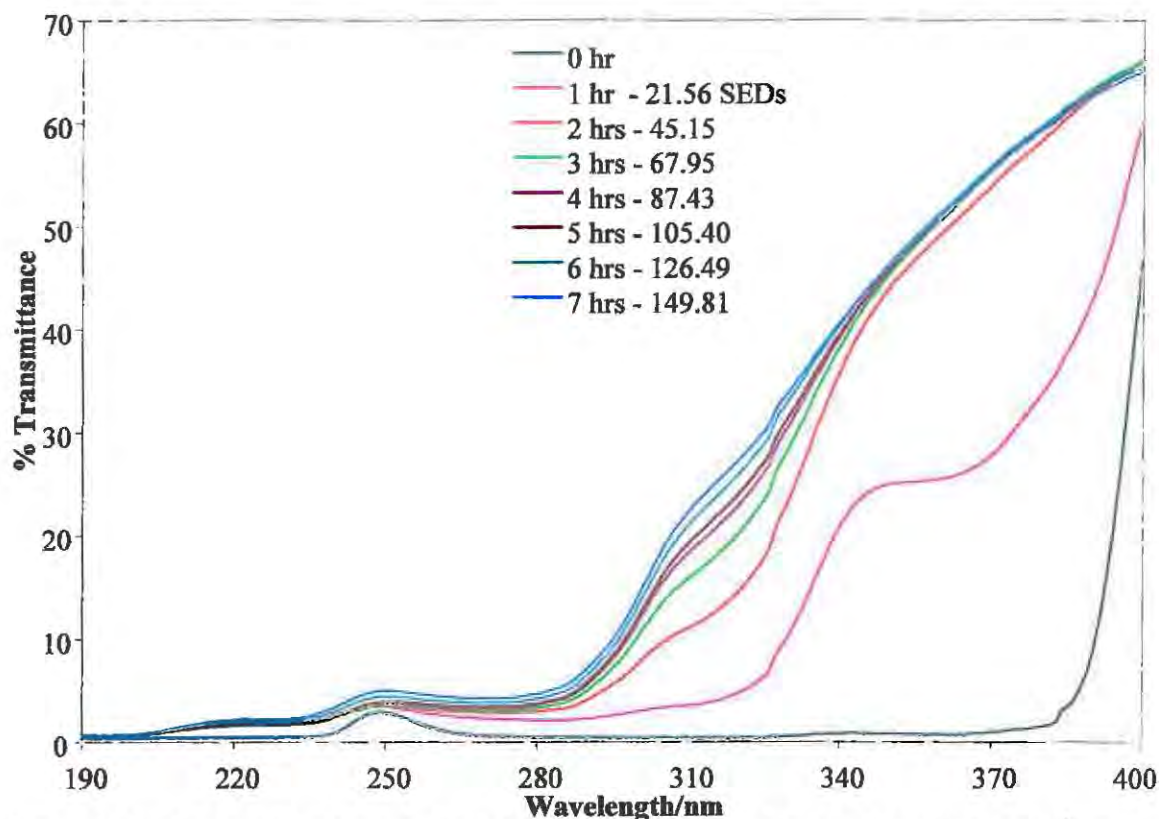


Figure 3.12: Changes in the spectral transmission of SA15 on a quartz plate (1 mg cm⁻²) with increasing solar irradiation.

However, the product was easily photo-inactivated upon exposure to sunlight. There was a sharp loss in photoprotection in the first hour of exposure to solar radiation. The shapes of the

transmission spectra of the product were significantly changed by exposure to sunlight. The product showed photoinstability in both the UVA and the UVB regions. Loss of photoprotection in the UVA region is attributed to the photoloss of AVO as observed for SA20. The photoinstability in the UVB region may be due to the photoisomerisation of OMC to the *cis*-isomer. In just two hours of irradiation in the sun, there was a loss of 8.80 and 41.37% of photoprotective power in the UVB and UVA regions, respectively. The photoinstabilities registered by SA15 are significantly higher than what was observed for SA20 (see Figure 3.8). Whereas SA15 was photounstable in the UVB region, SA20 displayed a high photostability. It can be surmised that the presence of TiO₂ photocatalysed the loss of OMC, thus resulting in a loss in the photostability of the sunscreen formulation in the UVB region. SA15 was also analysed in solution for its photostability behaviour.

Figure 3.13 shows the spectral transmission change registered by the product dissolved in solution upon irradiation in the sun.

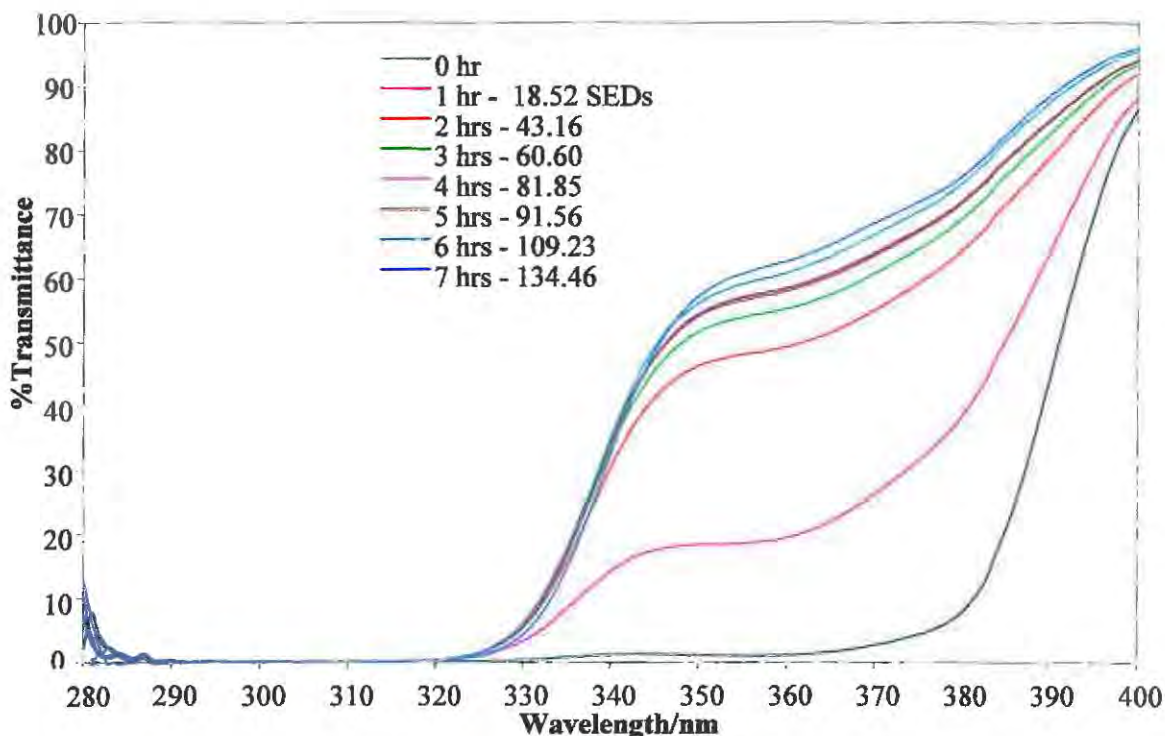


Figure 3.13: Changes in the spectral transmission of SA15 in solution (1 mg cm⁻³) with increasing solar irradiation. Transmission spectra were recorded in a 1-cm pathlength quartz cuvette with the solvent (isopropanol-cyclohexane-dichloromethane 50:37.5:12.5% (v/v)) in the reference beam.

The initial transmission spectra (before irradiation) of SA15 dispersed in solution and on a quartz plate look similar. As can be seen in Figure 3.13, the product displayed a high photostability in the UVB region, whereas in the UVA region, the product behaved in more or less the same way as observed on a quartz plate (Figure 3.12). Photostability in the UVB region can be ascribed to the stabilising effect of the solvent since it absorbs some of the UVR incident on the sample. The photostability behaviour of SA15 in solution was different from that observed in SA1, SA2, and SA20 where high photostabilities were observed. Photoinstabilities of SA15 in solution (36.59%) and on quartz plate (41.37%) for the UVA region were comparable. SA15 was photounstable both in solution and on quartz plate.

SA15 was analysed for its photostability by HPLC. Figure 3.14 presents the chromatogram of an unirradiated sample of SA15. The chromatogram showed the presence of two peaks. The peaks eluting at 10.776 and 12.282 minutes were assigned as AVO and OMC, respectively.

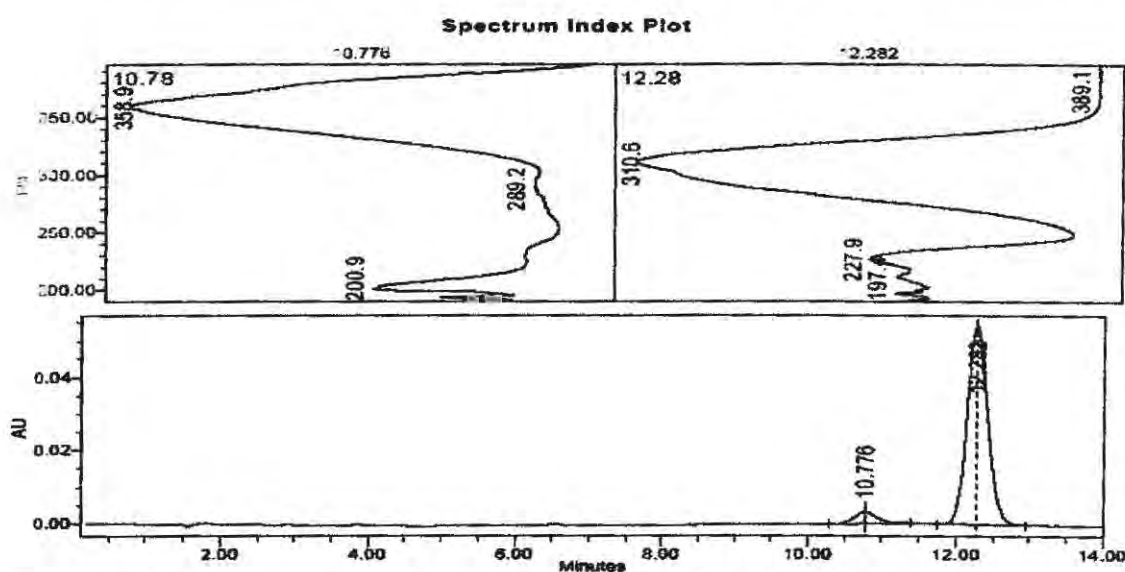


Figure 3.14: Chromatogram of an unirradiated sample of SA15. The chromatographic conditions used were: Phenomenex RP-C₁₂ 80 Å column, mobile phase - MeOH-H₂O 84:16% (v/v), injection volume - 20 µL, flow rate - 1 mL min⁻¹, and detection wavelength - 330 nm. The order of elution is AVO and OMC.

Analysis of an irradiated sample of SA15 by HPLC yielded the chromatogram shown in Figure 3.15. In Figure 3.14 only two peaks were observed, whereas for the irradiated sample, several peaks were observed in the chromatogram as displayed in Figure 3.15. The peaks eluting at 11.099 and 12.858 minutes were assigned as *cis*-OMC and *trans*-OMC, respectively. A comparison of the absorption spectrum of the peak eluting at 10.720 and the one assigned as *cis*-

OMC in Figure 3.11 (SA20) shows that it is the same photoproduct. The peak of AVO (10.776 min, Figure 3.14) could not be seen anymore in the irradiated sample even when the chromatogram was processed at 358 nm (λ_{\max} of AVO). The other unidentified peaks are probably of photoproducts formed from the photodegradation of AVO and/or OMC upon irradiation of SA15 in the sun. The photoproducts still remain to be identified.

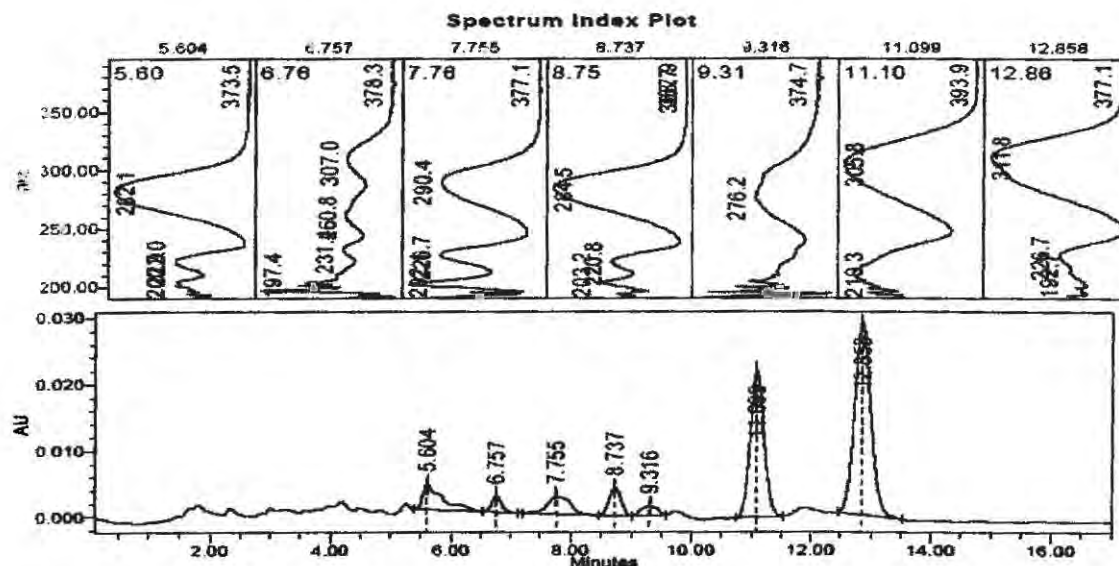


Figure 3.15: Chromatogram of an irradiated sample of SA15. The chromatographic conditions used were: Phenomenex RP-C₁₂ 80 Å column, mobile phase - MeOH-H₂O 84:16% (v/v), injection volume - 20 μ L, flow rate - 1 mL min⁻¹, and detection wavelength - 330 nm.

From Figure 3.15, the associated UV absorption spectra of the photoproducts show that they all absorb in the UVB and the longer wavelength UVC range. That probably explains the slight photoinstability of the product in the UVB region. The loss in photostability of SA15 in the UVB region could be a result of the photoloss of OMC through photoisomerisation and/or photodegradation.

The loss of photoprotection observed for SA15 in the UVA region can be attributed to the photodegradation and photoisomerisation of AVO. AVO is said to photodegrade to a number of photoproducts with the major ones being 4-*t*-butyl benzoic acid, 4-*t*-methoxy benzoic acid and the keto form that absorbs maximally at around 270 nm.¹¹³ It is known that AVO undergoes keto-enol tautomerisation upon exposure to solar radiation. The common enol form has a λ_{\max} of between 350 to 365 nm and the keto form absorbs around 270 nm. Andrea *et al.*²⁰⁸ observed a decrease in absorption of the common enol form ($\lambda_{\max} = 350$ nm) in irradiated solutions of AVO (in acetonitrile) which was replaced by an increase in absorption at 260 nm which they

attributed to the keto form. It can be speculated that some of the new peaks seen in Figure 3.15 are of isomers of the keto form since they show maximum absorption in the 270 - 290 nm range.

HPLC quantitation showed that about 37% of OMC is lost to photoisomerisation and/or photodegradation in SA15. This loss is relatively higher than the amount lost in SA20 after irradiation. The increased loss of OMC in SA15 can be said to be due to the synergy between the photosensitising effect of AVO and the photocatalytic effect of TiO₂.²⁰⁹ As mentioned above, AVO can act as a triplet photosensitiser,¹¹⁷ causing the photoloss of OMC through photo-isomerisation since its triplet energy is higher than that of OMC.¹¹⁶ Cantrell *et al.*²¹⁰ demonstrated that 266 nm laser photolysis of AVO solutions leads to the formation of the triplet state of the keto form which in turn is quenched by molecular oxygen. It can be surmised that AVO photosensitises the photoloss of OMC through energy transfer from the keto triplet state.

3.3.3.5 Sunscreens containing OMC, AVO, MBC and TiO₂

Figure 3.16 presents the change in the spectral transmission of SA6 on a quartz plate with irradiation time. From the 0 SED spectrum (dark blue), it is evident that this product offered broad spectrum protection, covering effectively both the UVA and UVB regions. In addition to AVO, TiO₂ and OMC, the UV filtering system of SA6 also contained MBC (see Figure 2.2c for the absorption spectrum) which is a UVB filter. The manufacturer claimed UVA and UVB protection which indeed was shown to be the case. The broad spectral coverage of SA6 can be ascribed to the presence of AVO and TiO₂.

The product registered an overall photoinstability of 5.60% and 0.54% in the UVA and UVB regions, respectively after 7 hours of irradiation. As opposed to the high photoinstability observed for SA15 and SA20, SA6 displayed a relatively high photostability in both the UVB and UVA regions. MBC is normally formulated in combination with AVO to stabilise the latter.^{134, 210} Therefore, the relatively high photostability in the UVA region can be ascribed to the stabilising effect of MBC on AVO. The product displayed a very high photostability yet it had an SPF value of only 8. There was a steady increase in photoinstability with increase in irradiation time.

SA6 was again analysed for its photostability behaviour in solution. The spectral transmission change of SA6 with irradiation time is shown in Figure 3.17. SA6 displayed a high photostability in solution as observed for SA1 and SA2 (see Figures 3.3 and 3.7). Even the loss



of AVO (which is normally characterized by an increase in transmittance in the long wavelength UVA region) was not observed in Figure 3.17.

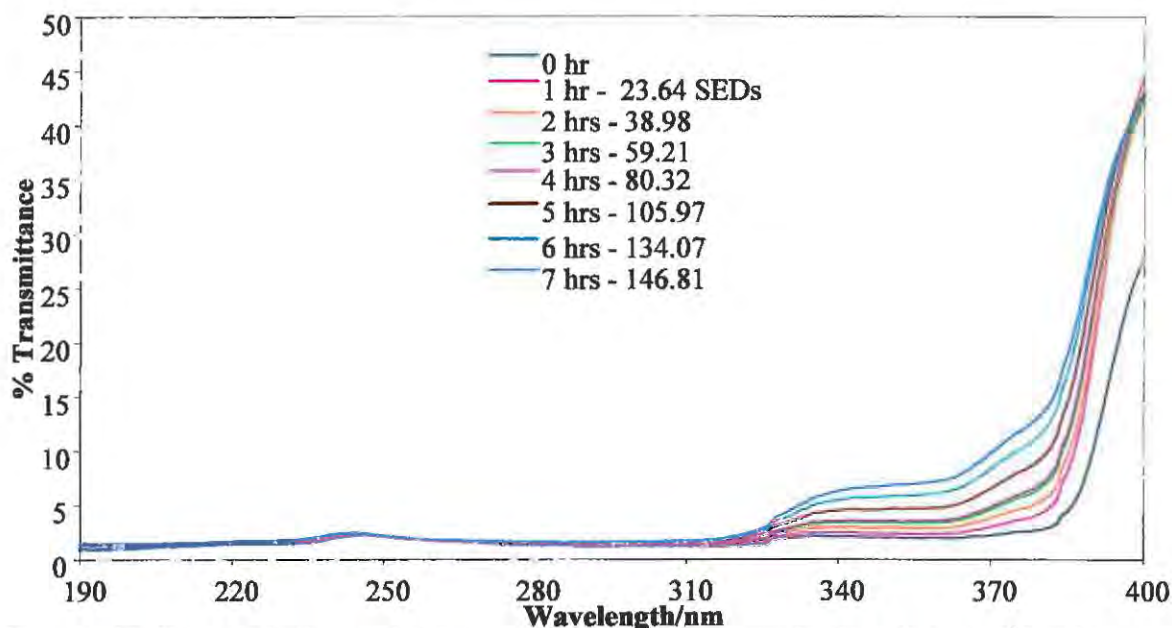


Figure 3.16: Changes in the spectral transmission of SA6 on a quartz plate (1 mg cm^{-2}) with increasing solar irradiation.

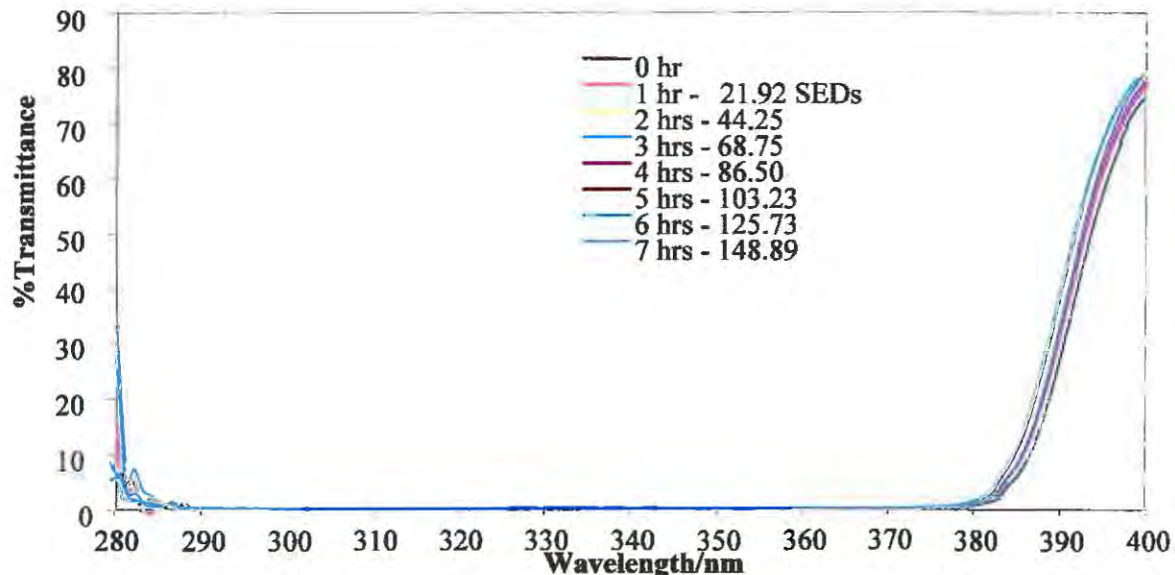


Figure 3.17: Changes in the spectral transmission of SA6 in solution (1 mg cm^{-3}) with increasing solar irradiation. Transmission spectra were recorded in a 1-cm pathlength quartz cuvette with the solvent (isopropanol-cyclohexane-dichloromethane 50:37.5:12.5% (v/v)) in the reference beam.

system as the last two products, SA6 and SA7 (see Table 3.9). The product displayed good broad-spectrum UV protection (in accordance with the claim on the label) and high photostability. The slight loss in overall photoprotection in the UVA (2.79%) and UVB (0.06%) regions was insignificant in view of the set threshold value of 5% for 2 hours of irradiation. Again, like SA6 and SA7, there was a slight loss in photoprotection in the long wavelength UVA (340 – 400 nm) region. The increase in transmittance with irradiation time observed in the long wavelength UVA range was ascribed to the photoloss of AVO. The photo-destabilising effect of AVO and TiO₂ on OMC is not evident in the products, SA6-8 as observed in SA15. Photoinstability increased with increase in irradiation time (or the UV dose delivered to the sample).

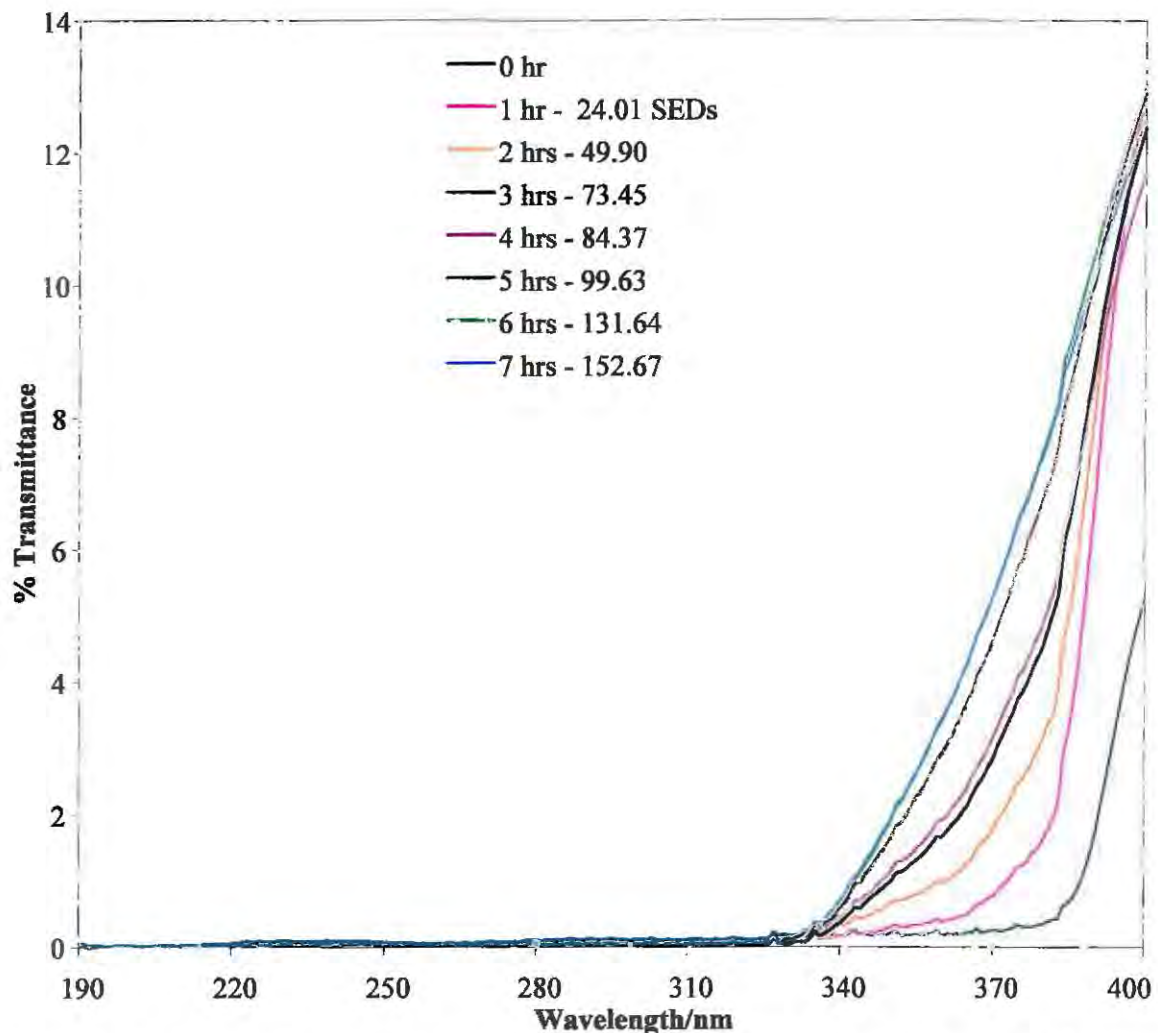


Figure 3.19: Changes in the spectral transmission of SA8 on a quartz plate (1 mg cm⁻²) with increasing solar irradiation.

Figure 3.18 shows the change in the spectral transmission of SA7 on a quartz plate with irradiation time. The product displayed very good broad-spectrum ultraviolet protection as evidenced by the coverage afforded by the 0 SED transmission spectrum (dark blue). After receiving a total UV dose of 152.67 SED, the product showed a photoinstability of 3.49% in the UVA region and 0.01% in the UVB region.

Products SA7 and SA6 were from the same manufacturer. Since they share a common UV filtering system and most probably, the same vehicle or emulsion, one would expect them to display the same spectral behaviour, which indeed is the case. The higher photostability displayed by the product here can be attributed to higher concentrations of the individual active ingredients in SA7 than SA6 (see Table 3.5). The slight photoinstability in the UVA region was again attributed to the photoloss of AVO upon exposure to sunlight. Photoinstability increased with increase in irradiation time.

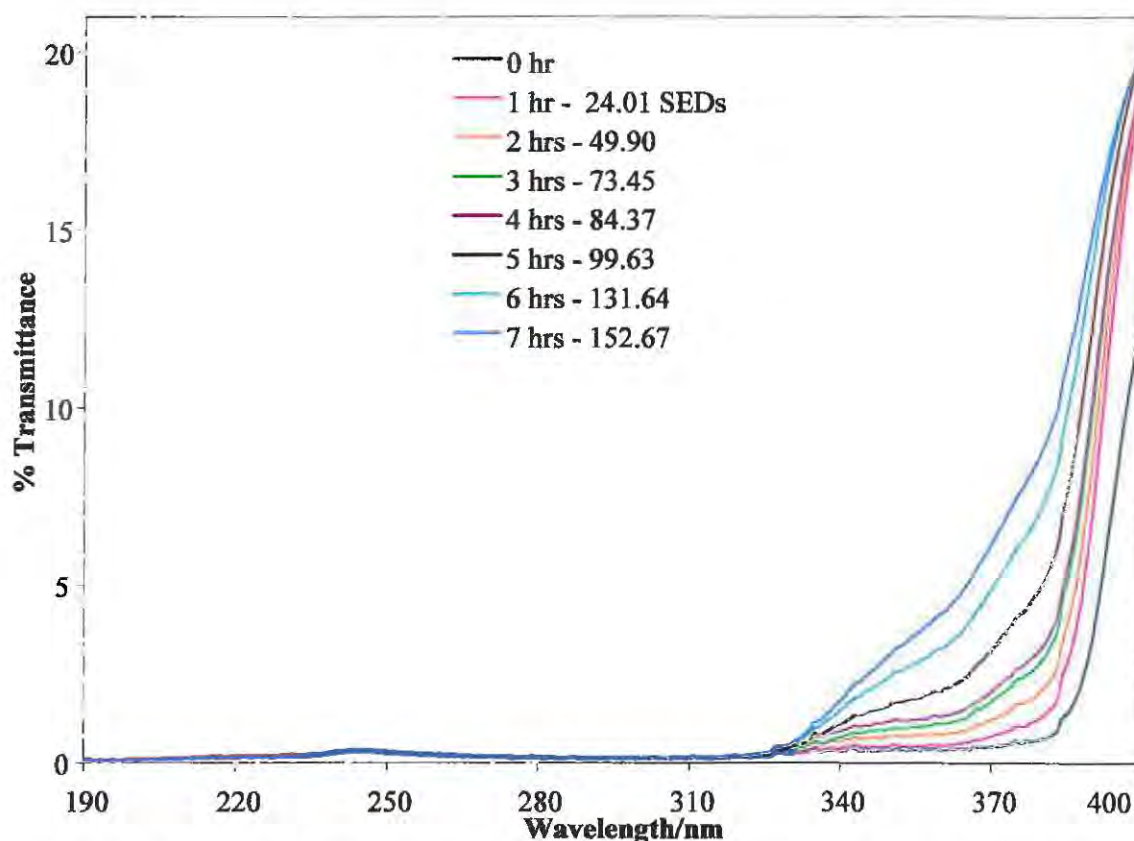


Figure 3.18: Changes in the spectral transmission of SA7 on a quartz plate (1 mg cm^{-2}) with increasing solar irradiation.

Figure 3.19 shows the change in the spectral transmission of SA8 on a quartz plate with irradiation time. This product was from the same manufacturer and had the same UV filtering

Figure 3.20 shows the spectral transmission change of SA21 on a quartz plate with irradiation time. SA21 shared a common UV filtering system with SA6-8 which consisted of MBC, AVO, OMC and TiO₂. The spectral coverage of the product (SA21) extended well into the longer wavelength UVA. Like SA6-8 that contained AVO and TiO₂, SA21 offered very good broad spectral coverage.

Exposure of the product to solar UVR caused a loss in photoprotection in the UVA region. The product remained photostable in the UVB region throughout the irradiation period of 7 hours. The product lost 6.63% of its photoprotective capacity in the UVA region after 2 hours of irradiation and was classified as photounstable. Photoinstability increased with increase in UV dose. The photostability behaviour of SA21 is different from that observed for SA6-8 which showed high photostability in both the UVB and UVA regions. SA21 also had an SPF value of 40+, yet it was found to be photounstable. This shows that a high SPF value does not necessarily mean high photostability. This difference in photostability behaviour can be attributed to the different emulsion or vehicle influence on the UV filtering system. SA21 was analysed for its photostability in solution as well.

Figure 3.21 gives the spectral transmission change of SA21 dispersed in solution with irradiation time. The product displayed a rapid increase in transmittance in the first 2 hours of exposure to UVR in the UVA region. However, the transmittance then remained constant upon further irradiation. Photostability in the UVB region remained unchanged (attributed to the photostabilising effect of the solvent on the UV filtering system). A photoinstability of 10.03% was registered for SA21 in solution and this is higher than that recorded on quartz plate (6.63%) for the same irradiation period (2 hours). The photoinstability for SA21 on a quartz plate steadily increased with irradiation time in the subsequent irradiations (after 2 hours), while the transmittance leveled off at about 10% for the same product in solution. The reason why the product showed no change in photostability in solution after 2 hours of irradiation is not clear.

Overall, SA21 displayed more photoinstability on a quartz plate than in solution. The product was classified as photounstable both in solution and on a quartz plate.

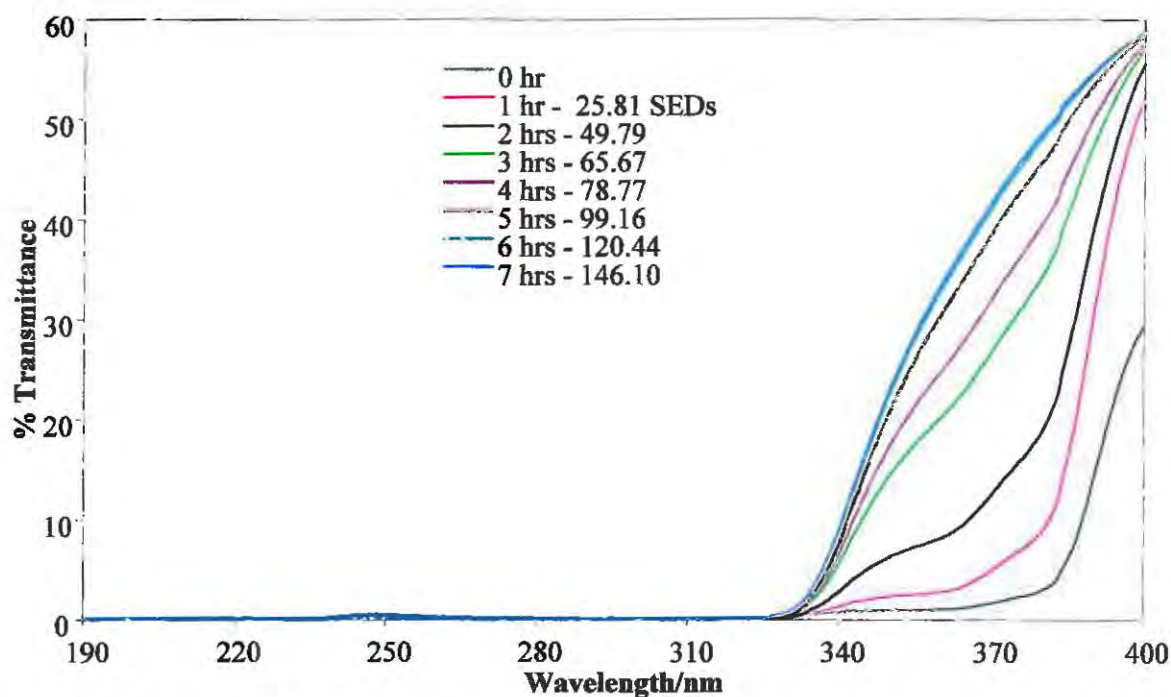


Figure 3.20: Changes in the spectral transmission of SA21 on a quartz plate (1 mg cm^{-2}) with increasing solar irradiation.

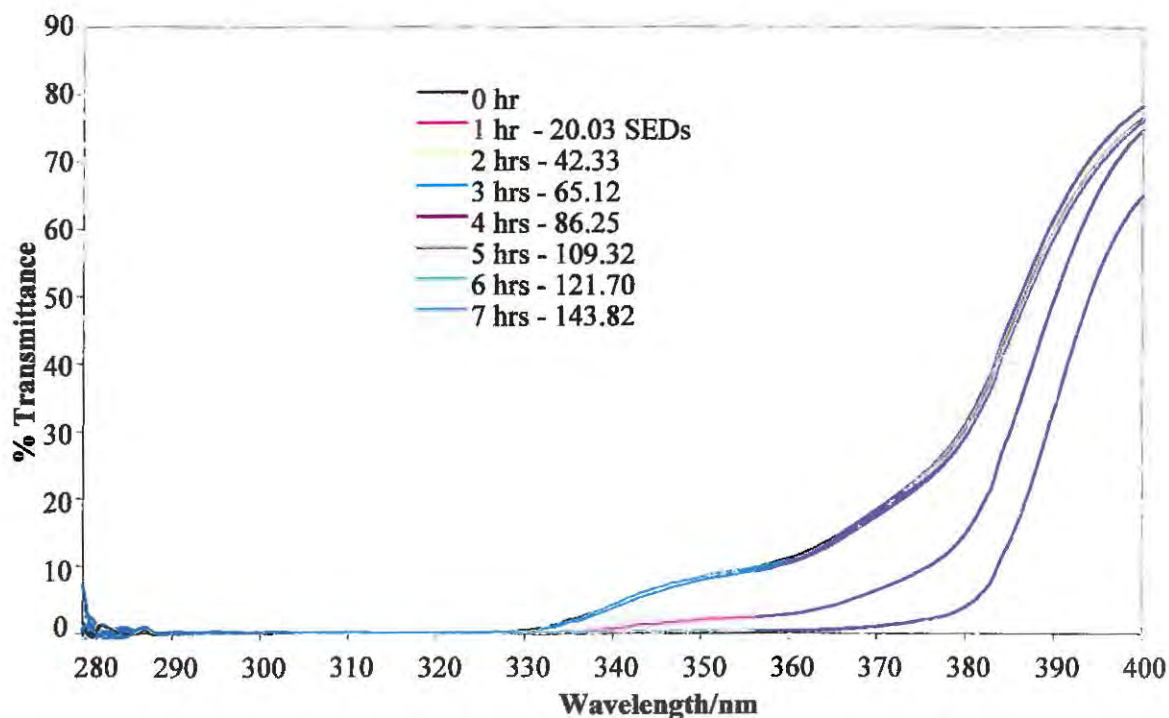


Figure 3.21: Changes in the spectral transmission of SA21 in solution (1 mg cm^{-3}) with increasing solar irradiation. Transmission spectra were recorded in a 1-cm pathlength quartz cuvette with the solvent (isopropanol-cyclohexane-dichloromethane 50:37.5:12.5% (v/v)) in the reference beam.

SA21 was analysed for its photostability by HPLC. The chromatogram of the unirradiated sample of SA21 is shown in Figure 3.22. Only three peaks can be seen in the chromatogram confirming the presence of three UV filters (see Table 3.9).

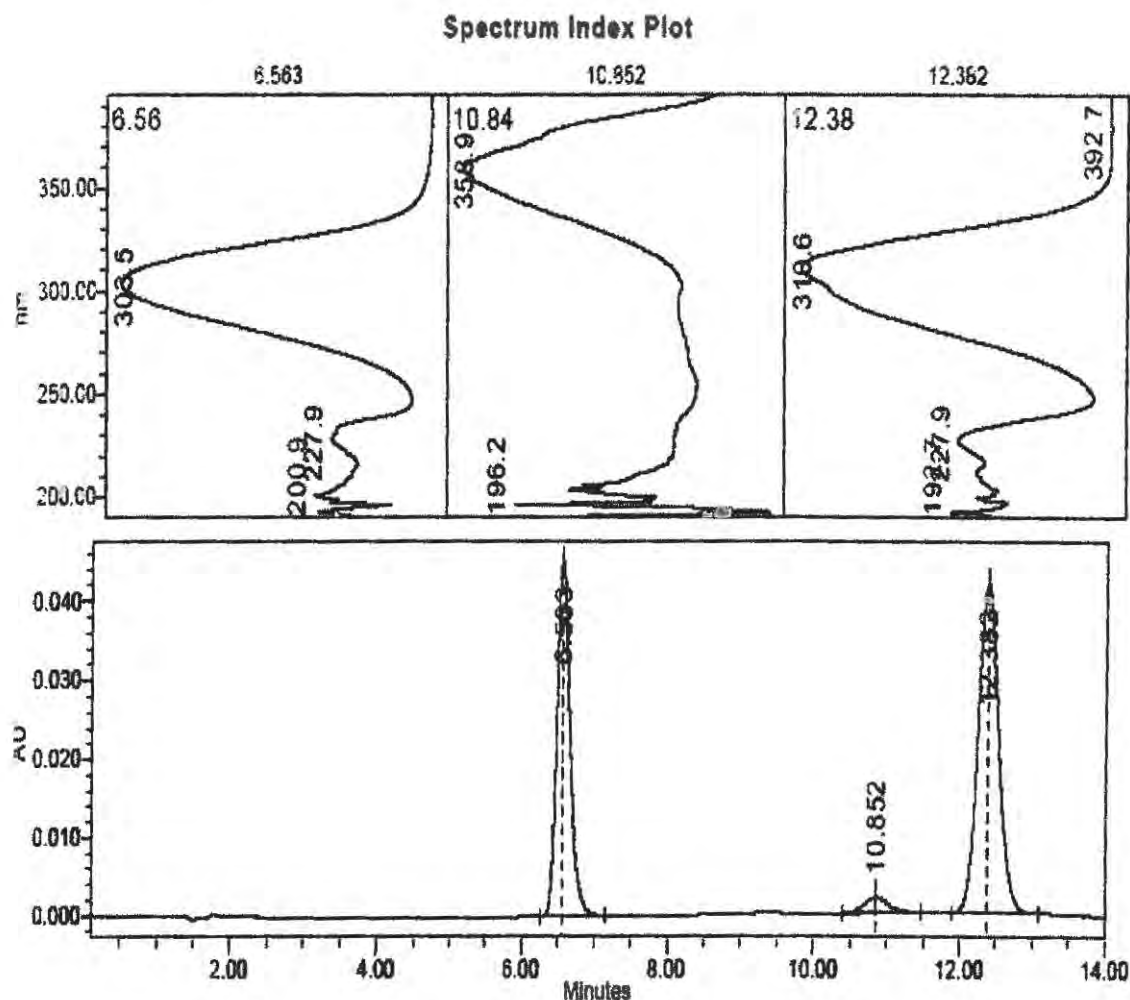


Figure 3.22: Chromatogram of an unirradiated sample of SA21. The chromatographic conditions used were: Phenomenex RP-C₁₂ 80 Å column, mobile phase - MeOH-H₂O 84:16% (v/v), injection volume - 20 µL, flow rate - 1 mL min⁻¹, and detection wavelength - 330 nm. The order of elution is MBC, AVO and OMC.

Analysis of the irradiated sample of SA21 by HPLC gave the chromatogram shown in Figure 3.23. The AVO peak which was supposed to show at 10.852 minutes could not be detected anymore. Again, processing the chromatogram at 358 nm (λ_{max} of AVO) did not show any peak. This finding shows that even the presence of MBC does not stop the complete loss of AVO. From the chromatogram shown in Figure 3.23, one can see two extra peaks. The two peaks in

Figure 3.23 were assigned as *cis*-MBC (7.393 min) and *cis*-OMC (12.439 min) as done for SA3 and SA16 below. It can be speculated that the same photoproducts were formed in the three products, SA3, SA16 and SA21. Tarras-Wahlberg *et al.*¹¹⁸ reported that MBC photoisomerises in more or less the same way as OMC upon exposure to solar UVR, reaching a photostationary equilibrium. HPLC quantitation revealed a loss of 10.52 and 32.40% for MBC and OMC, respectively. The amount of OMC lost in SA21 is comparable to that lost in the products, SA15 and SA20 above. MBC can be said to be relatively more photostable than OMC.

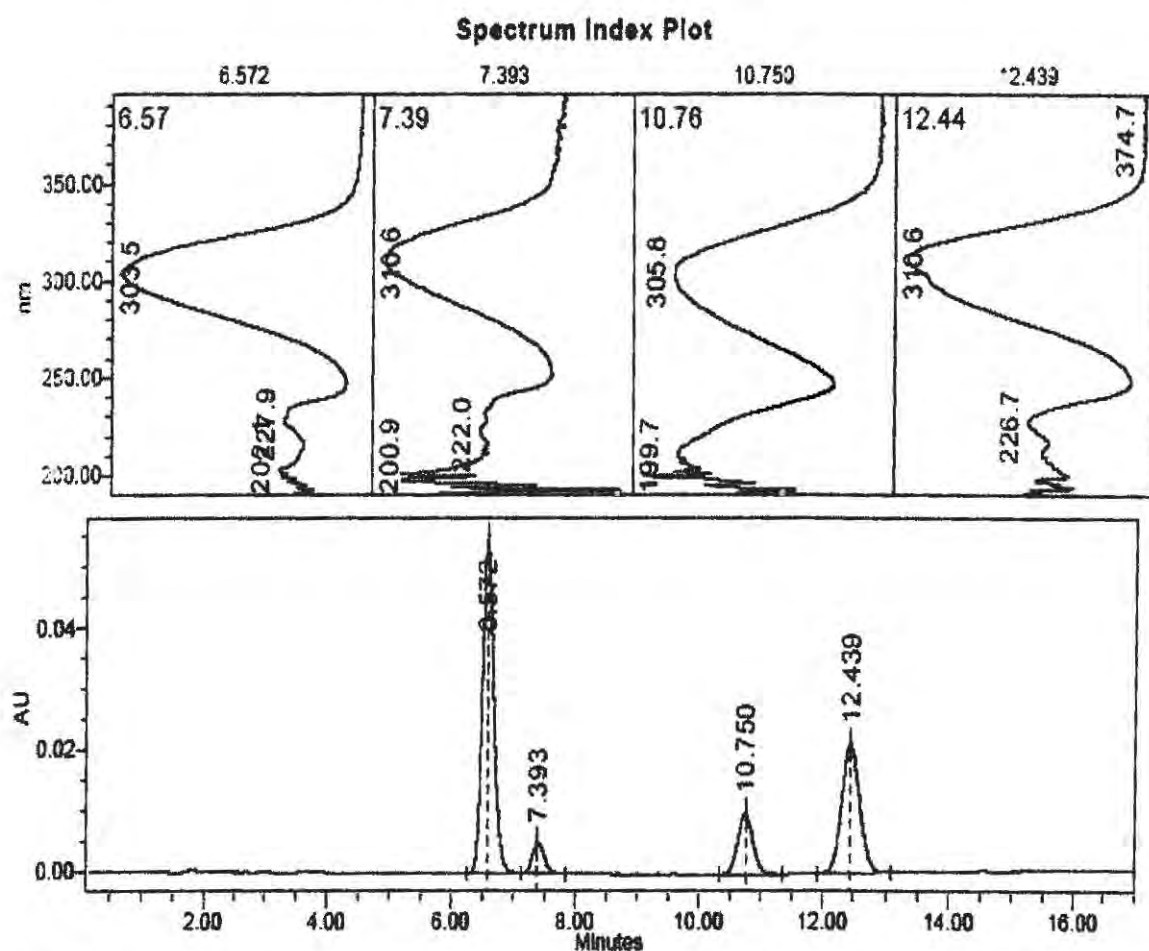


Figure 3.23: Chromatogram of an irradiated sample of SA21. The chromatographic conditions used were: Phenomenex RP-C₁₂ 80 Å column, mobile phase - MeOH-H₂O 84:16% (v/v), injection volume - 20 µL, flow rate - 1 mL min⁻¹, and detection wavelength - 330 nm. The order of elution is *trans*-MBC, *cis*-MBC, *cis*-OMC and *trans*-OMC.

SA22 had almost the same UV filtering system as the products, SA6-8 and SA21, except for the presence of an unidentified active ingredient which absorbed in the UVB region (see Figure F28

of Appendix F for chromatogram). Figure 3.24 shows the spectral transmission change of SA22 on a quartz plate with irradiation time.

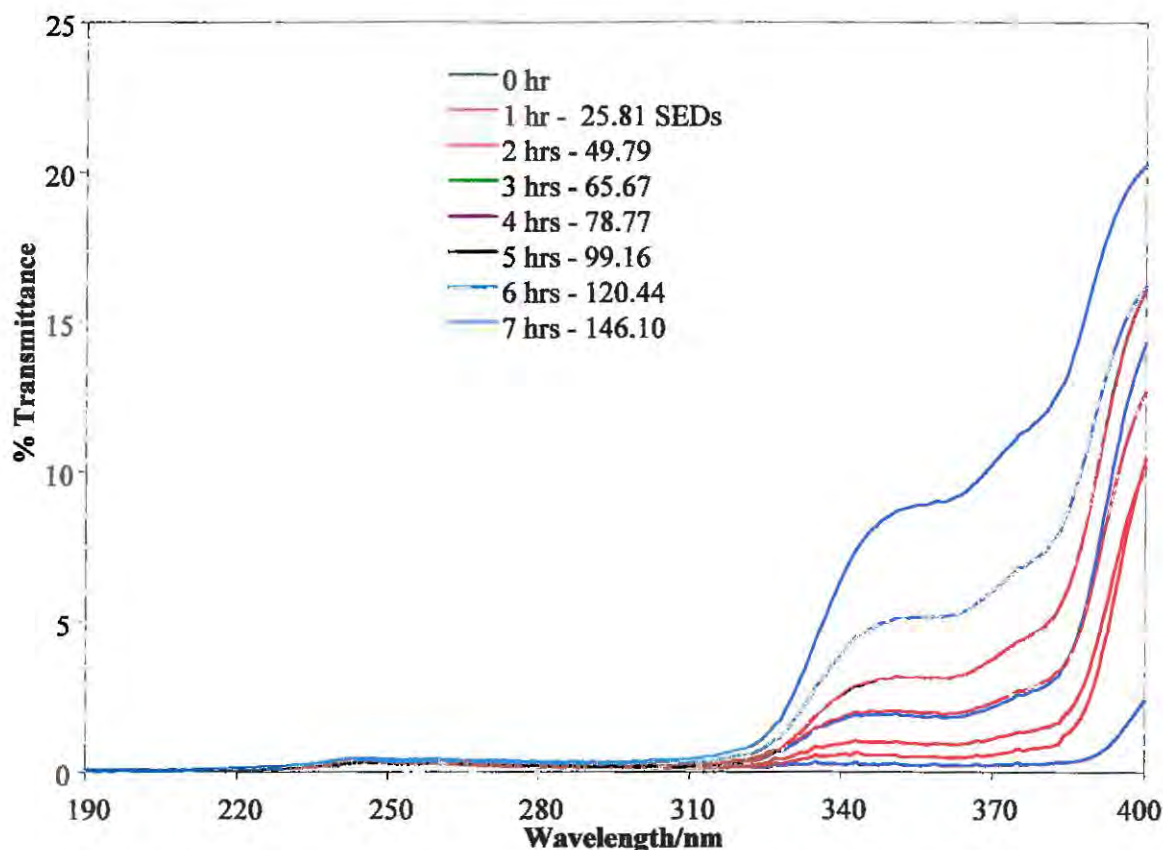


Figure 3.24: Changes in the spectral transmission of SA22 on quartz plate (1 mg cm^{-2}) with increasing solar irradiation.

The product offered very good broad spectral coverage. The broad-spectral coverage can be said to be due to the presence of AVO and TiO_2 in the UV filtering system.

Irradiation of the product resulted in a slight loss in photoprotection. Photoinstability increased steadily with irradiation time in the UVA region. However, the change in photostability was not that significant with the recorded photoinstabilities in the UVA and UVB regions after 2 hours of irradiation being 0.71% and 0.04%, respectively. The total photoinstability registered after 7 hours was 7.43% (UVA) and 0.30% (UVB). The photoinstability observed in the UVA region can be attributed to the photoloss of AVO. The product was classified as photostable. The transmission spectra of the products, SA6-8, SA21 and SA22 (containing the same active ingredients) looked quite similar though the photoinstabilities were different amongst products from different manufacturers.

3.3.3.6 Sunscreens containing OMC, MBC, Bz-3 and OS

Figure 3.25 shows the change in the spectral transmission of SA3 on a quartz plate. The product offered relatively poor spectral coverage as compared with SA6-8, SA15, SA21 and SA22 discussed above. The UV filtering system consisted of OMC, Bz-3, MBC and OS, all of which are essentially UVB-filters (see Figures 2.2b and c). OS is commonly used to enhance the efficacy of other UVB-filters and to minimise the degradation of other sunscreen active ingredients including AVO.⁷³ The product displayed poor protection especially in the longer wavelength UVA (340 – 400 nm) region. Nonetheless, the spectral coverage of SA3 is better than that observed for SA1 and SA2, and this is attributable to the higher concentration of Bz-3 in SA3 (4.83%) than in both SA1 (0.88%) and SA2 (1.43%).

Upon irradiation of SA3 on a quartz plate, there was a drastic loss in the protective power of the product in the first hour of exposure to solar radiation. Unlike the other products discussed thus far, the photoinstability (first hour) observed was quite pronounced for the UVB and shorter UVA regions. However, there was a decrease in transmittance in the long wavelength UVA (340 – 400 nm) range and that remained constant in the first three hours of irradiation. In addition to the loss of volatile organics in the first hour of irradiation, simultaneous photodegradation of UV filters occurred. Quite strangely, upon further irradiation from the fourth hour, the product regained photostability in the UVB and short wavelength UVA range (320 - 340 nm). This behaviour was attributed to the possible formation of photoproducts that absorbed in the same UV region as the initial UV filtering system.

The photostability behaviour of SA3 can also possibly be explained by the large water content in the product since it was a sprayable formulation. It can be speculated that the evaporation of water from the film took long, thus taking long to form a dry, firm sunscreen film on the quartz plate. SA3 was also analysed in solution to assess its photostability behaviour.

Figure 3.26 shows the change in the spectral transmission of SA3 in solution with irradiation time. In contrast to what was observed in Figure 3.25, SA3 showed high photostability in solution as shown in Figure 3.26. The unirradiated transmission profiles of the product (both in solution and on a quartz plate) appear similar. For a total UV dose of 148.89 SED, there was less than 0.5% loss in photostability for SA3 in solution.

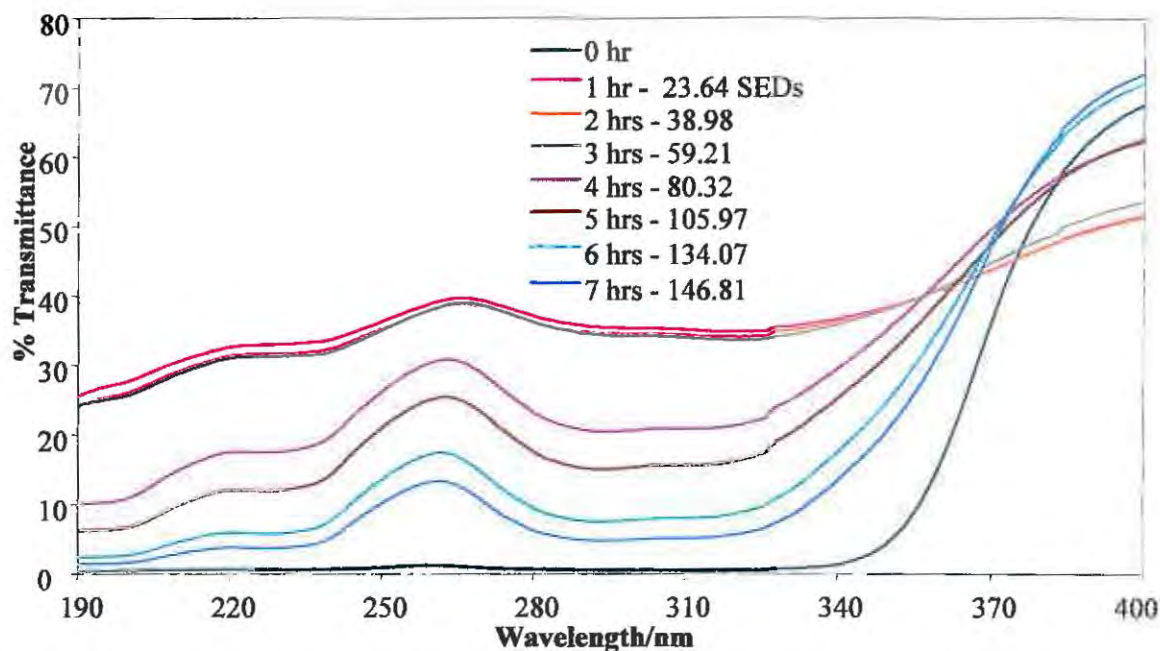


Figure 3.25: Changes in the spectral transmission of SA3 on a quartz plate (1 mg cm^{-2}) with increasing solar irradiation.

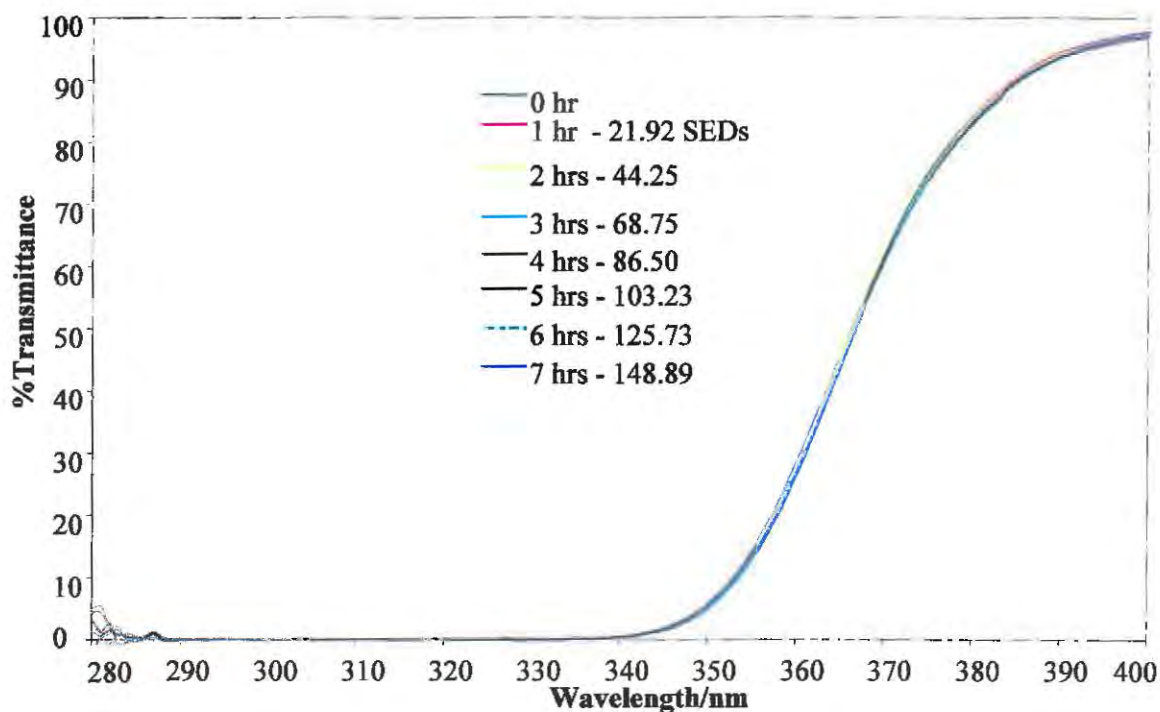


Figure 3.26: Changes in the spectral transmission of SA3 in solution (1 mg cm^{-3}) with increasing solar irradiation. Transmission spectra were recorded in a 1 cm path-length quartz cuvette with the solvent (isopropanol-cyclohexane-dichloromethane 50:37.5:12.5% (v/v)) in the reference beam.

SA3 was analysed for its photostability by HPLC. Figure 3.27 displays the chromatogram of an unirradiated sample of SA3. The chromatogram of the unirradiated sample showed four peaks and the associated UV absorption spectrum of each active ingredient. The peaks were identified as Bz-3 (3.851 min), MBC (6.519 min), OMC (12.219 min) and OS (14.214 min).

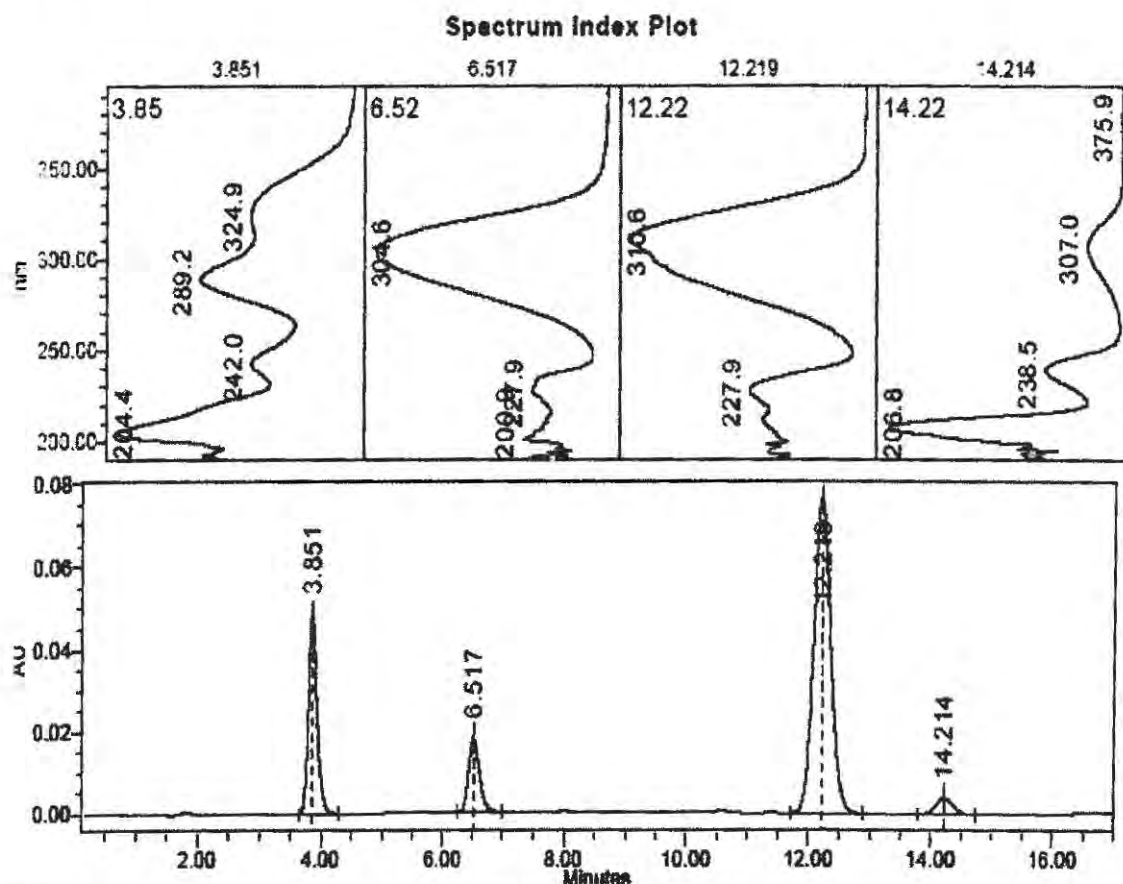


Figure 3.27: Chromatogram of unirradiated sample of SA3. The chromatographic conditions used were: Phenomenex RP-C₁₂ 80 Å column, mobile phase - MeOH-H₂O 84:16% (v/v), injection volume - 20 µL, flow rate - 1 mL min⁻¹, and detection wavelength - 310 nm. The order of elution is Bz-3, MBC, OMC and OS.

Because of its unique photostability behaviour as has been observed above, this product was irradiated in the sun for two irradiation periods and analysed by HPLC. Two petri-dishes were prepared, one was analysed after 3 hours of irradiation and the other sample after 6 hours of irradiation as described in Section 2.6. This was to check for any possible photoproducts and to see if the photoproducts were different for the two irradiation periods. However, it was observed that the chromatograms from the two samples gave the same peaks. The chromatogram displayed in Figure 3.28 is of the sample (SA3) irradiated in the sun for 6 hours.

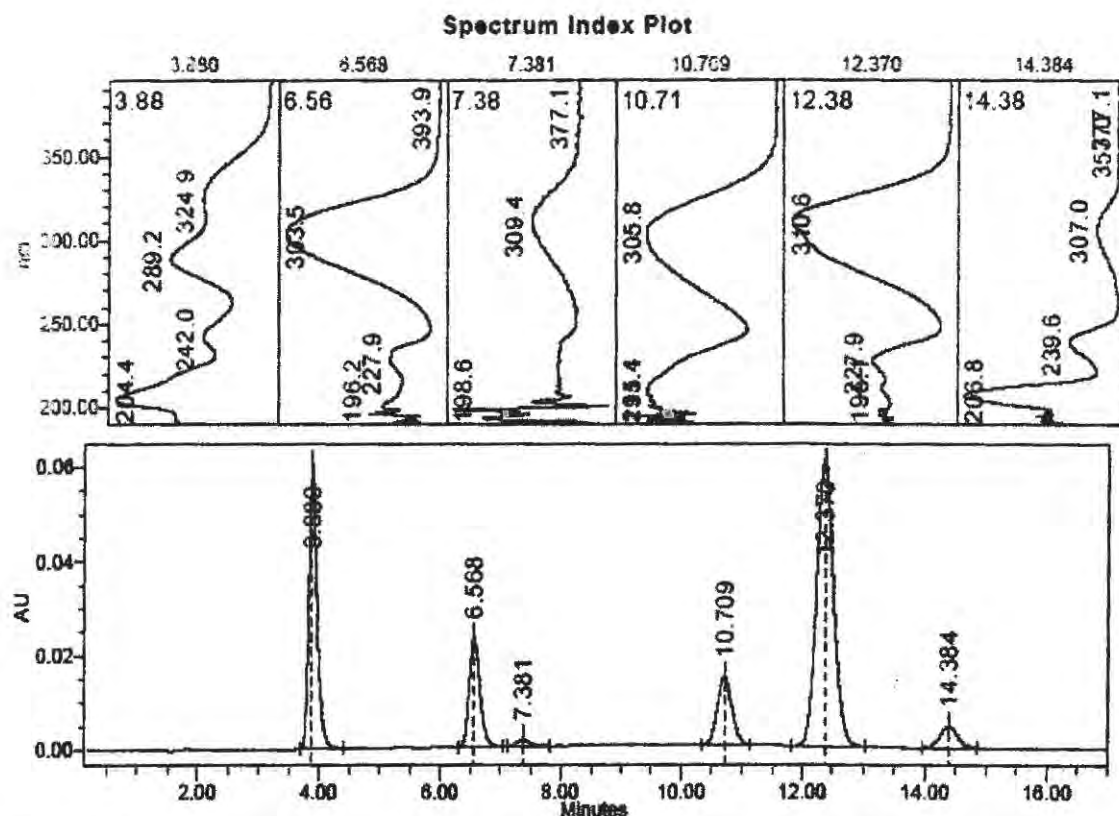


Figure 3.28: Chromatogram of sample of SA3 irradiated for 6 hours in the sun. The chromatographic conditions used were: Phenomenex RP-C₁₂ 80 Å column, mobile phase - MeOH-H₂O 84:16% (v/v), injection volume - 20 µL, flow rate - 1 mL min⁻¹, and detection wavelength - 310 nm. The order of elution is Bz-3, *trans*-MBC, *cis*-MBC, *cis*-OMC, *trans*-OMC and OS.

As can be seen in Figure 3.28, two new peaks were observed and they were assigned as *cis*-MBC (7.381 min) and *cis*-OMC (10.709 min). The assignment was done according to the peaks and UV absorption spectra observed in Figures 3.11, 3.15 and 3.23. The slight difference in the wavelength of maximum absorption of the spectrum of the peak eluting at 11.158 minutes in Figure 3.5 (SA1) and that at 10.709 minutes in Figure 3.28 (SA3) is probably due to the differences in polarities of the two sunscreen products, but it is the same photoproduct (*cis*-OMC). The peak eluting at 7.381 minutes was assigned to *cis*-MBC. As has been discussed above, *trans*-MBC (the common form) photoisomerises in more or less the same way as OMC.¹¹⁸ Bz-3 and OS are usually said to be highly photostable and are unaffected by solvent effects.¹⁶¹ A comparison of the chromatograms for irradiated SA21 (with TiO₂) and SA3 (without TiO₂) shows that essentially the same photoproducts are formed. Therefore, the presence of TiO₂ in the sunscreens does not seem to give rise to different photoproducts. This is of course with the exception of SA15, where a number of unidentified photoproducts were formed.

3.3.3.7 Sunscreens containing OMC, Bz-3, OS and TiO₂

Figure 3.29 shows the spectral transmission change of SA4 on a quartz plate with irradiation time. The UVA coverage of the product was more or less comparable to that of SA3. The UV-filters contained in SA4 were Bz-3, OMC, OS and TiO₂. TiO₂ is considered a broad-spectrum physical blocker though it maximally absorbs in the shorter wavelength UVA range (see Figure 1.1). It can be observed that the presence of TiO₂ without AVO does not improve the UVA coverage (broad-spectrum photoprotection) of the product that much. There was a claim of broad-spectrum UV protection on the label of the product. The spectral coverage of SA4 was comparable to that observed for SA1, SA2 and SA3 which did not contain TiO₂.

Irradiation of SA4 in the sun showed high photostability in both the UVB and UVA regions. There was a change in transmittance in the long wavelength UVA (340 – 400 nm) region in the first hour of irradiation. Also noticeable was the decrease in transmittance (stabilisation) in the UVB region in the first hour of exposure to sunlight. Photoinstability in the UVA region after a total dose of 146.81 SEDs was just 2.79%, which was below the set threshold of 5% for 2 hours of solar irradiation.

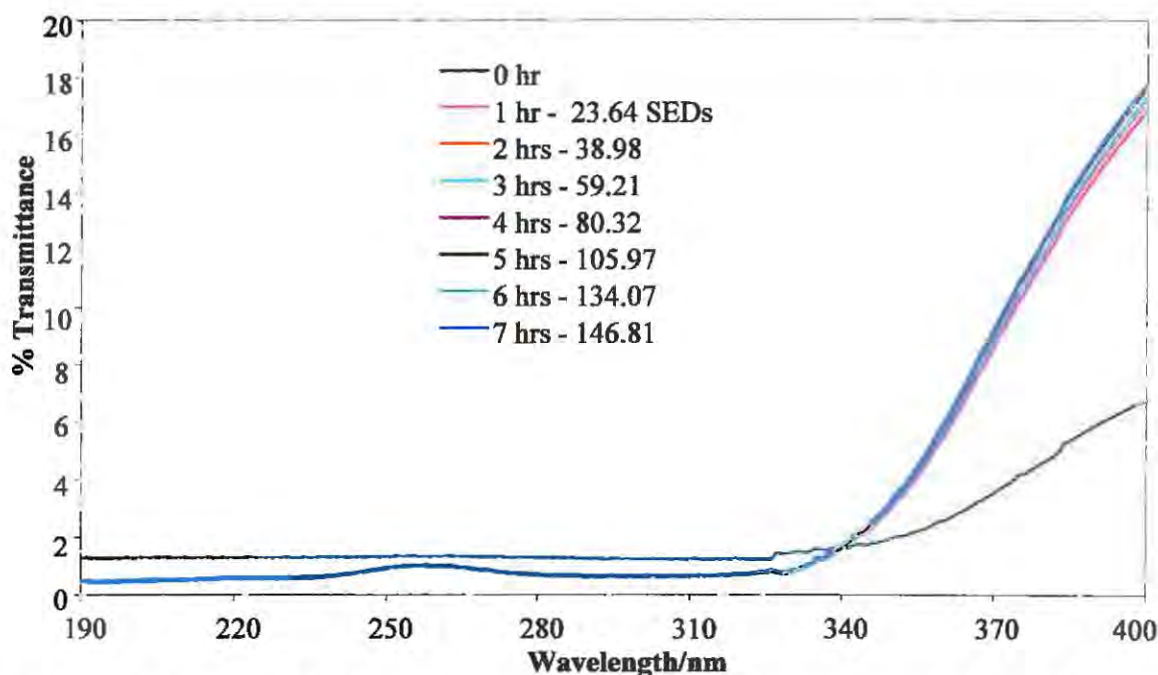


Figure 3.29: Changes in the spectral transmission of SA4 on a quartz plate (1 mg cm⁻²) with increasing solar irradiation.

Figure 3.30 shows the change in the spectral transmission of SA10 smeared on a quartz plate with irradiation time. The spectral coverage of this product did not extend much into the longer wavelength UVA region as observed for SA4 (see Figure 3.29) with which it shares a common UV filtering system (see Table 3.9). The manufacturer claimed broad-spectrum UV protection.

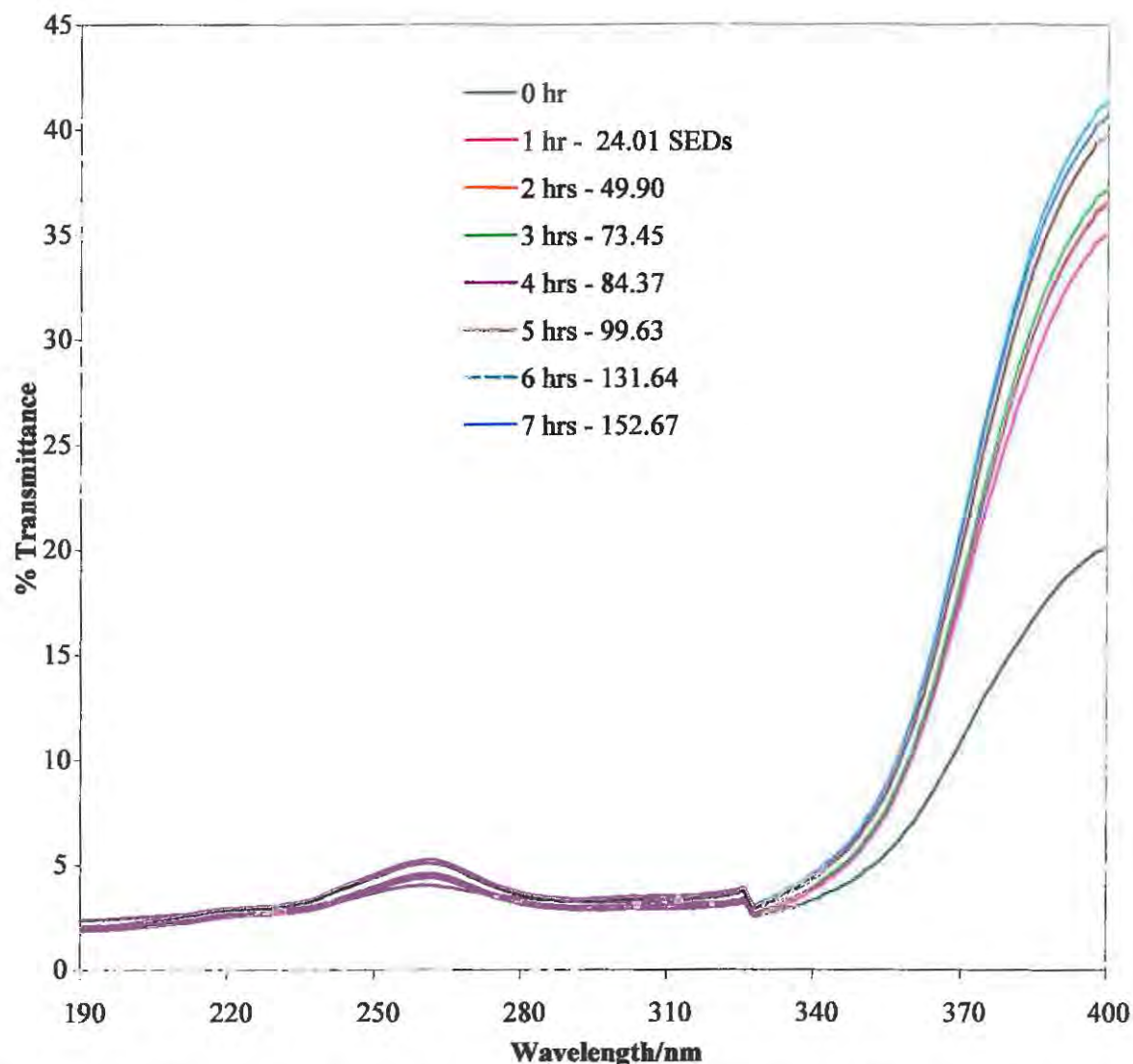


Figure 3.30: Changes in the spectral transmission of SA10 on a quartz plate (1 mg cm^{-2}) with increasing solar irradiation.

The first hour of exposure to the sun resulted in a jump in the transmittance of the product in the long wavelength UVA region. However, for the subsequent irradiations, the product showed high photostability in both the UVB and UVA regions. In addition to the UV filters (Bz-3, OMC, OS and TiO_2), the product contained mica and SiO_2 which probably help scatter and reflect harmful UVR, thus stabilizing the organic active ingredients. There was an overall

increase of 5% (UVA region) and 0.27% (UVB region) in transmittance after 7 hours of irradiation in the sun.

3.3.3.8 Sunscreens containing AVO, OT, DOBT and TiO₂

Figure 3.31 displays the spectral transmission change of SA19 on a quartz plate with irradiation time. The spectral coverage of the product (SA19) extended well into the UVA region, which is attributable to the presence of AVO. The UV filtering system contained DOBT, OT, AVO and TiO₂. The broad spectral coverage observed confirmed the claim that the product offers UVA protection. Both DOBT and OT absorb in the UVB region (see Figure 2.2a).

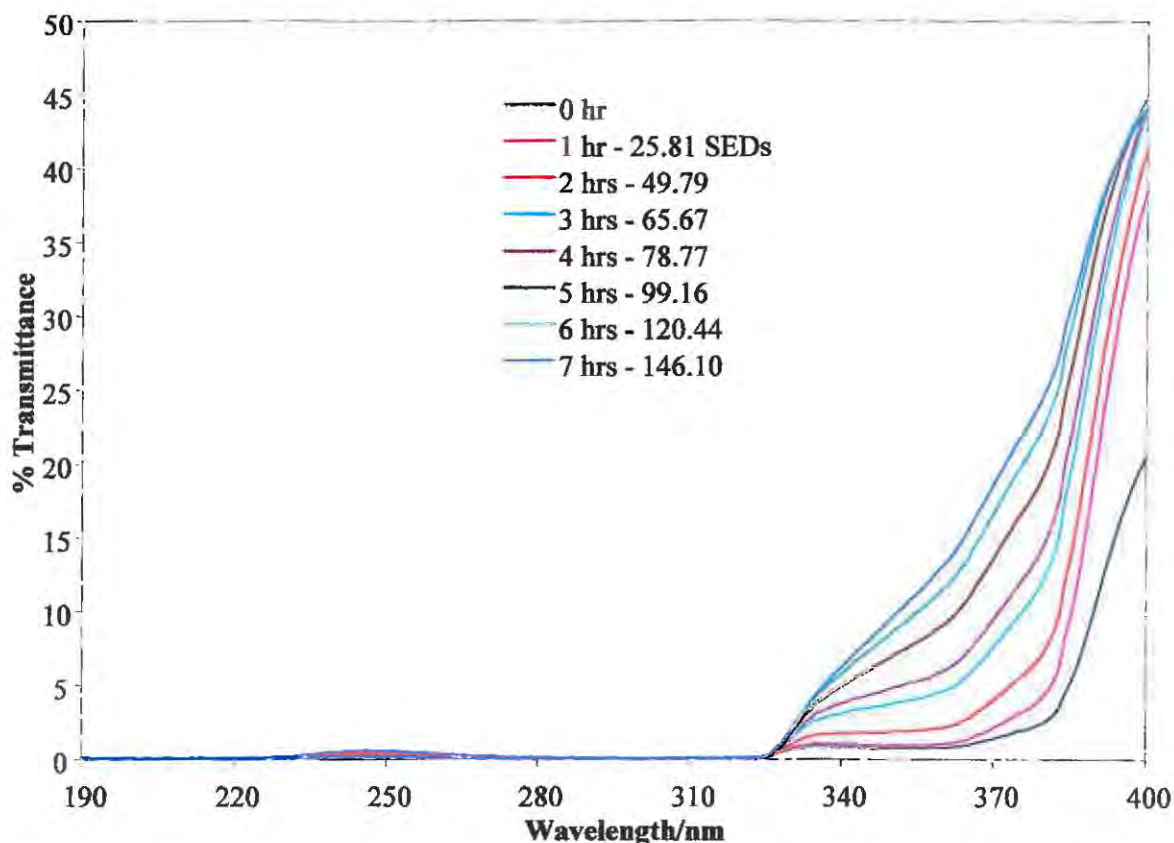


Figure 3.31: Changes in the spectral transmission of SA19 on a quartz plate (1 mg cm⁻²) with increasing solar irradiation.

However, there was a slight loss of photoprotection in the UVA region with exposure to solar UVR. Again, the loss in the photoprotective power of the product in the UVA region is ascribed to the photodegradation and photoisomerisation of AVO as discussed for the products, SA6-8, SA15 and SA20. The photostability remained constant in the UVB region. The

photoinstabilities of the product after 2 hours (49.79 SEDs) remained below the set threshold of 5% for both the UVB and UVA regions. Therefore, the product was classified as photostable. The shapes of the transmission spectra changed gradually with exposure to sunlight. Overall, the product registered an increase in transmittance of 0.01 and 10.57% in the UVB and UVA regions, respectively. Photoinstability increased with increase in UV dose.

3.3.3.9 Sunscreen containing OMC, OCR, BEMT and TiO₂

Figure 3.32 shows the change in the spectral transmission of SA13 on a quartz plate with irradiation time. The spectral coverage of the product extended quite well into the long wavelength UVA region confirming what was declared on the bottle. The UV filtering system of the product consisted of BEMT, OCR, OMC and TiO₂. The broad spectral coverage observed can be ascribed to the presence of BEMT, which is a broad-spectrum UV-filter (see Figure 2.2a), as well as TiO₂. OCR is a UVB absorber as shown in Figure 2.2c.

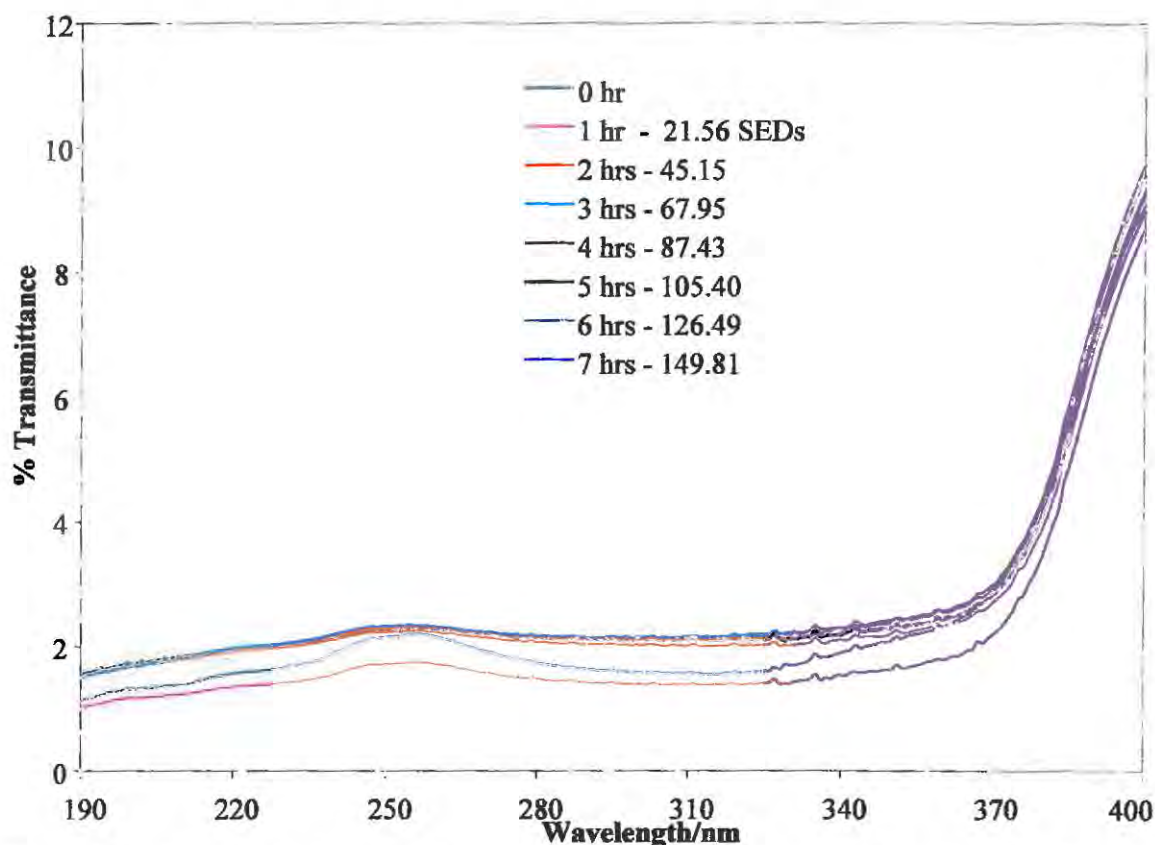


Figure 3.32: Changes in the spectral transmission of SA13 on a quartz plate (1 mg cm⁻²) with increasing solar irradiation.

There was not much change in photostability in both the UVB and UVA regions. All the photoinstability values were below 1% throughout the irradiation period of 7 hours. OCR is known to be photostable both in polar and non-polar solvents. The photostability of OCR is attributed to the lack of geometrical isomers¹⁶¹ in this trisubstituted double-bond system (see Section 1.3.3 for structure). The active ingredients, BEMT and OCR are normally used to photostabilise OMC.¹⁴⁴

3.3.3.10 Sunscreens containing OMC, MBC, MBBT and BEMT

Figure 3.33 displays the spectral transmission change of SA16 on a quartz plate with irradiation time. The product displayed very good broad spectral coverage. The broad spectral coverage observed in this product was in good agreement with the broad-spectrum UV protection claim made on the label. The UV filtering system consisted of MBC, OMC, MBBT and BEMT. As shown in Figure 2.2a, both BEMT and MBBT are broad-spectrum UV-filters.

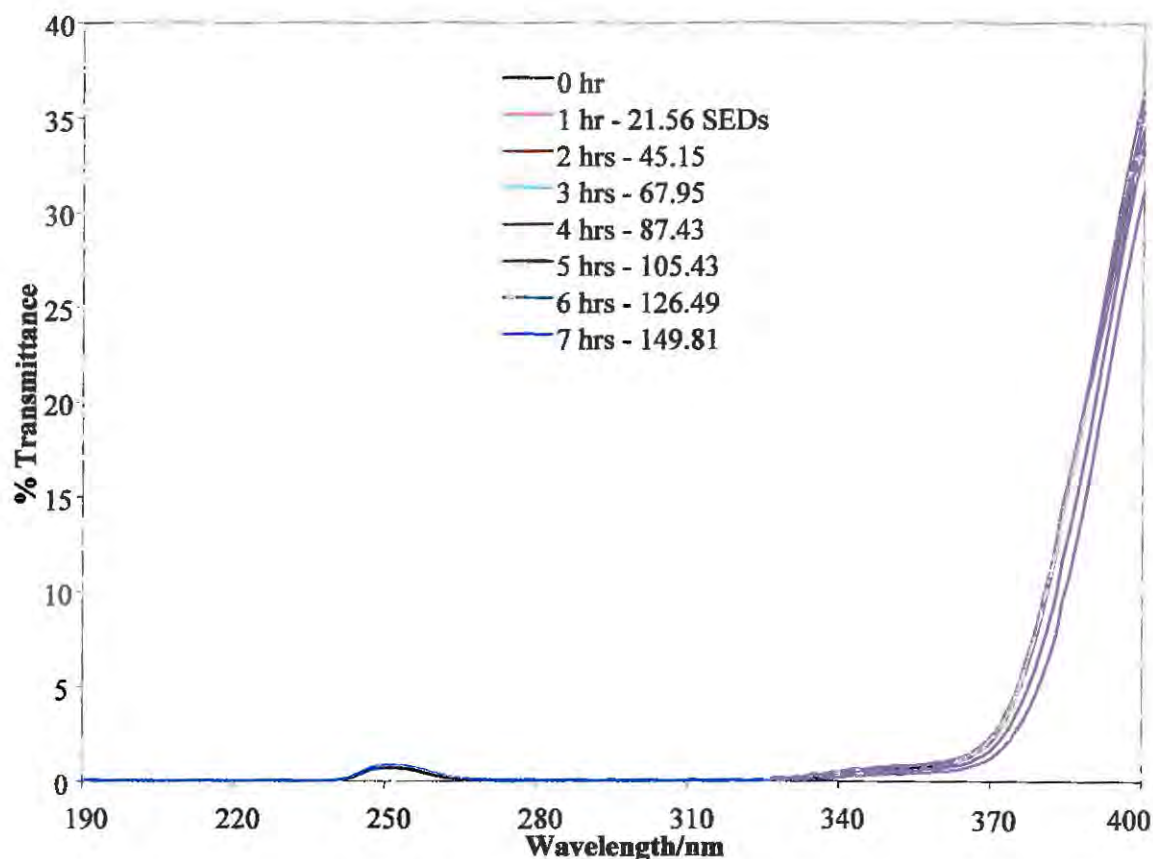


Figure 3.33: Changes in the spectral transmission of SA16 on a quartz plate (1 mg cm^{-2}) with increasing solar irradiation.

SA16 displayed very high photostability in both the UVA and UVB regions throughout the irradiation period. The broad-spectrum UV protection and high photostability of the product are probably due to the presence of MBBT and BEMT which have been shown to be highly photostable.¹³⁴ The UV filtering system of this product was the same as that of SA9 (see Figure 3.36 below) save for the absence of TiO₂ in this product.

As described in Section 2.6, SA16 was analysed by HPLC under two sets of chromatographic conditions. Analysis of the irradiated sample of SA16 under chromatographic conditions that eluted MBBT and BEMT only did not show any extra peaks except the two peaks of MBBT and BEMT (chromatogram not shown). Figure 3.34 shows the chromatogram of SA16 (unirradiated sample) obtained at chromatographic conditions used for eluting MBC and OMC (see Section 2.3.5). Only two peaks can be seen which were assigned to MBC (6.513 min) and OMC (12.299 min).

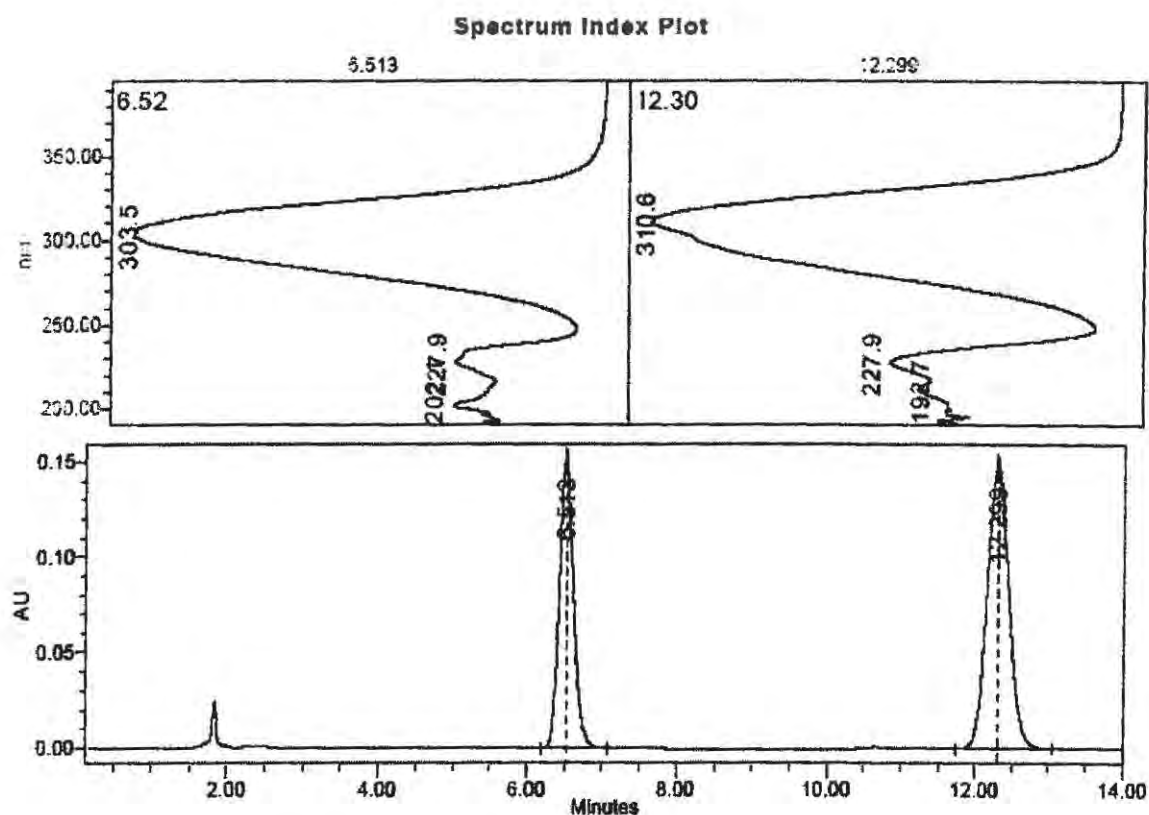


Figure 3.34: Chromatogram of an unirradiated sample of SA16. The chromatographic conditions used were: Phenomenex RP-C₁₂ 80 Å column, mobile phase – MeOH-H₂O 84:16% (v/v), injection volume – 20 µL, flow rate – 1 mL min⁻¹, and detection wavelength – 310 nm. The order of elution is MBC and OMC.

HPLC analysis of the irradiated sample of SA16 gave the chromatogram shown in Figure 3.35. The chromatogram was obtained under the chromatographic conditions used to elute OMC and MBC. As can be seen in Figure 3.35, two new peaks were observed. The new peaks, judging from their retention times and their associated UV/VIS absorption spectra, were assigned to *cis*-MBC (7.368 min) and *cis*-OMC (10.694 min) as discussed earlier (see Figures 3.23 and 3.28). There was a loss of 25.97% for OMC, and 9.90% for MBC after irradiation in the sun for 6 hours. This finding shows that the presence of the *tinisorbs* does not stop the photoisomerisation of OMC and MBC *per se*. Chatelain *et al.*¹³⁴ reported that BEMT prevented or greatly reduced the photodegradation of AVO when alone or in combination with OMC. They also reported achieving high recoveries of OMC after HPLC analysis of irradiated samples in which the two were formulated together.

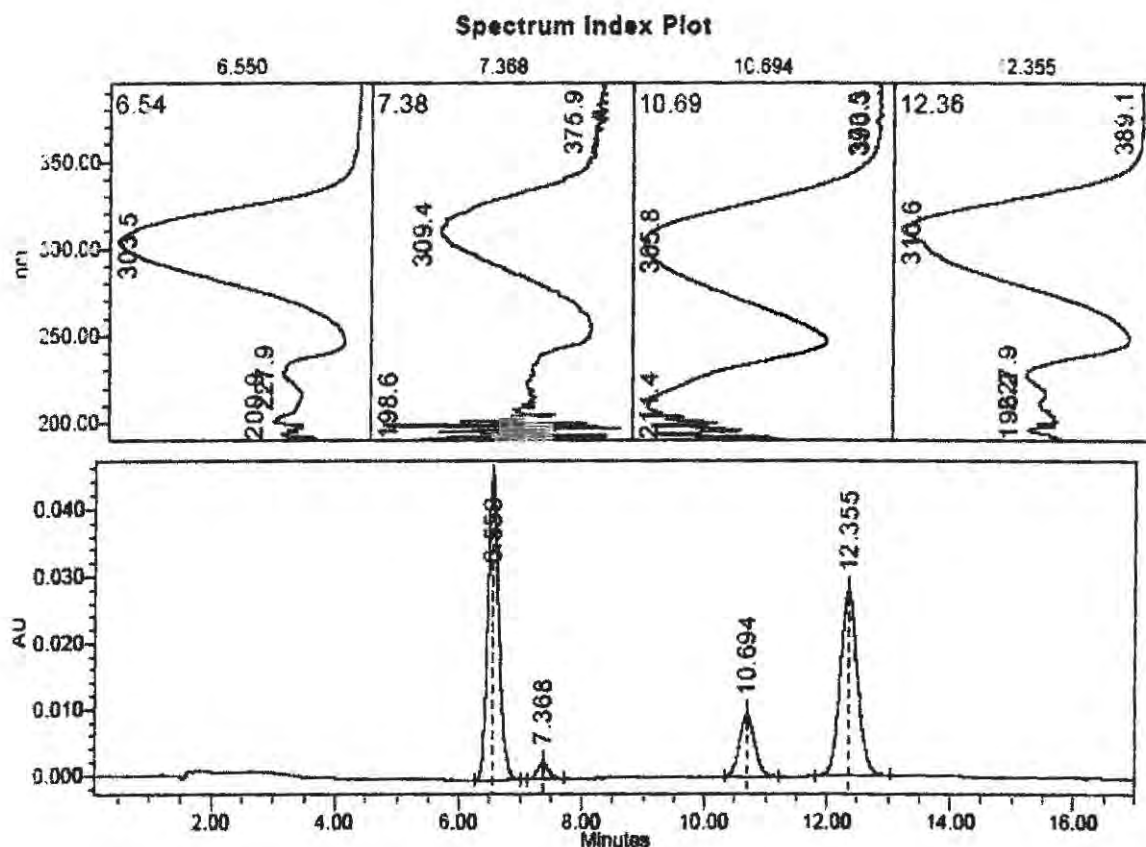


Figure 3.35: Chromatogram of an irradiated sample of SA16. The chromatographic conditions used were: Phenomenex RP-C₁₂ 80 Å column, mobile phase – MeOH-H₂O 84:16% (v/v), injection volume – 20 µL, flow rate – 1 mL min⁻¹, and detection wavelength – 310 nm. The elution order is *trans*-MBC, *cis*-MBC, *cis*-OMC and *trans*-OMC.

3.3.3.11 Sunscreens containing OMC, MBC, MBBT, BEMT and TiO₂

Figure 3.36 displays the spectral transmission change of SA9 on a quartz plate with irradiation time. The spectral coverage of the product extended well into the long wavelength UVA range. This confirmed the claim of broad-spectrum UV protection on the label. The UV filtering system of the product consisted of MBC, OMC, MBBT, BEMT and TiO₂. The two *tinorsorbs*, MBBT and BEMT are all broad-spectrum absorbers as shown in Figure 2.2a. However, the initial spectral coverage of SA9 is relatively poor as compared with SA16 discussed above. This may be because of the vehicle or emulsion influence on the absorption properties of the UV filtering system. The better spectral coverage offered by SA16 can also be due to slightly higher concentrations of MBBT (3.84%) and BEMT (2.59%) than in SA9 (MBBT – 3.39% and BEMT – 1.90%) as shown in Table 3.5.

SA9 exhibited high photostability in both the UVB and UVA regions. There was actually a decrease in transmittance upon exposure of the product to sunlight for one hour. This decrease in transmittance in the first hour can be explained by the formation of a firm, dry and uniform sunscreen film after the evaporation of organic volatiles and water.

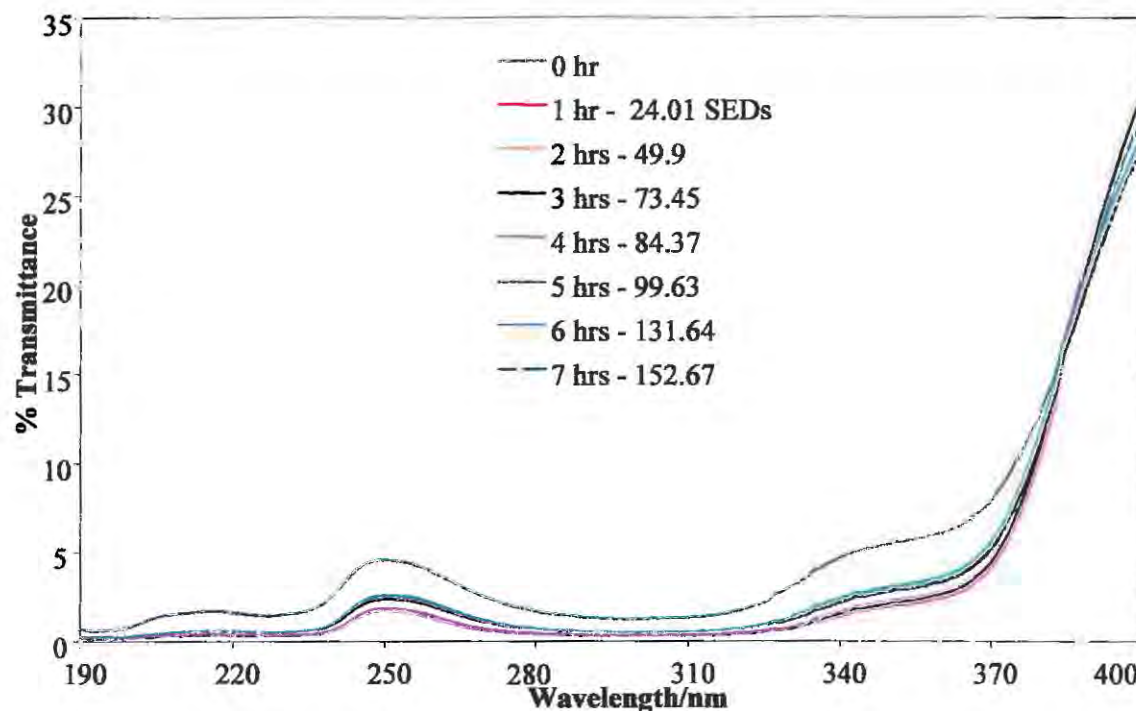


Figure 3.36: Changes in the spectral transmission of SA9 on a quartz plate (1 mg cm⁻²) with increasing solar irradiation.

While one would expect an increase in transmittance (photoinstability) with increase in the amount of UV dose delivered, SA9 showed a gradual decrease in transmittance with increase in irradiation time. The decrease in transmittance was exhibited in both the UVA and UVB regions. The transmission profiles of the product also remained essentially the same in shape throughout the seven hours of irradiation. This is contrary to what has been observed with the majority of products discussed so far. MBBT and BEMT have been shown to be highly photostable.^{134, 211, 212} Overall photoinstability was -1.93% (UVA region) and -0.81% (UVB region) after 7 hours of irradiation.

3.3.3.12 Sunscreens containing OMC, MBC, Bz-3, OS and TiO₂

Figure 3.37 displays the change in spectral transmission of SA5 smeared on a quartz plate with irradiation time. The product displayed a spectral coverage extending to the long wavelength UVA region. Hence, the product affords broad-spectrum UV protection. This observation confirmed the claim on the label of 'UV block' or 'broad-spectrum protection.' The product contained AVO in addition to the active ingredients contained in SA4 (OMC, MBC, OS and TiO₂) above as presented in Table 3.9. As discussed above, SA4 displayed poor protection in the long wavelength UVA (340 - 400 nm) region. Therefore, the improvement in protection in the longer wavelength UVA range observed for SA5 is due to the presence of AVO which absorbs maximally in the long wavelength UVA region.

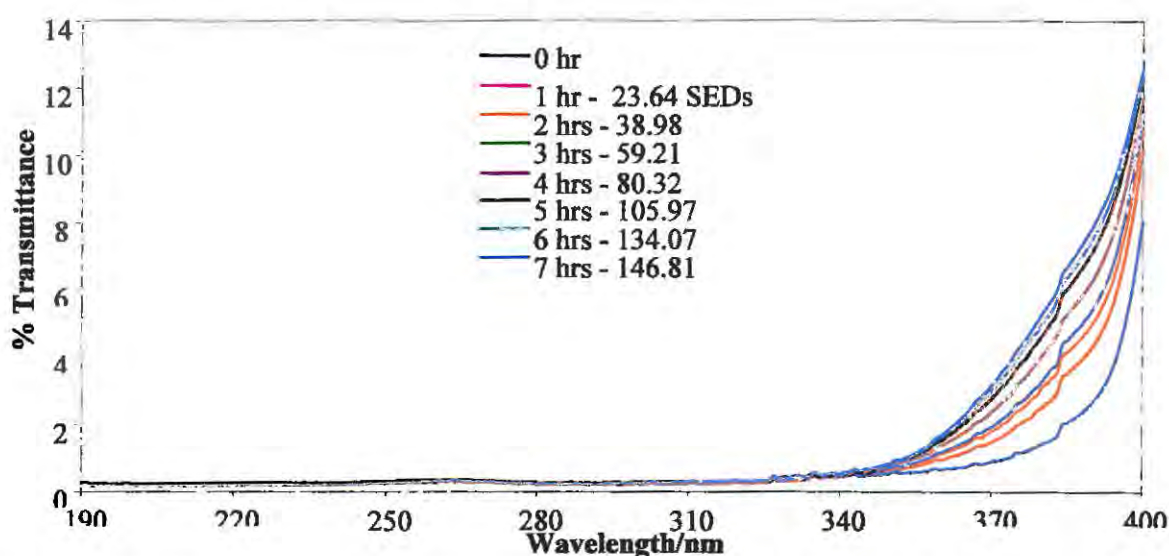


Figure 3.37: Changes in the spectral transmission of SA5 on a quartz plate (1 mg cm⁻²) with increasing solar irradiation.

The product was quite photostable, with an overall loss in photostability of 1.23% in the UVA region and 0.02% in the UVB region after receiving a total dose of 146.81 SEDs. The slight photoinstability in the long wavelength UVA region was attributed to the loss of AVO upon exposure to sunlight. There was a steady increase in photoinstability with irradiation time as observed with most of the products discussed so far.

3.3.3.13 Sunscreens containing OMC, Bz-3, AVO, OS and TiO₂

Figure 3.38 shows the change in the spectral transmission of SA11 on a quartz plate with irradiation time.

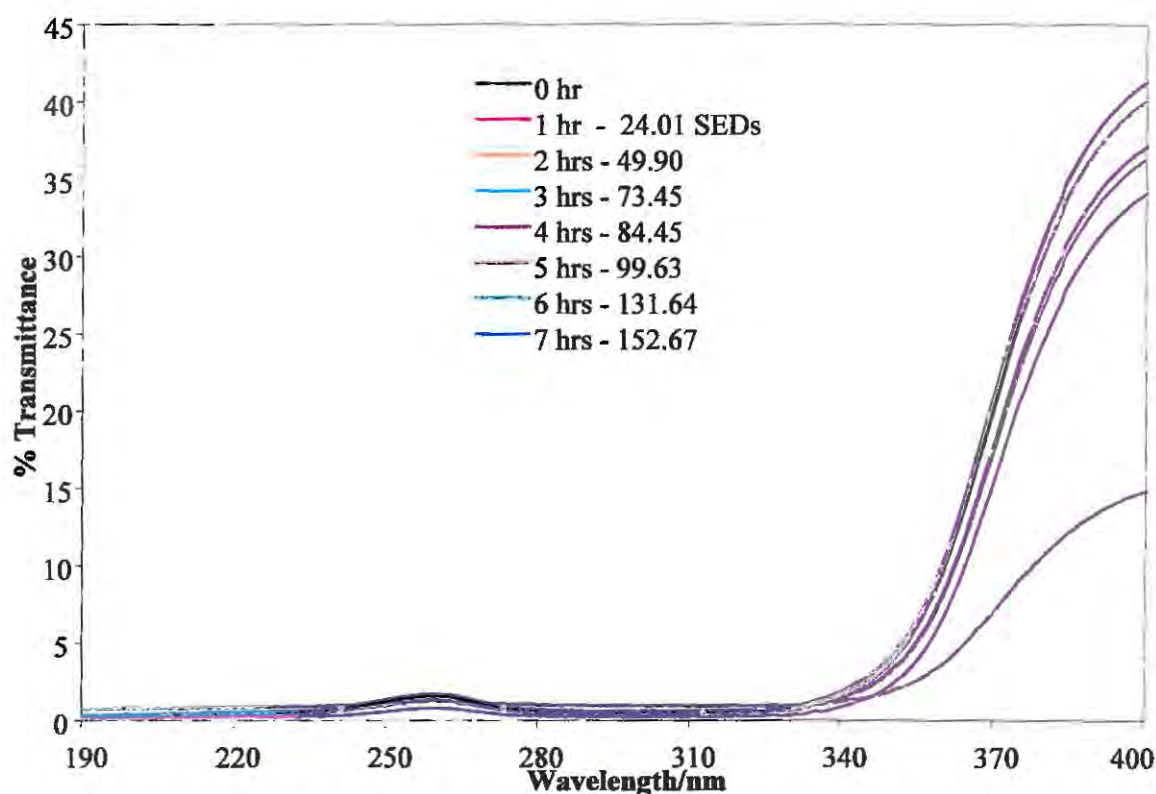


Figure 3.38: Changes in the spectral transmission of SA11 on a quartz plate (1 mg cm⁻²) with increasing solar irradiation.

SA11 had a UV filtering system quite close to that of SA10 (see Table 3.9) except for the presence of an additional active agent, MBC, initially not declared in SA11 (see Figure F15 of Appendix F for chromatogram). MBC absorbs in the UVB region like OMC and OS, hence the spectral transmission curves of the two products (SA10 and SA11) are expected to be similar. Like SA10 (see Figure 3.30), the spectral coverage of SA11 did not extend much into the long

wavelength UVA region as observed in the products, SA6-9, SA15, SA20, SA21 and SA22 discussed above. This is because we only have TiO₂ and Bz3 as the UVA absorbers whose spectral absorption is largely confined to the UVB (280 – 320 nm) and short wavelength UVA (320 – 340 nm) range.

SA11 again showed a large increase in transmittance in the long wavelength UVA range after exposure to sunlight in the first hour. Overall photoprotection loss was 7% (UVA region) and 0.55% (UVB region) after receiving a total UV dose of 152.67 SEDs. The two products, SA10 and SA11 were from the same manufacturer. SA11 also contained SiO₂ and mica.

3.3.3.14 Sunscreens containing OMC, AVO, OT, BEMT, DOBT and TiO₂

Figure 3.39 displays the change in the spectral transmission of SA14 on a quartz plate with irradiation time.

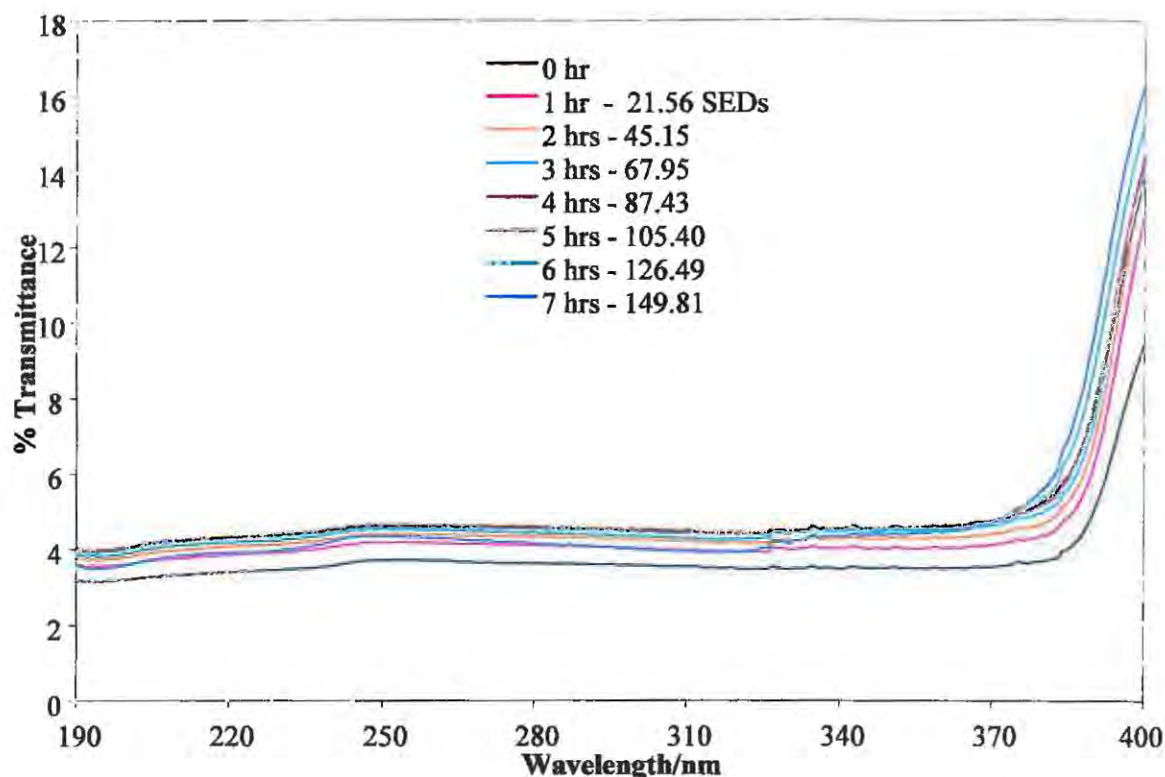


Figure 3.39: Changes in the spectral transmission of SA14 on a quartz plate (1 mg cm⁻²) with increasing solar irradiation.

SA14 had a complex UV filtering system comprising of up to six active ingredients namely: AVO, OT, TiO₂, BEMT, OMC and DOBT. DOBT and OT both absorb in the UVB region. The absorption spectrum of OT can be found in Figure 2.2a. The transmission spectra of SA14 extended more to the long wavelength UVA region than SA13 (see Figure 3.32) which can be attributed to the presence of AVO in addition to BEMT. The spectral coverage observed here agreed well with the claim on the bottle of offering protection in the UVA region.

Unlike some products containing AVO, there was no pronounced change in photoprotection in the UVA region throughout the irradiation period for SA14. BEMT is a broad-spectrum absorber and is known to be highly photostable as mentioned earlier. It has been shown to photostabilise AVO.¹³⁴ Overall loss in photoprotection was 0.57 and 0.31% for the UVB and UVA regions, respectively.

The photoinstability data for each product for the total 7-hour irradiation period was processed as detailed in Section 2.5.4.1. Tables 3.11 and 3.12 display the summarised results of the mean photoinstabilities of different sunscreen products analysed on a quartz plate and in solution, respectively. The method detailed in Section 2.5.4.1 was used to distinguish between photostable and photounstable products.

A mean photoinstability of $\geq 5\%$ for an irradiation time of 2 hours either in the UVB (ΔT_{UVB}) or in the UVA (ΔT_{UVA}) range was set as the threshold value (see Table 3.11). Of the twenty products analysed, 7 (in bold print) showed photoinstabilities that were significantly higher than 5% in the UVA region after 2 hours of irradiation or exposure to solar radiation. Only two products, SA3 and SA15, exhibited photoinstability in both the UVB and UVA regions ($\Delta T_{UVB/UVA}$). None showed photoinstability in the UVB region alone at about 40 SED (2 hours of irradiation). SA11 was classified as photostable though at 2 hours of irradiation, it exhibits a photoinstability (ΔT_{UVA}) of 5.06%. However, the photostability does not change that much at higher UVR doses. Besides the two products (SA3 and SA15) that showed photoinstability in both the UVA and UVB regions after 2 hours of irradiation, one product, SA1 showed an increase in transmittance of 7% plus in the UVB region at higher UV doses. For irradiation periods of 1, 3, 4, 5, 6, and 7 hours, the numbers of photounstable products are 6, 9, 10, 11, 11 and 13, respectively, in either the UVA or the UVB region. What is noticeable in these values is an increase in the number of photounstable products with increasing UV doses. Except for a few, we can confidently say photoinstability increases with increase in irradiation time in the two wavelength ranges.

Table 3.11: Mean photoinstability in the UVA (320 - 385 nm) range, ΔT_{UVA} (%), and the UVB (290 - 320 nm) range, ΔT_{UVB} (%), for an UV exposure of 1-7 hours for the sunscreen samples smeared on a quartz plate.

Sample	UVR region	Irradiation time/hour						
		1	2†	3	4	5	6	7
SA1	ΔT_{UVA}	-26.53	-31.13	-28.25	-33.52	-38.22	-36.57	-33.40
	ΔT_{UVB}	-1.94	-3.14	-3.34	-8.17	-11.09	-11.44	-10.79
SA2	ΔT_{UVA}	-21.67	-23.77	-22.89	-24.49	-27.55	-26.73	-26.94
	ΔT_{UVB}	-0.10	-0.28	-0.37	-1.65	-2.38	-2.76	-3.32
SA3	ΔT_{UVA}	-22.35	-22.11	-22.29	-20.71	-17.48	-13.76	-11.15
	ΔT_{UVB}	-34.68	-33.87	-33.50	-20.22	-14.97	-7.31	-4.46
SA4	ΔT_{UVA}	-2.41	-2.52	-2.54	-2.69	-2.75	-2.78	-2.79
	ΔT_{UVB}	0.57	0.62	0.58	0.58	0.60	0.59	0.59
SA5	ΔT_{UVA}	-0.34	-0.50	-0.59	-0.83	-1.04	-1.13	-1.23
	ΔT_{UVB}	0.01	0.04	-0.01	0.01	-0.04	-0.01	-0.02
SA6	ΔT_{UVA}	-0.64	-1.22	-1.83	-2.02	-3.28	-4.57	-5.60
	ΔT_{UVB}	-0.16	-0.22	-0.23	-0.25	-0.40	-0.47	-0.54
SA7	ΔT_{UVA}	-0.19	-0.53	-0.85	-1.08	-1.76	-2.75	-3.49
	ΔT_{UVB}	0.04	0.01	0.03	-0.01	0.01	0.02	0.01
SA8	ΔT_{UVA}	-0.34	-0.92	-1.49	-1.65	-2.45	-2.78	-2.79
	ΔT_{UVB}	0.08	0.07	0.08	0.07	0.07	0.07	0.06
SA9	ΔT_{UVA}	3.05	2.85	2.73	2.61	2.26	2.09	1.93
	ΔT_{UVB}	1.07	1.03	1.02	1.00	0.83	0.82	0.81
SA10	ΔT_{UVA}	-3.51	-3.83	-4.12	-3.84	-5.06	-5.61	-5.51
	ΔT_{UVB}	0.34	0.22	0.16	0.16	-0.12	-0.22	-0.27
SA11	ΔT_{UVA}	-3.93	-5.06	-5.27	-5.33	-6.48	-7.01	-6.66
	ΔT_{UVB}	0.72	0.49	0.48	0.45	0.38	0.35	0.55
SA13	ΔT_{UVA}	0.50	-0.04	-0.16	-0.17	-0.17	-0.27	-0.31
	ΔT_{UVB}	0.19	-0.44	-0.52	-0.51	-0.53	-0.56	-0.57
SA14	ΔT_{UVA}	-0.55	-0.83	-1.05	-1.13	-1.17	-1.15	-1.07
	ΔT_{UVB}	-0.44	-0.67	-0.89	-0.92	-0.95	-0.77	-0.42
SA15	ΔT_{UVA}	-21.79	-41.37	-43.78	-44.50	-44.88	-45.54	-45.57
	ΔT_{UVB}	-2.84	-8.80	-12.39	-14.22	-14.90	-16.29	-17.37
SA16	ΔT_{UVA}	0.40	-0.80	-0.89	-0.90	-0.91	-1.02	-0.99
	ΔT_{UVB}	0.00	0.00	0.00	0.00	-0.01	-0.03	0.00
SA18	ΔT_{UVA}	-24.14	-26.58	-29.21	-29.21	-27.00	-27.65	-27.17
	ΔT_{UVB}	-0.97	-1.11	-1.14	-1.14	-0.89	-1.16	-1.57
SA19	ΔT_{UVA}	-0.58	-1.83	-4.14	-5.30	-7.73	-9.48	-10.57
	ΔT_{UVB}	0.01	0.02	0.01	0.01	0.02	0.02	0.01
SA20	ΔT_{UVA}	-9.88	-19.18	-25.77	-29.68	-33.51	-35.07	-35.88
	ΔT_{UVB}	0.00	0.00	0.00	0.00	-0.01	-0.05	-0.07
SA21	ΔT_{UVA}	-2.10	-6.63	-14.80	-17.72	-21.32	-22.81	-23.28
	ΔT_{UVB}	0.08	0.09	0.08	0.08	0.09	0.08	0.08
SA22	ΔT_{UVA}	-0.30	-0.71	-1.58	-1.68	-2.70	-4.37	-7.43
	ΔT_{UVB}	0.04	0.01	-0.07	-0.07	-0.11	-0.19	-0.30

† A photoinstability of $\geq 5\%$ for an UV exposure period of 2 hours was used to distinguish between photostable and photounstable products (shown in bold).

The photoinstability data from the analysis of sunscreens in solutions are shown in Table 3.12. The associated transmission spectra of the products analysed in solution have been discussed above.

Table 3.12: Mean photoinstability in the UVA (320 - 385 nm) range, ΔT_{UVA} (%), and the UVB (290 - 320 nm) range, ΔT_{UVB} (%), for products analysed in solution.

Sample	UVR Region	Irradiation time/hour						
		1	2†	3	4	5	6	7
SA1	ΔT_{UVA}	-1.03	0.05	-1.40	-1.03	-1.37	-1.50	-1.51
	ΔT_{UVB}	-0.18	-0.18	-0.21	-0.18	-0.20	-0.21	-0.23
SA2	ΔT_{UVA}	-1.21	-1.11	-1.32	-1.35	-1.27	-1.76	-1.60
	ΔT_{UVB}	-0.11	-0.23	-0.34	-0.44	-0.53	-0.91	-0.95
SA3	ΔT_{UVA}	-0.41	-0.42	0.36	0.26	0.14	0.33	0.38
	ΔT_{UVB}	0.01	-0.02	-0.04	-0.02	-0.01	-0.01	0.02
SA6	ΔT_{UVA}	-0.08	-0.09	-0.14	-0.12	-0.14	-0.17	-0.10
	ΔT_{UVB}	0.04	0.02	0.00	0.00	0.00	-0.01	-0.01
SA15	ΔT_{UVA}	-16.42	-36.59	-40.48	-42.37	-42.40	-44.08	-44.09
	ΔT_{UVB}	-0.02	-0.02	-0.06	-0.06	-0.06	-0.01	-0.04
SA20	ΔT_{UVA}	-4.60	-5.05	-5.56	-6.42	-7.71	-8.76	-8.22
	ΔT_{UVB}	0.07	0.10	0.07	0.08	0.04	0.03	0.05
SA21	ΔT_{UVA}	-3.42	-10.03	-10.00	-10.17	-10.60	-10.37	-10.37
	ΔT_{UVB}	0.03	0.00	0.00	0.02	0.01	0.03	0.00

† A photoinstability of $\geq 5\%$ for an UV exposure period of 2 hours was used to distinguish between photostable and photounstable products (shown in bold).

From Table 3.12, it can be seen that most products analysed in solution displayed very high photostabilities. Only 2 of the products have shown significant photoinstability in solution. The products; SA1, SA2, SA3 and SA6 showed photoinstabilities of not greater than 1.60% in both the UVB and UVA regions when analysed in solution. However, SA15 and SA21, after 2 hours of irradiation displayed photoinstabilities of 36.59 and 10.03% in the UVA region, respectively. Overall, SA15 lost 44.09% of its photoprotective power and SA21 lost 10.37% after seven hours of irradiation in the UVA region. SA20 showed high photostability in solution. SA20

registered an overall increase in transmittance of 8.22% in the UVA region. Most products that showed high photoinstability on a quartz plate exhibited very high photostabilities here. None of the products analysed in solution showed photoinstability in the UVB region. The high photostabilities can be attributed to the stabilization of the active ingredients by the solvent itself, since it absorbs in the UVB region as shown in Fig. 2.9. The observations made from this analysis demonstrate that the behaviour of sunscreens in actual use (assumed to be thin, dry films on skin) cannot be predicted from results elicited from solution analysis.

3.3.4 Discussion

Almost all formulations with OMC and AVO in combination were photounstable to some degree. This was with the exception of SA14 which contained the broad-spectrum UV filter, BEMT. The broad-spectrum UV-filters, MBBT and BEMT, are known to be highly photostable and can be employed to photostabilise AVO- and OMC-containing formulations.^{211, 212} Probably that explains why there was no significant photoinstability in the products containing either of these two active agents. Besides BEMT and MBBT, OCR is also normally employed to photostabilise OMC though it only appeared in one product (SA13) which was found to be photostable. Only two products (SA5 and SA14) which contained both AVO and OMC displayed good photostability. As for why SA5 (without broad-spectrum stabilisers) did not show photoinstability is not clear. A plausible explanation can be that of the different solvent influence on the photochemical behaviour of sunscreen active ingredients. As mentioned earlier, AVO is photostable in polar protic solvents but unstable in non-polar or polar aprotic solvents.¹¹² The products with the same UV-filter system have shown similar, if not the same, spectral behaviour, e.g. SA6-8, SA21 and SA22. However, the photostability behaviour was not necessarily the same for products sharing a common UV filtering system, SA6-8 (photostable) and SA21 (photounstable).

The presence of TiO₂ may or may not affect the photostability and photochemical behaviour of sunscreen products. SA15 had a UV filtering system (AVO, OMC and TiO₂) almost close to that of SA20 (without TiO₂). Both products displayed high photoinstability in the UVA region on quartz plate but in solution, SA20 showed high photostability whereas SA15 still showed high photoinstability. The high photoinstability of SA15 can possibly be explained by the photocatalytic effect of TiO₂ or the vehicle influence on AVO and OMC. SA21 also (with TiO₂, AVO, MBC and OMC) showed photoinstability both in solution and on quartz plate. However,

SA6 with the same UV filtering system as SA21 displayed high photostability both on quartz plate and in solution. This probably points to the effect of the emulsion in which the sunscreen agents are dispersed. The differences in behaviour amongst products with the same UV filtering system can be attributed to the different vehicle influence on the photochemical behaviour of active ingredients.

Sharing a common UV filtering system does not necessarily mean the same photostability behaviour amongst products. This aspect has been demonstrated by the different photostability behaviour observed with sunscreen products, SA6 (photostable) and SA21 (photounstable). Nevertheless, except for SA14, all the products containing AVO have to some degree shown photoinstability in the UVA region. It is also worthy mentioning that most products with AVO afforded better broad-spectrum protection initially. All the photounstable commercial sunscreen products displayed photoinstability largely in the UVA region. This finding is in agreement with previous observations by Maier *et al.*¹⁴⁷

Antioxidants, such as vitamins, are normally incorporated in the formulation of sunscreen products. Topical vitamin E provides photoprotection by both antioxidant and UV absorptive properties.^{45, 213, 214} As an antioxidant, vitamin E scavenges free radicals and reactive oxygen species (ROS), thus reducing UV-induced oxidative stress on the skin.^{45, 153} By scavenging free radicals, vitamin E also reduces attack of sunscreen molecules by these reactive intermediate species, thus increasing the photostability and photoprotective capacity of a sunscreen formulation. Eleven sunscreen products analysed contained vitamin E and 2 showed photoinstabilities which were significantly higher than 5% in the UVB and/or UVA regions.

The photoinstability of sunscreens both in solution and on quartz plates was found to be UV dose dependent. There was an increase in photoinstability of sunscreens with increase in irradiation time. The photostability behaviour of sunscreens in solution was found not to be the same as that on a quartz plate. Quartz plates were used to mimic typical application conditions where a thin sunscreen film is applied onto the skin. Sunscreen products displayed higher photostabilities in solution than on a quartz plate. The higher photostabilities elicited in solution were ascribed to the photostabilising effect of the solvent since it absorbs in the UVB region.

In carrying out photostability studies on thin films of sunscreen product smeared on a quartz plate, it is desirable that the method of analysis be checked by a suitable independent method in order to validate the results and conclusions drawn from such a study. For that, the HPLC

technique was employed to analyse selected commercial sunscreens. The HPLC work was carried out to check if there was formation of any photoproducts after irradiation of sunscreens in the sun. Application of a separation technique (HPLC) in the assessment of the photostability of sunscreens affords quantitative as well as qualitative analysis of the sunscreen ingredients remaining and possible photoproducts formed after irradiation. Analysis of irradiated sunscreen samples by HPLC gives more insight into the type of photoproducts formed in photounstable formulations upon exposure to solar UVR. Separation and characterization of the different photoproducts yields structural information and phototoxicity tests can be carried out on the photoproducts.

An attempt was made to quantify the remaining active ingredients after 6 hours of irradiation in the sun, and to compare the remaining amounts to the determined concentrations displayed in Table 3.5. Quantitation of active ingredients was carried out as described in Section 2.3. Table 3.13 presents results of the percentage loss (% m/m) of active ingredients in different sunscreen products analysed by HPLC after irradiation in the sun.

Table 3.13: Percentage (% m/m) loss of active ingredients in different sunscreen products after irradiation.

Sample	% m/m loss of active ingredients				
	OMC	MBC	Bz3	OS	AVO
SA1	19.33	-	-5.56	-	-
SA3	25.00	5.17	3.84	-0.89	-
SA15	37.05	-	-	-	undetectable
SA16	25.97	9.90	-	-	-
SA20	35.35	-	-	-	undetectable
SA21	32.40	10.52	-	-	undetectable

From the chromatograms of irradiated suncare products (SA15, SA20 and SA21) containing AVO, it was shown that AVO completely photodegraded to unknown photoproducts. The chromatograms of the irradiated samples of the three products are shown in Figures 3.15, 3.11 and 3.23, respectively. The allowed levels of AVO in a formulation are low, with a maximum of 5%. The reason for such a small amount is probably due to the photoallergic and allergic reactions reported with AVO.²¹⁵ The determined levels of AVO in all products were below 3% and upon irradiation of some products, all the AVO was lost to photodegradation and photoisomerisation. This finding confirmed our suspicion that the increase in the spectral

transmittance in the UVA region in most products containing AVO was a result of the photoloss of AVO. The photoallergic reactions reported with AVO could be a result of the photoproducts formed upon exposure to UVR or generation of singlet oxygen via the triplet keto form of AVO.

The second most photounstable active ingredient as displayed in Table 3.13 was OMC. Photolosses of up to 37% were observed. The photoloss of OMC is said to be essentially due to its photoisomerisation to the *cis*-isomer.¹³¹ Ricci *et al.*²¹⁶ reported contact sensitisation to OMC though there are no reports of the generation of singlet oxygen by OMC. MBC showed up to 10% loss in concentration which is mainly attributed to its photoisomerisation to the *cis*-isomer as with OMC. It can also be seen in Table 3.13 that OMC and MBC are significantly lost even in the presence of MBBT and BEMT (SA16). Bz-3 and OS recoveries after irradiation were quite high. The latter two active ingredients are known to be photostable.¹⁶¹

HPLC analysis of irradiated SA3 gave two extra peaks in the chromatogram as shown in Figure 3.30. The new peak at 7.371 minutes was assigned to *cis*-MBC. The assignment is valid because the chromatograms for SA1, SA20 and SA15 in Figures 3.5, 3.11 and 3.15, respectively, where the UV filtering systems did not contain MBC, do not show this peak. It only showed in the three products: SA3 (Figure 3.28), SA16 (Figure 3.34) and SA21 (Figure 3.23), which contained MBC. Because the same peak showed in SA16 and SA21 which did not contain OS but MBC, it logically follows that it should be from MBC. MBC has been shown to photoisomerise to *cis*-MBC as reported by Tarras-Wahlberg *et al.*¹¹⁸ OS is known to be very photostable and there are no reports of its photodegradation. The high photostability of OS is attributed to the spatial arrangement of salicylates.¹⁶¹ The spatial arrangement allows for intra-hydrogen bonding in the molecule which shuts it away from interacting with solvent molecules.⁷³

The analysis of irradiated SA16 by HPLC showed that the two *tinorsorbs* (MBBT and BEMT) are photostable since the chromatogram did not show any new peaks (chromatogram not shown). Nevertheless, the chromatogram of the same product obtained under chromatographic conditions used to elute MBC and OMC showed the presence of two new peaks which were assigned to *cis*-MBC and *cis*-OMC. This finding shows that the presence of the *tinorsorbs* does not stop the photoloss of OMC and MBC to photoisomerisation *per se* as reported by Chatelain *et al.*¹³⁴ They reported that BEMT prevented or greatly reduced the photodegradation of AVO when alone or in combination with OMC. They also reported achieving higher recoveries of

OMC after irradiation in the presence of BEMT. This shows the importance of carrying out HPLC studies in addition to UV transmission.

If the results presented in Table 3.13 are anything to go by, it was shown that nearly 40% of OMC was lost in some sunscreen products after exposure to terrestrial solar UVR. There is also a lot of discussion about the possible photodegradation of OMC after exposure to UVR. Deflandre *et al.*¹⁴⁰ suggested that photoisomerisation takes place initially and is followed by photodegradation after a stationary phase has been established. Broadbent *et al.*¹¹⁴ isolated and identified photodimers of OMC from irradiated solutions of *trans*-OMC. The dimers are said to form via [2+2] cycloaddition reaction of the OMC molecule with itself. It is worth to note that all the experiments in which photodimers were isolated used simulated solar UVR where the UVR dose is normally of high intensity. It would be interesting to carry out such irradiation experiments in terrestrial solar UVR to see if these photodimers also form. Pattanaargson *et al.*¹³¹ used terrestrial solar UVR and just isolated the *cis*-isomer. Identification of the photoproducts formed in SA15 would probably shed more light on whether these photodimers are formed under application conditions.

3.4 Application of the *in vitro* critical wavelength method

The realisation that UVA plays an important role in the induction of skin cancer, chronic photoaging, photoimmune suppression and wrinkling of the skin has raised the need for sunscreen products to offer protection also in the UVA region. However, there is still no agreed method for the assessment of the broad-spectrum UV protection of a sunscreen formulation. One method of measuring the UVA protective efficiency of a formulation is the Star Rating (UVA/UVB ratio) according to the Boots Star Rating System. Diffey¹⁴⁹ proposed the critical wavelength (CW) *in vitro* method which is based on the absorption spectrum of a sunscreen formulation measured by UV/VIS absorption spectrophotometry. Diffey *et al.*¹⁵⁶ also applied the CW method to assess the broad-spectrum protective performance of sunscreen products. They proposed a minimum critical wavelength of 370 nm for broad-spectrum classification of a sunscreen formulation.¹⁵⁶ The CW method has been employed in the analysis of transmission spectroscopic data obtained in this study.

3.4.1 Broad-spectrum classification of sunscreens

The details of the calculation of the CW can be found in Section 2.5.4.2. Of the analysed sunscreen products, seventeen claimed broad-spectrum protection as listed in Table 2.1. The broad-spectrum protection was labelled by means of a star rating or by the 'UVB/UVA block' claim. In eight of the commercial sunscreens that declared broad-spectrum UV protection, the method of evaluation of the UVA protective efficiency was not given. Nine of the commercial sunscreens used the star rating system to indicate broad-spectrum protection. A comparison was made between the CW data obtained and the protection claimed on the label. It was assumed that those products using the number of stars to indicate broad-spectrum protection used the Star Rating method as proposed by Diffey.¹⁴⁹

Table 3.14 presents the calculated mean CW values, SPF numbers and the protection claims of the different products analysed. Each mean CW value is from 4 independent replicate product films. Critical wavelengths are also given for four products that did not make any claim of broad-spectrum ultraviolet protection. Table 3.15 gives the different CW ranges and the broad-spectrum rating or the number of stars for the respective ranges according to Diffey.¹⁴⁹ Table 3.15 was used to classify the broad-spectrum UV protection of products.

Of the nine products using the star rating system, it can be seen that two of the products agree with the calculated CW values (in bold). For the other 7 products (SA6, 9, 12, 13, 14, 15 and 16), the calculated CW values were higher than the range for the number of stars on the label. The variation could be a result of differences in sample preparation, but there is a strong correlation between the experimental data and the labelled information.

According to Table 3.15, a sunscreen formulation is said not to offer any UVA protection if the CW is less than 325 nm. From a CW value of 325 nm and up, the product can have the claim of offering broad-spectrum UV protection. A look at the calculated CW values and taking cognisance of the latter statement, we see that the CW data obtained agreed well with the broad-spectrum protection claims on 100% of the products. However, using the proposed minimum of 370 nm, three of the products claiming broad-spectrum protection would fail the test. SA18 without any UVA filter had a CW of 349 nm and according to Table 3.15, it offers some degree of UVA protection. Though no claim of UVA protection was on the label, such observations certainly call for a revision of the UVA star rating system. Perhaps that is the reason Diffey *et al.*¹⁵⁶ proposed a minimum of 370 nm.

Table 3.14: Details of the critical wavelength, SPF number and protection claim of the 21 commercial sunscreens analysed.

Sample Label.	SPF No.	λ_c /nm	Protection claim	
			UVA	UVB
SA1	5	360	✓	✓
SA2	10	354	✓	✓
SA3	30	360	✓	✓
SA4	40	381	✓	✓
SA5	40	381	✓	✓
SA6	8	382	***	✓
SA7	15	381	****	✓
SA8	30	382	****	✓
SA9	40	378	***	✓
SA10	15	377	✓	✓
SA11	30	371	✓	✓
SA12	5	372	***	✓
SA13	15	385	***	✓
SA14	30	387	***	✓
SA15	4	379	***	✓
SA16	30	373	***	✓
SA18	6	349	-	-
SA19	25	377	✓	-
SA20	30	368	-	-
SA21	40+	377	-	-
SA22	36	386	-	-

Table 3.15: The CW ranges and broad-spectrum rating (the number of stars).

Broad-spectrum classification of sunscreens	
Critical wavelength (λ_c)/nm	Broad-spectrum rating /no. of stars
$\lambda_c < 325$	0
$325 \leq \lambda_c < 335$	1
$335 \leq \lambda_c < 350$	2
$350 \leq \lambda_c < 370$	3
$370 \leq \lambda_c$	4

From Table 2.1 and Table 3.14, it can be seen that the products that would pass the proposed 370 nm threshold all contain AVO, MBBT, TiO₂ or BEMT in their formulation. That reiterates the finding by Diffey *et al.*¹⁵⁶ that a long-wave UVA-filter was necessary for achieving the highest proposed broad-spectrum classification of 370 nm or more. Sixteen products had CW

values greater than 370 nm. Nevertheless, a close look at the CW values and the spectral coverage afforded by some suncare products did not seem to show any correlation. A comparison of SA4 (Figure 3.29) and SA5 (Figure 3.37) shows that the latter offers a broader spectral coverage than the former, but the two share the same CW value. Again SA9, SA15, SA16, SA19 and SA21 displayed a broader spectral coverage than SA4. However, the CW values of these products are smaller than that of SA4. The reason for such inconsistencies is not clear but it can be attributed to a variation in the amplitude of the UV/VIS absorption spectra of the different suncare products, which in turn is related to the concentrations of sunscreen active agents in a formulation and the vehicle in which the active agents are dispersed.

An attempt was also made to apply the CW method to assess the photostability behaviour of sunscreen products.

3.4.2 Photostability assessment of sunscreens using the critical wavelength method

The analysis simply entailed the calculation of the change in the CW value with irradiation time for a few selected products. The selection was inclusive of both the photostable and photounstable products.

Table 3.16 shows the data of CW change with irradiation time for selected products and these data were used to construct the curves shown in Figure 3.39. Figure 3.39 shows the change in the CW values for the different products with irradiation time. SA15 was plotted separately because of the unique trend of its CW data.

The photounstable products, SA20 and SA21 showed a sharp decline in the CW values as displayed in Figure 3.39. This correlates well with the increase in photoinstability in the UVA region with irradiation time as discussed above (see Table 3.11, Figures 3.8 and 3.21). SA20 showed a decrease in CW value of 6.09% from 376 nm to 339 nm after 2 hours of irradiation in the sun. SA21 registered a decrease of 4.26% for the same irradiation period, showing that SA21 is more photostable than SA20. This agrees with the photoinstability data listed in Table 3.11 above. While it is difficult to set a threshold percentage decrease in CW in order to classify as photostable or photounstable, there is a strong association between the change in the CW observed and the photoinstabilities of the products. The gradient of SA19 is gentler than those of the photounstable products, SA20 and SA21. The percentage decrease in the CW of SA19

was 3.45%. SA6 showed more of a straight line, indicating high photostability. SA6 registered an overall decrease in CW of just 1%. According to the photoinstabilities displayed in Table 3.11, it was found that overall, SA6 was more photostable than SA19 and CW results confirm the same. Diffey *et al.*¹⁵⁶ found a decrease in the CW values with increasing doses of UVR.

Table 3.16: Changes of CW with irradiation time for different sunscreen products.

Irradiation time /hour	Critical wavelength (λ_c)/nm					
	SA3	SA15	SA6	SA19	SA21	SA20
0	359	380	382	377	376	361
1	385	376	380	373	367	348
2	386	372	379	371	360	339
3	385	374	379	370	352	336
4	378	374	379	369	350	334
5	375	376	379	366	345	332
6	367	376	378	365	344	333
7	364	377	378	364	345	332

SA3 started off with a low CW and upon irradiation, the CW sharply increased to 385 nm in the first hour. The CW remained fairly constant for three hours and then dropped but not to the original value of 360 nm. This behaviour can be explained by the change in the shapes and depths of the transmission spectra of the product in the first three hours (Figure 3.25). Figure 3.25 shows that there is a decrease in transmittance in the long wavelength UVA region and an increase in transmittance in the UVB and the short wavelength UVA regions upon irradiation in the first hour and that remains fairly constant for the next 2 hours. The increase in the CW value observed is a result of the increase in the amplitude of the absorption curves in the long wavelength UVA range. Figure 3.40 shows the changes in the absorption spectra of the product (SA3) with irradiation time. There is an overlap of the absorption spectra at around the 370 - 380-nm range as indicated in the graph. Overall, the CW of SA3 decreased by 5.70%.

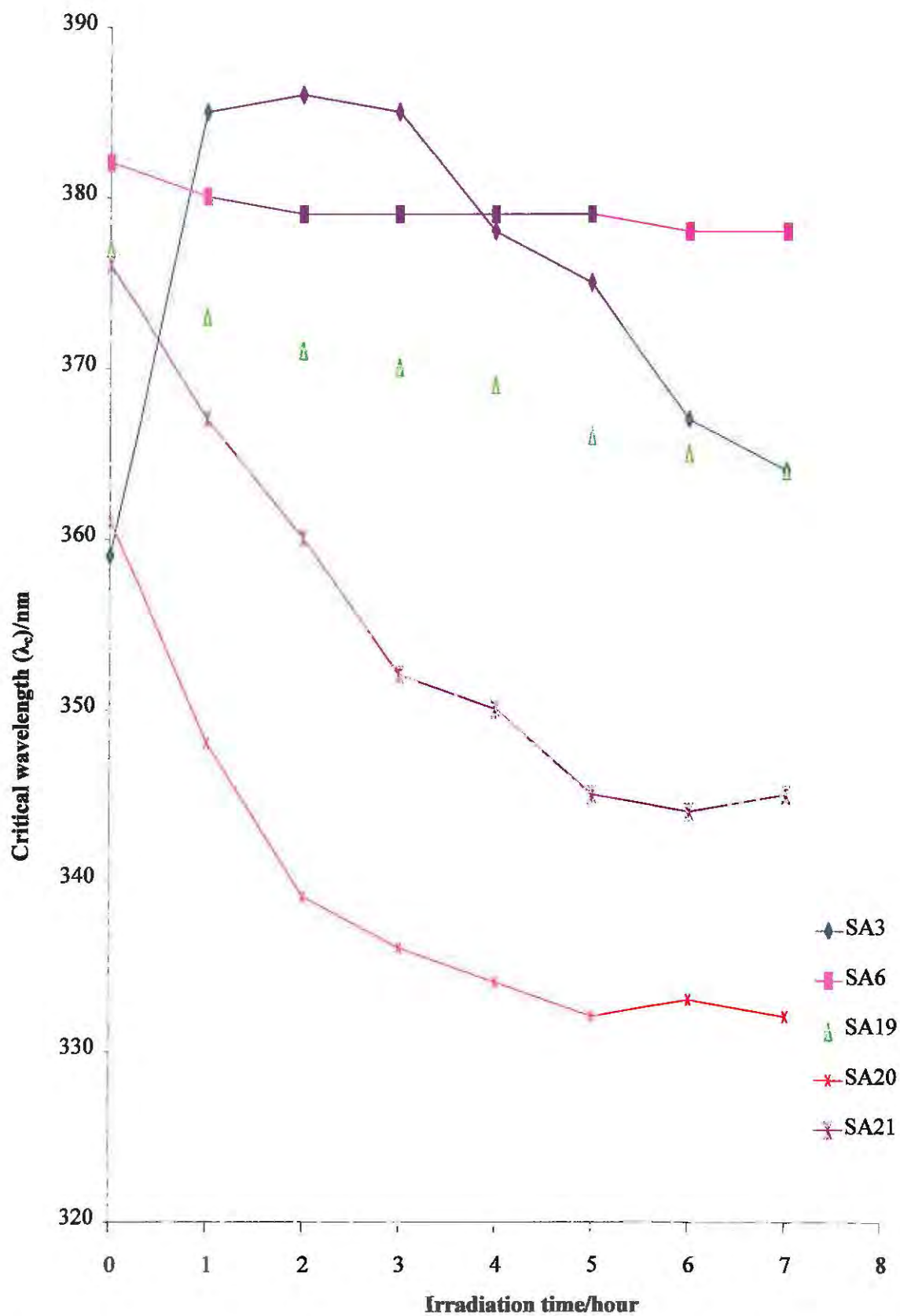


Figure 3.39: Changes in the critical wavelength of sunscreens on a quartz plate (1 mg cm^{-2}) with increasing solar irradiation.

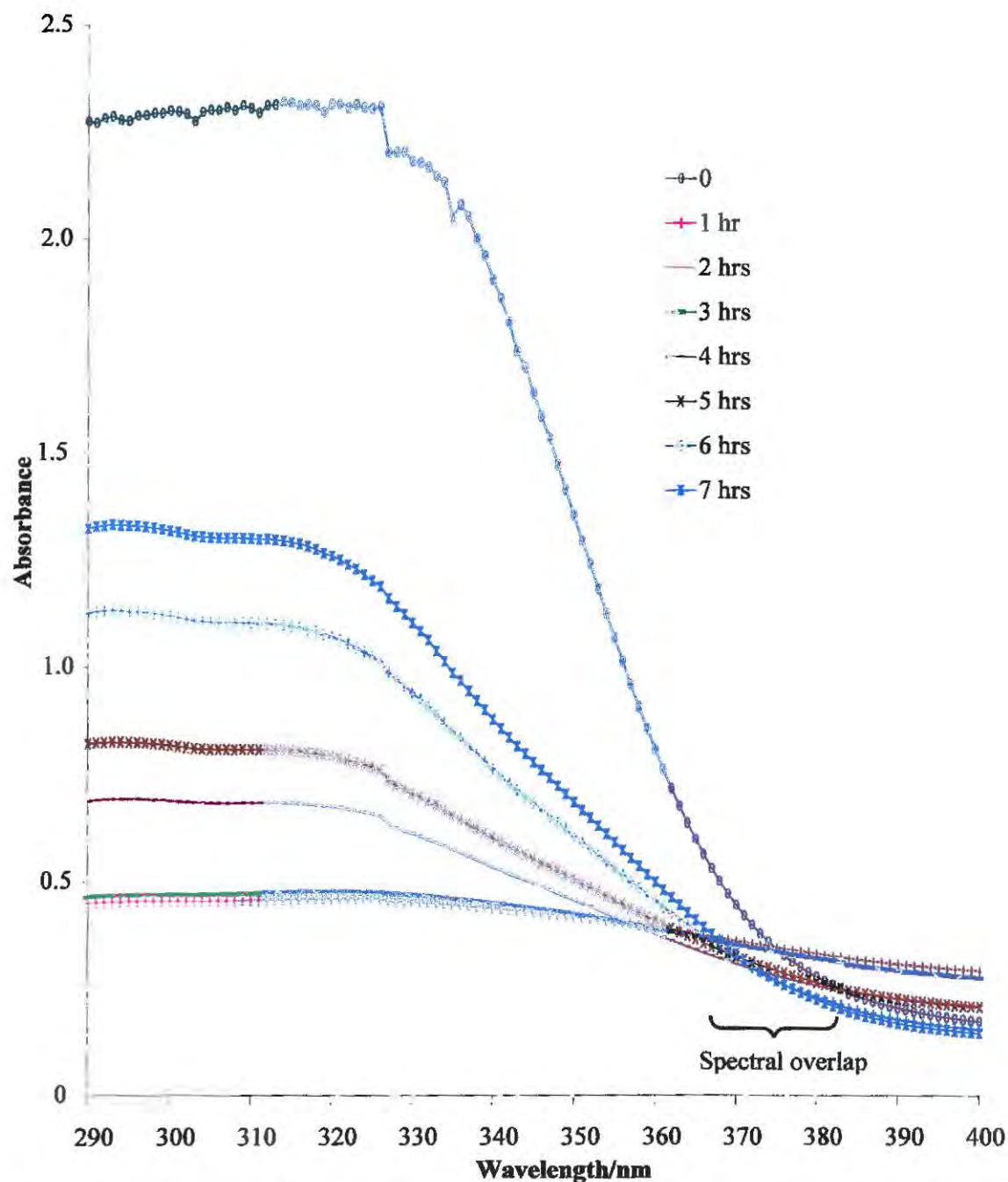


Figure 3.40: Changes in the absorption spectra of SA3 on a quartz plate (1 mg cm^{-2}) with increasing solar irradiation.

Figure 3.41 shows the changes in the critical wavelength values of SA15 with irradiation time. For this product, there was no systematic trend observed in the critical wavelength values with exposure to solar radiation. The photoinstabilities of the product presented in Table 3.11 showed an increase in photoinstability with increasing UV dose. However, there was no such correlation between the CW values and the irradiation time or the UV dose as displayed in Figure 3.41.

What can be noticed in Figure 3.41 is a decline in the CW value for the first two hours which then gradually rises with irradiation time. In an effort to explain this unique behaviour of SA15, the changes in the absorption spectrum of the product on quartz plate were plotted against irradiation time as shown in Figure 3.42.

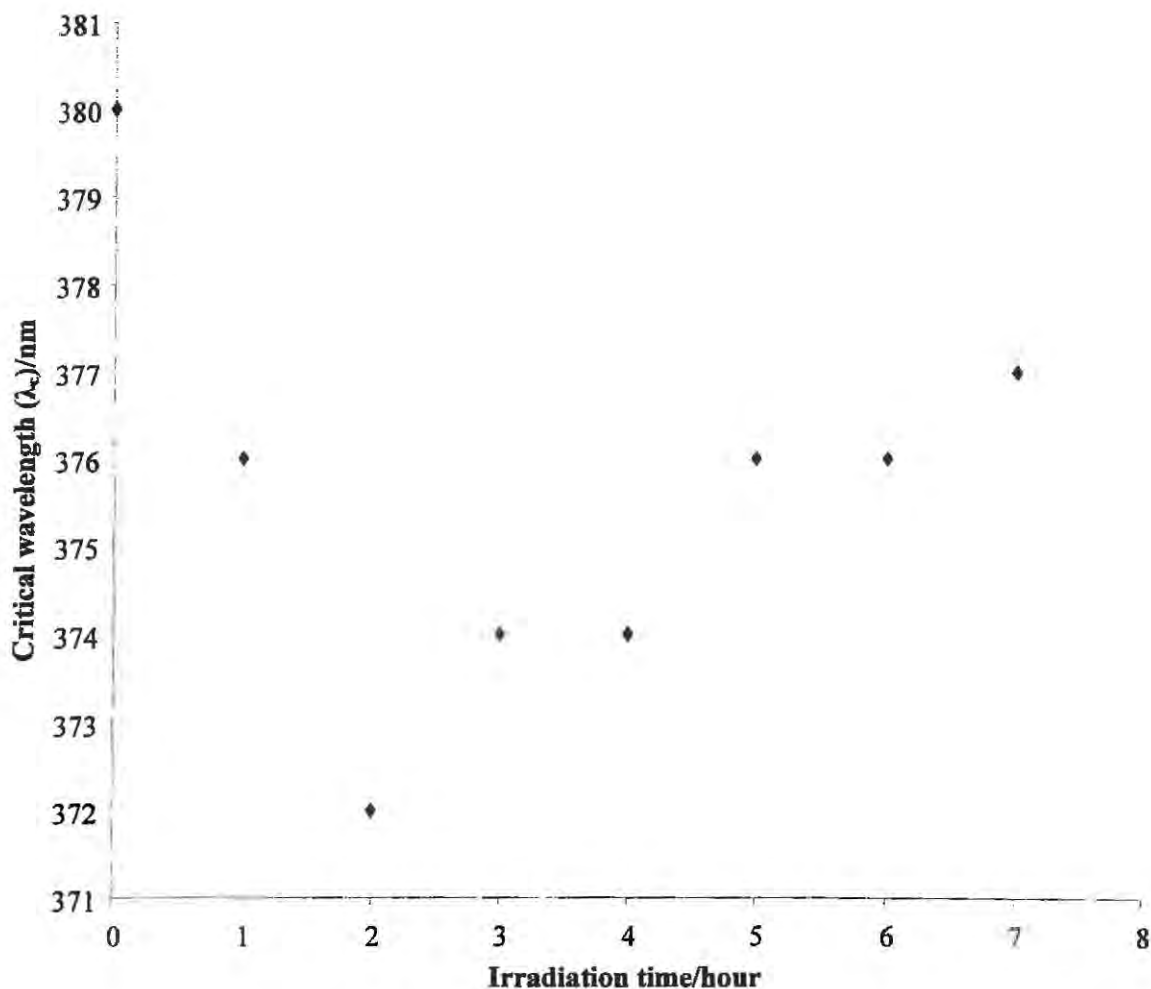


Figure 3.41: Changes in the critical wavelength of SA15 on a quartz plate (1 mg cm^{-2}) with increasing solar irradiation.

Figure 3.42 displays the change in the spectral absorption of SA15 with irradiation time. It can be seen that the shape and amplitude of the absorption spectra changed drastically in the first and second hours of irradiation. Further irradiation of the sample did not yield much change from the third hour and subsequent irradiations. The shape of the spectra remained essentially the same with slight changes in their amplitudes. The spectra overlap in the long wavelength UVA range from the third hour. That probably explains the scattered CW values. In such a situation, the photoinstability assessment of sunscreens by the CW method becomes weak.

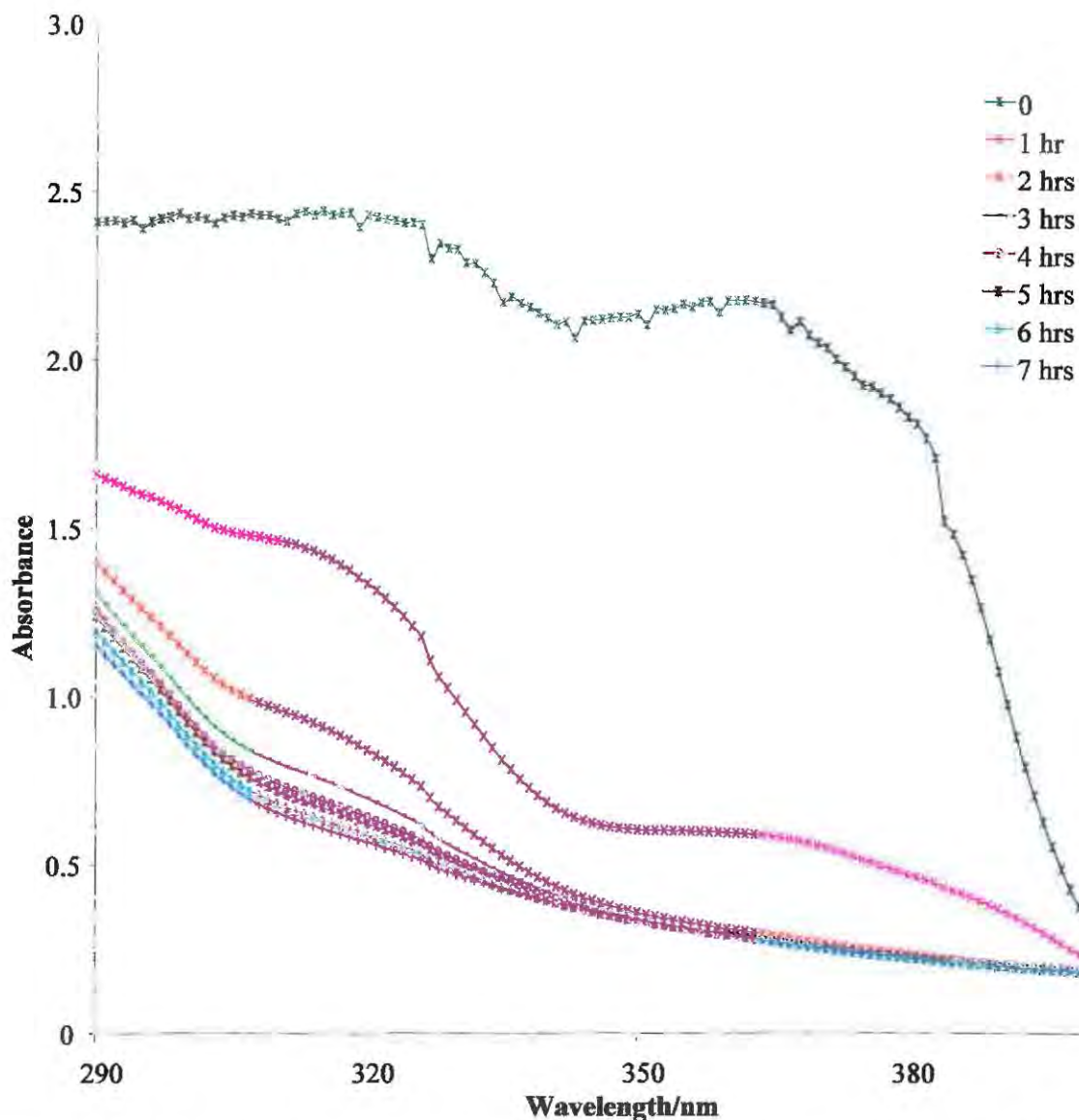


Figure 3.42: Changes in the spectral absorption of SA15 on a quartz plate (1 mg cm^{-2}) with increasing solar irradiation.

The findings from this section show that the *in vitro* CW method can be used with some degree of success, to measure the broad-spectrum UV protection of sunscreen products. Nonetheless, there is a need to revise the threshold CW for broad-spectrum classification of a sunscreen formulation. It was also shown that there is a fairly good correlation between the photoinstability and decrease in the calculated CW values. Therefore, the *in vitro* CW method can also be used to account for photoinstability of a sunscreen formulation, though there is need to set benchmarks in order to classify a sunscreen formulation as photostable or photounstable.

Chapter 4

CONCLUSION

There are two main concerns responsible for limiting chemical sunscreens for topical application: their potential for causing irritation and allergy, and the possibility of photochemical instability giving rise to potentially toxic photoproducts. Indeed, there are several reports of photocontact sensitivity reactions with some active ingredients. Investigations have also shown that these products may not be photostable *per se*. It has been demonstrated that some active ingredients used in sun care products photodegrade upon exposure to solar radiation. Consequently, that causes a reduction in the photoprotective capacity of sunscreen products besides the potential phototoxicity of the photodegradation products.

In the light of these concerns, the aims of this study were to assess the photostability behaviour of commercial sun care products available on the South African market as well as to determine the amounts of the active ingredients in these products.

The first part of the study involved the quantitative as well as qualitative analysis of commercial sunscreens by HPLC. The second part involved the photostability assessment of the commercial sunscreens by irradiation in terrestrial solar radiation. The analysis was carried out both on thin sunscreen films on quartz plates and after dispersion in solution. This was mainly to investigate if there is a correlation between the two methods. UV/VIS transmission spectroscopy and HPLC were used for the photostability assessment of sun care products.

The quantitative analysis of commercial sunscreens by HPLC showed that, generally, the levels of all sunscreen active ingredients in sun care products were within COLIPA acceptable limits. The determined mean concentration ranges were: 0.53 – 2.84% (AVO), 1.63 – 10.00% (OMC), 0.88 – 6.28% (Bz-3), 1.17 – 4.67% (MBC), 1.62 – 2.59% (BEMT), 3.38 – 3.85% (MBBT), 1.19 – 3.17% (OT) and 3.96% (OCR). The amount of TiO₂ measured in the commercial sunscreens ranged from 0.05 to 3.21%. This is far lower than the COLIPA approved level of a maximum of 25% in sun care products.

Judging from these results, it can be concluded that the levels of all sunscreen active ingredients contained in sun care products available on the South African market are within internationally

stipulated levels. Nevertheless, it is recommended that the levels of sunscreen active ingredients be constantly monitored to ensure the safety of the public.

From the photostability studies, it was observed that the products showed high photoinstability in the UVA region. There was generally a high photostability of the sun care products in the UVB region. This finding was in agreement with the findings of Maier *et al.*^{146, 147} who found that sun care products showed a high photostability in the UVB region, but were very photolabile in the UVA region. This is because sunscreens are selected and measured for their efficacy against erythema or sunburn whose action spectrum lies in the UVB region. The sun protection factor (SPF, see Section 1.3) of a sun care product is essentially a measure of the protective capacity of a sunscreen formulation against UVB radiation and does not account for the protective efficiency of a sunscreen formulation against UVA radiation.

There are just a few UVA filters available. The most commonly used is AVO, which absorbs maximally in the longer wavelengths UVA range. Unfortunately, as has been demonstrated in this study from the HPLC results, AVO is highly photolabile. The other available broad-spectrum filters, Tinosorb M (MBBT) and Tinosorb S (BEMT) are just new on the market and have been approved for use in sun care products only in Europe.¹⁶⁶ The United States Food and Drug Administration is yet to approve these two for use in the country. The two active ingredients were found to appear in just a few sun care products in this study. The poor protection in the UVA region is of concern as epidemiologic evidence has shown that UVA radiation plays a significant role in the induction of melanoma skin cancer.^{15, 42, 56}

In total, 35% of the commercial sunscreen products analysed were photounstable in the UVA region and only 10% were photolabile in both the UVB and UVA regions. The photoinstability in the UVA region was largely due to the photodegradation of AVO. There is therefore, a need to develop sunscreen active ingredients that offer high protective efficiency in the UVA region and they should also be highly photostable. Since the two broad-spectrum absorbers, MBBT and BEMT, have been shown to be highly photostable, manufacturers should not continue to use photolabile active ingredients when photostable ones are available. All the products (SA9, SA13, SA14 and SA16) containing the two *tinorsorbs* have displayed very good broad-spectral coverage as well as high photostability in both the UVB and UVA regions.

The photostability analysis of commercial sunscreen products by irradiation in the sun has shown that photoinstability is dose-dependent. There was generally an increase in

photoinstability with increase in irradiation time. In simple terms, the longer one stays in the sun the less the protection one gets from these products. Normally, manufacturers recommend that sunscreens be reapplied after every two hours. However, a study by Wright *et al.*⁶⁴ on beach goers in the USA (Texas) showed that the application of sunscreen was below that normally recommended and that most beach goers did not re-apply the sunscreens while in the sun. This then increases their risk of developing skin cancer. Overexposure to the longer wavelength UVA radiation may contribute to the reportedly high level of incidence of skin cancer in South Africa since most of the suncare products analysed offer poor protection in this spectral range and are photolabile.

The photostability analysis of suncare products in solution yielded higher photostabilities than on a quartz plate. The high photostabilities in solution were attributed to the stabilising effect of the solvent on the sunscreen active ingredients especially in the UVB region since the solvent shows absorption in this region. This means that the solvent system employed in the Australian/New Zealand UV Transmittance Standard is not ideal for sunscreen analysis. It would be interesting to try other solvent systems for such photostability studies. AVO was shown to exhibit high photostabilities when dispersed in MeOH,¹¹² but was photolabile in cyclohexane so these would not be a good choice for the photostability analysis of this active ingredient. The choice of an ideal solvent for sunscreen analysis is a complex process and does not simulate application conditions. Therefore, analysis of the unmodified suncare product smeared on a quartz plate should become the method of choice as it is more representative of the photophysical and photochemical processes occurring in thin sunscreen films on the skin.

Products with the same filter combination, namely SA6 and SA21, have displayed different photostability behaviour. The high photostability shown by SA6 and the poor photostability exhibited by SA21 point to the different emulsion or vehicle influences on the photochemical behaviour of the active ingredients. This finding highlights the importance of carefully choosing the emulsion for a particular UV filtering system. The photostability behaviour of SA6 (SPF8 - photostable), SA20 (SPF30 - photolabile) and SA21 (SPF30 - photolabile) also showed that a high sun protection factor does not necessarily mean high photostability.

Photostability analysis of commercial sunscreens by HPLC has shown that some active ingredients used in these products are photolabile. The analysis of irradiated commercial sunscreens by HPLC showed that OMC photoisomerises to the *cis*-form upon exposure to solar radiation. It has been shown that close to 40% of OMC is lost to photoisomerisation in some

products. MBC was also observed to undergo photoisomerisation but not to the same extent as OMC and AVO. AVO was shown to photodegrade completely in some products, leading to the formation of unknown photoproducts. These findings are in agreement with results from previous investigations.^{74, 113, 118, 140, 142}

The use of the *in vitro* critical wavelength method to assess the photostability behaviour of suncare products gave mixed results. While there was a strong correlation between the decrease in the critical wavelength value and the increase in photoinstability in most of the products (SA6, SA19, SA20 and SA21), SA15 showed the very opposite of what was expected. Nonetheless, the strong correlation observed means that the *in vitro* critical wavelength method can be applied to account for the photoinstability of suncare products upon exposure to sunlight. Moreover, most of the broad-spectrum protection data on the labels agreed well with the calculated critical wavelength data, though there is a need to revise upwards the threshold critical wavelength value for the broad-spectrum classification of suncare products.

In view of the findings from this study, it should be made mandatory for manufacturers in the cosmetic industry to test the photostability and the broad-spectrum protective capacity of their products before marketing. It therefore, calls for the development of standard methods (as for the sun protection factor measurement) for the assessment of these two important parameters in sunscreen development. This should be part of the broad effort in the fight against skin cancer.

I followed with keen interest the lawsuit filed against five of the leading US manufacturers of sunscreen lotions and sprays for deceptively promoting their products as 'All day Sunblocks.' The incidence of skin cancer in the country is said to be increasing despite people using these suncare products.²¹⁷ The bone of contention is the ability of these sunscreen products to protect against the longer wavelength UVA radiation which causes premature aging of the skin and is believed to induce the development of skin cancer. A month later, the European Commission issued a statement urging all sunscreen manufacturers to revise their product-labelling guidelines. 'Among the labels judged unacceptable were: sunblocker, total protection – and those that use unclear or imprecise terminology such as "broad spectrum", "strengthened protection UVA", and "100 per cent anti-UVA/UVB/IR".²¹⁸ In addition to previous similar findings, indeed this study has shown that commercial sunscreens are photounstable and therefore offer poor protection in the UVA region.

Future studies can be conducted on the photostability of commercial sunscreens in different solvents and be compared with the thin sunscreen film method. Other areas of study can include investigating the sunscreen application rate used by beach goers in South Africa. The public ought to be educated on the importance of applying the correct amount of sunscreen before going into the sun. Since photoinstability was mainly due to the photodegradation and/or photoisomerisation of OMC and AVO, efforts should be made to try and stabilise the two already approved active ingredients by means of intercalation in zeolites or hydrotalcites,²¹⁹ or encapsulation in cyclodextrins.¹³⁵ Plant extracts containing flavanoids have also been reported to be potent in mitigating the harmful effects of solar radiation on the skin.^{214, 220} Photostabilisation of these two active ingredients can also be achieved by use of polyphenols contained in these plant extracts.¹¹²

Appendix A

MATERIALS

The chemicals used for the purposes of this study have been categorized below together with the manufacturers' name and where relevant, the grade of chemical.

A1 Chemicals used for the quantitation of UV filters by HPLC

Methanol (99.8%)	-	BDH HiperSolv™ Chemicals, Ltd.
Acetonitrile (99.9%)	-	BDH HiperSolv™ Chemicals, Ltd.
Tetrahydrofuran (99.8%)	-	Lab-Scan Analytical Sciences, Ltd.
Chloroform (99%)	-	Waters Division of HPLC Pvt, Ltd.
DMSO (99.7%)	-	Riedel-de Haën
Dichloromethane (99%)	-	Saarchem
Isopropanol (99.5%)	-	Sigma-Aldrich
MBC	-	Merck
Bz-3	-	BASF
AVO	-	BASF
OMC	-	BASF
OS	-	Haamann & Reimer
OCR	-	BASF
OT	-	BASF
MBBT	-	Ciba Specialty Chemicals, Ltd.
BEMT	-	Ciba Specialty Chemicals, Ltd.

A2 Chemicals used for Actinometry (Gas Chromatography)

Valerophenone (99%)	-	Sigma-Aldrich
Acetone (99.8%)	-	Riedel-de Haën
Air	-	Fedgas
Hydrogen	-	Fedgas

Nitrogen - Fedgas

A3 Determination of titanium dioxide

Titanium dioxide (99.8%) - Riedel-de Haën

Sulphuric acid (98.0%) - Associated Chemical Enterprises C.C.
BDH Chemicals Ltd, Poole, England.

Potassium hydrogen sulphate (KHSO_4) - BDH Chemicals Ltd, Poole, England.

Appendix B

EQUIPMENT

All the equipment used in achieving the aims of this study is listed below.

B1 Equipment

Perkin Elmer Lambda 35 UV/VIS spectrophotometer

Waters 600 HPLC multisolvent delivery system with 225 μ l pumpheads, a Perkin Elmer Series 200 autosampler, a Waters 996 photodiode array detector, and a De' Mark Pentium II computer with Waters Millennium³² software

Phenomenex Synergi Max-RP-C₁₂ 80 Å column

Perkin Elmer Autosystem XL gas chromatograph

Millipore Milli-Q⁵⁰ ultra pure water apparatus

Millipore Durapore® 0.45 μ m membrane filters

Millipore Millex-LCR Hydrophilic PFTE 0.45 μ m syringe filters

Ultrasonic bath: Ultrasonic Manufacturing Company (UMC 20)

Appendix C

CALIBRATION AND ACTINOMETRY DATA

The following tables present the calibration data for all the active ingredients quantified in this study. The calibration curve for each active ingredient is presented in Appendix D.

Table C1: Calibration data for the determination of Bz-3.

Concentration /mol dm ⁻³	1 x 10 ⁻⁵	2 x 10 ⁻⁵	3 x 10 ⁻⁵	4 x 10 ⁻⁵	5 x 10 ⁻⁵	6 x 10 ⁻⁵	7 x 10 ⁻⁵
1	184304	350323	532797	715204	889221	1097280	1307445
	183503	351156	535634	714947	889012	1092609	1292631
	182964	352446	533370	716061	887180	1094164	1289533
	183584	351879	534843	715668	888047	1092627	1287854
	183139	352001	536149	715430	890698	1089773	1310075
2	180298	361385	562719	722141	919364	1057362	1259513
	181401	360621	565045	730214	921440	1062325	1259526
	179704	362828	567204	728555	914090	1054218	1256552
	180584	363814	571365	730171	911174	1061946	1256224
	181300	364247	575645	731329	924609	1053877	1265747
3	187486	368591	568634	730247	917004	1126942	1319433
	187622	368711	569843	732083	915047	1132421	1307177
	188436	369324	570149	731421	919526	1133831	1321648
	188894	367444	568797	732161	919611	1127333	1319513
	189102	368726	567875	729634	918180	1119164	1317520
Mean	184154.73	360899.73	557337.93	725017.73	908280.20	1093058.13	1291359.40
Std Dev	3324.94	7357.12	16925.92	7377.92	14584.23	29853.10	25618.90
RSD/%	1.81	2.04	3.04	1.02	1.61	2.73	1.98

Table C2: Calibration data for the determination of MBC.

Concentration /mol dm ⁻³	1 x 10 ⁻⁵	2 x 10 ⁻⁵	3 x 10 ⁻⁵	4 x 10 ⁻⁵	5 x 10 ⁻⁵	6 x 10 ⁻⁵	7 x 10 ⁻⁵
1	290901	582011	854899	1159971	1446482	1750204	2041997
	289914	579344	855547	1160122	1445284	1745711	2046640
	291401	581225	856974	1154174	1445018	1749014	2046691
	290256	580254	857096	1159241	1446102	1748101	2039732
	290184	581333	856403	1159546	1447038	1749127	2044680
2	287912	578234	904899	1169791	1476848	1700224	2021997
	287830	579434	904547	1170202	1474248	1694181	2026640
	287834	582125	906749	1164741	1482078	1700611	2026691
	287352	585027	909609	1179471	1484260	1708602	2037732
	288818	586490	920343	1179564	1486132	1699171	2034680
3	290882	589770	883554	1179540	1472590	1745292	2025897
	293662	586345	891997	1172690	1486663	1761972	2032505
	292284	588830	887812	1177660	1479688	1753704	2018319
	291139	589637	884334	1179274	1473890	1746834	2016945
	290122	588411	881245	1176822	1468743	1740732	2027708
Mean	290032.73	583898.00	883733.87	1169520.60	1467670.83	1732898.67	2032590.20
Std Dev	1807.75	4075.57	22851.52	9136.25	16635.56	24263.65	10043.47
RSD/%	0.62	0.70	2.59	0.78	1.13	1.40	0.49

Table C3: Calibration data for the determination of OS.

Concentration /mol dm ⁻³	1 x 10 ⁻⁵	2 x 10 ⁻⁵	3 x 10 ⁻⁵	4 x 10 ⁻⁵	5 x 10 ⁻⁵	6 x 10 ⁻⁵	7 x 10 ⁻⁵
1	103175	205295	292802	406133	515145	598113	704862
	103852	208238	295799	413020	516419	595666	698201
	103597	206010	293073	410805	514452	597320	701355
	102230	207742	290950	410600	523719	600841	691708
	103806	207066	291548	410786	519612	596541	691582
2	102750	207875	305991	412899	514983	614109	717168
	102502	210314	306921	411756	513740	614631	725583
	103222	208203	307353	412552	515348	615927	718300
	101670	206246	306773	410656	509570	616669	721548
	99481	207050	308086	412257	511598	613606	724322
3	103917	206773	307358	409057	508782	602419	709937
	104599	209737	308000	405921	510065	599954	713300
	104342	207493	305255	405705	508084	601620	710433
	102966	209237	307145	408520	507345	605167	714276
	104553	208556	305733	407700	508245	600836	713250
Mean	103110.80	207722.33	302185.80	409891.13	513140.47	604894.60	710388.33
Std Dev	1317.33	1391.96	6958.58	2570.46	4672.13	7785.04	10867.43
RSD/%	1.28	0.67	2.30	0.63	0.91	1.29	1.53

Table C4: Calibration data for the determination of AVO.

Concentration /mol dm ⁻³	1 x 10 ⁻⁵	2 x 10 ⁻⁵	3 x 10 ⁻⁵	4 x 10 ⁻⁵	5 x 10 ⁻⁵	6 x 10 ⁻⁵	7 x 10 ⁻⁵
1	345495	720444	1078186	1439757	1812989	2180384	2561636
	344997	721422	1081470	1438245	1826828	2178133	2558096
	345601	722022	1092100	1438069	1841700	2173441	2547220
	346075	720810	1089008	1435089	1827334	2176303	2556422
	346801	719689	1085031	1437831	1844735	2172520	2563830
2	348907	725196	1124053	1446766	1836355	2196280	2548838
	347417	724091	1122341	1454561	1828515	2186903	2551168
	347553	724375	1142781	1455128	1829230	2187759	2546103
	348430	725202	1134063	1446777	1833845	2193278	2553587
	352538	725764	1119934	1447899	1855465	2219136	2546047
3	346766	719697	1140204	1447686	1844550	2071205	2563573
	347460	720508	1127203	1449532	1812807	2080175	2551380
	348642	728608	1139994	1444914	1827151	2096187	2556166
	349722	723929	1134716	1440119	1826645	2113817	2547841
	350562	728406	1117748	1444044	1841515	2102970	2533468
Mean	347797.73	723344.20	1115255.47	1444427.80	1832644.27	2155232.73	2552358.33
Std Dev	2061.10	2964.20	23417.31	6135.60	11714.99	47910.37	8045.71
RSD/%	0.59	0.41	2.10	0.42	0.64	2.22	0.32

Table C5: Calibration data for the determination of OCR.

Concentration /mol dm ⁻³	1 x 10 ⁻⁵	2 x 10 ⁻⁵	3 x 10 ⁻⁵	4 x 10 ⁻⁵	5 x 10 ⁻⁵	6 x 10 ⁻⁵	7 x 10 ⁻⁵
1	144175	292295	450033	593145	743113	902748	1051813
	143852	292321	449120	592419	742666	901666	1052201
	143597	291910	448805	591452	747320	903320	1049355
	144230	291742	449600	591719	740841	902841	1046708
	143806	292122	448986	589612	746541	902541	1052582
2	147013	295619	453518	617823	749937	917756	1089058
	147759	293260	453303	613593	749489	916172	1079387
	148393	292961	452096	614126	750144	919330	1070531
	146967	294165	452282	616396	750665	917849	1077892
	148337	294887	456634	615288	749364	916548	1076765
3	143941	286857	443100	599512	742262	890554	1056780
	142656	284567	440075	595406	741820	889017	1047395
	143379	284278	439866	595924	742468	892081	1038801
	143994	285445	438696	598126	742985	890644	1045944
	142611	286146	438877	597050	741697	889381	1044850
Mean	144980.67	290571.67	447666.07	601439.40	745420.80	903496.53	1058670.80
Std Dev	2072.34	3935.87	5969.54	10615.47	3708.29	11551.85	15639.76
RSD/%	1.43	1.35	1.33	1.76501	0.50	1.28	1.48

Table C6: Calibration data for the determination of OT.

Concentration /mol dm ⁻³	1 x 10 ⁻⁶	2 x 10 ⁻⁶	3 x 10 ⁻⁶	4 x 10 ⁻⁶	5 x 10 ⁻⁶	6 x 10 ⁻⁶	7 x 10 ⁻⁶
1	159534	284228	444557	587072	734010	867420	980754
	157455	287445	443993	588336	735600	868321	984640
	155704	285196	443864	585344	734104	869229	983482
	153549	286961	440122	584621	733986	868978	985616
	154889	285869	439572	586425	734125	867884	988796
2	147551	274284	430156	547108	726615	870937	992141
	148752	272609	428590	546874	724117	872248	991025
	147610	273813	432967	546696	723138	872217	994872
	145606	272850	433173	546327	725023	872103	988170
	148035	273388	429722	546417	722999	871539	989289
3	155720	274557	439083	597788	724878	878472	1031990
	153639	277777	437517	599054	726470	879374	1025869
	151886	275526	441393	596058	724972	880284	1024710
	149728	277293	439648	595334	724854	880032	1026846
	151070	276200	440099	597140	724993	878937	1030030
Mean	152048.53	278533.07	437630.40	576706.27	727992.27	873198.33	1001215.33
Std Dev	4138.08	5654.94	5381.81	22463.09	4774.85	4823.36	19889.69
RSD/%	2.72	2.03	1.23	3.90	0.66	0.55	1.99

Table C7: Calibration data for the determination of BEMT.

Concentration /mol dm ⁻³	4.0 x 10 ⁻⁶	8.0 x 10 ⁻⁶	1.2 x 10 ⁻⁵	1.6 x 10 ⁻⁵	2.0 x 10 ⁻⁵	2.4 x 10 ⁻⁵	2.8 x 10 ⁻⁵
1	201414	396017	574795	795596	968663	1196522	1358926
	196950	393203	575591	795992	969996	1178292	1362132
	197915	394721	573080	794432	965900	1183790	1373573
	198752	395414	573964	796004	966752	1179674	1369445
	200483	393975	574023	794564	967223	1185426	1365466
2	195189	391514	568260	786550	957650	1173032	1363248
	194710	388732	569046	787151	958967	1178736	1366417
	195664	390233	566564	785310	954918	1180217	1367947
	194528	390918	567438	786617	955760	1176148	1363778
	193696	389495	567496	787441	956226	1171948	1360033
3	200421	396694	577668	809623	973506	1192454	1385820
	199985	395169	575945	810021	974845	1198253	1399091
	198745	397391	576893	808454	970729	1199758	1410697
	198904	397997	576833	810034	971585	1195622	1396409
	197934	395944	578468	808586	972059	1191353	1392368
Mean	197686.00	393827.80	573070.93	797091.67	965651.93	1185415.00	1375690.04
Std Dev	2448.86	2982.96	4164.52	9719.74	7023.12	9492.23	16655.70
RSD/%	1.24	0.76	0.73	1.22	0.73	0.80	1.21

Table C8: Calibration data for the determination of MBBT.

Concentration /mol dm ⁻³	1 x 10 ⁻⁵	2 x 10 ⁻⁵	3 x 10 ⁻⁵	4 x 10 ⁻⁵	5 x 10 ⁻⁵	6 x 10 ⁻⁵	7 x 10 ⁻⁵
1	88902	166708	255307	346104	438534	520036	609629
	87640	165910	256051	347306	435729	519659	609682
	88958	164958	256642	344889	437257	516821	612282
	89554	165563	256341	345642	436992	518641	611131
	89897	166021	253543	345789	436254	520465	610542
2	88047	173933	259143	350538	429091	518817	605757
	88673	172157	260784	349308	427812	517469	606087
	89670	172768	260058	350071	427547	517573	605708
	89950	172244	260779	350219	426808	519684	605752
	90940	173136	259358	351756	426282	518632	605637
3	93013	176920	260118	346519	429048	520660	606355
	91749	176121	260363	347722	426239	521283	607810
	91067	175167	261789	345302	427769	520444	606008
	91663	175773	262315	346056	427504	520598	606858
	92007	176232	260855	346203	426765	521525	607269
Mean	90115.33	171574.07	258896.40	347561.60	430642.07	519487.13	607767.13
Std Dev	1570.04	4457.82	2639.20	2225.69	4724.55	1438.51	2274.07
RSD/%	1.74	2.60	1.02	0.64	1.10	0.28	0.37

Table C9: Calibration data for the determination of OMC.

Concentration /mol dm ⁻³	1 x 10 ⁻⁵	2 x 10 ⁻⁵	3 x 10 ⁻⁵	4 x 10 ⁻⁵	5 x 10 ⁻⁵	6 x 10 ⁻⁵	7 x 10 ⁻⁵
1	314865	551370	804237	1178975	1542907	1718596	2048784
	311922	553894	801643	1186231	1495813	1722160	2053603
	317052	547722	795466	1183863	1502002	1716425	2051081
	309430	554312	807827	1193953	1504109	1719630	2049656
	310244	543478	797662	1192653	1506518	1726252	2056393
2	295159	561971	835071	1120093	1444349	1720314	2030406
	292213	564057	833475	1127357	1457268	1723882	2025635
	293345	564590	835877	1126988	1453454	1718141	2033315
	293723	565175	834660	1125076	1455563	1721349	2021585
	294338	564488	834495	1120772	1458038	1727978	2028509
3	316044	583556	903243	1177712	1459215	1762670	2068371
	314265	584930	900652	1192614	1464444	1758792	2062631
	315156	584740	894482	1200718	1457322	1757220	2055502
	317143	583483	906829	1198004	1463482	1760450	2039553
	317549	583868	896675	1197390	1461305	1751605	2025258
Mean	307496.53	566108.93	845486.27	1168159.93	1475052.60	1733697.60	2043352.13
Std Dev	10340.77	14653.08	42742.70	32973.93	28019.50	18272.40	15041.76
RSD/%	3.36	2.59	5.06	2.82	1.90	1.05	0.74

Table C10: Calibration data for the determination of TiO₂.

Concentration /ppm	0.475	2.378	3.567	4.756	7.134	9.512
1	502.85	2479.8	3809.4	5159.6	7422.4	9576
2	550.31	2667.1	3959.5	4946	7204.6	9812.9
3	511.56	2506.7	3638.9	4882.9	7178.7	9580.7
Mean	521.57	2551.20	3802.60	4996.17	7268.57	9656.53
Std Dev	25.26	101.27	160.41	145.01	133.85	135.44
RSD/%	4.84	3.97	4.22	2.90	1.84	1.40

Table C11: Data of the change in valerophenone concentration with irradiation time.

Time/s	Concentration/M
0	1.15×10^{-3}
600	1.03×10^{-3}
1200	8.04×10^{-4}
3240	3.78×10^{-4}

Table C12: Physical constants used for the calculation of photon flux.

Constant	Value
h	6.63×10^{-34} J s
c	3.00×10^8 m s ⁻¹
λ	3.10×10^{-7} m
A	3.90×10^{-4} m ²
V	3.00×10^{-3} cm ³
N_A	6.02×10^{23} mol ⁻¹

Table C13: Summary of the mean % m/m concentrations of the various sunscreen active ingredients in the different products analysed.

Product	AVO	OMC	Bz-3	MBC	OS	MBBT	BEMT	OT	OCR	TiO ₂
SA1	-	1.63	0.88	-	-	-	-	-	-	-
SA2	-	2.84	1.43	-	-	-	-	-	-	-
SA3	-	7.70	4.83	1.17	2.14	-	-	-	-	-
SA4†	-	9.99	3.82	-	6.37	-	-	-	-	3.21
SA5	0.72	7.51	6.28	-	3.69	-	-	-	-	1.41
SA6	1.83	2.25	-	2.28	-	-	-	-	-	0.33
SA7	2.15	5.12	-	3.87	-	-	-	-	-	1.14
SA8	1.69	6.84	-	3.99	-	-	-	-	-	1.58
SA9†	-	7.03	-	4.27	-	3.39	1.90	-	-	1.09
SA10	-	4.49	3.45	-	1.61	-	-	-	-	1.42
SA11	-	8.82	5.34	1.18	3.28	-	-	-	-	1.28
SA12	2.41	7.78	-	-	-	-	-	-	-	-
SA13	-	4.03	-	-	-	-	1.63	-	3.89	1.61
SA14	2.83	5.23	-	-	-	-	1.81	1.20	-	1.79
SA15	1.12	4.06	-	-	-	-	-	-	-	0.05
SA16	-	6.31	-	3.88	-	3.84	2.59	-	-	-
SA18	-	4.78	-	-	-	-	-	-	-	-
SA19	1.12	-	-	-	-	-	-	3.43	-	1.26
SA20	0.53	9.45	-	-	-	-	-	-	-	-
SA21†	1.49	7.58	-	4.69	-	-	-	-	-	1.03
SA22	2.44	6.31	-	2.18	-	-	-	-	-	0.82
COLIPA	5	10	10	4	5	10	10	5	10	25

- Denotes absence of the specific sunscreen active ingredients from the respective product.

† Products containing active ingredients with levels higher than COLIPA set limits (shown in bold).

Appendix D

CALIBRATION CURVES AND RESIDUAL PLOTS

The following are the calibration curves and the residual plots used for the quantitation of active ingredients in sun care products analysed in this study.

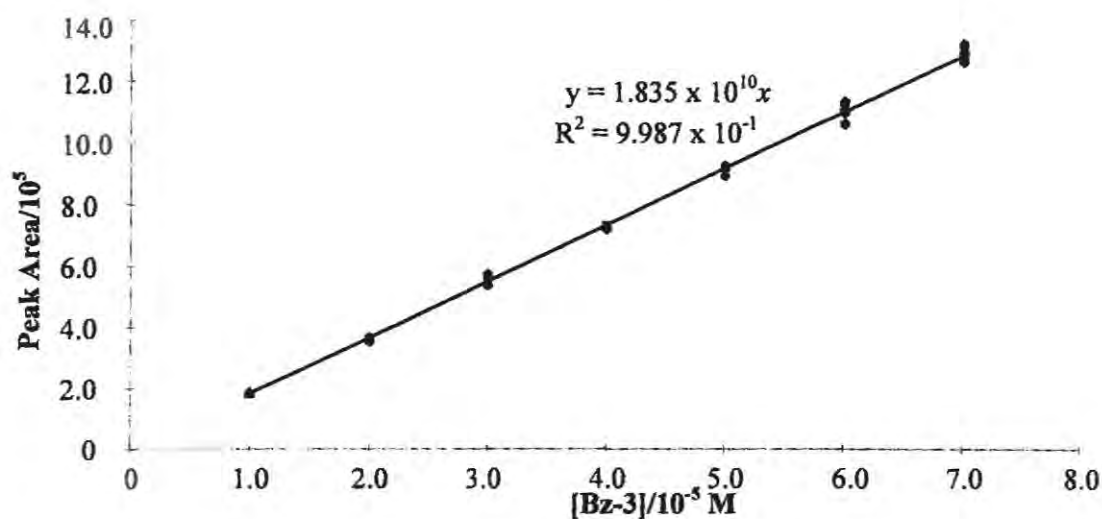


Figure D1: HPLC calibration curve for the determination of Bz-3. The chromatographic conditions used were: Phenomenex Synergi Max-RP-C₁₂ 80 Å column, mobile phase - MeOH-H₂O 84:16% (v/v), injection volume - 20 µL, flow rate - 1 mL min⁻¹, and detection wavelength - 290 nm.

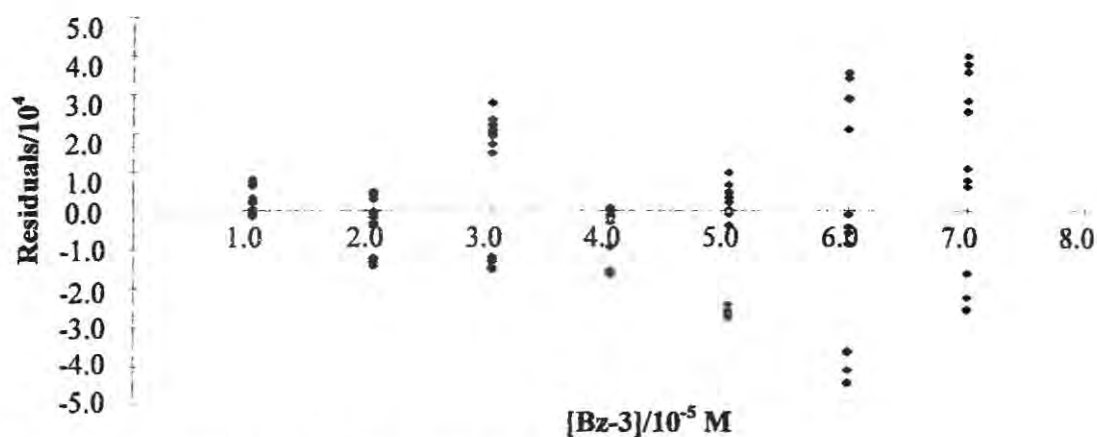


Figure D2: Residual plot for the calibration curve of Bz-3.

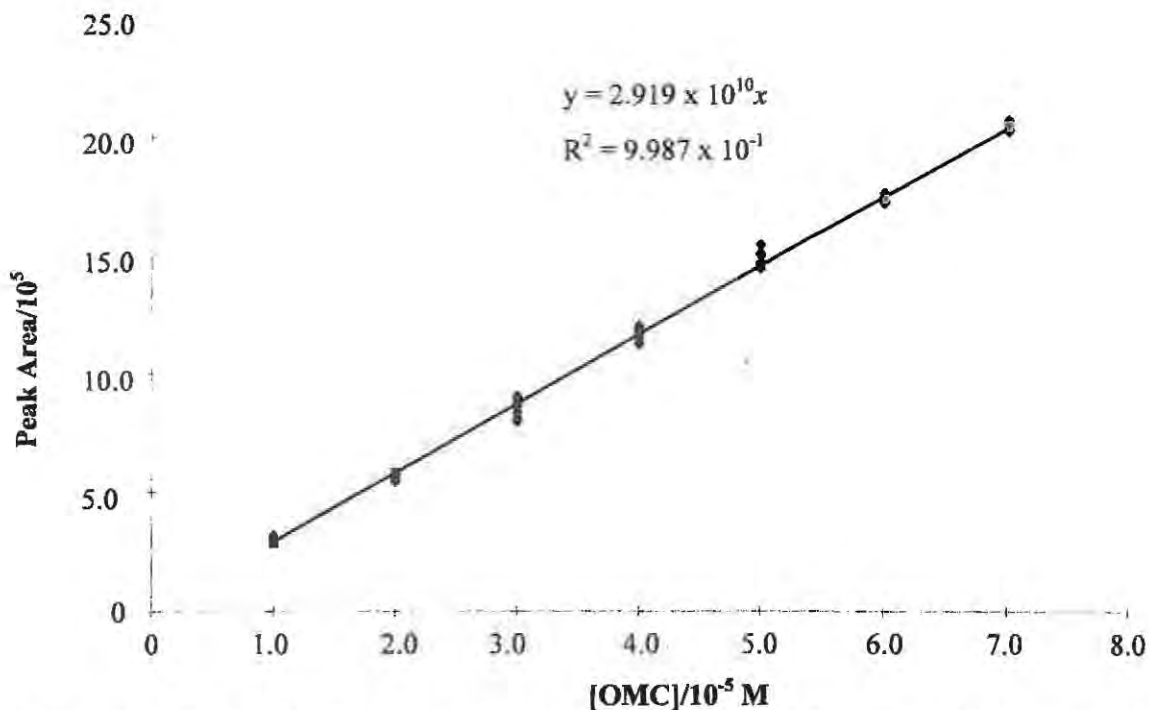


Figure D3: HPLC calibration curve for the determination of OMC. The chromatographic conditions used were: Phenomenex Synergi Max-RP-C₁₂ 80 Å column, mobile phase - MeOH-H₂O 84:16% (v/v), injection volume - 20 µL, flow rate - 1 mL min⁻¹, and detection wavelength - 310 nm.

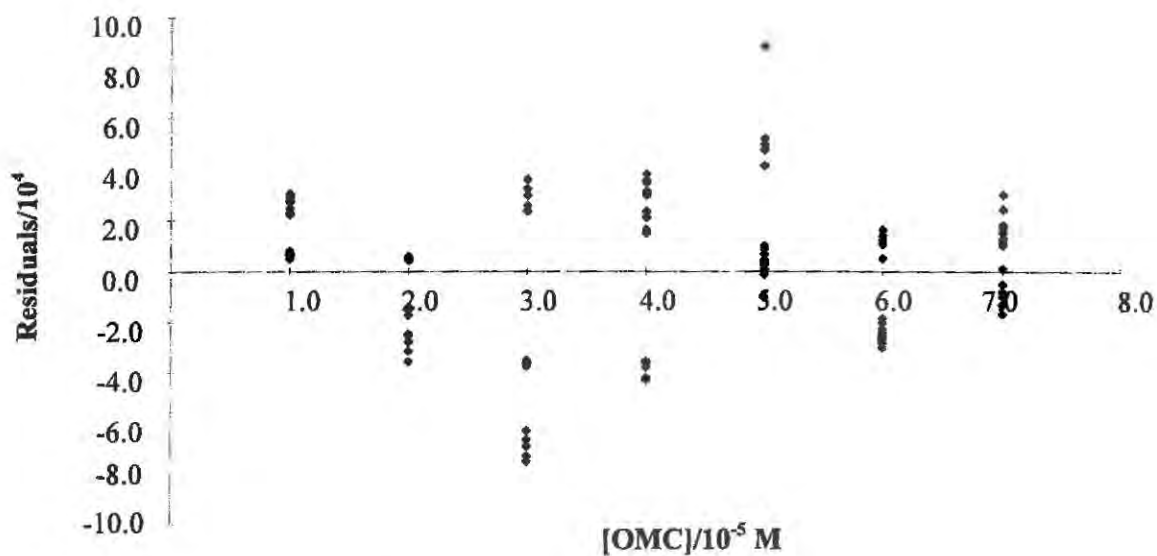


Figure D4: Residual plot for the calibration curve of OMC.

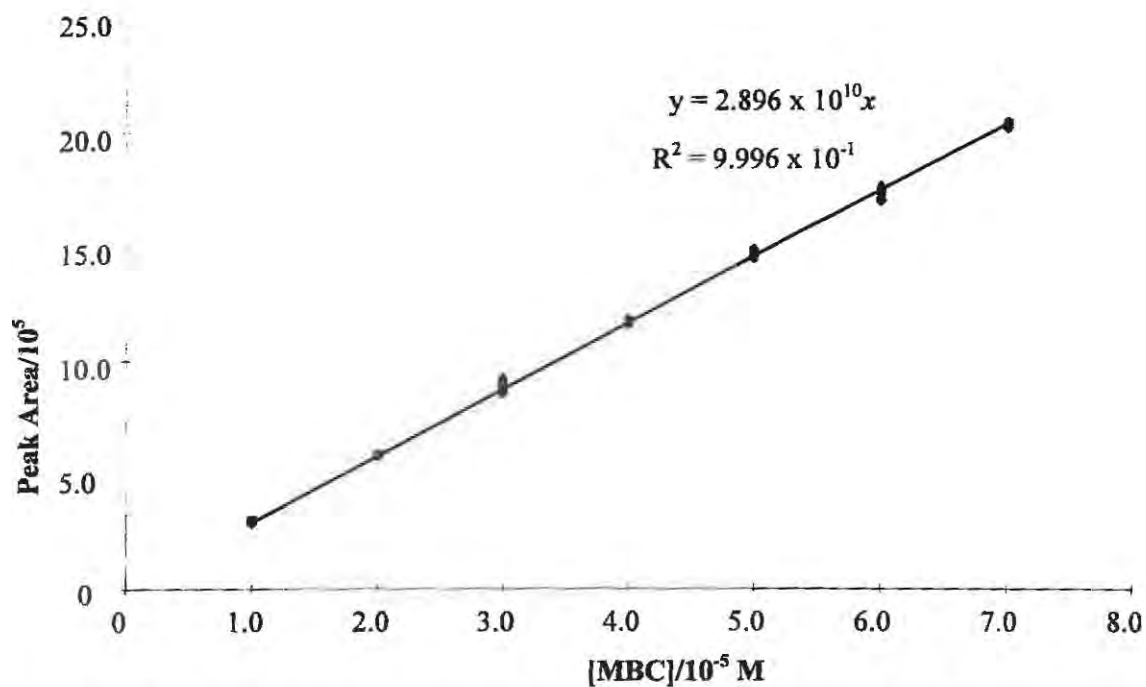


Figure D5: HPLC calibration curve for the determination of MBC. The chromatographic conditions used were: Phenomenex Synergi Max-RP-C₁₂ 80 Å column, mobile phase - MeOH-H₂O 84:16% (v/v), injection volume - 20 µL, flow rate - 1 mL min⁻¹, and detection wavelength - 302 nm.

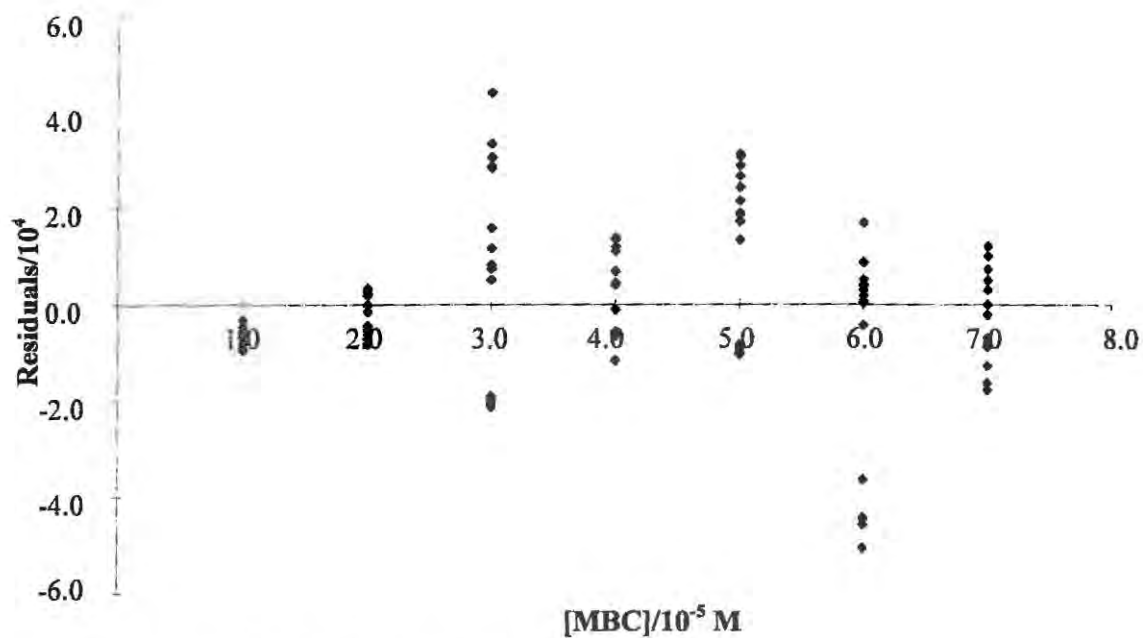


Figure D6: Residual plot for the calibration curve of MBC.

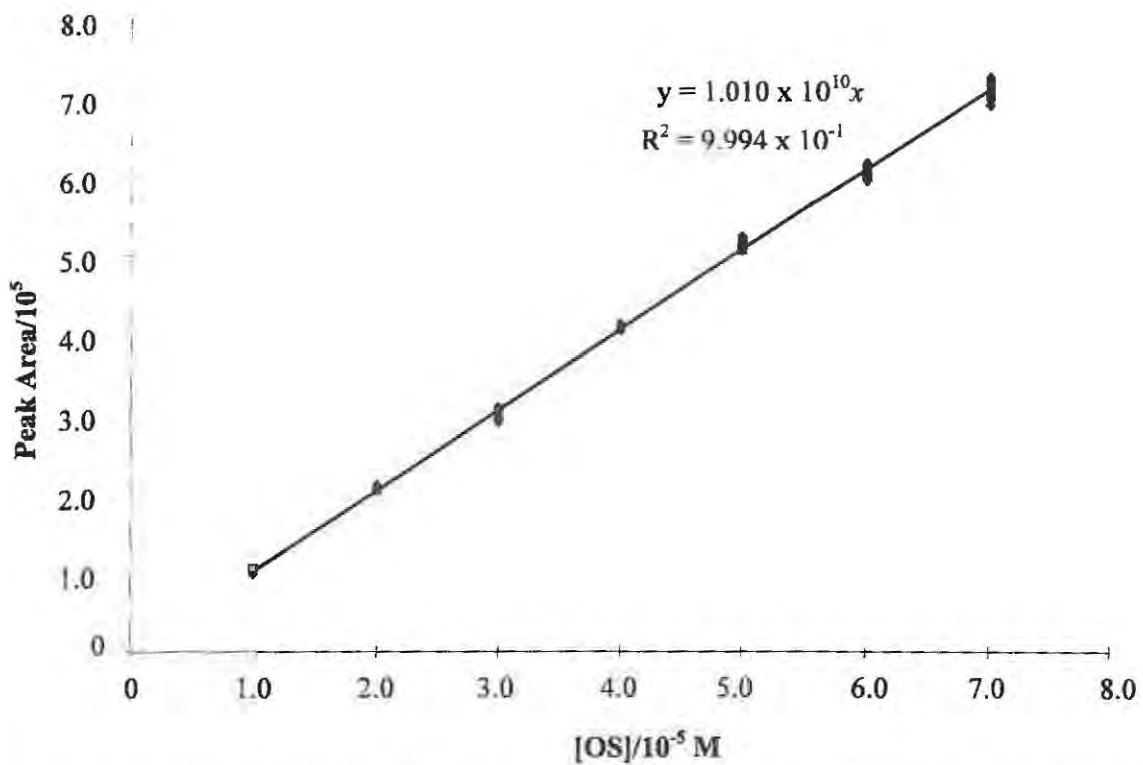


Figure D7: HPLC calibration curve for the determination of OS. The chromatographic conditions used were: Phenomenex Synergi Max-RP-C₁₂ 80 Å column, mobile phase - MeOH-H₂O 84:16% (v/v), injection volume - 20 µL, flow rate - 1 mL min⁻¹, and detection wavelength - 242 nm.

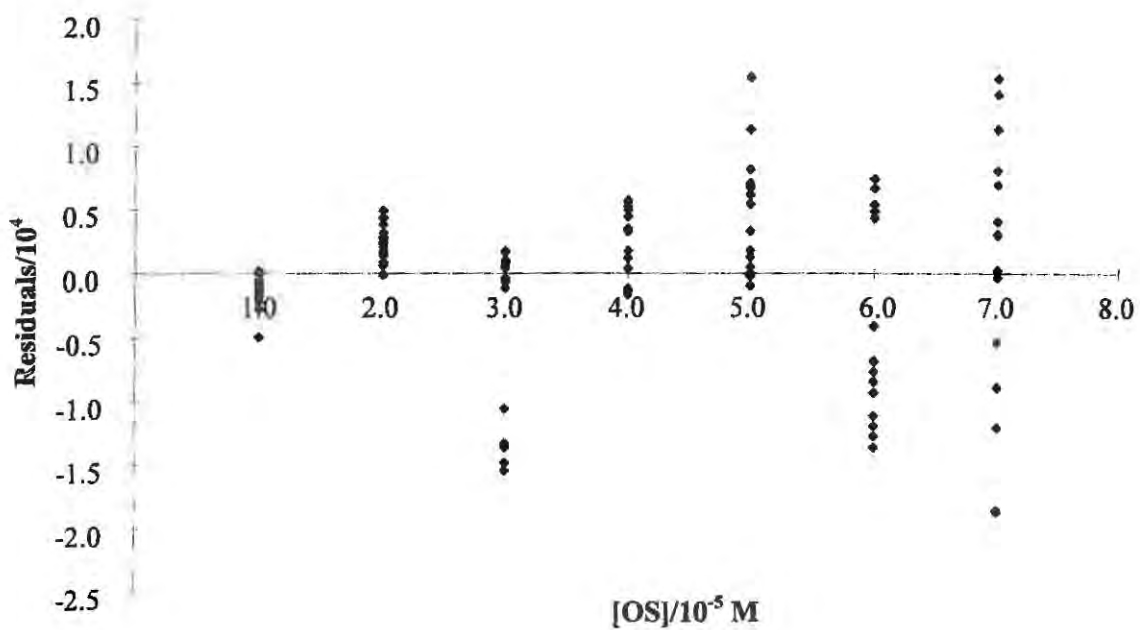


Figure D8: Residual plot for the calibration curve of OS.

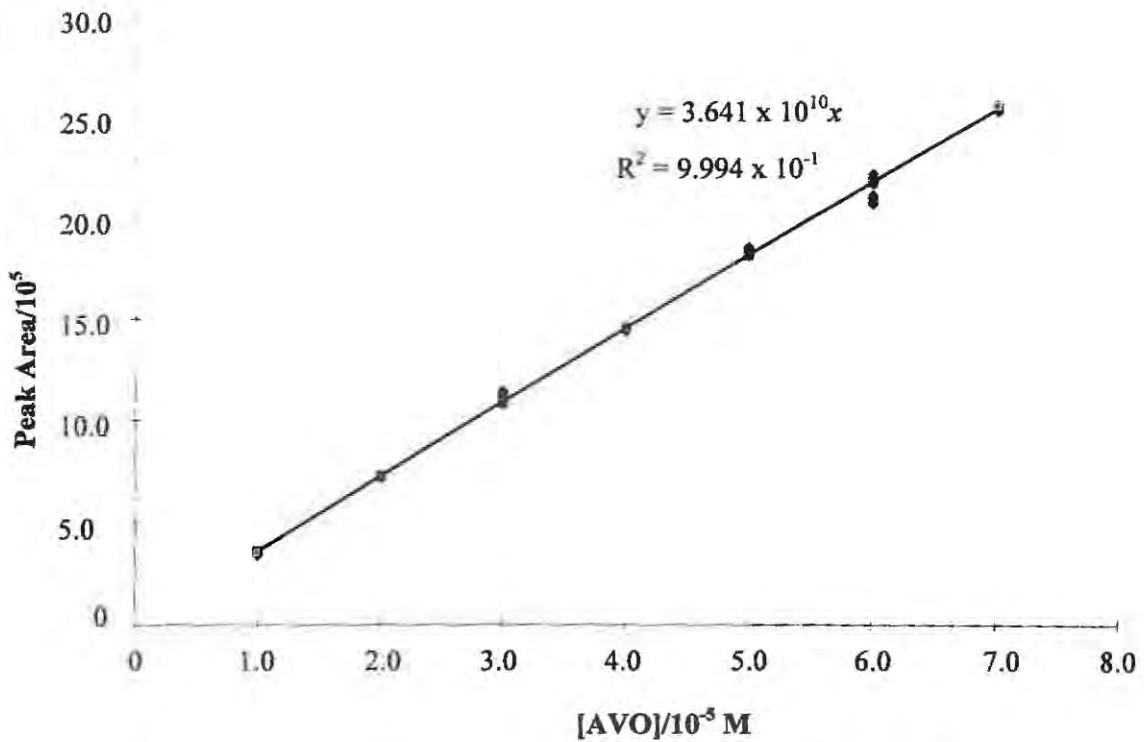


Figure D9: HPLC calibration curve for the determination of AVO. The chromatographic conditions used were: Phenomenex Synergi Max-RP-C₁₂ 80 Å column, mobile phase - MeOH-H₂O 84:16% (v/v), injection volume - 20 µL, flow rate - 1 mL min⁻¹, and detection wavelength - 358 nm.

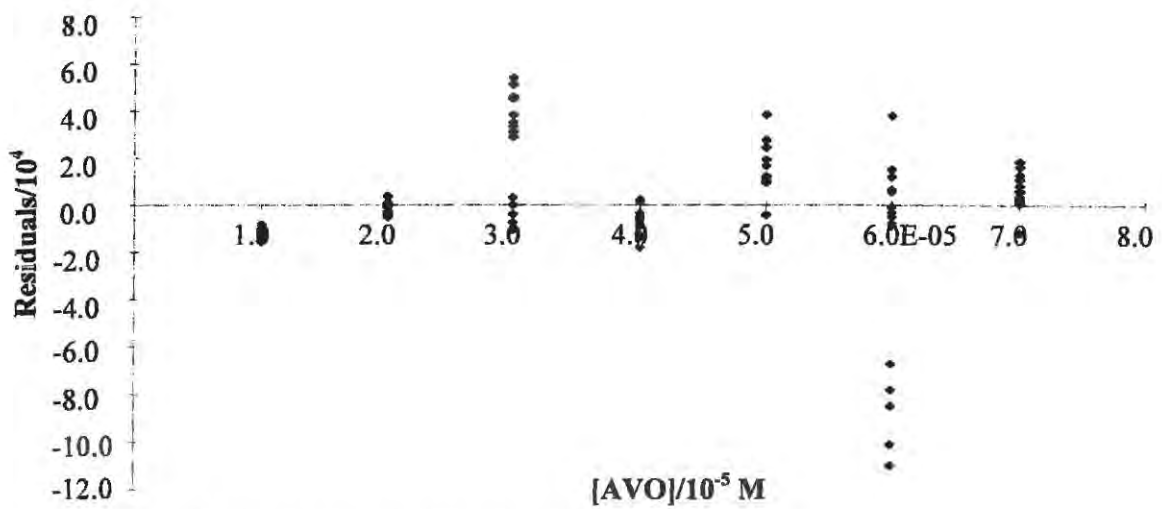


Figure D10: Residual plot for the calibration curve of AVO.

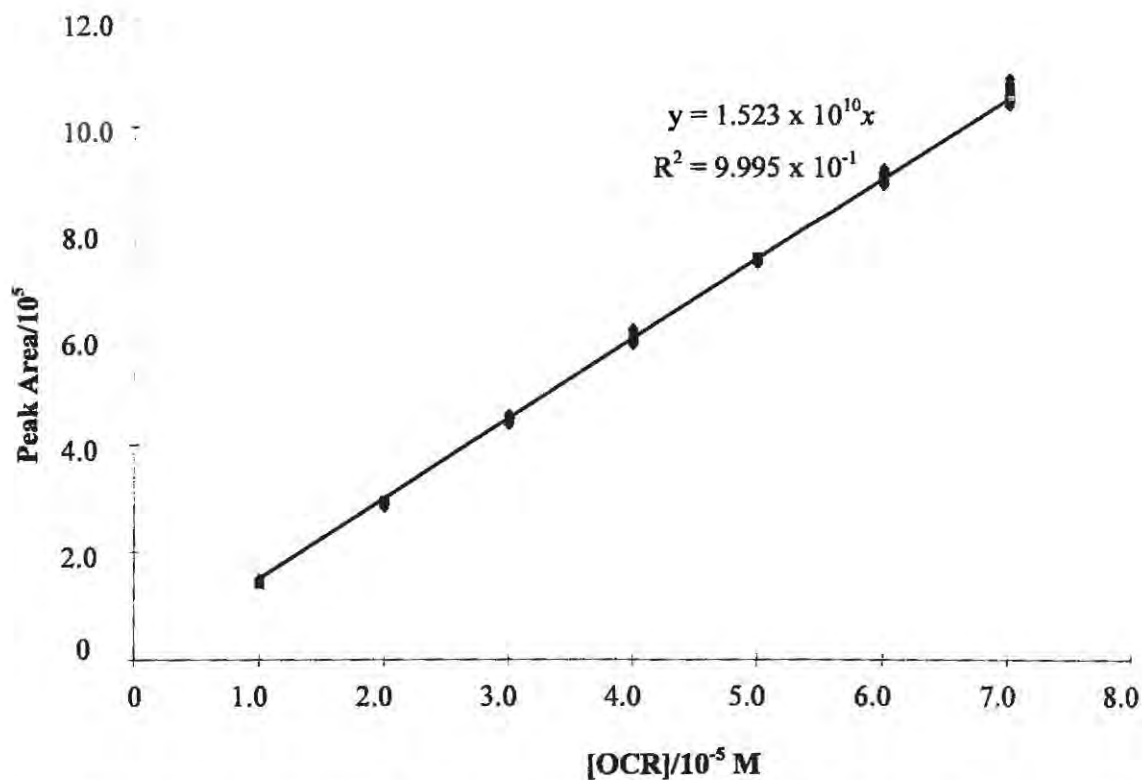


Figure D11: HPLC calibration curve for the determination of OCR. The chromatographic conditions used were: Phenomenex Synergi Max-RP-C₁₂ 80 Å column, mobile phase - MeOH-H₂O 84:16% (v/v), injection volume - 20 µL, flow rate - 1 mL min⁻¹, and detection wavelength - 305 nm.

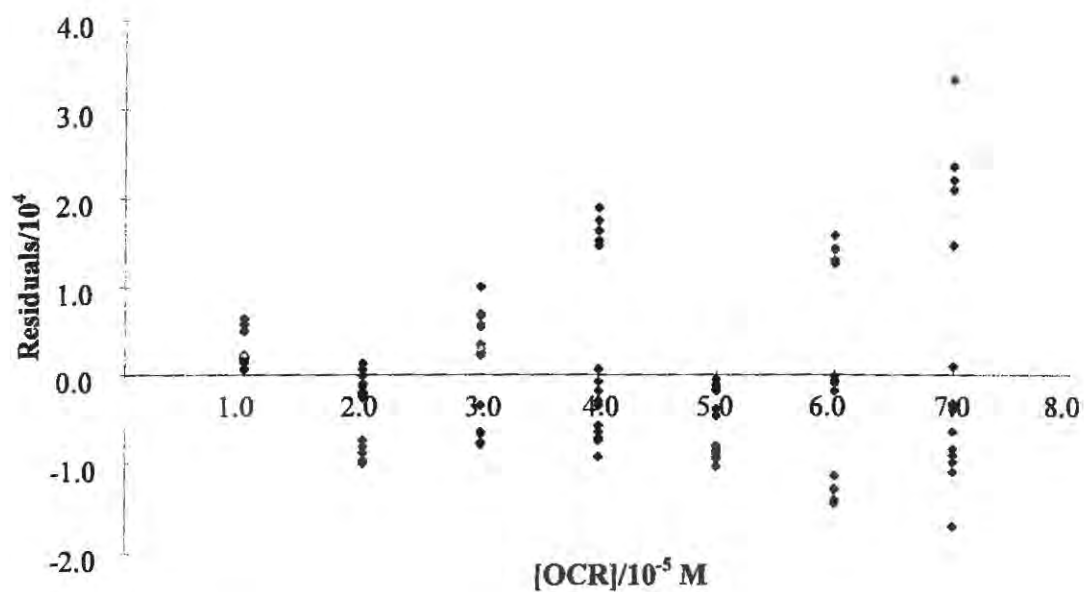


Figure D12: Residual plots for the calibration curve of OCR.

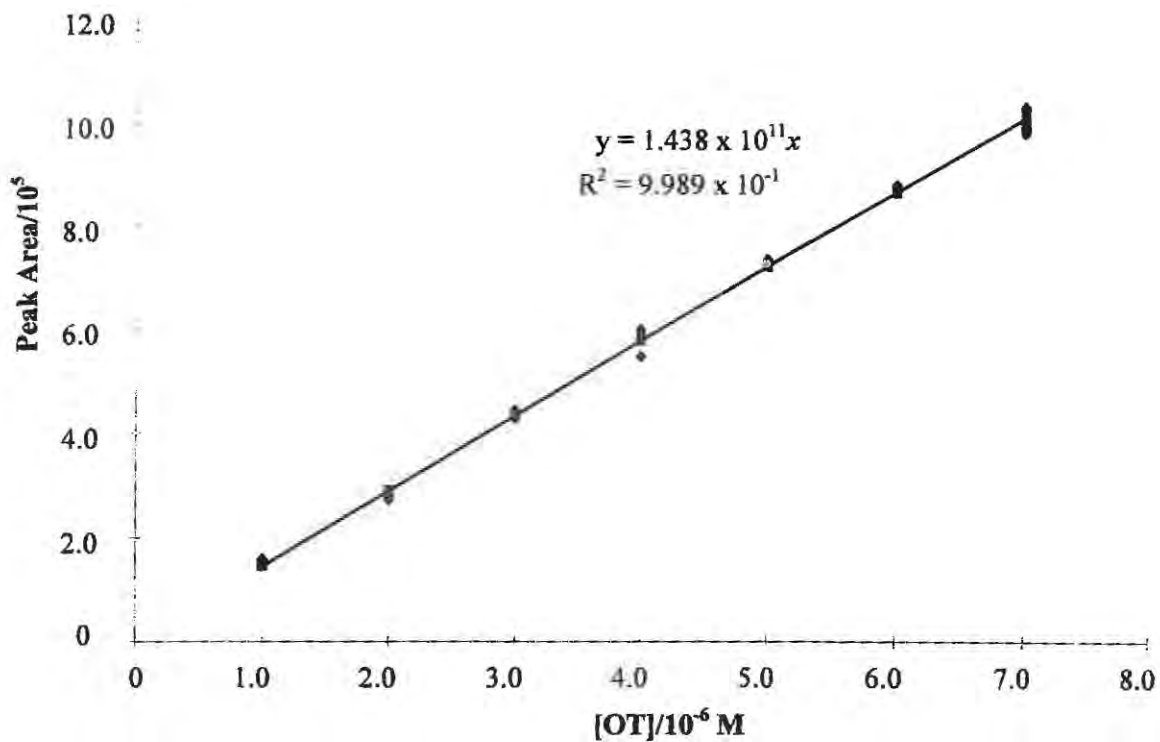


Figure D13: HPLC calibration curve for the determination of OT. The chromatographic conditions used were: Phenomenex Synergi Max-RP-C₁₂ 80 Å column, mobile phase - MeOH-ACN 90:10% (v/v), injection volume - 20 µL, flow rate - 1 mL min⁻¹, and detection wavelength - 311 nm.

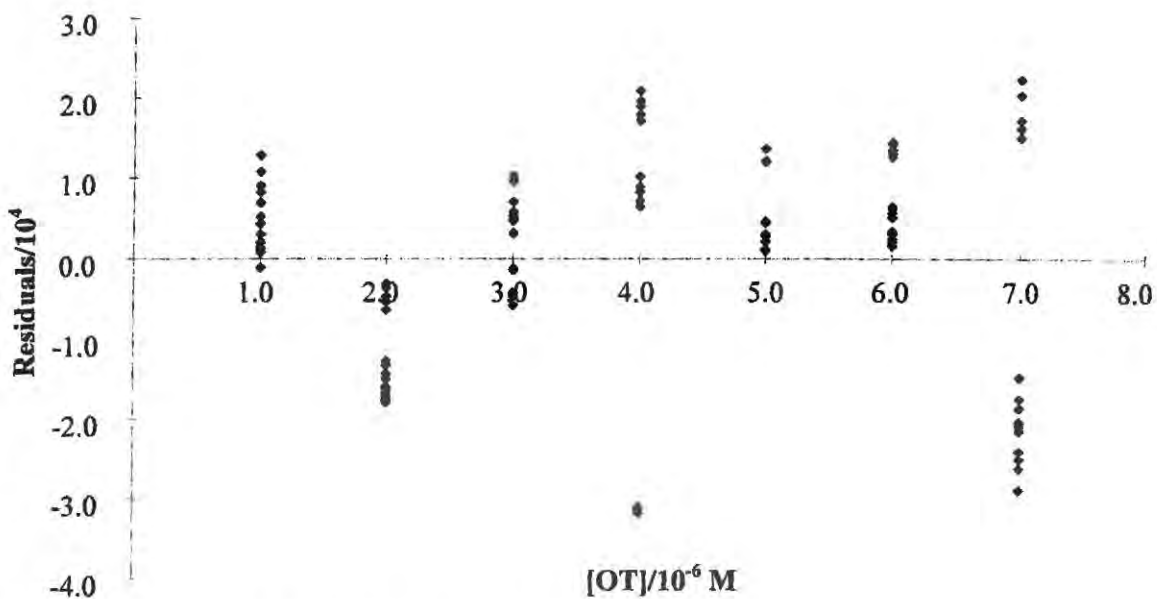


Figure D14: Residual plot for the calibration curve of OT.

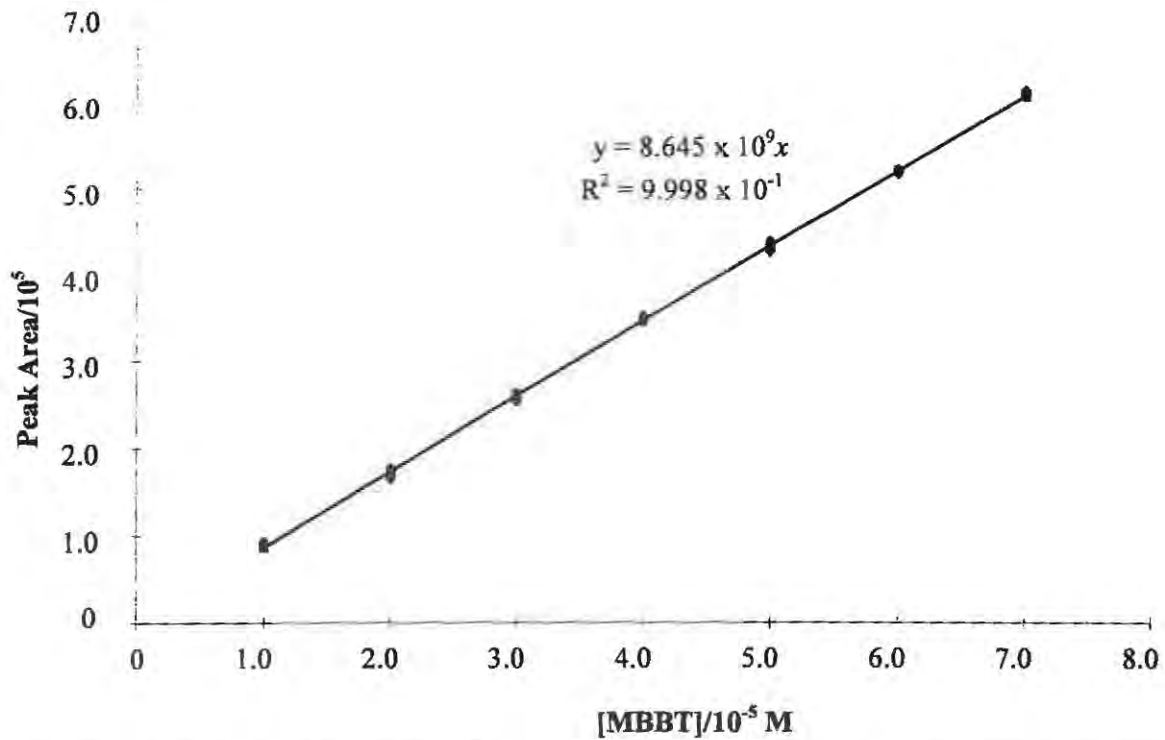


Figure D15: HPLC calibration curve for the determination of MBBT. The chromatographic conditions used were: Phenomenex Synergi Max-RP-C₁₂ 80 Å column, mobile phase - MeOH-ACN 90:10% (v/v), injection volume - 20 μL, flow rate - 1 mL min⁻¹, and detection wavelength - 342 nm.

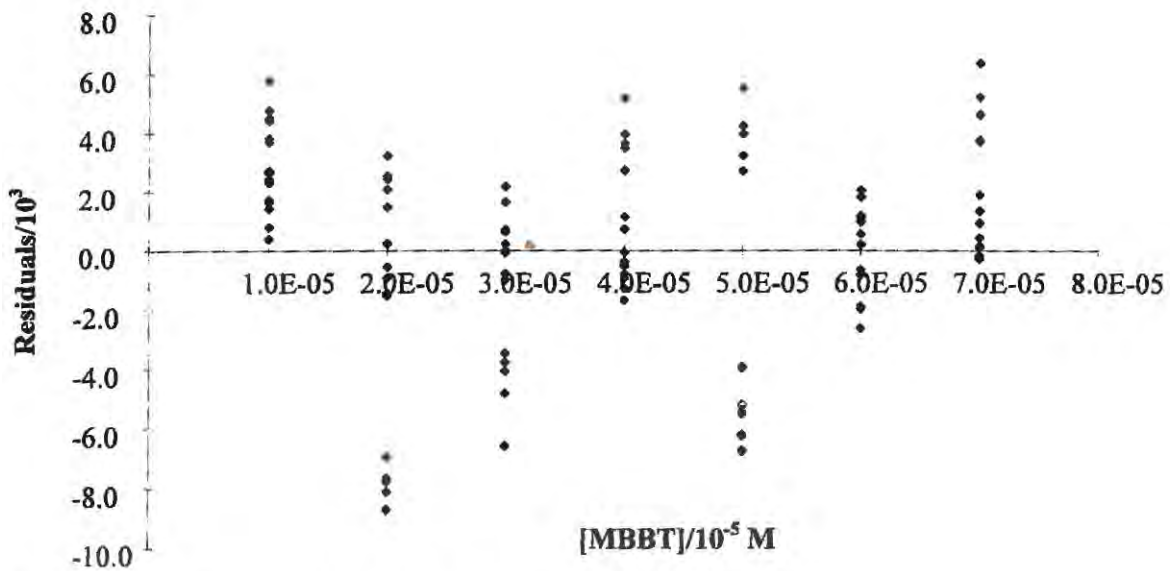


Figure D16: Residual plot for the calibration curve of MBBT.

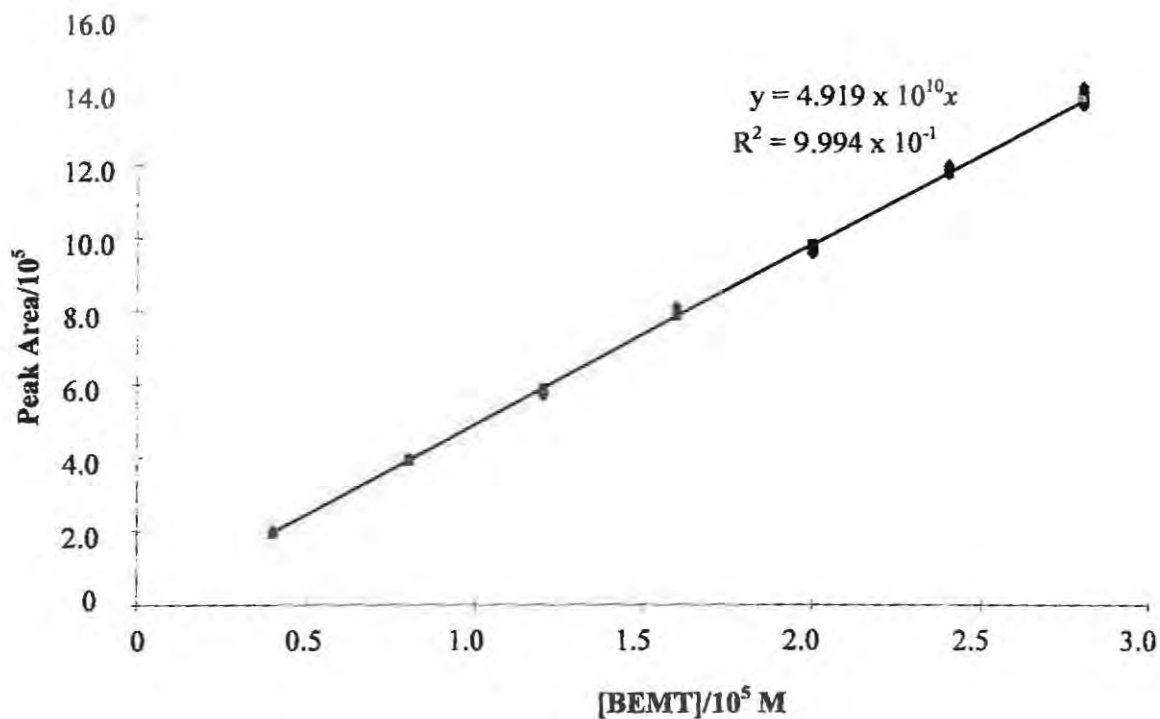


Figure D17: HPLC calibration curve for the determination of BEMT. The chromatographic conditions used were: Phenomenex Synergi Max-RP-C₁₂ 80 Å column, mobile phase - MeOH-ACN 90:10% (v/v), injection volume - 20 μL, flow rate - 1 mL min⁻¹, and detection wavelength - 342 nm.

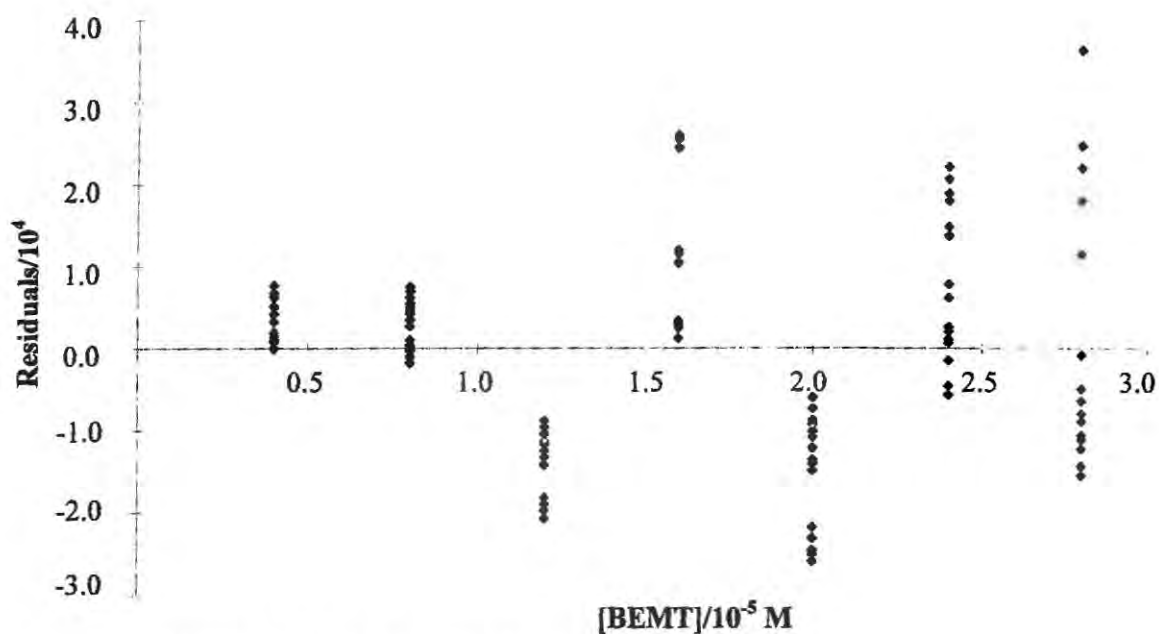


Figure D18: Residual plot for the calibration curve of BEMT.

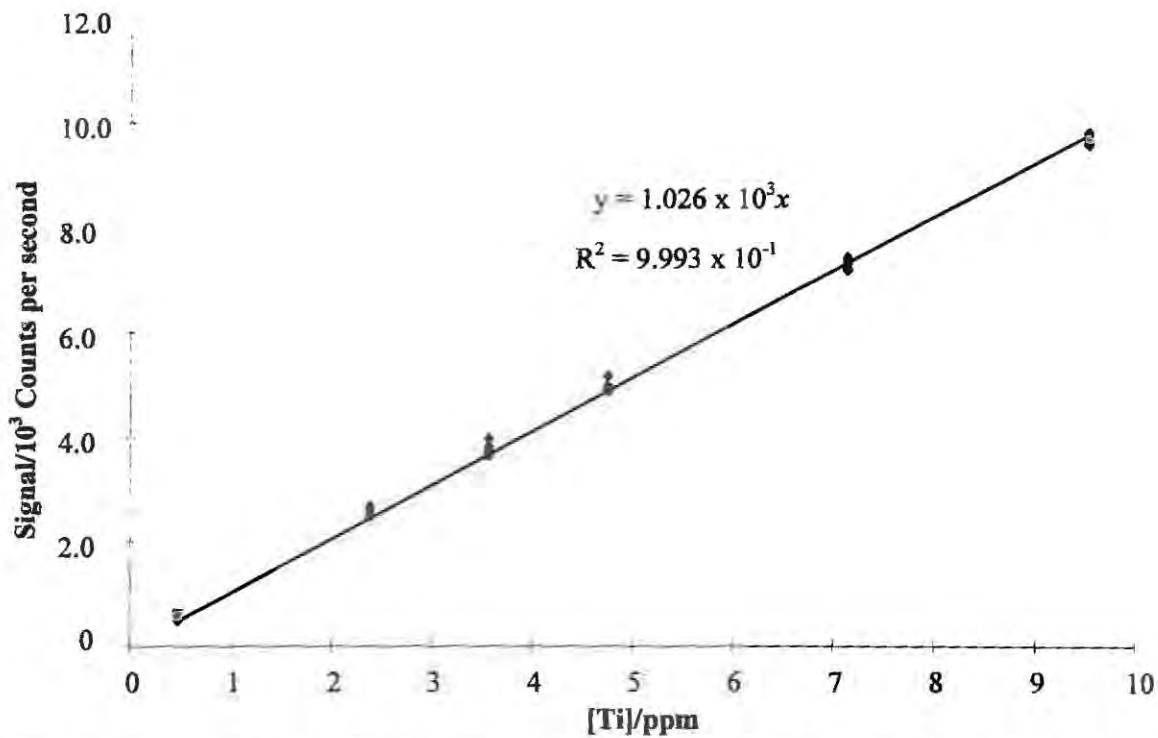


Figure D19: ICP-OES calibration curve for the determination of titanium dioxide. The experimental conditions were: wavelength, 337.280 nm; generator power, 1000 W; plasma gas flow rate, 12 L min⁻¹; auxiliary gas flow rate, 0.00 L min⁻¹; sheath gas flow rate, 0.2 L min⁻¹; nebuliser pressure, 3 bars; sample flow rate, 1 mL min⁻¹.

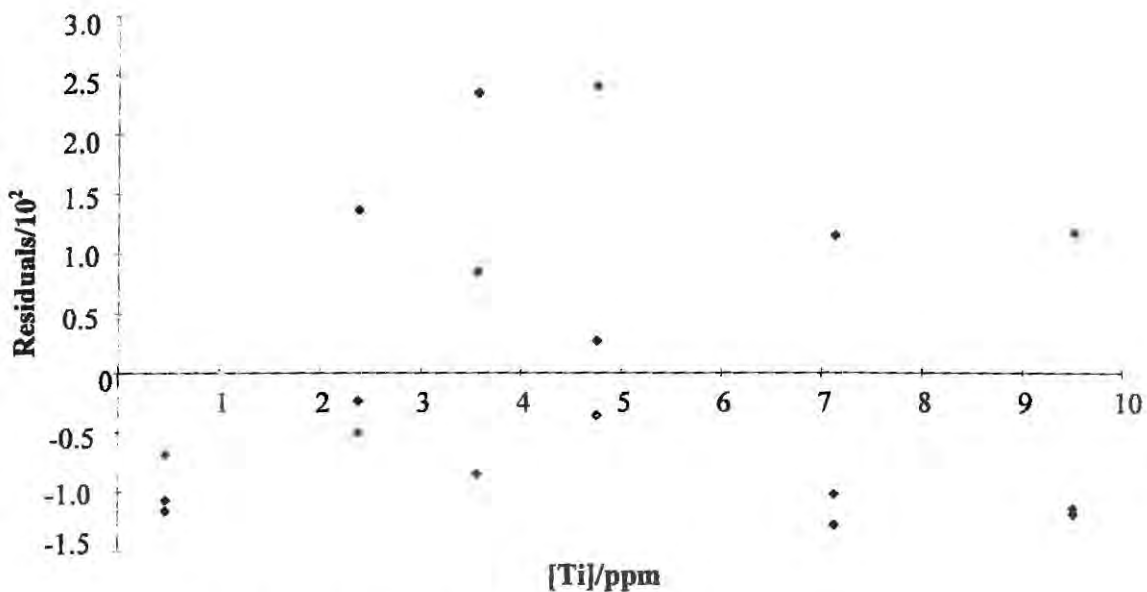


Figure D20: Residual plot for the calibration curve of TiO₂.

Appendix E

Straight-line calibration with intercept zero

(Draft: please do not quote without the author's permission.)

Iain L. MacDonald
Actuarial Science, University of Cape Town
7701 Rondebosch, South Africa
imacдона@commerce.uct.ac.za

1 Introduction

Straight-line calibrations are an important tool of the analytical chemist, but involve some nontrivial statistical questions. An excellent review is provided by Miller (1991). Miller rightly emphasizes the 'inverse regression' nature of the problem: once one has fitted a satisfactory straight line $y = a + bx$ to the calibration data (x_i, y_i) , $i = 1, \dots, n$, one then seeks to use the line to infer the x -value (usually a concentration) corresponding to a given y_0 . Of course it is a simple matter to find the x_0 corresponding to a given y_0 if one can assume that y_0 is observed without error and that a and b are known exactly. Neither of these assumptions is always reasonable in practice, which implies that the 'point estimate' $x_0 = (y_0 - a)/b$ alone is of limited utility: to be more useful it needs to be supplemented with confidence limits, even if they are only approximate.

Miller (1991, equation (9) and the sentence following) provides such approximate confidence limits, which can be derived by using the method known to statisticians as the delta method. In outline, what is done is to take account of the error in each of y_0 , a and b , and thereby to produce an estimated standard deviation s_{x_0} for the point estimate $x_0 = (y_0 - a)/b$. The required approximate confidence limits are then of the form $x_0 \pm ts_{x_0}$, where t is (e.g.) the upper $2\frac{1}{2}\%$ point of the relevant t distribution.

One apparent gap in the literature easily available to chemists is the case in which it is reasonable to assume $a = 0$. If this assumption is made, only b needs to be determined to establish the calibration line. The usual simple linear regression formulas do not apply to this case, however, nor does equation (9) of Miller (1991). Our purpose here is take the reader through the case $a = 0$. As one might expect, this case is simpler than the situation in which one cannot assume that $a = 0$, but an explicit treatment is perhaps useful to those chemists who have never had the advantage of a course in statistics: the majority in many universities? We include the derivation of the relevant formulas, but we are not so unrealistic as to assume that the hard-worked laboratory chemist has time for such frivolity! The methods described are easy to implement, especially if one uses the freeware package R (R Development Core Team, 2005), which is fast becoming the standard for much statistical work. But Excel will also work well.

2 Simple linear regression with intercept zero

We suppose we have observations y_i ($i = 1, 2, \dots, n$), satisfying

$$y_i = bx_i + e_i,$$

where e_i has a normal distribution with mean zero and variance σ^2 , and e_i and e_j are independent if $i \neq j$. The least-squares estimate of b is $\hat{b} = \sum_i x_i y_i / \sum_i x_i^2$, all sums being over values of i from 1 to n . (To prove this result, just differentiate $\sum_i (y_i - bx_i)^2$ with respect to b , set the derivative equal to zero, and solve for b .) Because one is assuming normality, the estimate $\hat{b} = \sum_i x_i y_i / \sum_i x_i^2$ is also the maximum-likelihood estimate.

With $u_i = x_i / \sum_i x_i^2$, \hat{b} is then the linear combination $\sum_i u_i y_i$ of the normal random variables y_i , and thereby normally distributed. It has mean $\sum_i u_i (bx_i) = b$, so it is an unbiased estimate of b . Somewhat less obviously, \hat{b} can be shown to have variance $\sigma^2 / \sum_i x_i^2$.

Our i th fitted y -value is $\hat{y}_i = \hat{b}x_i$, and the corresponding residual is $y_i - \hat{y}_i$. The quantity σ^2 is estimated by the sum of squared residuals divided by $(n-1)$, i.e. by:

$$s^2 = \frac{1}{n-1} \sum_i (y_i - \hat{y}_i)^2.$$

This can also be shown to be unbiased, and has, apart from a constant factor, a chi-squared distribution with $n-1$ degrees of freedom.

3 Calibration

Now suppose we have observed a single value y_0 , and we want to estimate the corresponding x_0 . That is, y_0 is an observed value of $Y_0 = bx_0 + e_0$, where e_0 has a normal $(0, \sigma^2)$ distribution independent of the e_i s. The point estimate for x_0 is $\hat{x}_0 = Y_0/b$; more precisely it is $\hat{x}_0 = Y_0/\hat{b}$, as we don't know b itself, but we do have an estimate of it, \hat{b} . But to put confidence limits on x_0 we need to estimate the variance of $\hat{x}_0 = Y_0/\hat{b}$; call this ratio $g(Y_0, \hat{b})$.

The 'delta method' tells us that, approximately:

$$\text{Variance } g(Y_0, \hat{b}) = \left(\frac{\partial g}{\partial Y_0} \right)^2 \text{Variance } (Y_0) + \left(\frac{\partial g}{\partial \hat{b}} \right)^2 \text{Variance } (\hat{b}). \quad (1)$$

The derivatives are evaluated at the observed values of the random variables Y_0 and \hat{b} , which we denote by y_0 and (loosely) b . There is also a covariance term to be taken into account, but fortunately the relevant covariance, that of Y_0 and \hat{b} , is zero. (In passing: if we did not assume $a = 0$, we would have to find the variance of $(Y_0 - \hat{a})/\hat{b}$. This involves three variance terms and one nonzero covariance term, and Miller's equation (7) then results.)

In our case the variance of \hat{x}_0 is approximately

$$\left(\frac{1}{b} \right)^2 \sigma^2 + \left(-\frac{y_0}{b^2} \right)^2 \frac{\sigma^2}{\sum_i x_i^2} = \frac{\sigma^2}{b^2} \left[1 + \frac{y_0^2}{b^2 \sum_i x_i^2} \right].$$

With $s^2 = \frac{1}{n-1} \sum_i (y_i - \hat{y}_i)^2$ our approximate result for s_{x_0} , corresponding to Miller's equation (7), is therefore:

$$s_{x_0} \approx \frac{s}{b} \left[1 + \frac{y_0^2}{b^2 \sum_i x_i^2} \right]^{\frac{1}{2}}.$$

If Y_0 represents not one determination but the average of m , Variance (Y_0) in our equation (1) is σ^2/m instead of σ^2 . The above expression for s_{x_0} then becomes:

$$s_{x_0} \approx \frac{s}{b} \left[\frac{1}{m} + \frac{y_0^2}{b^2 \sum_i x_i^2} \right]^{\frac{1}{2}}, \quad (2)$$

which corresponds to Miller's equation (9). Confidence limits for x_0 given y_0 are of the form

$$x_0 \in \hat{x}_0 \pm t s_{x_0}, \quad (3)$$

t being a figure from tables of the t distribution with $n-1$ degrees of freedom. For instance, if $n = 105$, an approximate 95% confidence interval is $x_0 \in \hat{x}_0 \pm 1.983 s_{x_0}$; 1.983 is the upper $2\frac{1}{2}\%$ point of the t distribution with 104 degrees of freedom, the point above which lies $2\frac{1}{2}\%$ of the probability associated with the distribution. (Notice how close this is to 1.960, the corresponding figure for a standard normal distribution.)

4 A complication

One complication that sometimes arises is this. A number of determinations of y_{0i} are made for each of several concentrations (x). However, all the relevant concentrations correspond to a single mass%, and it is that mass% that we wish to estimate. The mass percentages are known constants times the relevant concentrations. To get a point estimate of the mass%, multiply each of the q values y_{0i} by the relevant conversion factor f_i (that which converts from concentration to mass %). Call the q resulting values u_i , average them to get \bar{u} and divide by \hat{b} . That is, \bar{u}/\hat{b} is the point estimate of mass%.

To get a confidence interval on the mass% we find the variances of the quantities $u_i = f_i y_{0i}$, and hence that of $\bar{u} = q^{-1} \sum_{i=1}^q f_i y_{0i}$. Subject to the 'usual assumptions', the variance of \bar{u} is

$$q^{-2} \sum_{i=1}^q f_i^2 \sigma^2.$$

So just replace $1/m$ in the formula (2) by $q^{-2} \sum_{i=1}^q f_i^2$, and replace y_0^2 there by \bar{u}^2 . (All we are thereby doing is replacing y_0 and its variance by \bar{u} and its variance.) Proceed otherwise as before to get a confidence interval for the mass%. Note that s^2 , b and $\sum_{i=1}^n x_i^2$ are all (still) as determined by the original calibration data. Formulas (2) and (3) for the confidence limits are therefore replaced by:

$$\text{mass\%} \in \frac{\bar{u}}{b} \pm \frac{ts}{b} \left[q^{-2} \sum_{i=1}^q f_i^2 + \frac{\bar{u}^2}{b^2 \sum_i x_i^2} \right]^{\frac{1}{2}}. \quad (4)$$

Note that this equation can be checked — to some extent — against (2) and (3) by setting all the factors f_i equal to 1.

Appendix: Alternative derivation of the confidence limits

An alternative derivation of the confidence limits given by (2) and (3), which is messier but more elementary in the sense that it does not use the delta method, is as follows. This derivation also has the advantage of displaying the nature and extent of the approximation involved in (2).

The variance of $U = Y_0 - \hat{b}x_0$ is:

$$\text{Var}U = \text{Var}(Y_0 - \hat{b}x_0) = \sigma^2/m + x_0^2 \text{Var}(\hat{b}) = \sigma^2 \left(\frac{1}{m} + \frac{x_0^2}{\sum_i x_i^2} \right), \quad (5)$$

i.e. if Y_0 is the average of m determinations. Now let s.e. U denote the standard error of U , i.e. the following estimate of its standard deviation:

$$\text{s.e. } U = s \left(\frac{1}{m} + \frac{x_0^2}{\sum_i x_i^2} \right)^{\frac{1}{2}}.$$

(As before, s is defined by $s^2 = \frac{1}{n-1} \sum_i (y_i - \hat{y}_i)^2$.) If t denotes the upper $\alpha/2$ point of the t distribution with $n-1$ degrees of freedom, it then follows that (exactly)

$$1 - \alpha = P(|U/\text{s.e. } U| < t).$$

Symmetric $100(1 - \alpha)\%$ confidence limits for x_0 can therefore be found by solving the following equation for x_0 :

$$\left| (y_0 - bx_0) / \left\{ s \left(\frac{1}{m} + \frac{x_0^2}{\sum_i x_i^2} \right)^{\frac{1}{2}} \right\} \right| = t.$$

Equivalently we consider the more obviously quadratic equation for x_0 :

$$(y_0 - bx_0)^2 = t^2 s^2 \left(\frac{1}{m} + \frac{x_0^2}{\sum_i x_i^2} \right),$$

the solution of which is:

$$x_0 = \frac{y_0}{b(1-g)} \pm \frac{ts}{b(1-g)} \left(\frac{1-g}{m} + \frac{y_0^2}{b^2 \sum_i x_i^2} \right)^{\frac{1}{2}},$$

where g denotes $t^2 s^2 / (b^2 \sum_i x_i^2)$.

If g is sufficiently close to zero, the confidence limits can therefore be approximated by

$$\frac{y_0}{b} \pm \frac{ts}{b} \left(\frac{1}{m} + \frac{y_0^2}{b^2 \sum_i x_i^2} \right)^{\frac{1}{2}}$$

which yields the same conclusion as our equations (2) and (3). Miller (1991) reports (in the slightly different context he considers) that $g < 0.05$ is sufficiently small. Peculiarities can arise, however, if g is large, e.g. because the estimated b is very small; note that the quadratic equation for the confidence limits on x_0 has no real roots if g is sufficiently large.

References

- Miller, J.N. (1991). Basic Statistical Methods for Analytical Chemistry, Part 2. Calibration and Regression Methods: A Review. *The Analyst* **116**, 3–14.
- R Development Core Team (2005). R: A language and environment for statistical computing. R Foundation for Statistical Computing, Vienna, Austria. ISBN 3-900051-07-0, URL <http://www.R-project.org>.

Appendix F

CHROMATOGRAMS FOR SUNCARE PRODUCTS

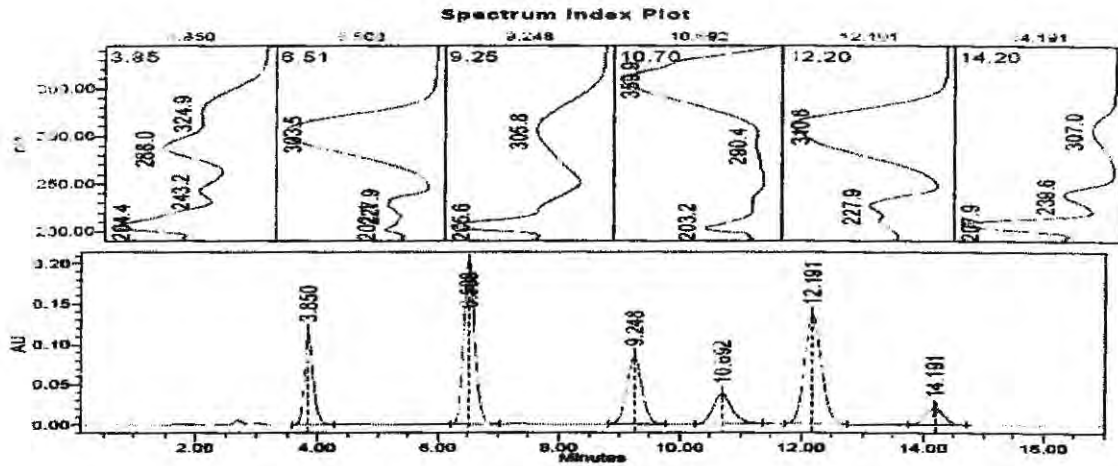


Figure F1: Typical chromatogram of a standard mixture of sunscreen agents for the non-*tinosorb* set. The chromatographic conditions used were: Phenomenex Synergi Max-RP-C₁₂ 80 Å column, mobile phase MeOH-H₂O 84:16% (v/v), injection volume – 20 µL, flow rate - 1 mL min⁻¹, and detection wavelength – 310 nm. The order of elution is Bz-3, MBC, OCR, AVO, OMC and OS.

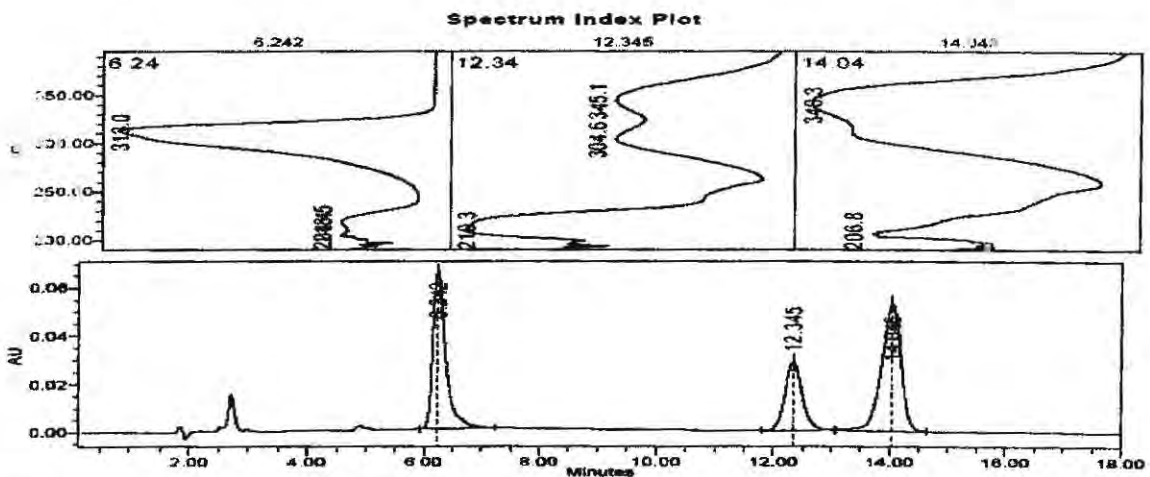


Figure F2: Chromatogram for a standard mixture of sunscreen active ingredients in the *tinosorb* set. The chromatographic conditions used were: Phenomenex Synergi Max-RP-C₁₂ 80 Å column, mobile phase MeOH-ACN 90:10% (v/v), injection volume – 20 µL, flow rate - 1 mL min⁻¹, and detection wavelength - 311 nm. The order of elution is OT, MBBT and BEMT.

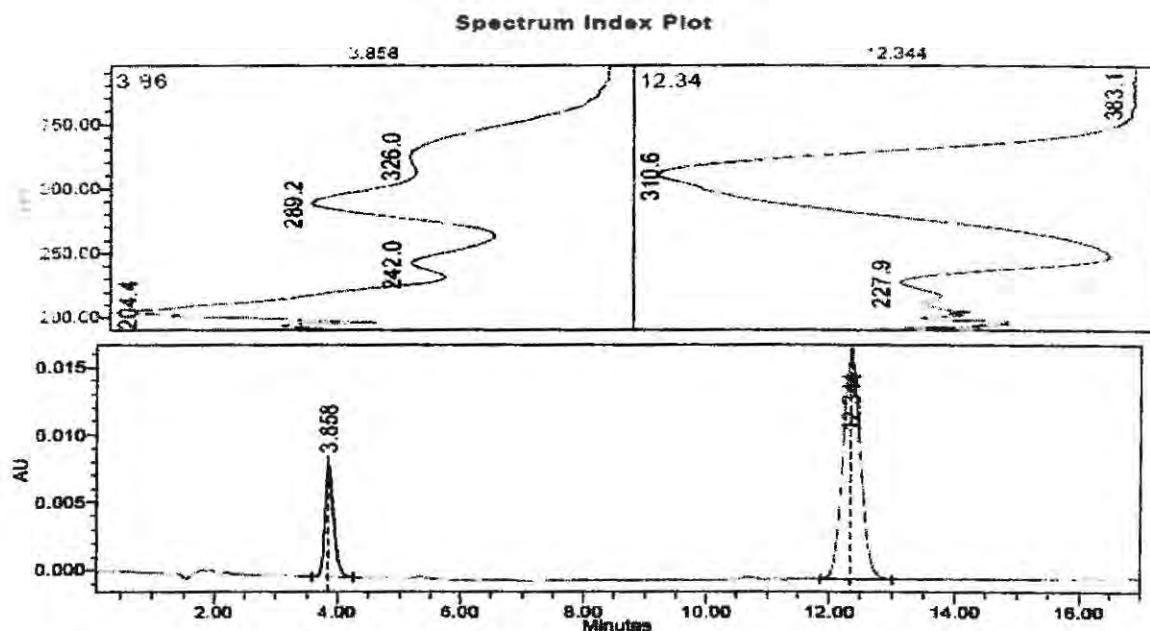


Figure F3: Chromatogram for unirradiated SA1. The chromatographic conditions used were: Phenomenex RP-C₁₂ 80 Å column, mobile phase - MeOH-H₂O 84:16% (v/v), injection volume - 20 µL, flow rate - 1 mL min⁻¹, and detection wavelength - 310 nm. The order of elution is Bz-3 and OMC.

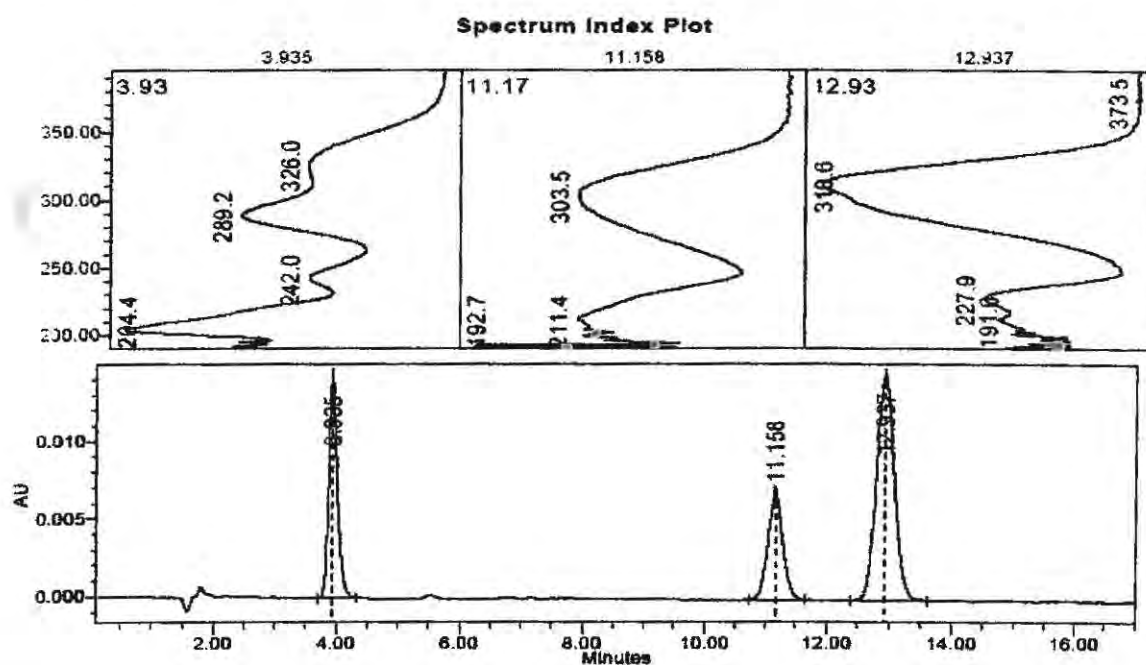


Figure F4: Chromatogram for irradiated SA1. The chromatographic conditions used were: Phenomenex RP-C₁₂ 80 Å column, mobile phase - MeOH-H₂O 84:16% (v/v), injection volume - 20 µL, flow rate - 1 mL min⁻¹, and detection wavelength - 310 nm. The order of elution is Bz-3, *cis*-OMC and *trans*-OMC.

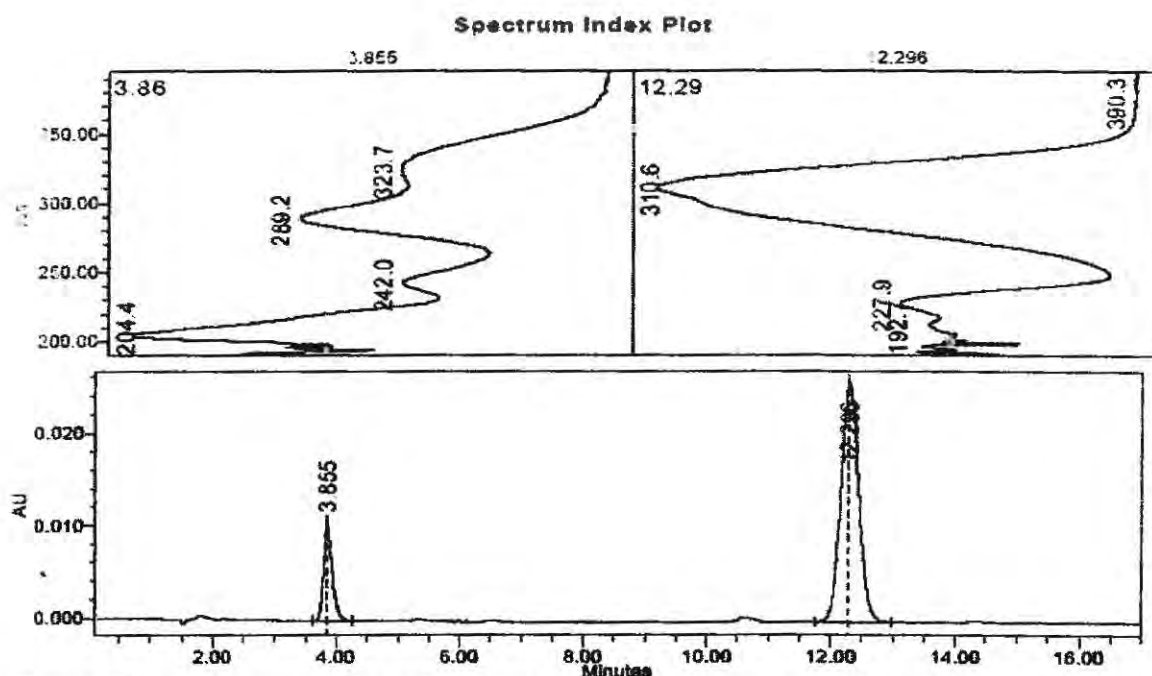


Figure F5: Chromatogram for unirradiated SA2. The chromatographic conditions used were: Phenomenex RP-C₁₂ 80 Å column, mobile phase - MeOH-H₂O 84:16% (v/v), injection volume - 20 µL, flow rate - 1 mL min⁻¹, and detection wavelength - 310 nm. The order of elution is Bz-3 and OMC.

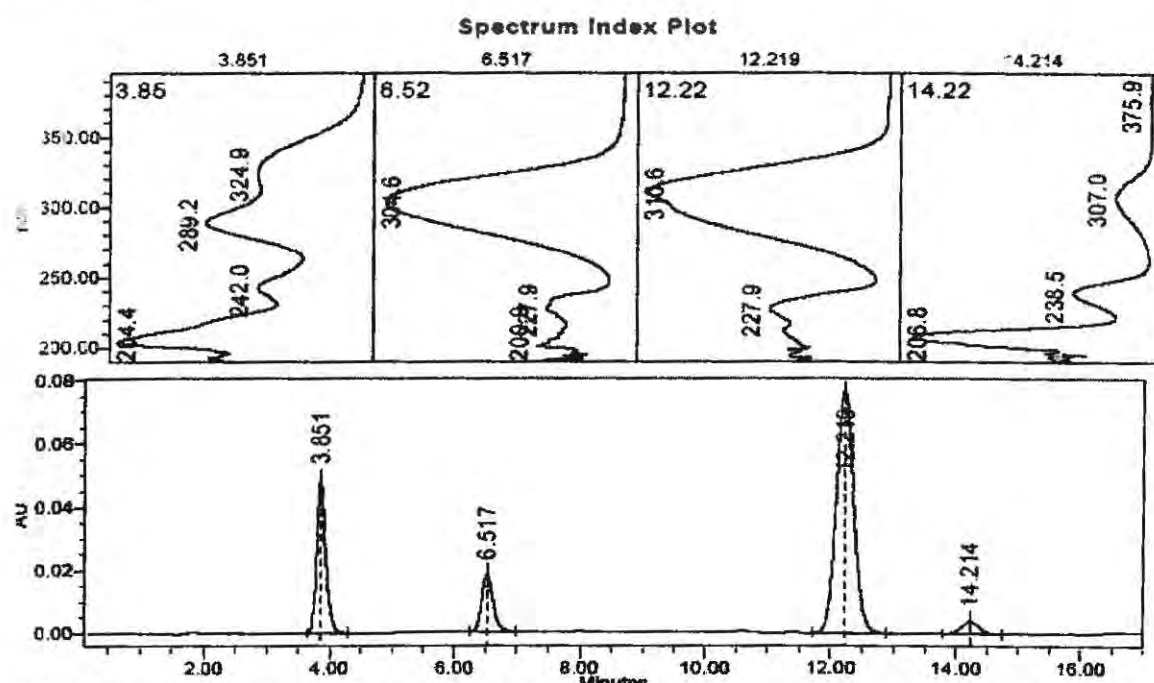


Figure F6: Chromatogram for unirradiated SA3. The chromatographic conditions used were: Phenomenex RP-C₁₂ 80 Å column, mobile phase - MeOH-H₂O 84:16% (v/v), injection volume - 20 µL, flow rate - 1 mL min⁻¹, and detection wavelength - 310 nm. The order of elution is Bz-3, MBC, OMC and OS.

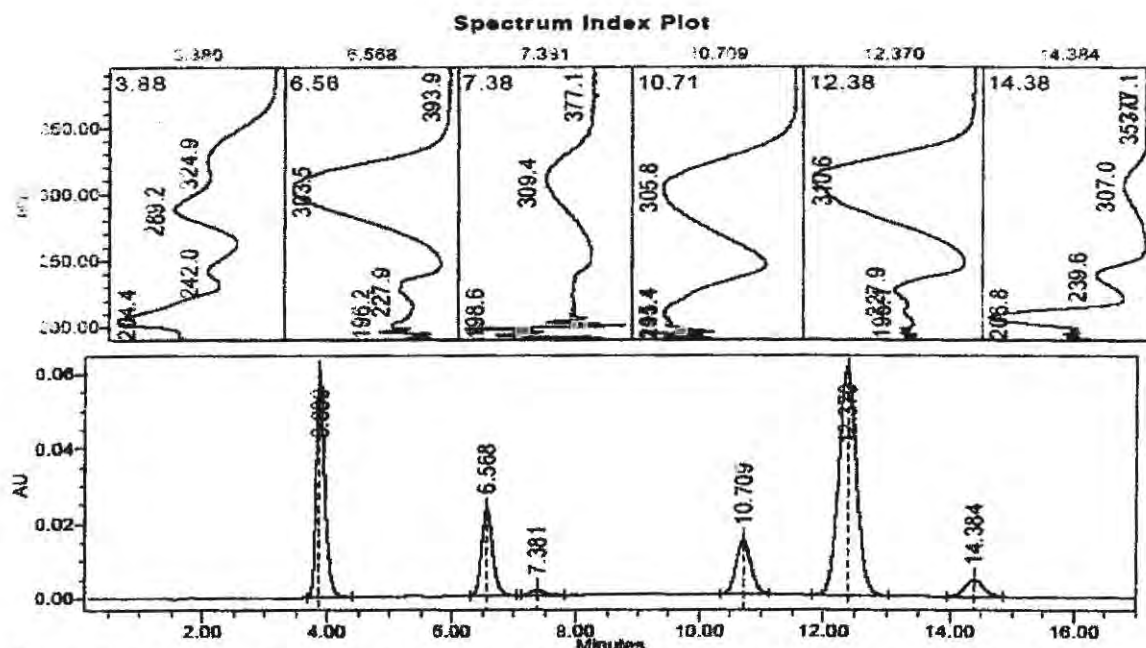


Figure F7: Chromatogram for irradiated SA3. The chromatographic conditions used were: Phenomenex RP-C₁₂ 80 Å column, mobile phase - MeOH-H₂O 84:16% (v/v), injection volume - 20 µL, flow rate - 1 mL min⁻¹, and detection wavelength - 310 nm. The order of elution is Bz-3, MBC, *cis*-MBC, *cis*-OMC, *trans*-OMC and OS.

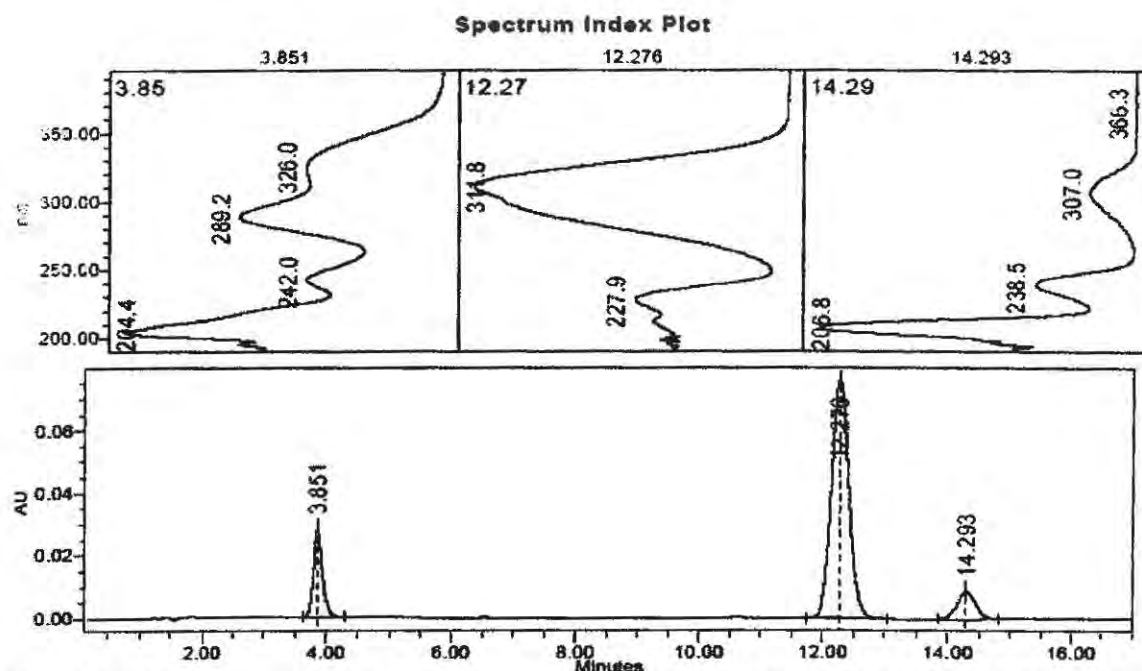


Figure F8: Chromatogram for unirradiated SA4. The chromatographic conditions used were: Phenomenex RP-C₁₂ 80 Å column, mobile phase - MeOH-H₂O 84:16% (v/v), injection volume - 20 µL, flow rate - 1 mL min⁻¹, and detection wavelength - 310 nm. The order of elution is Bz-3, OMC and OS.

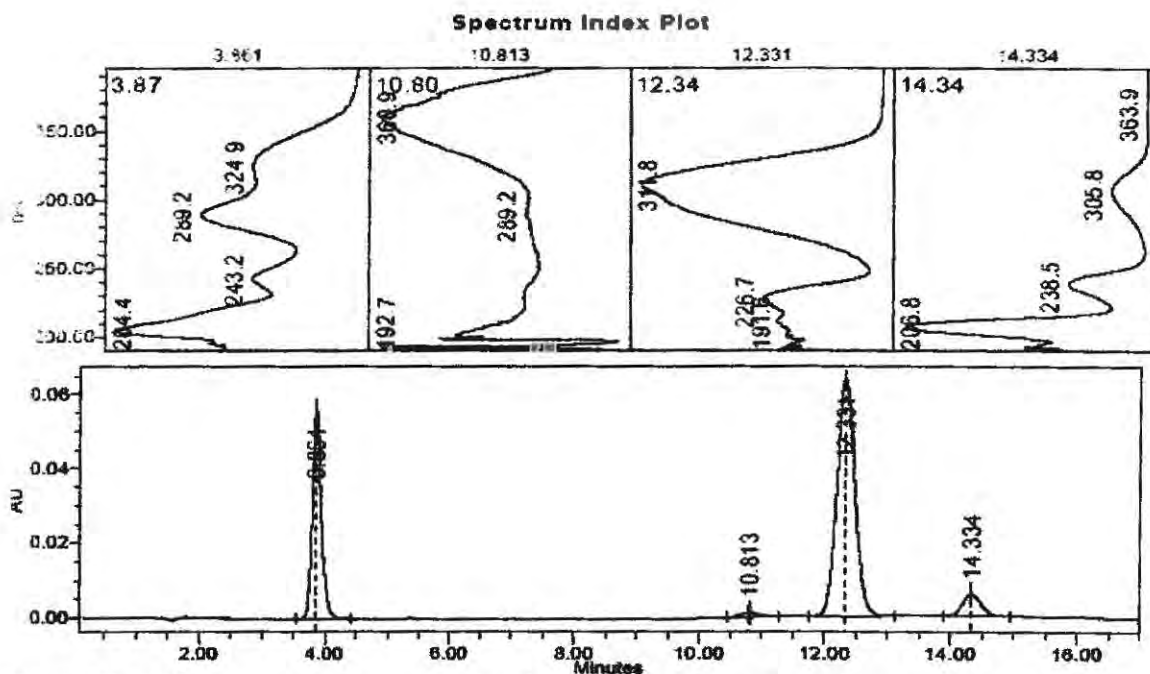


Figure F9: Chromatogram for unirradiated SA5. The chromatographic conditions used were: Phenomenex RP-C₁₂ 80 Å column, mobile phase - MeOH-H₂O 84:16% (v/v), injection volume - 20 µL, flow rate - 1 mL min⁻¹, and detection wavelength - 310 nm. The order of elution is Bz-3, AVO, OMC and OS.

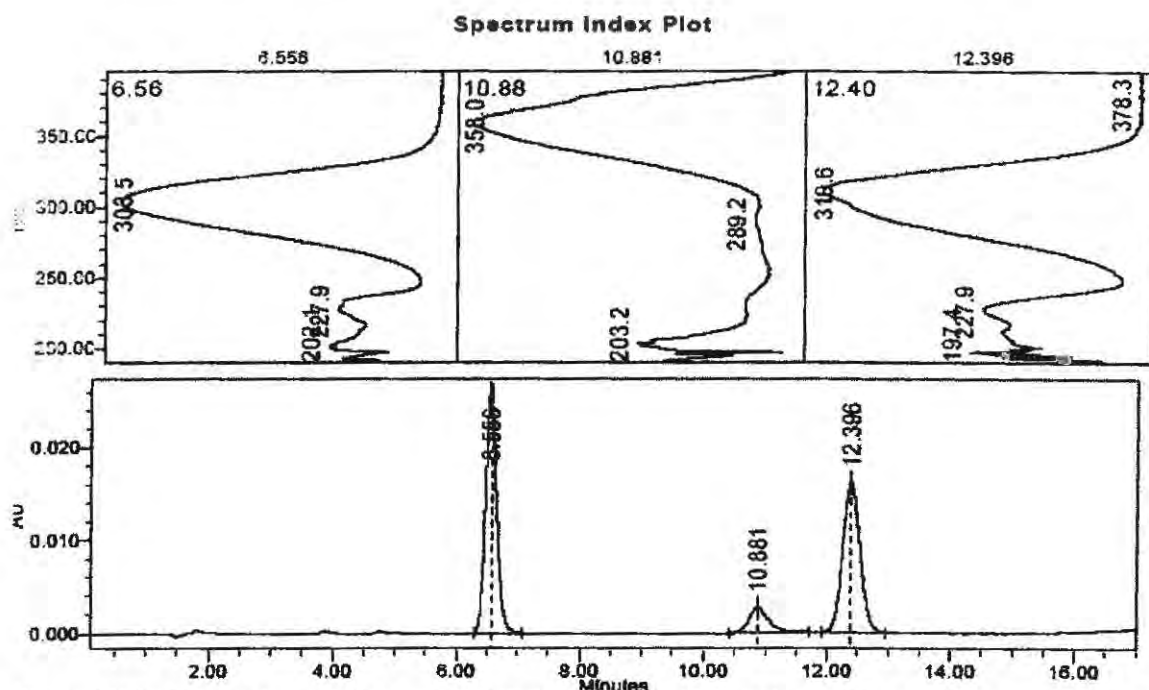


Figure F10: Chromatogram for unirradiated SA6. The chromatographic conditions used were: Phenomenex RP-C₁₂ 80 Å column, mobile phase - MeOH-H₂O 84:16% (v/v), injection volume - 20 µL, flow rate - 1 mL min⁻¹, and detection wavelength - 310 nm. The order of elution is MBC, AVO and OMC.

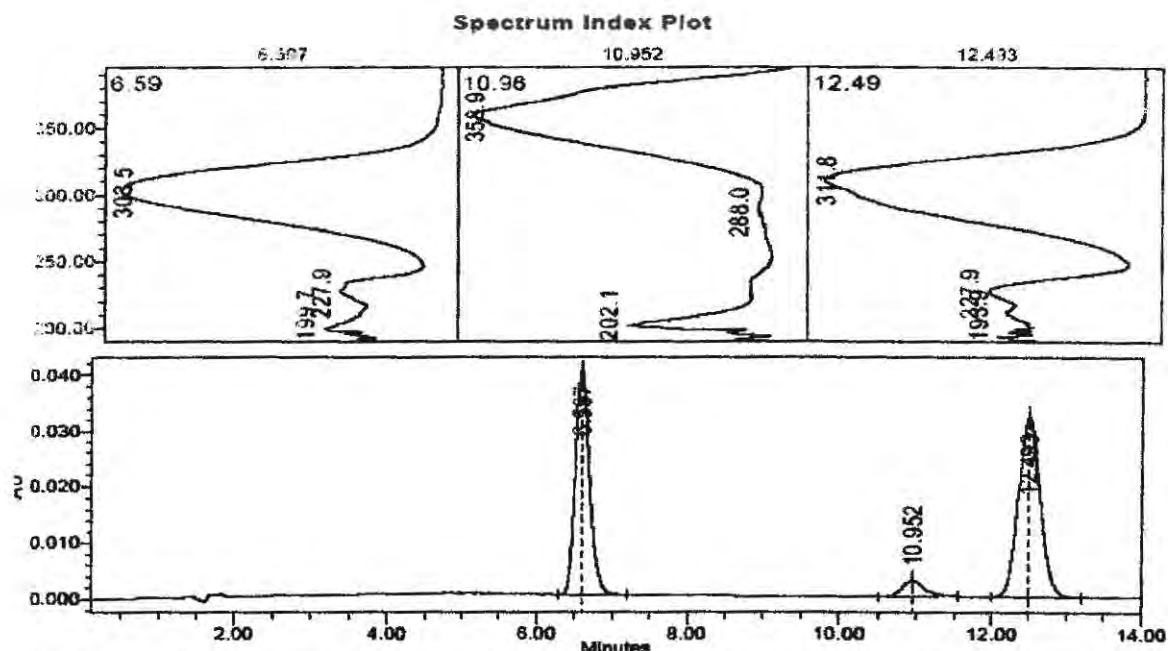


Figure F11: Chromatogram for unirradiated SA7. The chromatographic conditions used were: Phenomenex RP-C₁₂ 80 Å column, mobile phase - MeOH-H₂O 84:16% (v/v), injection volume - 20 µL, flow rate - 1 mL min⁻¹, and detection wavelength - 310 nm. The order of elution is MBC, AVO and OMC.

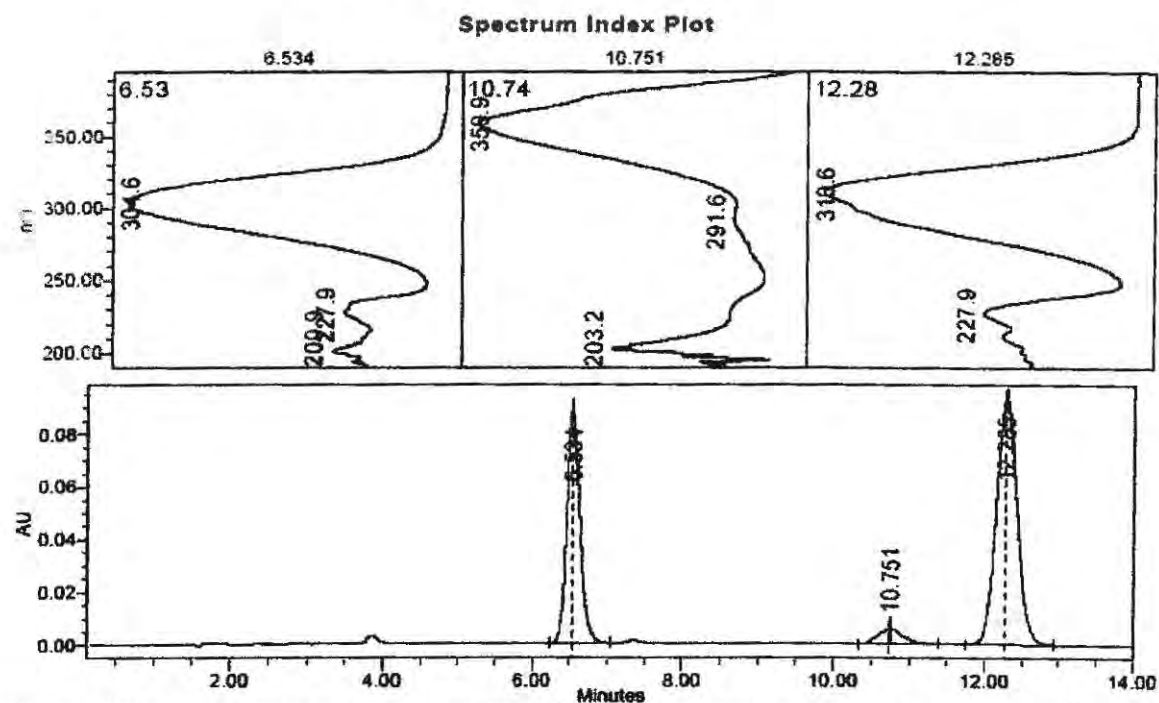


Figure F12: Chromatogram for unirradiated SA8. The chromatographic conditions used were: Phenomenex RP-C₁₂ 80 Å column, mobile phase - MeOH-H₂O 84:16% (v/v), injection volume - 20 µL, flow rate - 1 mL min⁻¹, and detection wavelength - 310 nm. The order of elution is MBC, AVO and OMC.

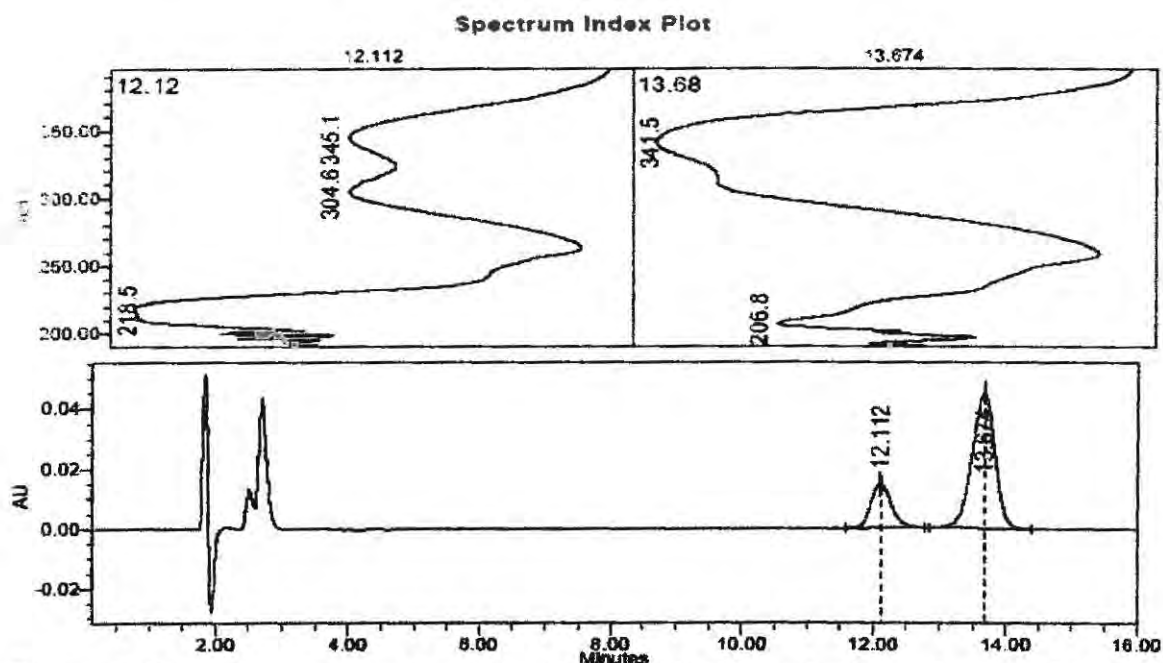


Figure F13a: Chromatogram for unirradiated SA9 (determination of *timosorbs*). The chromatographic conditions used were: Phenomenex Synergi Max-RP-C₁₂ 80 Å column, mobile phase - MeOH-ACN 90:10% (v/v), injection volume - 20 µL, flow rate - 1 mL min⁻¹, and detection wavelength - 342 nm. The order of elution is MBBT and BEMT.

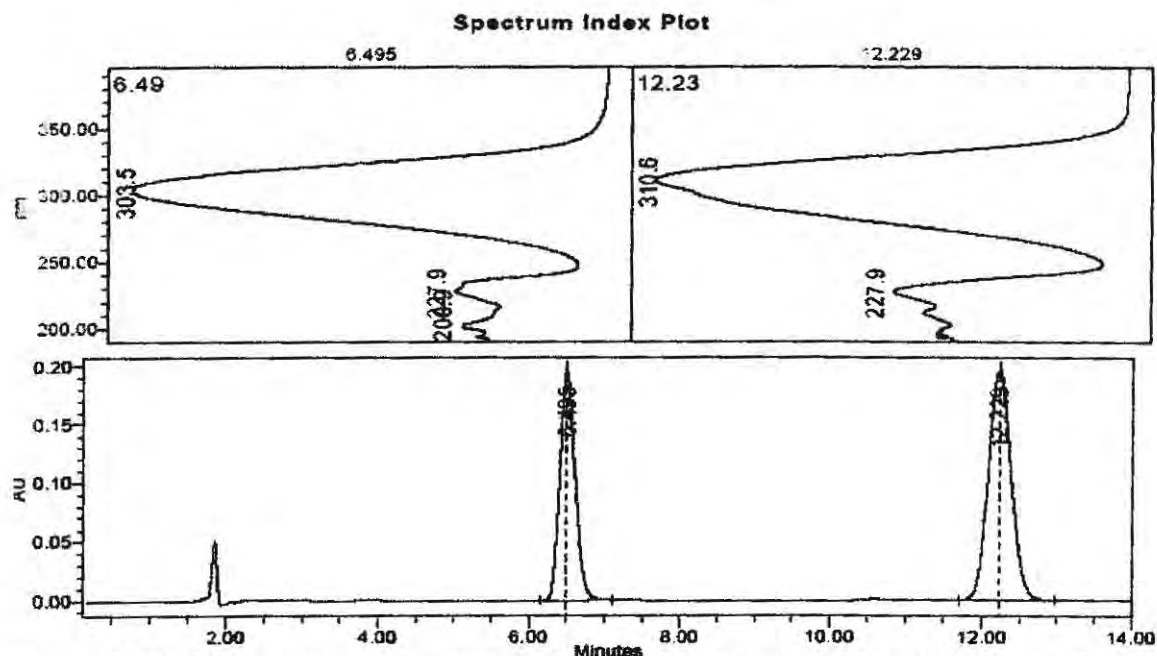


Figure F13b: Chromatogram for unirradiated SA9 (determination of OMC and MBC). The chromatographic conditions used were: Phenomenex RP-C₁₂ 80 Å column, mobile phase - MeOH-H₂O 84:16% (v/v), injection volume - 20 µL, flow rate - 1 mL min⁻¹, and detection wavelength - 310 nm. The order of elution is MBC and OMC.

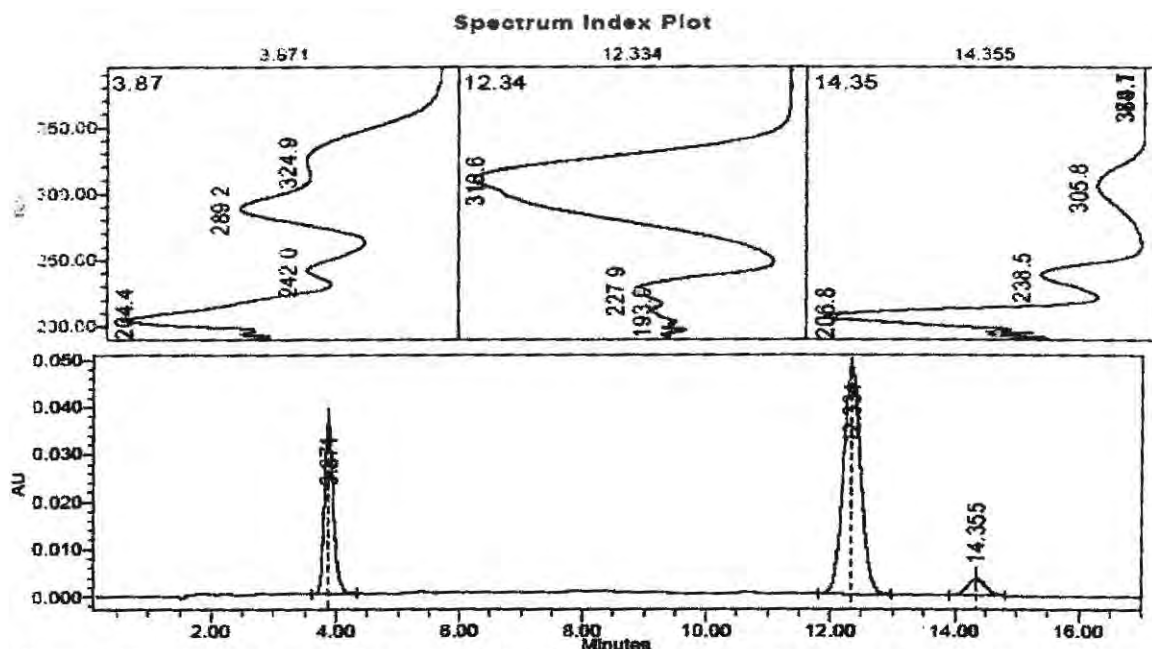


Figure F14: Chromatogram for unirradiated SA10. The chromatographic conditions used were: Phenomenex RP-C₁₂ 80 Å column, mobile phase - MeOH-H₂O 84:16% (v/v), injection volume - 20 µL, flow rate - 1 mL min⁻¹, and detection wavelength - 310 nm. The order of elution is Bz-3, OMC and OS.

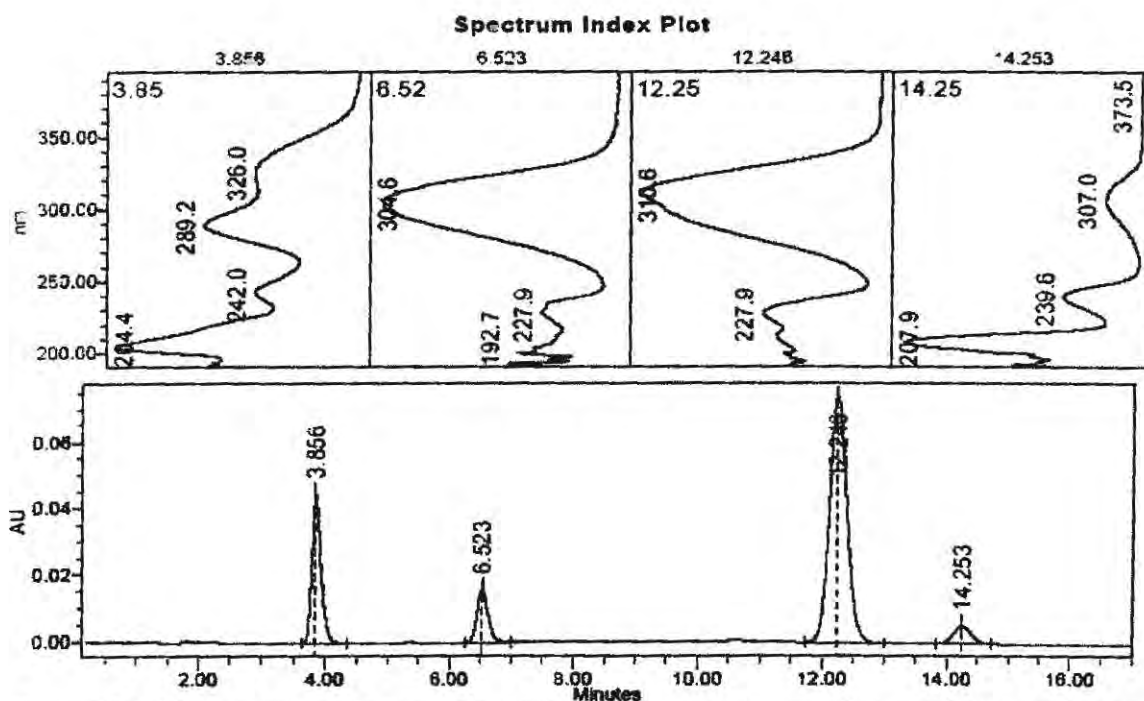


Figure F15: Chromatogram for unirradiated SA11. The chromatographic conditions used were: Phenomenex RP-C₁₂ 80 Å column, mobile phase - MeOH-H₂O 84:16% (v/v), injection volume - 20 µL, flow rate - 1 mL min⁻¹, and detection wavelength - 310 nm. The order of elution is Bz-3, MBC, OMC and OS.

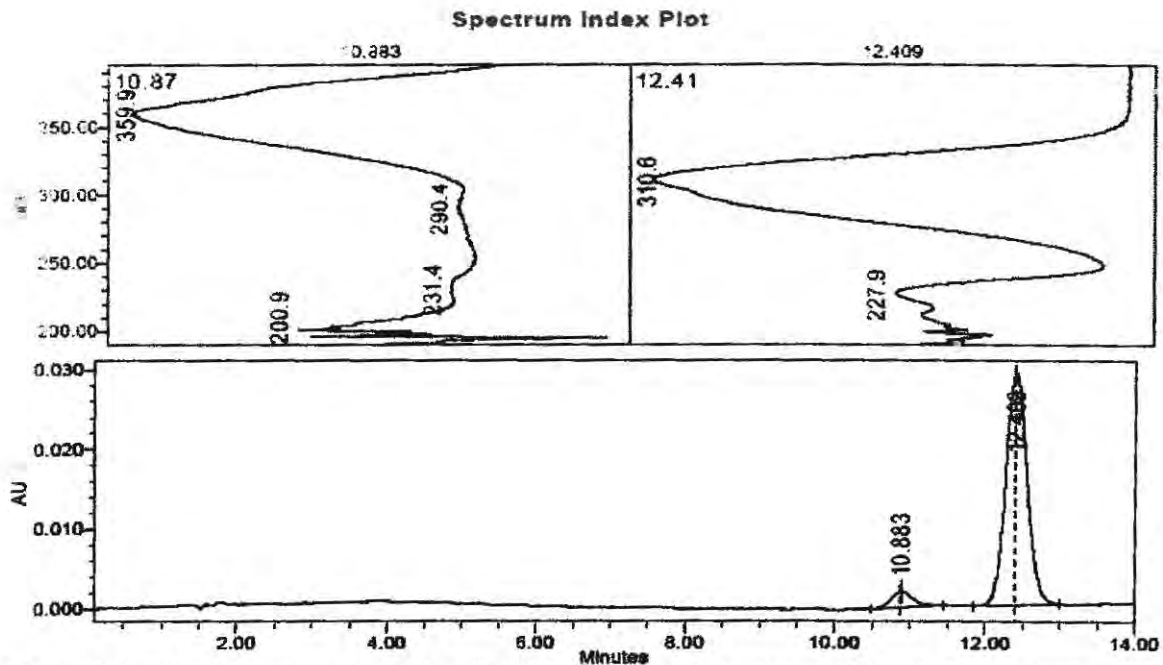


Figure F16: Chromatogram for unirradiated SA12. The chromatographic conditions used were: Phenomenex RP-C₁₂ 80 Å column, mobile phase - MeOH-H₂O 84:16% (v/v), injection volume - 20 µL, flow rate - 1 mL min⁻¹, and detection wavelength - 330 nm. The order of elution is AVO and OMC.

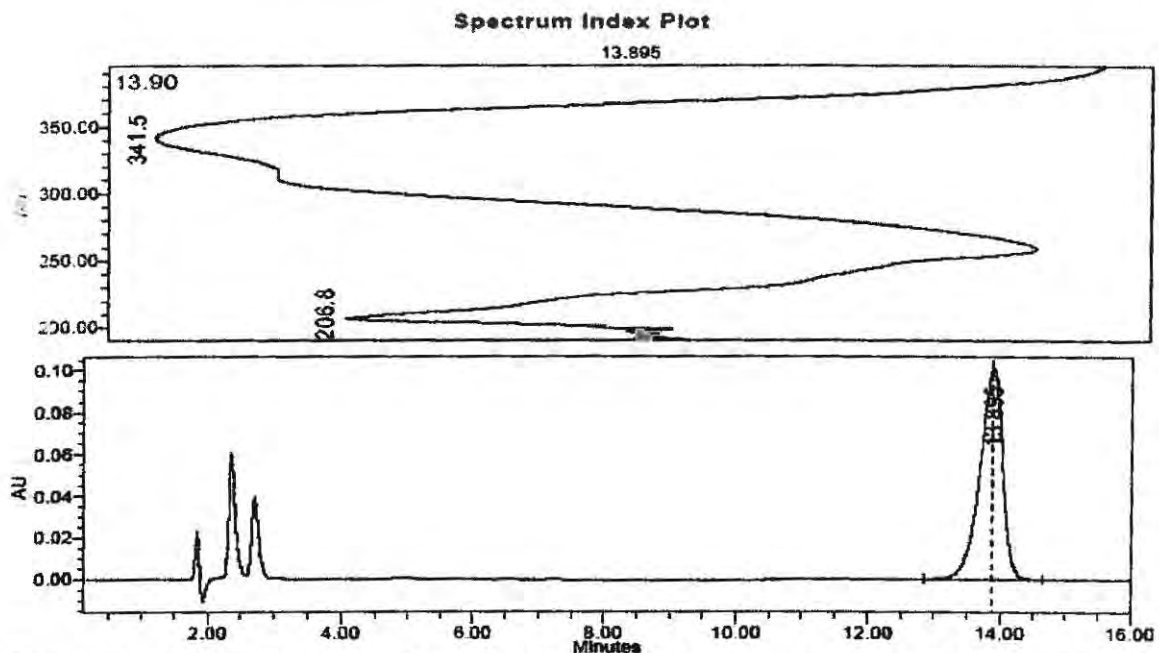


Figure F17a: Chromatogram for unirradiated SA13 (determination of tinosorbs). The chromatographic conditions used were: Phenomenex Synergi Max-RP-C₁₂ 80 Å column, mobile phase - MeOH-ACN 90:10% (v/v), injection volume - 20 µL, flow rate - 1 mL min⁻¹, and detection wavelength - 342 nm. The marked peak is BEMT.

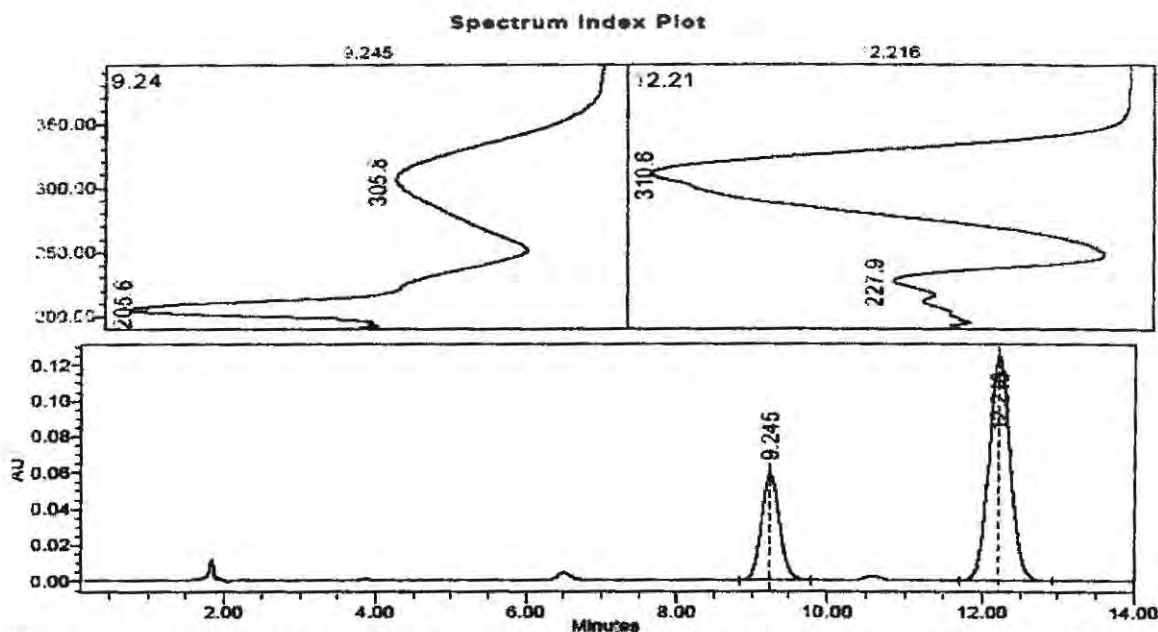


Figure F17b: Chromatogram for unirradiated SA13 (determination of OMC, OCR). The chromatographic conditions used were: Phenomenex RP-C₁₂ 80 Å column, mobile phase - MeOH-H₂O 84:16% (v/v), injection volume - 20 µL, flow rate - 1 mL min⁻¹, and detection wavelength - 310 nm. The order of elution is OCR and OMC.

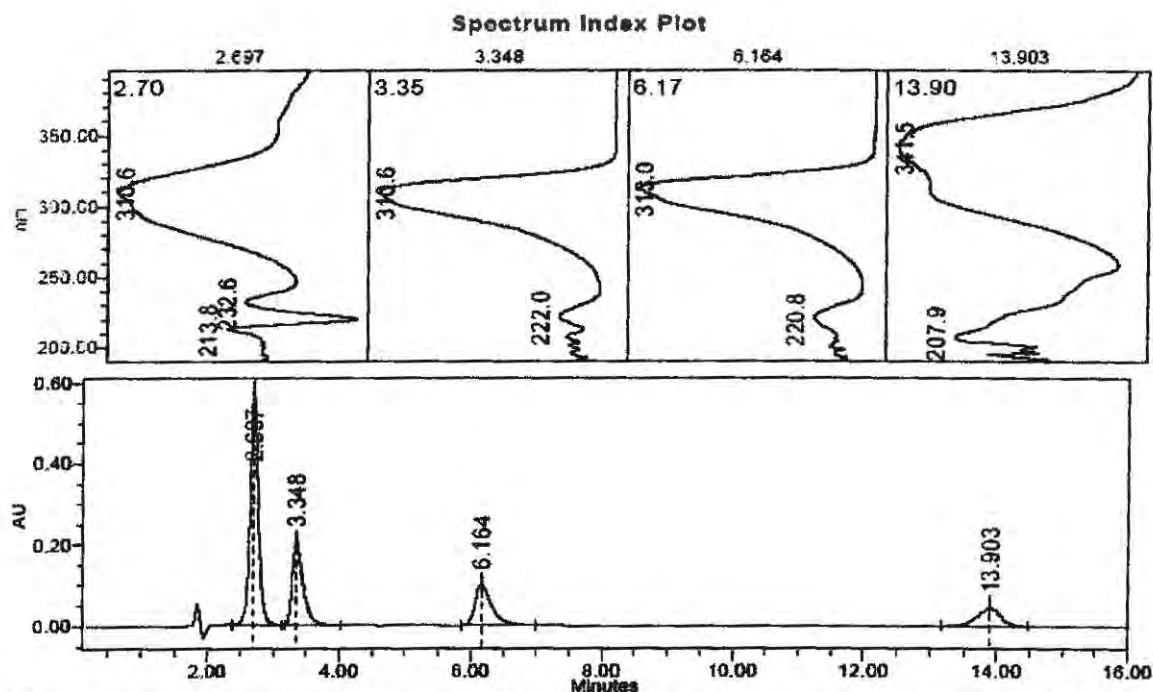


Figure F18a: Chromatogram for unirradiated SA14 (determination of OT and BEMT). The chromatographic conditions used were: Phenomenex Synergi Max-RP-C₁₂ 80 Å column, mobile phase - MeOH-ACN 90:10% (v/v), injection volume - 20 µL, flow rate - 1 mL min⁻¹, and detection wavelength - 311 nm. The order of elution is "unknown," DOBT, OT and BEMT.

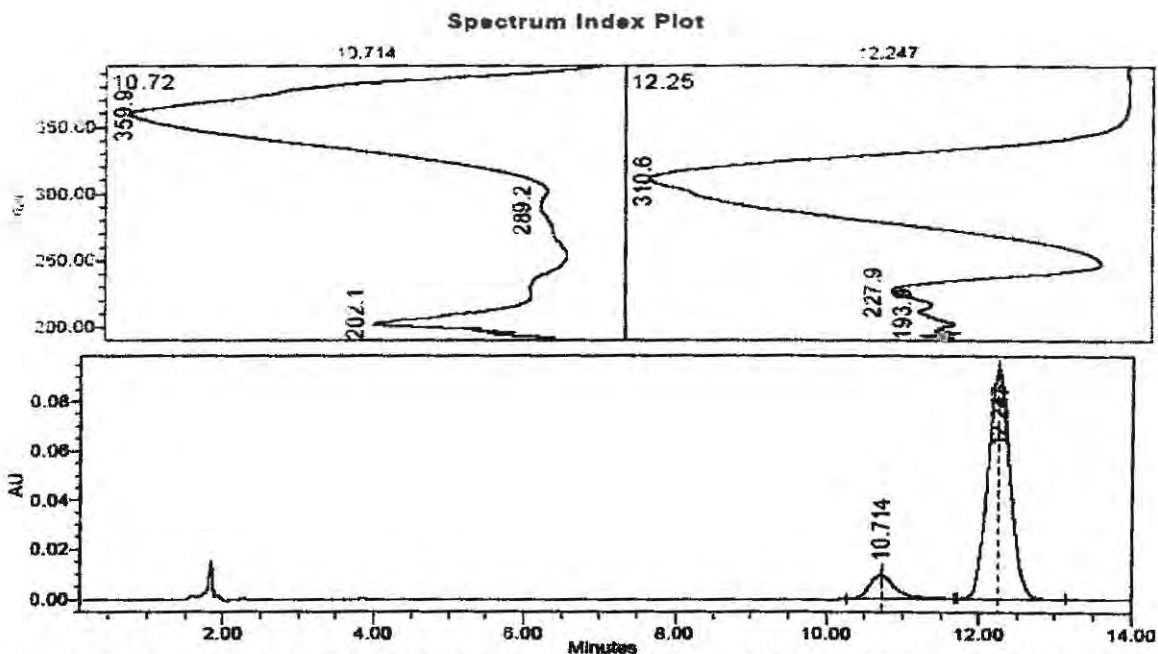


Figure F18b: Chromatogram for unirradiated SA14 (determination of AVO and OMC). The chromatographic conditions used were: Phenomenex RP-C₁₂ 80 Å column, mobile phase - MeOH-H₂O 84:16% (v/v), injection volume - 20 µL, flow rate - 1 mL min⁻¹, and detection wavelength - 310 nm. The order of elution is AVO and OMC.

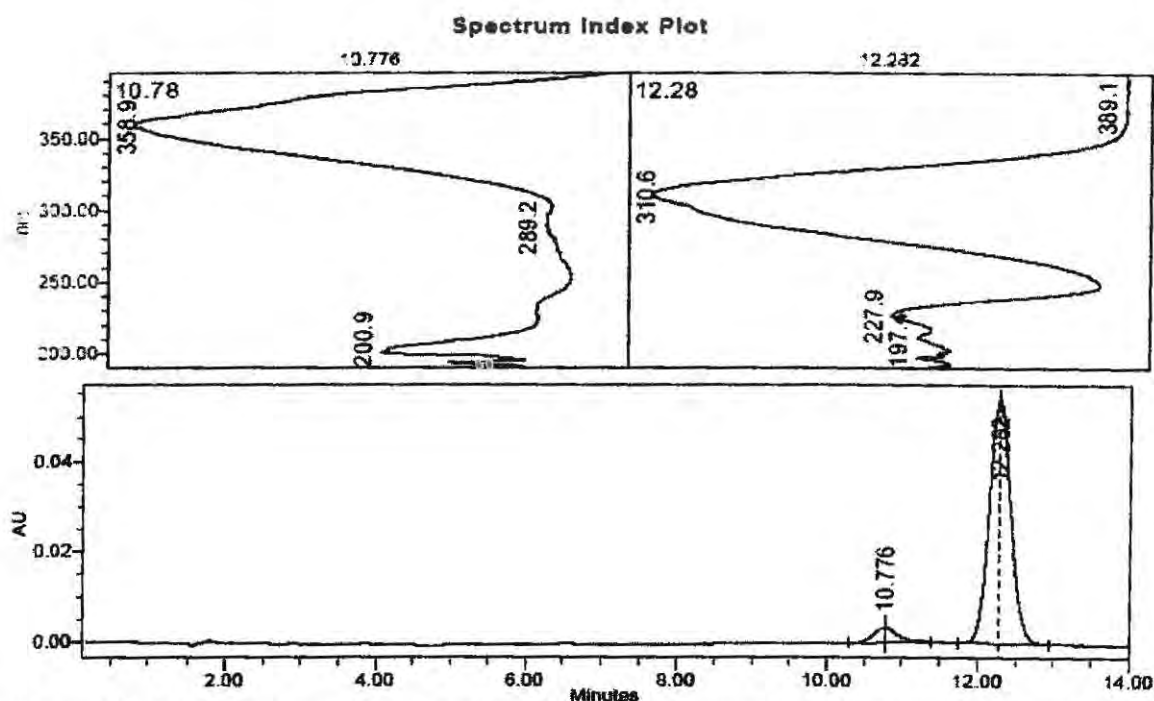


Figure F19: Chromatogram for unirradiated SA15. The chromatographic conditions used were: Phenomenex RP-C₁₂ 80 Å column, mobile phase - MeOH-H₂O 84:16% (v/v), injection volume - 20 µL, flow rate - 1 mL min⁻¹, and detection wavelength - 330 nm. The order of elution is AVO and OMC.

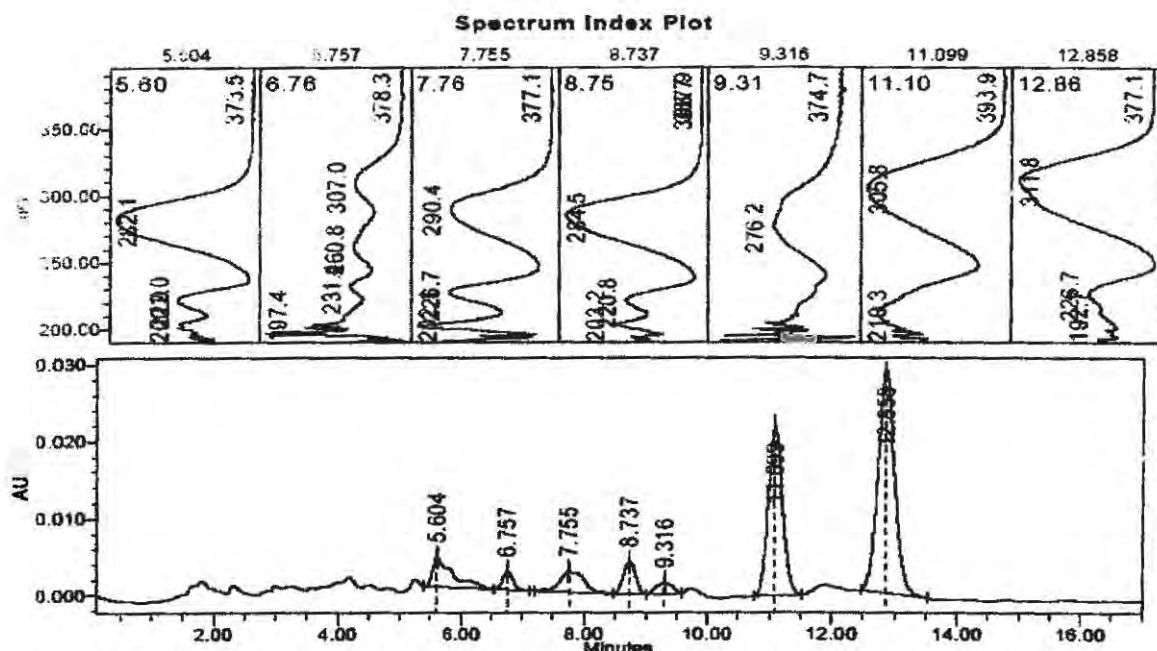


Figure F20: Chromatogram for irradiated SA15. The chromatographic conditions used were: Phenomenex RP-C₁₂ 80 Å column, mobile phase - MeOH-H₂O 84:16% (v/v), injection volume - 20 µL, flow rate - 1 mL min⁻¹, and detection wavelength - 330 nm. The peaks eluting at 11.099 and 12.858 minutes are for *cis*-OMC and *trans*-OMC, respectively.

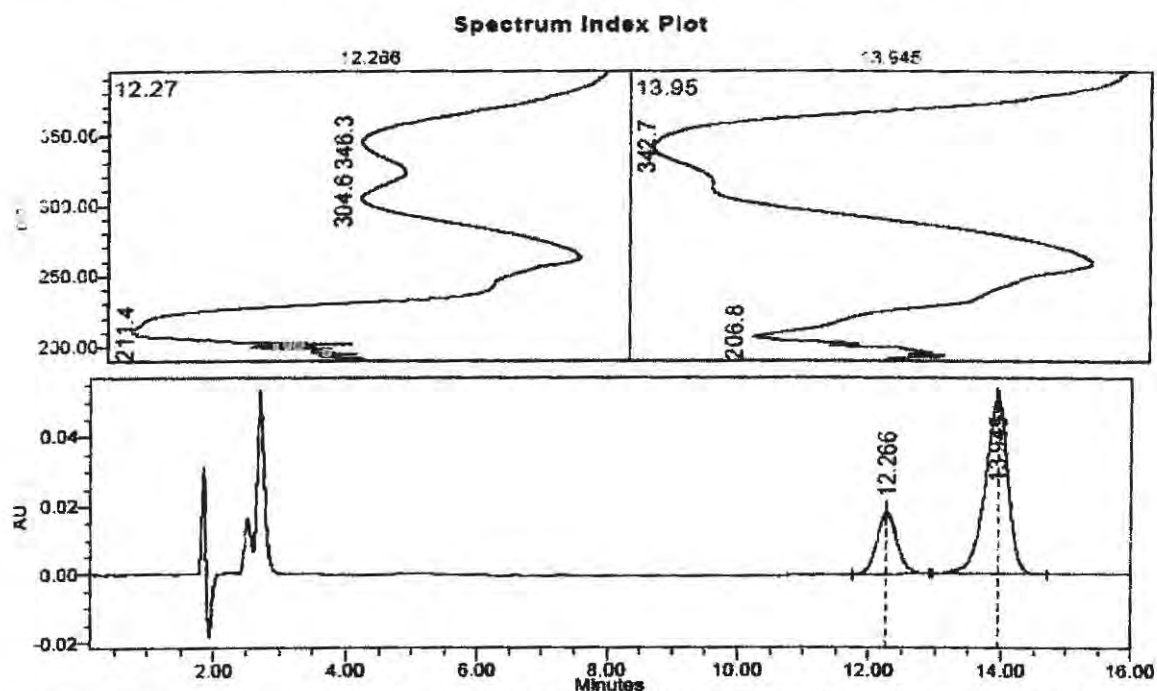


Figure F21a: Chromatogram for unirradiated SA16 (determination of the *timosorbs*). The chromatographic conditions used were: Phenomenex Synergi Max-RP-C₁₂ 80 Å column, mobile phase - MeOH-ACN 90:10% (v/v), injection volume - 20 µL, flow rate - 1 mL min⁻¹, and detection wavelength - 342 nm. The order of elution is MBBT and BEMT.

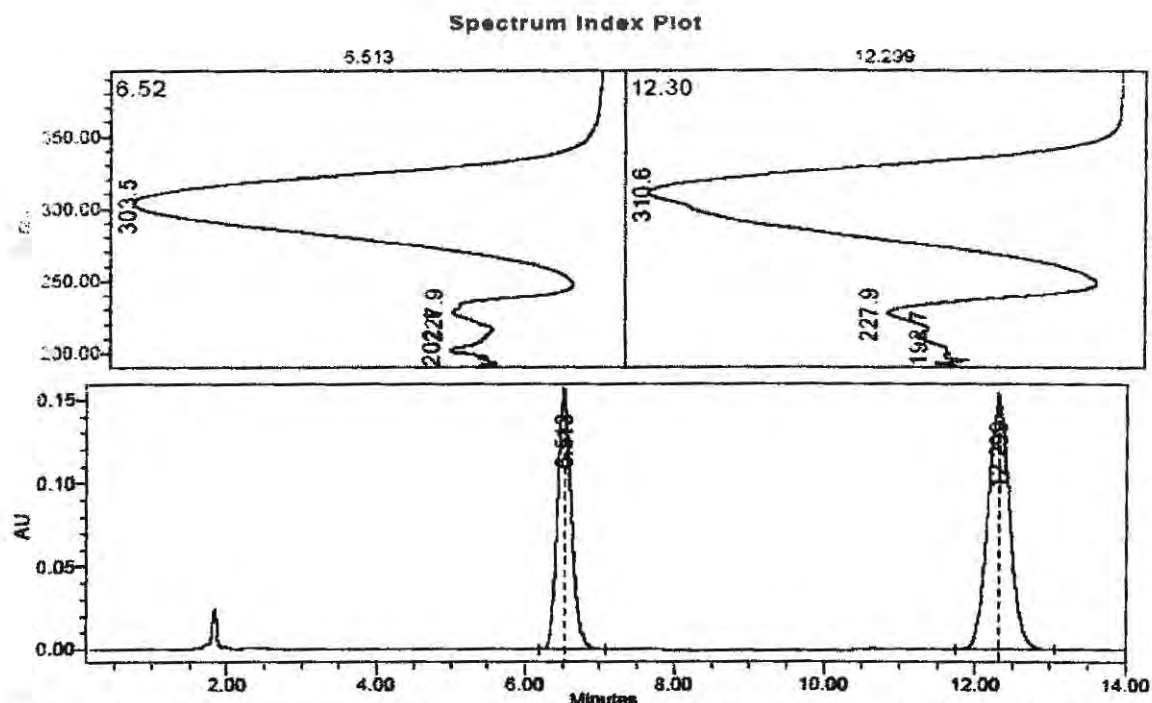


Figure F21b: Chromatogram for unirradiated SA16 (determination of OMC, MBC). The chromatographic conditions used were: Phenomenex RP-C₁₂ 80 Å column, mobile phase - MeOH-H₂O 84:16% (v/v), injection volume - 20 µL, flow rate - 1 mL min⁻¹, and detection wavelength - 310 nm. The order of elution is MBC and OMC.

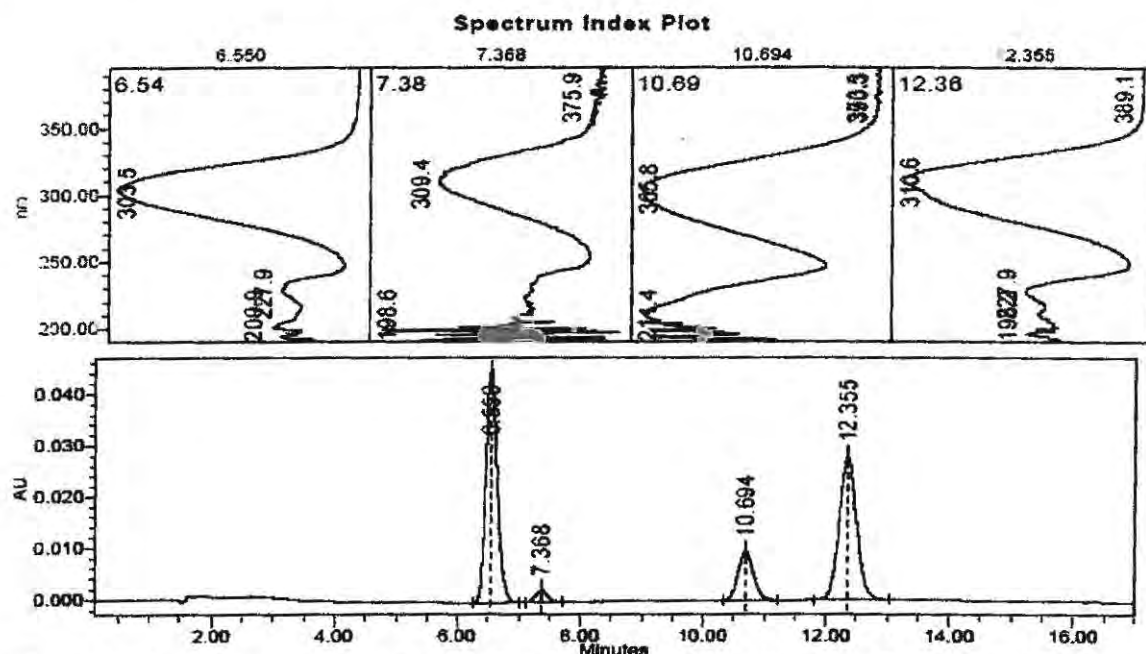


Figure F22: Chromatogram for irradiated SA16 (determination of OMC, MBC). The chromatographic conditions used were: Phenomenex RP-C₁₂ 80 Å column, mobile phase - MeOH-H₂O 84:16% (v/v), injection volume - 20 µL, flow rate - 1 mL min⁻¹, and detection wavelength - 310 nm. The order of elution is *trans*-MBC, *cis*-MBC, *cis*-OMC and *trans*-OMC.

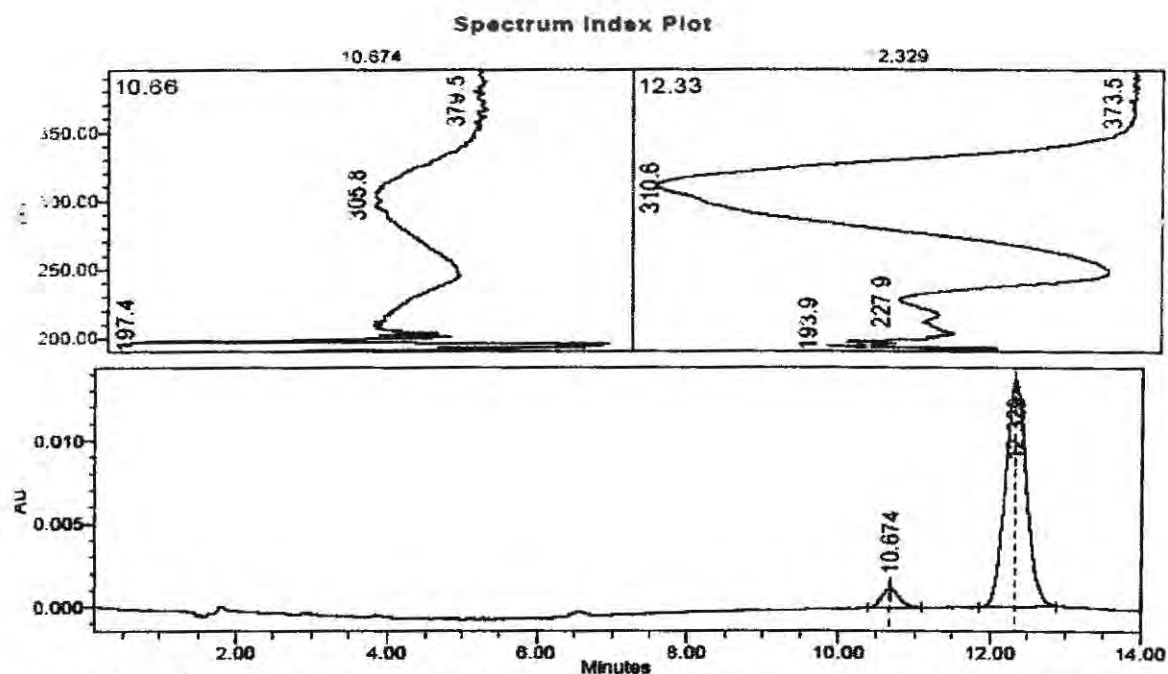


Figure F23: Chromatogram for unirradiated SA18. The chromatographic conditions used were: Phenomenex RP-C₁₂ 80 Å column, mobile phase - MeOH-H₂O 84:16% (v/v), injection volume - 20 µL, flow rate - 1 mL min⁻¹, and detection wavelength - 310 nm. The order of elution is *cis*-OMC and *trans*-OMC.

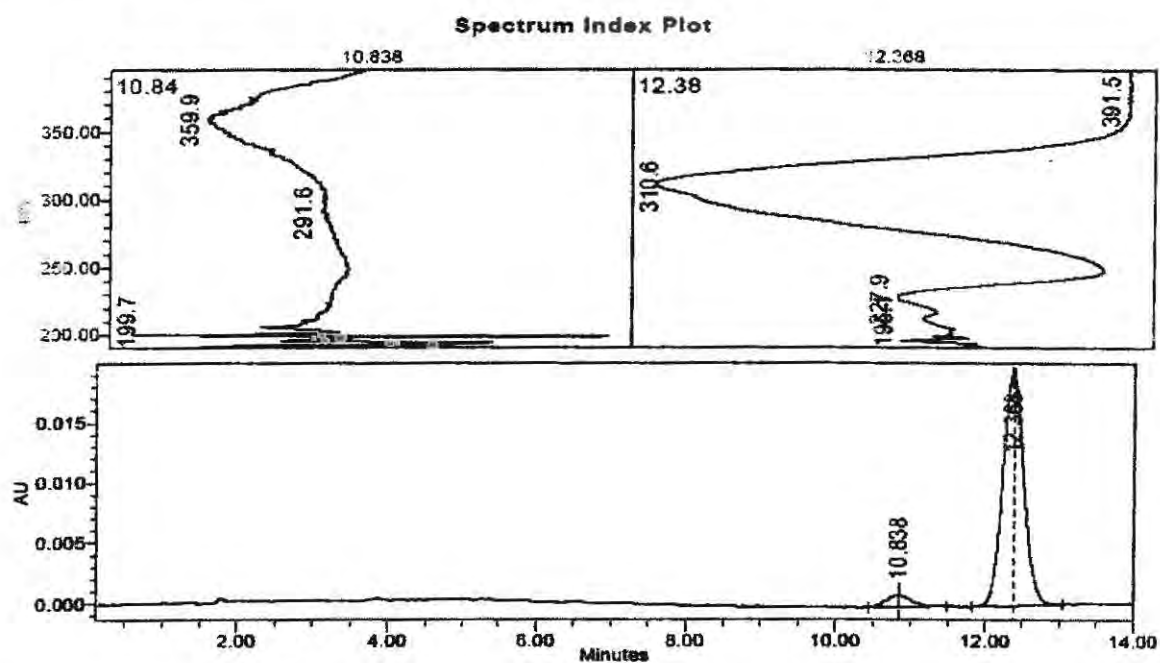


Figure F24: Chromatogram for unirradiated SA20. The chromatographic conditions used were: Phenomenex RP-C₁₂ 80 Å column, mobile phase - MeOH-H₂O 84:16% (v/v), injection volume - 20 µL, flow rate - 1 mL min⁻¹, and detection wavelength - 330 nm. The order of elution is AVO and OMC.

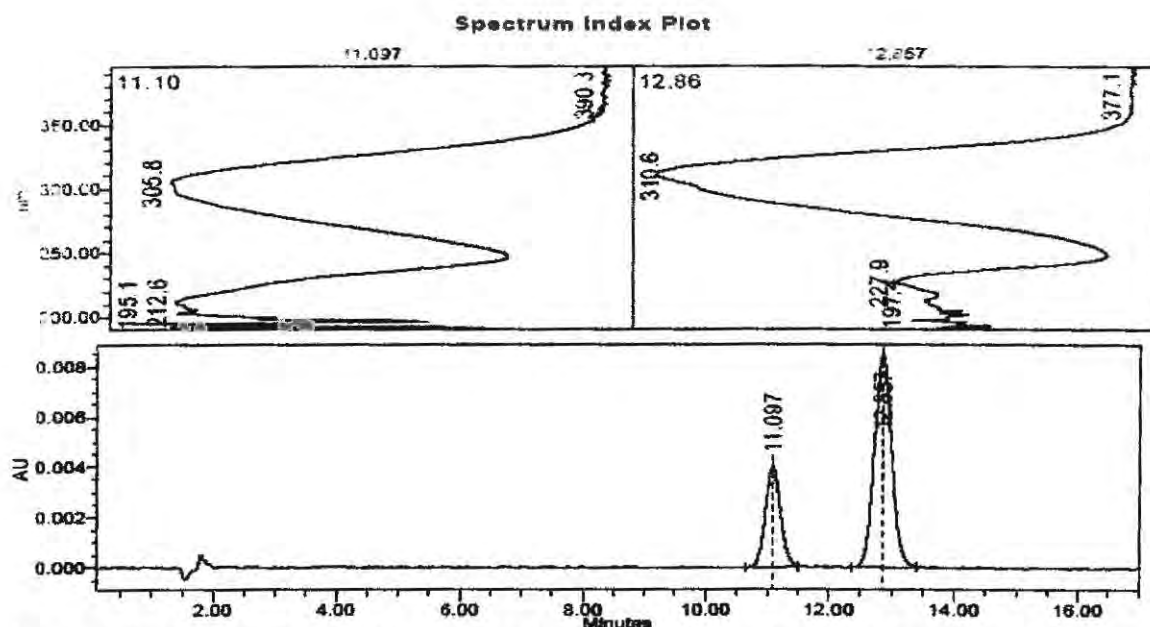


Figure F25: Chromatogram for irradiated SA20. The chromatographic conditions used were: Phenomenex RP-C₁₂ 80 Å column, mobile phase - MeOH-H₂O 84:16% (v/v), injection volume - 20 µL, flow rate - 1 mL min⁻¹, and detection wavelength - 330 nm. The order of elution is *cis*-OMC and OMC.

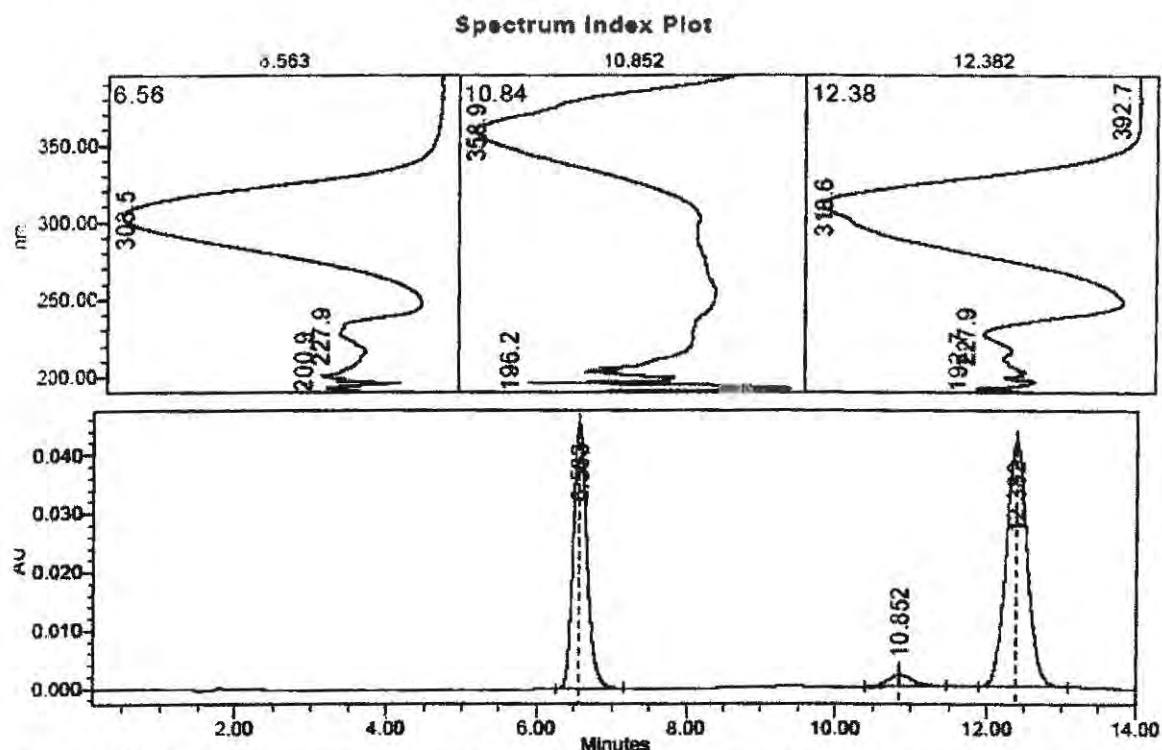


Figure F26: Chromatograms for unirradiated SA21. The chromatographic conditions used were: Phenomenex RP-C₁₂ 80 Å column, mobile phase - MeOH-H₂O 84:16% (v/v), injection volume - 20 µL, flow rate - 1 mL min⁻¹, and detection wavelength - 330 nm. The order of elution is MBC, AVO and OMC.

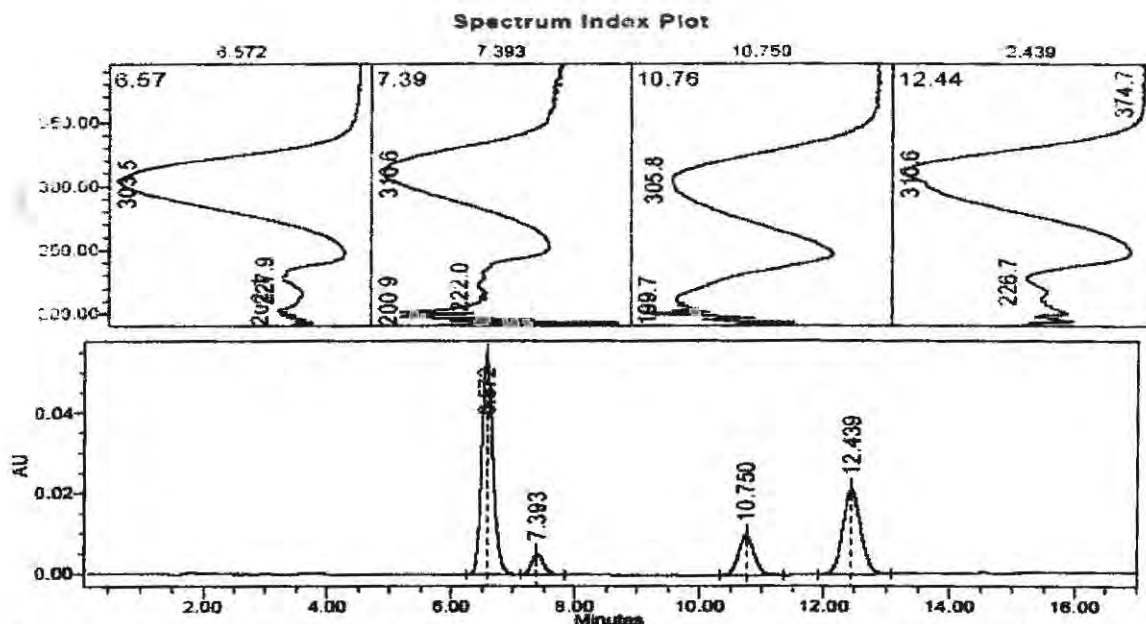


Figure F27: Chromatogram for irradiated SA21. The chromatographic conditions used were: Phenomenex RP-C₁₂ 80 Å column, mobile phase - MeOH-H₂O 84:16% (v/v), injection volume - 20 µL, flow rate - 1 mL min⁻¹, and detection wavelength - 330 nm. The order of elution is *trans*-MBC, *cis*-MBC, *cis*-OMC and *trans*-OMC.

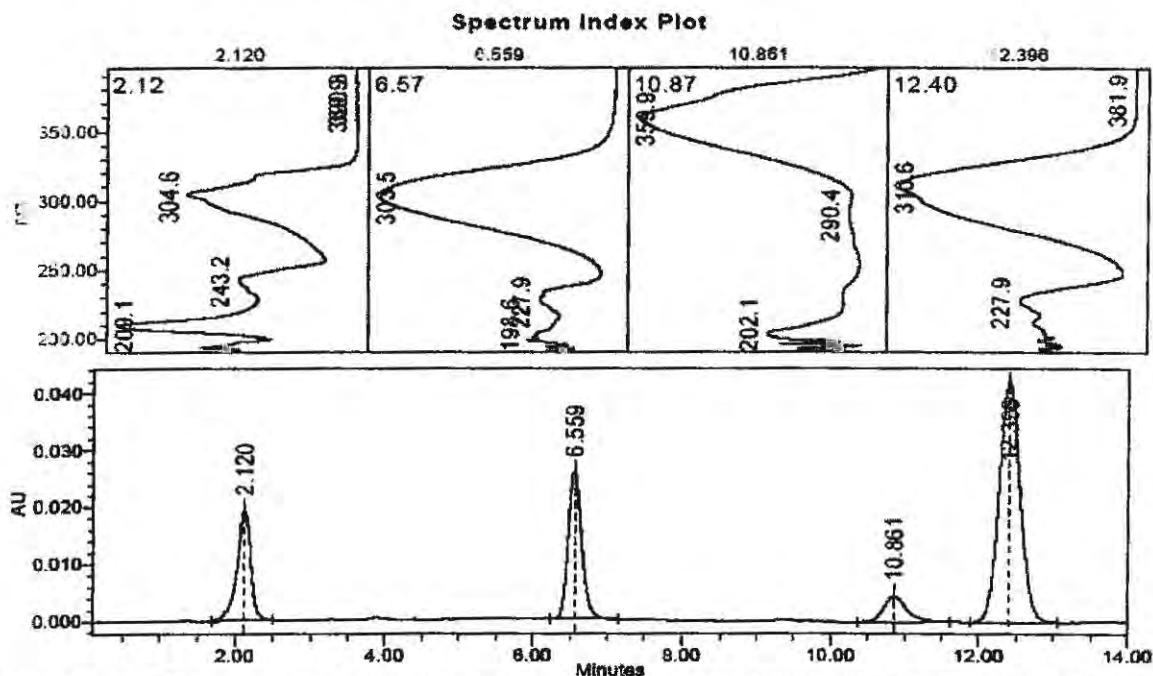


Figure F28: Chromatogram for unirradiated SA22. The chromatographic conditions used were: Phenomenex RP-C₁₂ 80 Å column, mobile phase - MeOH-H₂O 84:16% (v/v), injection volume - 20 µL, flow rate - 1 mL min⁻¹, and detection wavelength - 310 nm. The order of elution is "unknown," MBC, AVO and OMC.

Appendix G

RAW DATA FOR SUNCARE PRODUCTS

The following tables list the peak areas obtained for the active ingredients in the different suncare products analysed by HPLC.

SA1		SA2		SA3			
OMC	Bz-3	OMC	Bz-3	OMC	Bz-3	MBC	OS
761310	351910	1012180	441762	1010958	531101	187236	115518
756697	355823	1009698	442271	1021412	533703	187977	115200
755254	353490	1015097	440555	1038032	538850	184374	115062
735690	351895	1250721	472495	1091055	541098	177199	114498
727745	345786	1233458	472782	1092615	513664	178001	110195
735711	343504	1222766	466318	1076995	508841	174382	113100
903122	327155	1169862	457896	958859	482356	165766	112217
902648	330264	1203654	460253	956324	485512	168533	115632
905687	332645	1185642	462351	954658	480253	164453	114235
SA4			SA5			SA18	
OMC	Bz-3	OS	OMC	Bz-3	OS	AVO	OMC
360945	213161	92141	1483101	1058338	305607	178248	5643463
364450	210215	91628	1476437	1055280	297689	155435	5798652
361040	212875	90151	1445141	1039430	315959	154231	5967823
369953	111956	94135	1352109	904607	267065	147671	1203254
365234	110889	93576	1403562	910236	270869	145210	1187564
370213	112452	97149	1386547	915763	275463	142564	1243256
722337	116956	187897	1504334	954550	287285	178521	1187546
723548	113889	185523	1541325	947895	281456	170254	1216548
720546	115452	184254	1482578	951263	277859	174632	1255784
SA8			SA9				
AVO	OMC	MBC	OMC	MBC	MBBT	BEMT	
593759	2013325	1302210	2431881	1645138	62713	206402	
595637	1965861	1273122	2429339	1652776	63040	208628	
589578	1982567	1267895	2414878	1644075	63346	207054	
511021	1954631	1320102	2451921	1809021	312789	1043273	
509877	1962364	1330862	2469295	1822573	312989	1063799	
510700	1974121	1321542	2474906	1858694	311438	1069930	
577905	1867905	1250461	2594752	1685127	333517	1128949	
575689	1872445	1242135	2630501	1692812	334490	125146	
571452	1898675	1245263	2629850	1674104	333976	125146	

SA6			SA7			SA12	
AVO	OMC	MBC	AVO	OMC	MBC	OMC	AVO
1254996	1303625	1498693	1427630	2890201	2479821	8967007	3426323
1236458	1326458	1478564	1456328	2956346	2513679	9004526	3485638
1265897	1298698	1523678	1473654	2923654	2456398	8945627	3471313
1235999	1302625	1498559	563374	1177917	1000123	910675	304485
1243569	1295876	1456789	567489	1203564	999785	905683	305642
1236875	1326587	1463568	570245	1152634	1054263	914563	307856
1010031	1086542	1276795	641254	1347527	1152436	1121339	406287
998795	1045263	1204563	635426	1267859	1075623	1154263	410365
992465	1053548	1245624	633142	1297856	1105642	1102312	409555
SA15		SA16		SA19			
OMC	AVO	OMC	MBC	MBBT	BEMT	AVO	OT
636615	183976	2990965	2080729	94524	379280	153226	1253626
635126	180245	3000863	2090768	95112	377896	151485	1251959
631562	185763	3006752	2096913	93896	378356	151023	1223553
1349172	435349	2363373	1655023	474122	1857809	165593	1428572
1253421	440636	2372332	1663710	473836	1852398	159755	1414551
1296543	434562	2381714	1679742	474850	1857504	166515	1410626
677011	221004	2951021	2010684	376875	1557781	275784	2399136
681452	225463	2940903	2030802	371659	1552426	292515	2394731
676942	222456	2936810	2052896	372429	1557481	282124	2380819
SA20		SA21		SA22			
AVO	OMC	AVO	OMC	MBC	AVO	OMC	MBC
186696	2908351	750284	3078231	2410932	283927	642298	264621
189602	3004532	745632	3058923	2345617	285468	645879	265789
187809	2953452	746522	3045637	2378964	279658	650235	268954
118564	1856245	119004	538115	344544	176742	365248	141746
115632	1845692	121000	539023	345698	180425	361524	145687
116254	1799984	122364	537689	350142	179856	359784	146257
121444	1821365	234950	1049776	726678	605669	1456236	535624
117854	1859864	232356	1053456	730542	615362	1503625	529634
123666	1814235	233463	1052654	724653	610524	1402536	520142

SA13			SA14			
OMC	OCR	BEMT	OMC	AVO	OT	BEMT
1509798	594531	368412	1969048	1254424	320425	215235
1516460	596555	369124	1972614	1249437	319945	216456
1523673	597939	369453	1969849	1256324	320145	215245
2359876	988631	1887076	2333559	1203559	1628593	1106052
2428053	987448	1888949	2351710	1208853	1646189	1101454
2397402	990125	1878009	2372629	1869849	1635353	1116567
1499805	593476	1522038	2019102	1304385	1825548	1236499
1456500	592612	1516979	2042589	1319396	1826172	1241524
1439711	591895	1512894	2030210	1326295	1824054	1238713
SA10			SA11			
OMC	Bz-3	OS	OMC	Bz-3	OS	MBC
6865392	4100353	978101	5464415	2556976	824536	825345
6817892	4156785	972678	5390236	2578394	827865	822722
6890134	4178905	973728	5418953	2517853	821356	828956
754556	469976	101195	352227	163787	55457	53603
756235	470563	104987	353562	164562	52275	55623
753698	467236	106745	350153	160745	51523	56523
664116	403253	98202	1321339	702104	193034	196116
654789	400031	100235	1353624	705623	195642	195342
659786	405362	102345	1395632	703436	199563	198452

Appendix H

CONFERENCE PRESENTATIONS

The following have been presented at conferences:

T. Bunhu, and B. S. Martincigh, *Photostability and photochemical analysis of commercial sunscreens*, The 11th Congress of the European Society for Photobiology, Aix-les-Bains, France, September 3-8 2005,

T. Bunhu, and B. S. Martincigh, *Photostability and photochemical analysis of commercial sunscreens*, Faculty of Science and Agriculture Research Day, University of KwaZulu-Natal, 20 September 2005.